DOE/ID-10571
February 1997

Development of a More Fish-Tolerant Turbine Runner Advanced Hydropower Turbine Project

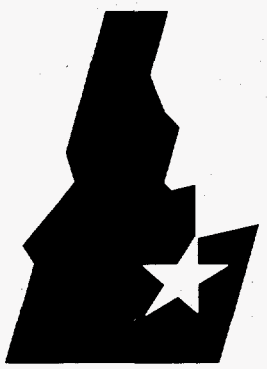

Idaho National Engineering Laboratory

U.S. Department of Energy • Idaho Operations Office

DISCLAIMER

This report was prepared by Alden Research Laboratory, Inc. (ARL) and Northern Research And Engineering Corporation (NREC) to document the work prepared as part of the Advanced Hydropower Turbine Program sponsored by the U.S. Department of Energy (DOE). Neither the DOE, any cosponsor of the program, ARL, NREC, nor any person acting on behalf of them:

A) Makes any warranty or representation whatsoever, expressed or implied, with respect to the use of any information disclosed in this report, or that the use of the information disclosed in this report does not infringe on or interfere with privately owned rights; or

B) Assumes responsibility for any damages or other liabilities whatsoever resulting from use of this report or any information disclosed in this report.

DOE/ID-10571
ARL Report No. 13-97/M63F

Development of a More Fish-Tolerant Turbine Runner Advanced Hydropower Turbine Project

Thomas C. Cook, Project Engineer
George E. Hecker, President
Alden Research Laboratory, Inc.

Henry B. Faulkner, Senior Project Engineer
Willem Jansen, Technical Director
Northern Research and Engineering Corporation

Published February 1997

Prepared for the
U.S. Department of Energy
Assistant Secretary for Energy Efficiency and Renewable Energy
DOE Idaho Operations Office
and
Hydropower Research Foundation, Inc.
Contract DE-AC07-95ID13383

ABSTRACT

Alden Research Laboratory, Inc. (ARL) and Northern Research and Engineering Corporation (NREC) conducted a research program to develop a turbine runner which will minimize fish injury and mortality at hydroelectric projects. ARL/NREC have developed a runner shape which minimizes the number of blade leading edges, reduces the pressure versus time and the velocity versus distance gradients within the runner, minimizes or eliminates the clearance between the runner and runner housing, and maximizes the size of the flow passages, all with minimal penalty on turbine efficiency.

An existing pump impeller provided the starting point for developing the fish tolerant turbine runner. The Hidrostal pump is a single bladed combined screw/centrifugal pump which has been proven to transport fish with minimal injury. The focus of the ARL/NREC research project was to develop a new runner geometry which is effective in downstream fish passage and hydroelectric power generation. A flow of 1,000 cfs and a head in the range of 75 ft to 100 ft were selected for conceptual design of the new runner.

Conceptual design of the new runner began with a re-evaluation of studies which have been previously conducted to identify probable sources of injury to fish passing through hydraulic turbines. Criteria relative to hydraulic characteristics which are favorable for fish passage were prepared based on a reassessment of the available information. Important criteria used to develop the new runner design included low pressure change rates, minimum absolute pressures, and minimum shear. Other criteria which are reflected in the runner design are a minimum number of blades (only two), mimimum total length of leading edges, and large flow passages.

Flow characteristics of the new runner were analysed using two-dimensional and three-dimensional Computational Fluid Dynamic (CFD) models. The basic runner geometry was initially selected using the two-dimensional model. The three-dimensional model was used to investigate the flow characteristics in detail through the entire runner and to refine the design by eliminating potential problem areas at the leading and trailing edges. Results of the analyses indicated that the runner has characteristics which should provide safe fish passage with an overall power efficiency of approximately 90%.

The size of the new runner, which is larger than conventional turbine runners with the same design flow and head, will provide engineering, fabrication, and installation challenges related to the turbine components and the civil works. A small reduction in the overall efficiency would reduce the size of the runner considerably, would simplify the turbine manufacturing operations, and would allow installation of the new turbine at more hydroelectric sites.

DISCLAIMER

ACKNOWLEDGEMENTS

The Advanced Hydropower Turbine Program Phase I - Develop Conceptual Engineering Designs, was initiated by an agreement between the U.S. Department of Energy and the Hydropower Research Foundation, Inc. This foundation is a non-profit organization representing the participants of the industry who are providing funds for Phase I. The participants include:

Chelan County PUD
Electric Power Research Institute
Georgia Power Company
Grant County PUD
Idaho Power Company
New England Power
Niagara Mohawk Power Corporation
Pacific Gas & Electric
Tennessee Valley Authority
Washington Water Power Company

The Technical Review Committee consisted of representives of these participants and representatives from:

U.S. Department of Energy
U.S. Army Corps of Engineers
Bonneville Power Administration
National Marine Fisheries
Department of Interior
Bureau of Reclamation
Nortwest Power Planning Council
Native American Tribes
Oak Ridge National Laboratory
Idaho National Engineering Laboratory
Other utilities and private companies

The Technical Review Committee provided valuable input toward development of the more fish tolerant turbine runner.

DEVELOPMENT OF A MORE FISH TOLERANT TURBINE RUNNER

TABLE OF CONTENTS

TABLE OF CONTENTS (Continued)

TABLE OF CONTENTS (Continued)

LIST OF TABLES

LIST OF FIGURES

LIST OF FIGURES (Continued)

LIST OF FIGURES (Continued)

LIST OF FIGURES (Continued)

EXECUTIVE SUMMARY

Alden Research Laboratory, Inc. (ARL) and Northern Research and Engineering Corporation (NREC) conducted the first phase of a multi-year research program to develop a turbine runner which will minimize fish injury and mortality at hydroelectric projects. Toward that goal, ARL and NREC completed the conceptual design of a new runner geometry with physical features and flow characteristics which are conducive for fish passage, with minimal penalty on turbine performance.

The first step in the conceptual design of the new fish tolerant runner was a review of existing turbine mortality studies to assess the reasons why fish are injured when passing through turbines. This assessment formed the basis for defining criteria used for evaluating the effectiveness of the new runner geometry for safe fish passage. The criteria selected to evaluate runner performance characteristics for safe fish passage included the following parameters:

(1) Peripheral runner speed;
(2) Minimum pressure;
(3) Maximum pressure change rate;
(4) Minimum shear;
(5) Minimum number and total length of leading blade edges;
(6) Minimum clearance between runner and fixed turbine housing components; and,
(7) Maximum size of flow passages.

The assessment of fish injury sources in turbines identified two additional parameters which could be contributors to fish injury: (1) distance between the runner and wicket gates, and (2) travel time from the intake to the runner. Flow control (wicket gates) and plant configuration (distance between the intake and runner) were not evaluated in the conceptual design of the new turbine. The conceptual design concentrated on development of the new runner with the boundaries of the computational models set at the runner inlet and exit.

Available data were reviewed to identify typical operating parameters for existing hydraulic turbines which could be used to select the design point for the fish tolerant turbine. A flow of 1,000 cfs and a design head range between 75 ft and 100 ft were selected for the conceptual design of the new turbine. This design point is representative of the flow and head range (500 cfs to 2,000 cfs and 25 ft to 150 ft) for most hydroelectric turbines installed in the United States.

An existing pump impeller was selected as the starting point for the new turbine runner. The Hidrostal pump is a single-bladed combined screw/centrifugal pump used in the food processing industry to transport fish and vegetables with minimal damage. This pump has been applied as a fish pump in diversion and bypass systems, and ARL has conducted biological evaluations of the pump which verify the effectiveness of the pump for transporting live fish back to their natural environment. As a result of these studies, Hidrostal pumps are currently in use for this purpose at a number of steam electric plants, and the U. S. Bureau of Reclamation is conducting a pilot study at the Red Bluff Diversion Dam on the Sacramento River to evaluate the biological effectiveness of a 36 inch inlet diameter Hidrostal pump.

The focus of ARL/NREC's Phase I conceptual design efforts has been to develop a turbine runner to effectively pass fish like the pump impeller. An impeller casting was purchased and a computer file defining the initial trial impeller geometry was developed using "reverse engineering" techniques. Two-dimensional analysis indicated that the impeller geometry was not acceptable for turbine operation and a new design had to be developed for the runner. A grid (mesh) for the computational codes was prepared to analyse the new geometry.

Flow characteristics of the new runner were analyzed using two-dimensional and three-dimensional Computational Fluid Dynamic (CFD) models prepared by NREC. The basic new runner geometry was developed using the two-dimensional model. The three-dimensional model was used to investigate flow characteristics through the entire runner, and to refine the design to eliminate potential problem areas, particularly at the leading and trailing edges. Results of the analysis indicates that the runner has characteristics which should provide safe fish passage at an overall power efficiency of about 90%.

The next step in developing the ARL/NREC fish tolerant turbine is a pilot scale test to directly observe if fish passing through the runner sustain any injury. Results of the CFD analyses performed in the Phase I conceptual design indicate that the new runner has flow characteristics which should provide fish passage without injury; however, this can only be proven by testing the turbine with fish. The pilot test would include hydraulic measurements to verify the turbine efficiency at the design point. After the basic benefits of the turbine to fish have been proven, additional CFD analyses and model testing would be conducted to refine the runner design, thus reducing fish injury even further while increasing the hydraulic efficiency.

GLOSSARY OF TERMS

A number of terms are used repeatedly in this report. To clearly identify their intended meaning, the following glossary is provided. General schematic diagrams of Francis and Kaplan turbines are provided in Section 2, Development of Biological Design Criteria, on Figures 2-1 and 2-2, respectively.

Abrasion damage - Damage to fish resulting from rubbing contact with moving or stationary objects in a turbine flow passage (adapted from COE 1995a).

Absolute pressure - Atmospheric pressure plus gauge pressure.

Anadromous fish - Fish that ascend rivers from the sea to breed.

Approximate Factorization - A numerical scheme for solving the finite difference form of the Navier-Stokes equations by reducing the equations to an equivalent set of simpler equations that approximate the original equations.

Approximate Factorization Error- The numerical inacurracy resulting from approximate factorization.

Atmospheric pressure - The force per unit area of air; varies with elevation; at sea level atmospheric pressure (1 atmosphere) equals 14.7 psia (101.3 kPa).

Best efficiency point - The operating point at which a turbine produces the highest ratio of power output relative to the flow through the unit and the net head across the unit.

Bulb turbine - Axial flow turbine that has the generator, enclosed in a bulb-shaped housing, within the water passage to the runner (adapted from COE 1991).

Cavitation - Formation and implosion of water vapor bubbles that occur in water. The formation occurs when local pressure is reduced to vapor pressure.

Clupeid species - Family of fish that includes several anadromous species such as alewife, blueback herring, and American shad.

Critical sigma - The runner sigma at which cavitation is initiated; the value of critical sigma is lower than the value of plant sigma, with the difference representing the margin of safety against cavitation.

Decompression - Lowering of pressure from the value at which fish are acclimated.

Discharge ring - The stationary cylinder surrounding the blades.

Distributor area - The upstream area where flow is uniformly distributed to the turbine runner; generally includes the stay ring, wicket gates, head cover, and bottom ring (COE 1991).

Francis turbine - A reaction turbine, named for the inventor, in which water passes through the runner first in a radial and then axial direction.

Grinding damage - Damage to fish drawn into narrow gaps between turbine components. "Gap damage" to fish is considered to be the same as grinding damage.

Gamma - Gamma (γ) is the ratio of specific heats and is calculated by dividing the specific heat at constant pressure (Cp) by the specific heat at constant volume (Cv) of a fluid. This ratio is 1.4 for air at atmospheric conditions and is 1.0 for incompressible fluids.

Kaplan turbine - A propeller turbine, named for the inventor, with runner blades which are adjustable in angle when the unit is in operation (adapted from COE 1991). Flow downstream of the wicket gates is turned in an axial direction prior to reaching the runner.

Leading edge - The edge of the runner blade on the upstream side of the runner.

Leakage - Flow through gaps between rotating and stationary turbine components.

Mechanical injury - Damage to fish resulting from abrasion, grinding, and/or strike (as defined elsewhere) on turbine rotating or stationary components.

Meridional - Meridional refers to a component of a direction or vector that lies in the plane through the rotational axis (the cross-sectional plane).

Naturally-entrained - Fish that were present in a water body and have passed through a hydraulic turbine on their own volition.

Navier-Stokes equations - The set of partial differential equations that govern the unsteady, incompressible, viscous flow of fluids.

On-cam operation - Operating a Kaplan turbine using an automatic control system to set the blade angle versus wicket gate opening (at a given head) with the intent of producing maximum efficiency.

Peripheral runner speed - The speed at which the outside edge(s)of the runner travels (tip speed).

Plant sigma - The value of sigma for the site conditions and turbine setting.

Pressure damage - Damage to fish resulting from increases or decreases in the pressure from values to which the fish have acclimated (COE 1995b).

Pressure Surface - The side of the runner blades with higher pressure than the other side.

Runner sigma - The value of sigma at referenced to a particular place elevation of the runner; usually calculated at the centerline or bottom of the runner in a vertical axis turbine, or at the highest point of the runner in a horizontal axis turbine.

Sigma - A non-dimensional parameter (σ) representing pressure conditions at a turbine runner; the ratio of the pressure above vapor pressure on the underside of the runner and the total pressure across the runner; see equation (5).

Stagnation Point - The point of zero relative velocity near the leading edge of a blade where the flow is divided into the portion that passes over the pressure surface and the portion that passes over the suction surface (see Figure 6-49).

Shear damage - Damage to fish resulting from their passing through regions of rapid velocity changes (shear zones) (COE 1991).

Shear zone - Adjacent flow regions in a turbine having different velocities.

Shroud - Surface of revolution associated with the tips of the turbine blade.

Specific heat at constant pressure - The amount of energy (heat) necessary to raise the temperature of one unit mass of fluid one degree while the fluid is held at constant pressure.

Specific heat at constant volume - The amount of energy (heat) necessary to raise the temperature of one unit mass of fluid one degree while the fluid is held at constant volume.

Strike damage - Damage to fish resulting from their direct collision with rotating or stationary turbine components (COE 1995a).

Suction surface - The side of the runner blade with lower pressure than the other side.

Throat - The minimum cross-section in the discharge ring; usually downstream of the runner.

Turbine efficiency - Percent of useful shaft power developed relative to hydraulic input power.

Turbine (runner) setting - The runner elevation relative to the tailwater level.

Vapor pressure - Pressure at which water vaporizes (boils); varies with water temperature.

Vortex - Water flowing in a well defined circular motion with a lower pressure in the center; vortices may be caused by flow disturbances at the runner's leading edge and by leakage through gaps (COE 1995a); vortices in the turbine draft tube are caused by residual swirl leaving the runner (COE 1995a).

Wicket gate - One of a series of gates in the flow passage leading to the runner which regulates quantity and direction of water; the series of movable, flow-regulating gates impart rotation to the flow (adapted from COE 1991).

SECTION 1
INTRODUCTION

The U.S. Department of Energy (DOE) and the hydropower industry have initiated an Advanced Hydropower Turbine System Program. The hydropower industry recognizes that hydropower plants can have an adverse effect on the environment and that there is a need to improve turbine design to mitigate fish passage through turbines and water quality issues. The goal of the Advanced Hydropower Turbine System Program is to design, develop, build, and test environmentally friendly hydropower turbine systems. The program is planned in three phases: Phase I - develop conceptual engineering designs; Phase II - build and test fully engineered scale models of the most promising designs; and Phase III - build and test full-scale prototypes of the most promising models.

In October 1995, the DOE awarded a contract (No. DE-AC07-95ID13383) to Alden Research Laboratory Inc. (ARL) to develop a fish friendly turbine runner design. ARL's approach to developing a fish tolerant runner was initiated based on the characteristics of a commercially available pump impeller. ARL and its subcontractor, Northern Research and Engineering Corporation (NREC) employed Computational Fluid Dynamic (CFD) analyses, a mathematical modeling technique, to change the initial geometry for application as a turbine and to develop a new runner which should minimize fish injury and mortality. The new turbine runner characteristics were evaluated by comparing hydraulic features in the new runner to the features in existing turbines which are known to affect fish mortality.

Section 2 of this report, Development of Biological Design Criteria, presents the ARL's assessment of available fish mortality information used to identify criteria for evaluating the new runner geometry potential to pass fish without injury. This biological criteria section presents a review of studies conducted to identify the mechanisms causing fish injury and mortality as a result of passage through hydraulic turbines. The criteria indicate how development of a new turbine runner might avoid or alleviate fish injury in existing runner designs. Insight into the physical, mechanical, and hydrodynamic forces that injure fish was particularly useful in interpreting CFD analyses results, and in selecting runner geometry improvements.

Section 3, Selection of Turbine Design Parameters, and Section 4, The Hidrostal Impeller Concept And Past Applications, identify design operating conditions selected for the new turbine, and give the characteristics for the selected pump impeller. These sections describe the process of selecting the

operating design point and the initial geometry for the new runner, and provide information on the Hidrostal pump design and experience as a fish pump.

Section 5, Description of Computational Methods, and Section 6, Results of Computational Analyses, discuss the CFD analyses. The general approach to the design process, the CFD codes, and the basic assumptions are presented in Section 5. A summary of preliminary analyses using the one-dimensional power performance model, the two-dimensional model to develop the new runner geometry, and the results of the three-dimensional CFD analyses for three design iterations of the new runner are presented in Section 6. The discussion on the general approach describes major steps in the design process for developing the new runner in general, reviews existing turbine types and performance characteristics, and presents blade loading options used in turbine design. The discussion on the basic assumptions addresses the consequences of the biological criteria, and describes the inlet and outlet conditions, flow control, and rotation simulation. The results section describes validation of the analytical methods by comparing predicted pump performance to pump performance data, and summarizes the analyses of the various iterations of the runner geometry which were investigated to arrive at the final design. The predicted operating characteristics and a comparison of the flow characteristics to the biological criteria are presented for various runner geometries investigated in the two-dimensional analyses, and for the refinements to the runner geometry analysed with the three-dimensional CFD model.

Basic biological, engineering, manufacturing, and installation considerations for completing turbine component design for the new runner, and for application of the new turbine at hydroelectric sites have been identified for the final runner design. A discussion on these issues is presented in the section entitled Evaluation of Final Runner Design. The last two sections of the report present the conclusions of the analyses and a brief discussion on future efforts that are necessary to verify how effective the new turbine will be in passing fish without injury. A list of cited literature within this report and a list of other literature reviewed as part of the project development efforts are presented at the end of the report.

SECTION 2
DEVELOPMENT OF BIOLOGICAL DESIGN CRITERIA

2.1 Introduction

Available information was reviewed (1) to identify hydraulic parameters that may contribute to fish injury while passing through turbine runners, and (2) to establish allowable values for parameters such as velocity and pressure gradients and absolute pressures that could be used as limiting values in the design of the new turbine runner. Criteria for design of the new runner were established based on ARL's re-evaluation of the available mortality studies of fish passing through turbines and other cause-and-effect studies conducted to date.

Studies designed to identify causes of fish stress, injury, and mortality in fish passing through hydraulic turbines have been ongoing for decades. The studies have been conducted by hydroelectric project owners, the U.S. Department of Energy (DOE), the Electric Power Research Institute (EPRI), the Federal Energy Regulatory Commission (FERC), the National Marine Fisheries Service (NMFS), the U.S. Fish and Wildlife Service (USFWS), and state resource agencies during licensing and relicensing efforts. While a variety of causes have been identified, the ability to use the available data base in a predictive manner, when considering improved runner designs, is somewhat limited because of the study methods.

The process of accurately defining the causes of fish injury and stress during turbine passage for the purpose of developing new runner designs is extremely difficult. Direct observations and physiological examinations of fish exiting operating turbines is perhaps the most realistic method for identifying injury. However, such studies are very complex and costly, and results can be biased due to stress and injury resulting from mark, release, and/or recapture techniques. Further, it is difficult to accurately attribute an observed injury or stress to a specific causal mechanism (e.g., differentiating between mechanical effects from strike, abrasion, and grinding). Since it has not been possible to observe fish passing through a full-scale operating turbine, defining the actual mechanisms causing mortality at specific study sites has been somewhat speculative. As a result, attempts to draw general conclusions based on the combined results of the various turbine passage studies conducted to date have not resulted in definitive cause and effect relationships.

To provide additional insight into the causes of turbine injury, researchers have conducted smaller-scale experiments that attempt to isolate the effects of individual mechanisms. While this study

approach has yielded useful data, and even resulted in the definition of threshold levels of injury for selected parameters and species, smaller-scale experiments may not accurately account for the effect of a given parameter within the dynamic environment of a turbine. Further, the synergistic effects of multiple stresses encountered by fish during turbine passage is not considered in such studies. Therefore, the ability to interpret results from small-scale experiments as they relate to full-scale installations has been limited.

As a result of these limitations, ARL's re-evaluation of the results of past research efforts, as presented in the following discussions, has been used to formulate criteria that provide a baseline for comparing runner characteristics to improve fish passage. The criteria are intended to provide guidelines for identifying runner modifications to reduce the potential for injury, not to assess the overall effectiveness of the new turbine runner. The effectiveness of the new runner for passing fish with minimal injury can only be verified through biological evaluation of a prototype runner in a subsequent phase of the runner development.

2.2 Review of Past Research

In 1992, EPRI prepared a review of many turbine entrainment and mortality studies that had been completed at hydroelectric plants (EPRI 1992). This review was different from previous reviews in that it included data from many projects outside the Pacific Northwest that encounter riverine rather than anadromous fish species. Many of these studies were conducted in the early 1990's as part of the FERC relicensing process, and employed research techniques that were not available for earlier studies. The findings of this EPRI review relative to turbine mortality can be summarized as follows:

1) Estimated mortality caused by turbine passage in the studies reviewed averaged 20% for Francis turbines, 12% for Kaplan turbines, and 9% for bulb turbines.

2) A wide variety of species suffer similar mortality rates in a given turbine type.

3) Several studies, which compared mortality rates of entrained fish (sometimes referred to as "naturally-entrained" fish) with artificially introduced fish, indicated lower rates of mortality for the entrained fish (averaging 6% mortality for both Francis and Kaplan turbines).

4) Studies of juvenile clupeid species (American shad and blueback herring) conducted since 1987 indicated a mortality of about 16% for Francis turbines and about 4% for Kaplan turbines.

The authors of the 1992 EPRI review attributed the lower mortality of naturally-entrained fish to the smaller size of fish (an artifact of the testing protocol; i.e., fish available for artificial introduction at the time of the tests were larger than those passing through turbines "naturally"). The lower mortality rates of juvenile clupeid species observed in studies after 1987 are attributed by the 1992 EPRI reviewers at least in part to improved handling techniques and evaluation technologies that were used in the more recent studies.

The 1992 EPRI review also addresses fish mortality at hydroelectric plants associated with spillway flows and fish bypass systems. Such information provides insight into the causes injury and stress in fish subjected to rapid changes in flow direction and magnitude. For example, at Bonneville Dam, fish released into flows discharged over a spillway had higher survival than fish released in the surface back eddy in the draft tube discharge, while fish released into the back eddy had a higher survival rate than the fish released into the turbine and the bypass system. Fish losses due to predation at the exit for the Bonneville bypass system appear to be higher than the fish losses associated with either spillway flow or with passage through the Kaplan turbines.

Two other studies reviewed in the 1992 EPRI report address the mortality of fish passing over spillways and through bypass systems. At the Crescent Hydroelectric Project, the spillway studies indicated negligible immediate mortality and about 12% mortality after 48 hours for juvenile blueback herring passing over a 12 ft high spillway discharging 40 cfs. At the Bellows Falls Hydroelectric Project, the fish bypass studies indicated a 0 to 4% immediate mortality rate and no additional delayed mortality after 48 hours with Atlantic salmon smolts passing through an ice-log sluiceway sloping approximately 30 ft over a 500 ft length and terminating in a 30 ft drop into the tailrace.

EPRI also assessed spillway and bypass systems in an earlier report (EPRI 1986). The 1986 EPRI assessment indicates that the mortality associated with fish bypass systems and spillways with free-falling water can be similiar to turbine mortality. The orifice bypass systems from the gatewells and ice and trash sluiceways at McNary Dam and Ice Harbor Dam both had estimated mortality rates of salmonids in the 4 to 22% range (EPRI 1986). Studies conducted on salmonids indicated a 0 to 2% mortality of fish under free-fall spill flow conditions to a pool of water at velocities up to 50 ft/sec, and a 2 to 7% mortality for fish which entered a pool of water through a hydraulic jump (COE 1972). At Glines Dam, yearling coho salmon had an 8% mortality after passing through a spillway gate and free-falling 180 ft into a plunge pool (COE 1972). The results of the bypass and free-fall studies conducted prior to 1986 indicate that impact forces, surface friction, and differential pressure changes are major contributors to fish mortality in bypass systems, and that all these factors which must be addressed in designing a turbine runner for effective fish passage (EPRI 1986).

The combined mortality evaluations for spillways and other alternative fish bypass routes indicate that development of a turbine that causes minimal stress and injury could eliminate the high cost of spilling and fish passage structures.

Turbine design and operating characteristics that may contribute to the mortality of fish passing through turbines in general, and specifically through Kaplan and Francis units, have been identified by EPRI (1987). General schematic diagrams of Kaplan and Francis turbines are provided on Figures 2-1 and 2-2. The 1987 EPRI assessment indicates that fish mortality through turbines is affected by the number of leading edges on the runner, changes in pressure versus time, the size of flow passages through the turbine, and clearances between the runner and other turbine components. Pertinent findings of the 1987 EPRI assessment relative to understanding the possible causes of fish stress and injury during turbine passage are presented below.

General

1) Subatmospheric pressures (including cavitation) in a turbine increase fish mortality.

2) Fish mortality tends to be inversely proportional to turbine efficiency (higher turbine efficiencies generally result in lower mortality).

3) Higher runner elevations with respect to tailwater levels increase fish mortality (presumably because of lower pressures in the runner).

4) The exact location of fish damage within a turbine is difficult to identify (injury type and character may be related to various causes).

5) The impracticality of observing fish injury within a turbine has been a primary obstacle in determining factors causing fish mortality.

6) Stress of fish passing through turbines is discriminate (only those fish exposed to discrete areas are presumed to be damaged).

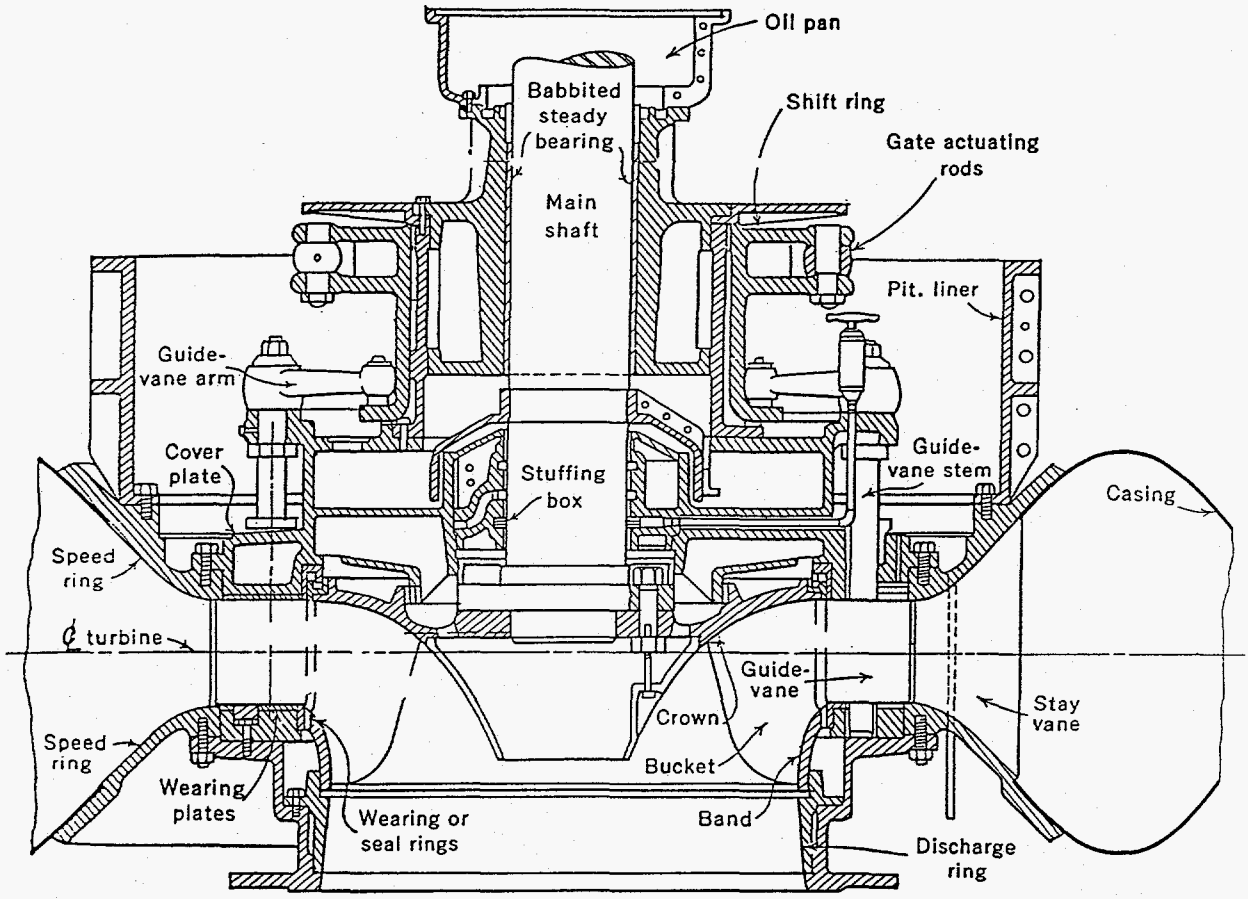

Figure 2-1
Cross-Section Through Francis Turbine
Source: Doland 1954

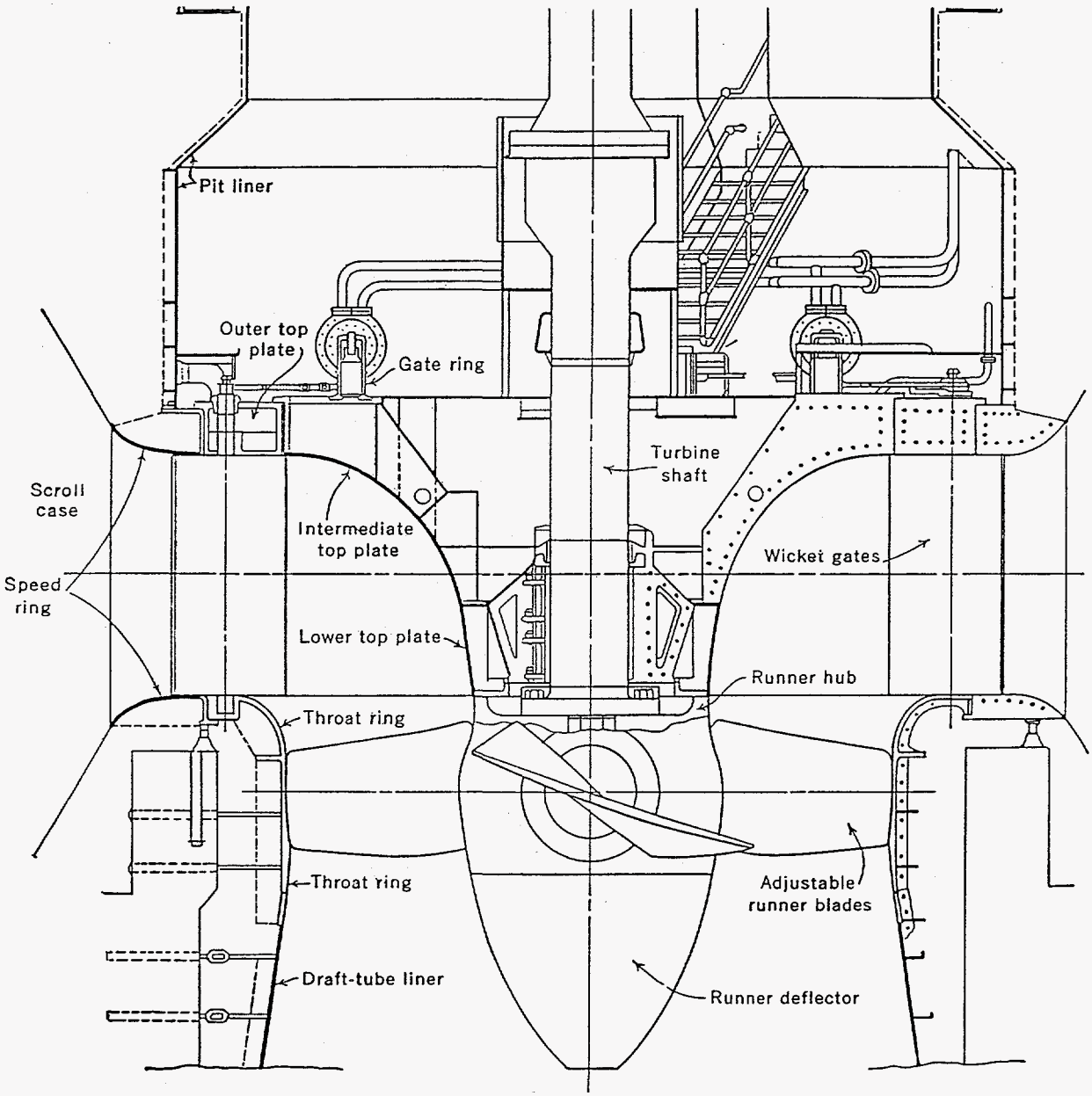

Figure 2-2
Cross-Section Through Kaplan Turbine
Source: Doland 1954

Francis Turbines

1) A major area of concern is the runner entrance, where the wicket gates, the blades, and the runner's peripheral speed may damage fish.

2) Higher peripheral runner speeds have been correlated to higher mortality.

3) There is little relationship between plant operating head and fish mortality (similar mortality at 40 ft and 410 ft heads).

4) Greater wicket gate openings have been correlated to higher mortality rates (perhaps due to less clearance between the trailing edge of the wicket gates and the runner).

Kaplan Turbines

1) A major area of concern is the clearance between the blade tips and the throat (discharge) ring where fish may be caught.

2) There is little correlation between peripheral runner speed and fish mortality.

3) There is little relationship between plant operating head and fish mortality (similar mortality at 20 ft and 110 ft heads).

4) In one model study, the speed at which young salmon struck the blades was a factor affecting mortality.

In contrast to the above conclusions regarding operating head, it is often stated that head is a major contributing factor to turbine mortality, and that head and mortality are directly related. This relationship was not obvious in the EPRI review. It is possible that the higher mortality rates observed in earlier studies at projects with higher heads may be due to the fact that Francis turbines, which generally have higher mortality rates than Kaplan turbines due to inherent turbine characteristics, are typically installed at higher head sites.

In 1995, the U.S. Army Corps of Engineers held a Turbine Passage Survival Workshop in Portland, Oregon. A compilation of available information related to injury of fish passing through turbines provided a basis for discussions at the workshop on the uncertainties of the sources of fish injury in

turbines. The workshop handout and proceedings indicated that operating turbines at best efficiency reduces injury to fish (COE 1995a; COE 1995b). The best efficiency point occurs at 85 to 95% of rated load for Francis turbines, 95% of rated load for fixed blade turbines, and 65 to 70% of rated load for Kaplan turbines (COE 1995b). Rated load is presumed to be power output at full gate and design head and speed. The lowest fish mortality through a Francis turbine occurs at peak efficiency, which occurs at about 75% of full gate (Cramer 1964; Bell 1981; Collins 1984). At Foster Dam, the lowest mortality of fingerling chinook passing through a Kaplan turbine occurred at a 25% blade angle with the wicket gates set at the best efficiency position, and was 2 to 8% at heads ranging between 86 to 110 ft, respectively (Bell 1981). Other blade angle settings on the Foster Dam units had mortality as high as 31% with the wicket gates set at best efficiency positions (Bell 1981). The best efficiency for a Kaplan turbine is a function of blade angle and typically occurs at about 75% of full gate (Collins 1984), but can occur between at 40% to 99% of full gate setting..

The participants in the 1995 Corps of Engineers workshop generally agreed that fish stress and injury resulting from turbine passage can be grouped loosely into the following categories: 1) mechanical, 2) cavitation, 3) shear, and, 4) pressure. Mechanical damage was subdivided into fish injury resulting from strike, abrasion, and grinding. Important information that was brought to light regarding each of these sources of stress and injury is summarized below.

1) Mechanical Injury

Strike

Strike damage to fish is the result of direct collision with turbine components. Smaller fish passing through Francis turbines have lower mortality than larger fish, suggesting that strike is a contributor to fish injury in Francis turbines (Collins 1984). Stationary turbine components cause fewer injuries than moving parts (Monten 1985 cited in COE 1995b).

The probability of strike is a function of the opening between the blades, the number of blades, the blade velocity, and fish length (Monten 1985 cited in COE 1995b). A number of models have been developed to predict the probability of strike occurring in different types of runners. Since the strike probability for the models are in percent, the models can be compared directly with the percent mortality rate determined from field studies. In 1957, Von Raben developed the first model for estimating the probability of fish striking a Kaplan blade (Cada 1990). Von Raben's model is:

$$P = (l * n * N * a * \cos \beta * 100) / Q \qquad \text{(eq. 1)}$$

where: P = probability of strike (%);
l = fish length (ft);
n = number of blades;
N = unit speed (rpm);
a = cross-sectional area of water passage at the blade (ft^2);
β = blade angle relative to the axis of the shaft (degrees);
Q = discharge (cfs).

Monten developed a model which approximates the probability of strike in a Kaplan unit as a function of fish length and blade spacing (COE 1995b):

$$P = [\ (l/2) / S\ ]*100 \qquad \text{(eq. 2)}$$

where: P = strike probability (%);
l = fish length (ft);
S = spacing between blades (ft).

The Corps of Engineers developed a model to estimate the probability of strike in a Kaplan unit as a function of the distance that the blade travels along an arc over a time period and the distance between the blades along the arc at the blade tips (COE 1991). The Corps of Engineers model for Kaplan units is:

$$P = (N*n*l*\cos\theta) / (60*Va) \qquad \text{(eq. 3)}$$

where: P = probability of strike (%);
N = unit speed (rpm);
n = number of blades;
l = fish length (ft);
θ = angle between the actual entrance velocity and axial velocity components;
Va = axial water velocity at blades (ft/sec).

Figure 2-3 shows a schematic diagram defining the velocity components used in equation (3). Since equation (3) does not have a parameter related to the turbine size, the blade tip speed is not taken explicitly into account in the Corps of Engineers strike probability model.

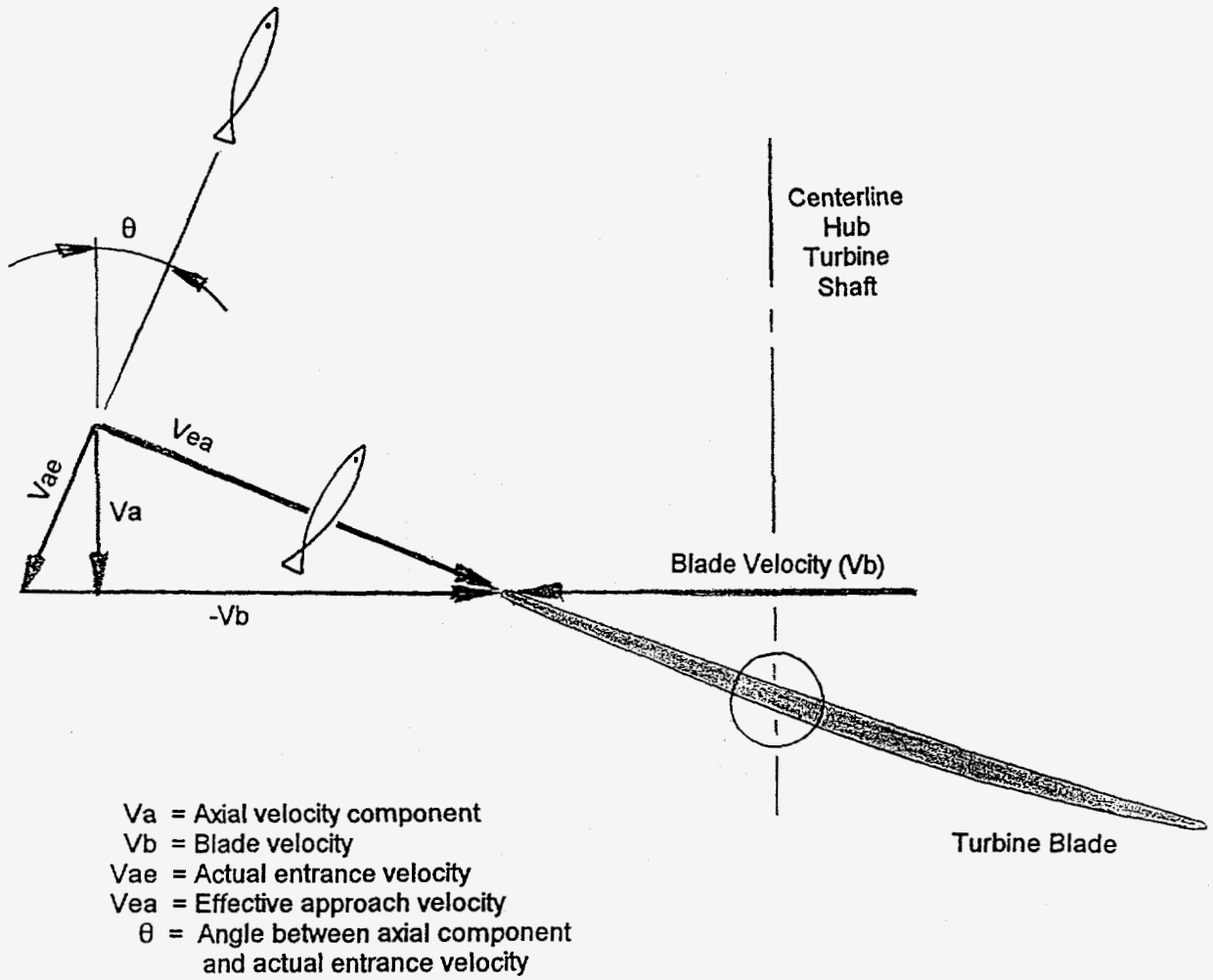

Figure 2-3
Velocity Vector Diagram
Kaplan Turbine Blade Leading Edge

The Corps of Engineers also has a model to estimate the probability of strike in a Francis turbine (COE 1991):

$$P = (N*n*l*\cos \alpha) / (60*Vr) \qquad \text{(eq. 4)}$$

where: P = probability of strike (%);
N = unit speed (rpm);
n = number of blades;
l = fish length (ft);
α = angle between the actual entrance velocity and a line tangent to the runner;
Vr = radial water velocity (ft/sec).

Figure 2-4 shows a schematic diagram defining the velocity components used in equation (4).

Available data suggests that a portion of fish injury and mortality can be attributed to direct collisions with the turbine (COE 1995b). However, there are no direct visual observations available to correlate mortality to strike (COE 1995b) and to verify the strike probability models. Data on specific causes of injury to fish passing through turbines is very limited.

One recent study, which may eventually lend itself to evaluation of the strike equations, was conducted by the Corps of Engineers during 1995 at Lower Granite Dam (Normandeau 1995). The 1995 Lower Granite Dam study estimated 1 hour and 120 hour survival probabilities of spring migrant chinook salmon passing through a Kaplan turbine. The survival estimates were based on statistical analyses of fish released in one or two of the three intake bays, downstream of the extended length submerged travelling screen, and recaptured in the tailrace using the balloon tag method. Figures 2-5 and 2-6 show the general arrangement of Lower Granite Dam facilities and a cross-section through one of units, respectively. Six test scenarios were evaluated including: four releases with the unit operating near peak efficiency and 18,000 cfs (one release in the upper portion of the end intake bay A, one release in the middle portion of end intake A, one release in the middle of the center intake bay B, one release in the middle of intake bays B and C); one release in the middle of intake bay A with the unit operating near peak efficiency and 13,500 cfs; and, one release in the middle of intake bay B with the unit operating at cavitation conditions and 19,000 cfs.

Fish injuries in the Lower Granite Dam study were categorized according to three probable causes: (1) mechanical (strike, grinding, and abrasion); (2) pressure related; and, (3) shear. The study results indicated a range of 2 to 5% for the 1 hour mortality probability and 3 to 6% for the 120 hour

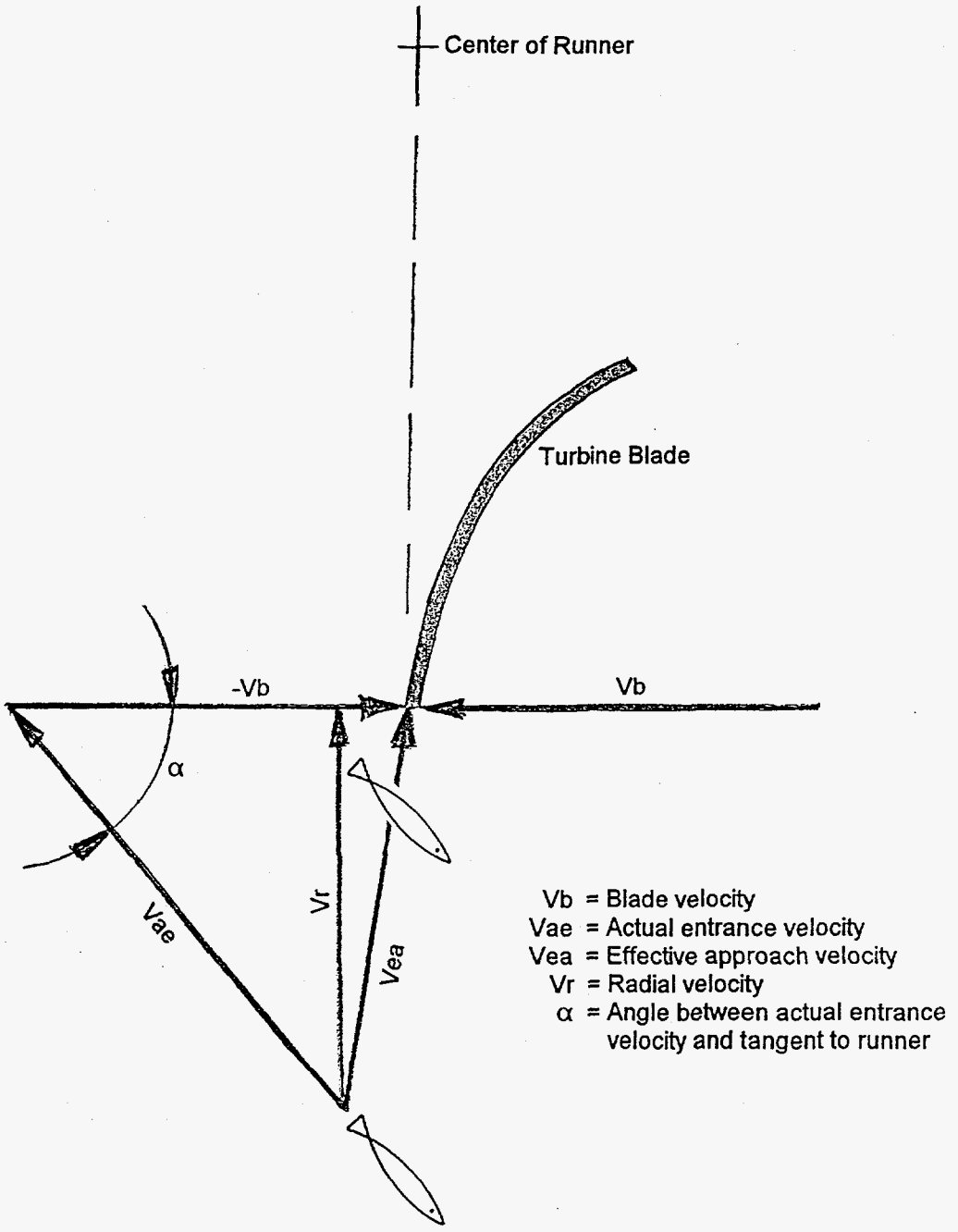

Figure 2-4
Velocity Vector Diagram
Francis Turbine Blade Leading Edge

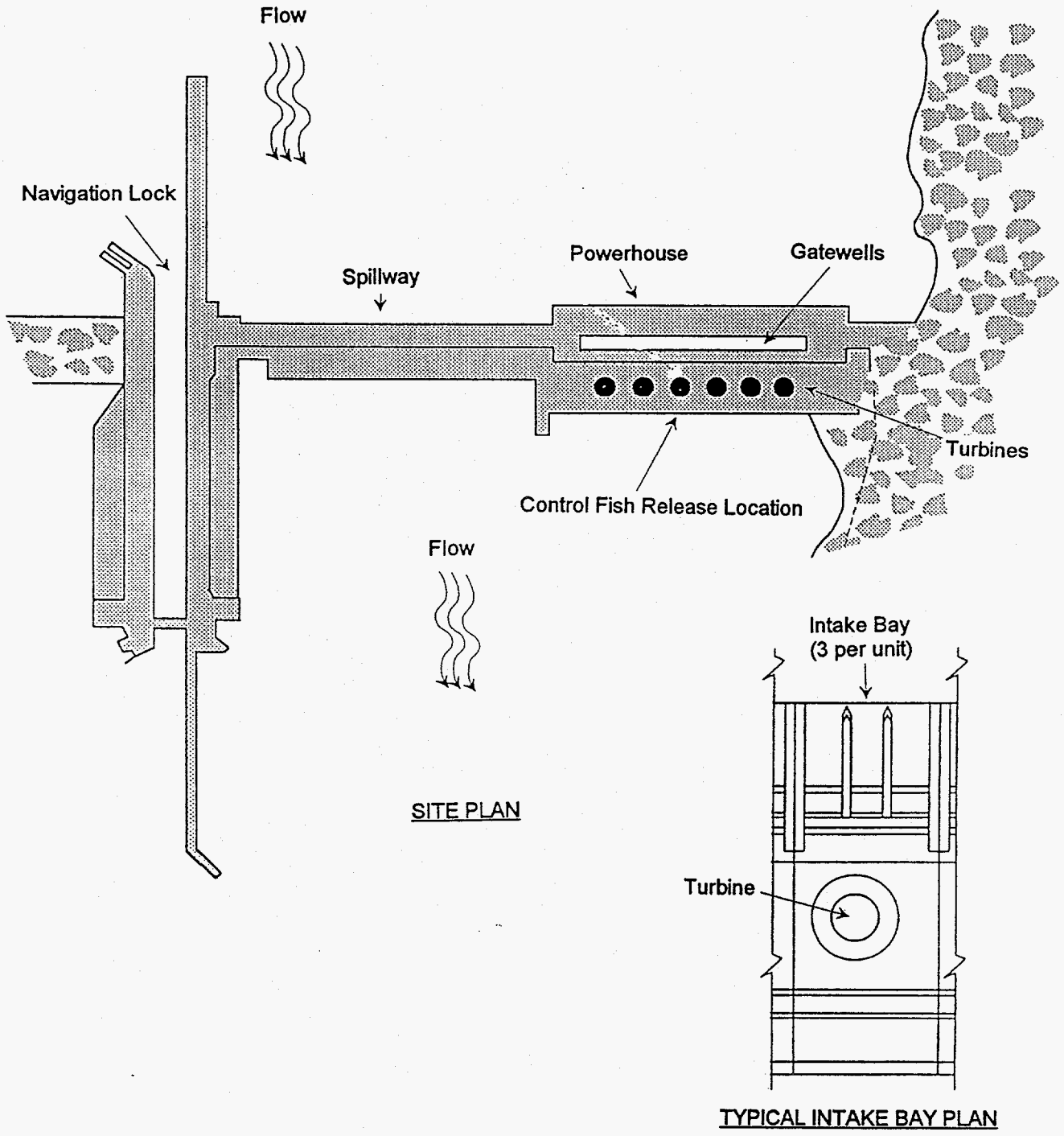

Figure 2-5
General Arrangement, Lower Granite Dam
Source: Normandeau 1995

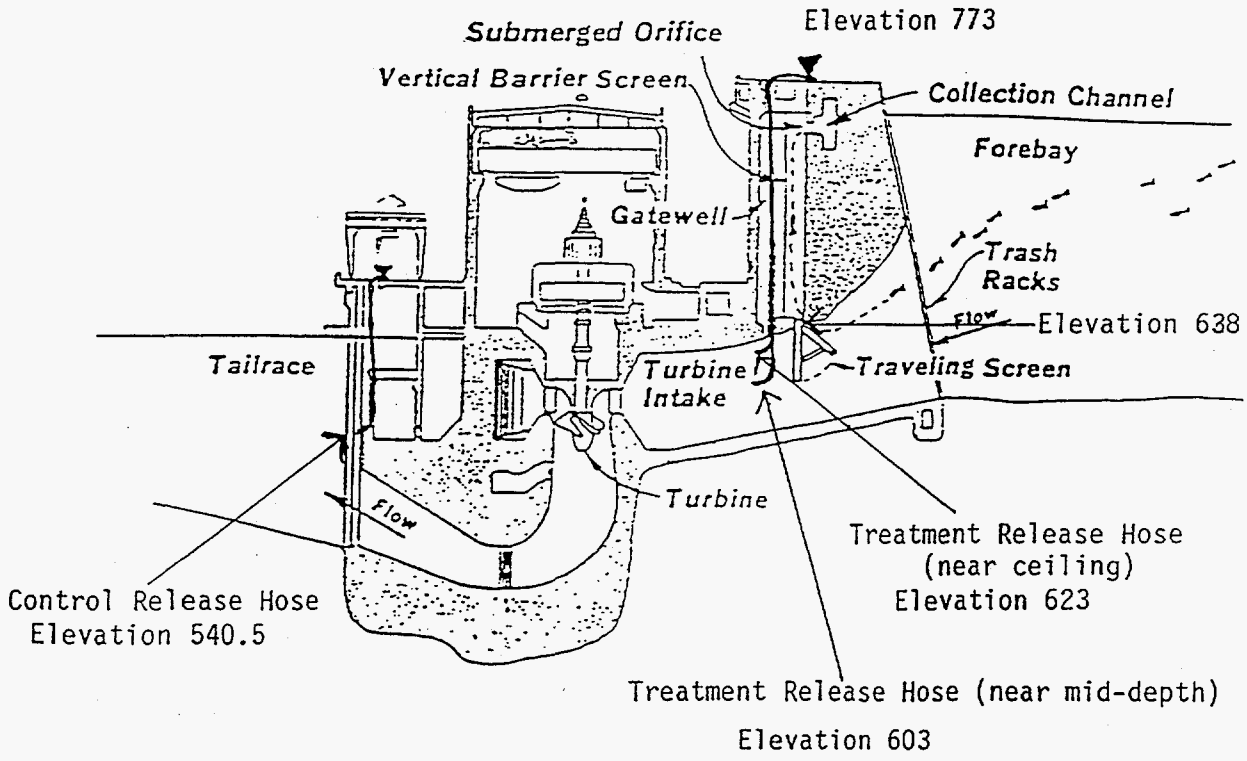

Figure 2-6
Section Through Centerline Turbine, Lower Granite Dam
Source: Normandeau 1995

mortality probability for all six test conditions with the Kaplan unit at Lower Granite Dam, significantly less than the 12% mortality rate reported in the 1992 EPRI report for Kaplan turbines in general. Fifty percent (50%) of the injuries in the Lower Granite Dam study were attributed to mechanical sources with the remaining injuries attributed to multiple sources (17%), pressure changes (19%), and shear (14%).

Unfortunately, the Lower Granite Dam study report does not include sufficient data to calculate strike probability with the three mathematical models for comparison to the number of observed injuries attributed to strike. Blade angles (β) and the unit characteristics, including the spacing between the blades (S), the area of flow passage (a), and the angle between the entrance and axial water velocity vectors (θ) for each of the test conditions are necessary to predict strike probability with the models. Evaluation of strike equations would be possible if these data were made available.

Strike calculations using Von Raben's model, equation (1), have been compared to total mortality rates at some projects. Blade contact injuries at a STRAFLO (low-head, propellor type) turbine have been shown to be close to predicted strikes using equation (1) (Dadswell et al. 1986 cited in Cada 1990). At Townsend Dam, field data with the two horizontal Kaplan turbines indicate no mortality for 8 to 13 cm largemouth bass, 4 to 24% mortality for 20 to 23 cm largemouth bass, 1 to 15% mortality for 13 to 15 cm rainbow trout, and 4 to 25% mortality for 33 to 36 cm rainbow trout (RMC 1994). The predicted strike probability for these species and the Kaplan units at Townsend using equation (1) are 8% for 8 to 13 cm largemouth bass, 10 to 18% mortality for 20 to 23 cm largemouth bass, 7 to 12% mortality for 13 to 15 cm rainbow trout, and 15 to 27% mortality for 33 to 36 cm rainbow trout (RMC 1994). The observed mortality data for the species evaluated at Townsend Dam is lower than the probability of strike predicted with Von Raben's model equation (1). Mortality should be less than strike since not all fish which are struck will die. For example, fish passing near the runner hub would be struck at a lower angular velocity, possibly not as injurious as the velocity at the blade tip. In addition, the report on Townsend Dam indicates that observed mortality for clupeids less than 23 cm in length is about 4% at other Kaplan turbine installations, compared to a 5% strike probability using equation (1) (RMC 1994).

The strike calculations based on the Corps of Engineers model, equation (3), indicate that the predicted 10% strike for the Kaplan turbines at Big Cliff Hydroelectric Plant is high compared to the mortality estimate of 5% obtained by tests at the project, and that the predicted strike of 6% for the bulb units at Racine is slightly lower than mortality rate of 8% determined from passage studies (COE 1991).

Calculations indicate that the strike probability, based on the Corps of Engineers model for Francis turbines, equation (4), is about 27% for 9 cm trout, 32% for 11 cm trout, and 40% for 14 cm trout at the Lequille Hydroelectric Project (COE 1991). The predicted strike probability was 18% for 7 cm fish and 35% for 14 cm fish at the Cushman Hydroelectric Project, and 8% for 7 cm fish representative of chinook, 16% for 14 cm fish representative of steelhead, and 24% for 21 cm fish representative of rainbow trout found at the Shasta Hydroelectric Project (COE 1991). The predicted strike probability for most of these projects and species are greater than the total mortality rate of 12% for Francis turbines presented in the 1992 EPRI report.

Calculations using equation (4) indicate that the wicket gate position does not effect the strike probability in Francis turbines having a radial velocity in the 25 to 40 ft/sec range (COE 1991). However, there are no available field data to verify the mathematical predictions.

Data on fish mortality resulting from entry into water and impact on solid objects have been summarized by the Corps of Engineers (COE 1991). This data, which may be indicative of injury resulting from shear as well as strike, are summarized on Figure 2-7. The mortality of fish entering a pool of water varies linearly between 0% at 65 ft/sec and 100% at 145 ft/sec based on actual test data. Data indicates that fish mortality resulting from impact on solid objects varies linearly between 0% at 15 ft/sec and 100% at 95 ft/sec.

The 1987 EPRI assessment also provides peripheral runner velocity and mortality data that can be used to determine what turbine runner speeds produce low strike potential (low mortality). A plot of this data, provided in Figure 2-8, indicates that mortalities increase with runner peripheral velocities. A best fit straight line of the data points indicates minimal fish mortality could be expected with runner peripheral velocities of 40 ft/sec or lower. The correlation coefficient (r) and the probability value (p) for the line shown on Figure 2-8 indicates that there is a significant correlation between the variables, and that there is a low probability that the linear relationship occurred randomly. The trend in the data on Figure 2-8 may show that, if tip speed were related to strike, more strikes would occur at higher tip speeds. A secondary trend with the number of turbine buckets may also exist but cannot be determined due to scatter in the field data and the relatively small variation in the number of buckets among the various Francis runners. An upper boundary envelope of the data presented on Figure 2-8 indicates that a peripheral runner velocity of 20 ft/sec or less may be more appropriate to eliminate strike mortality.

In addition, the data on Figure 2-8 can be used to verify the Corps of Engineers model to determine the strike probability in Francis turbines, equation (4). As indicated on the figure, mortality rates

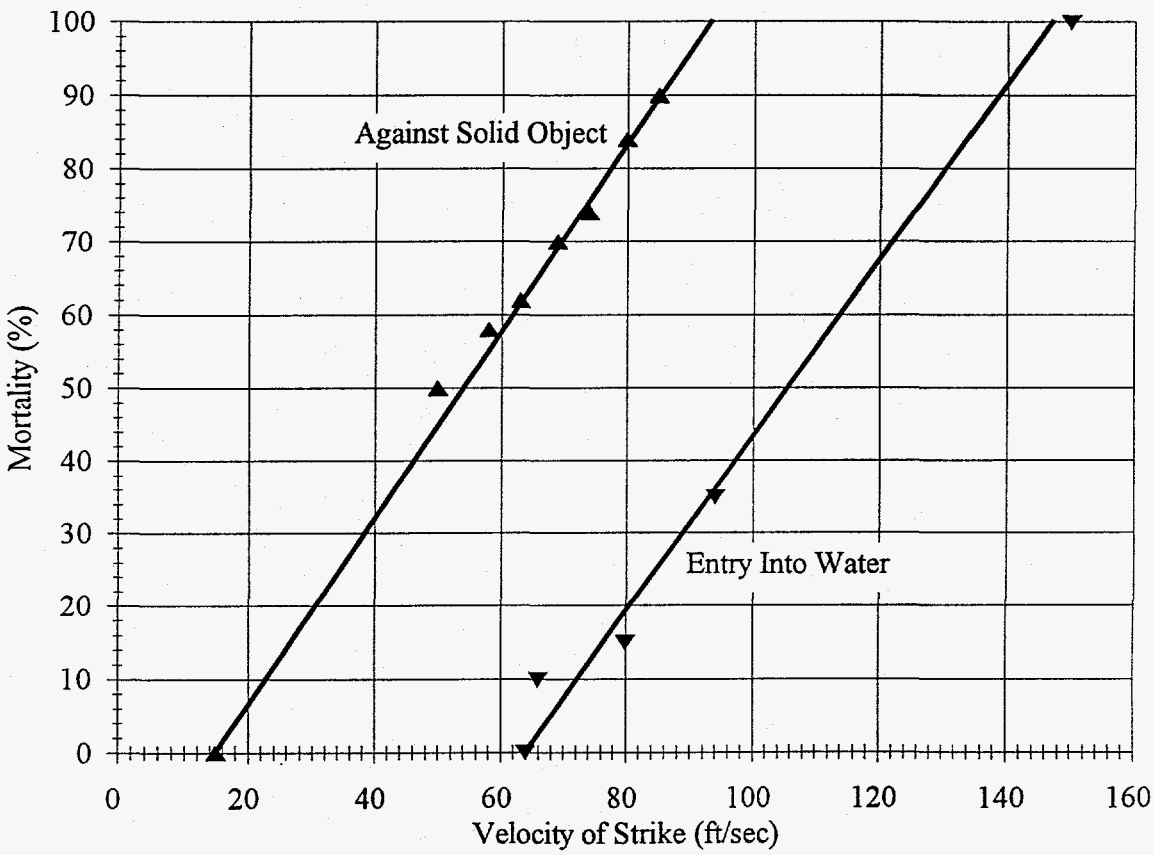

Figure 2-7
Fish Mortality When Flow Strikes Water Surface and Solid Objects
Source: Adapted from COE 1991

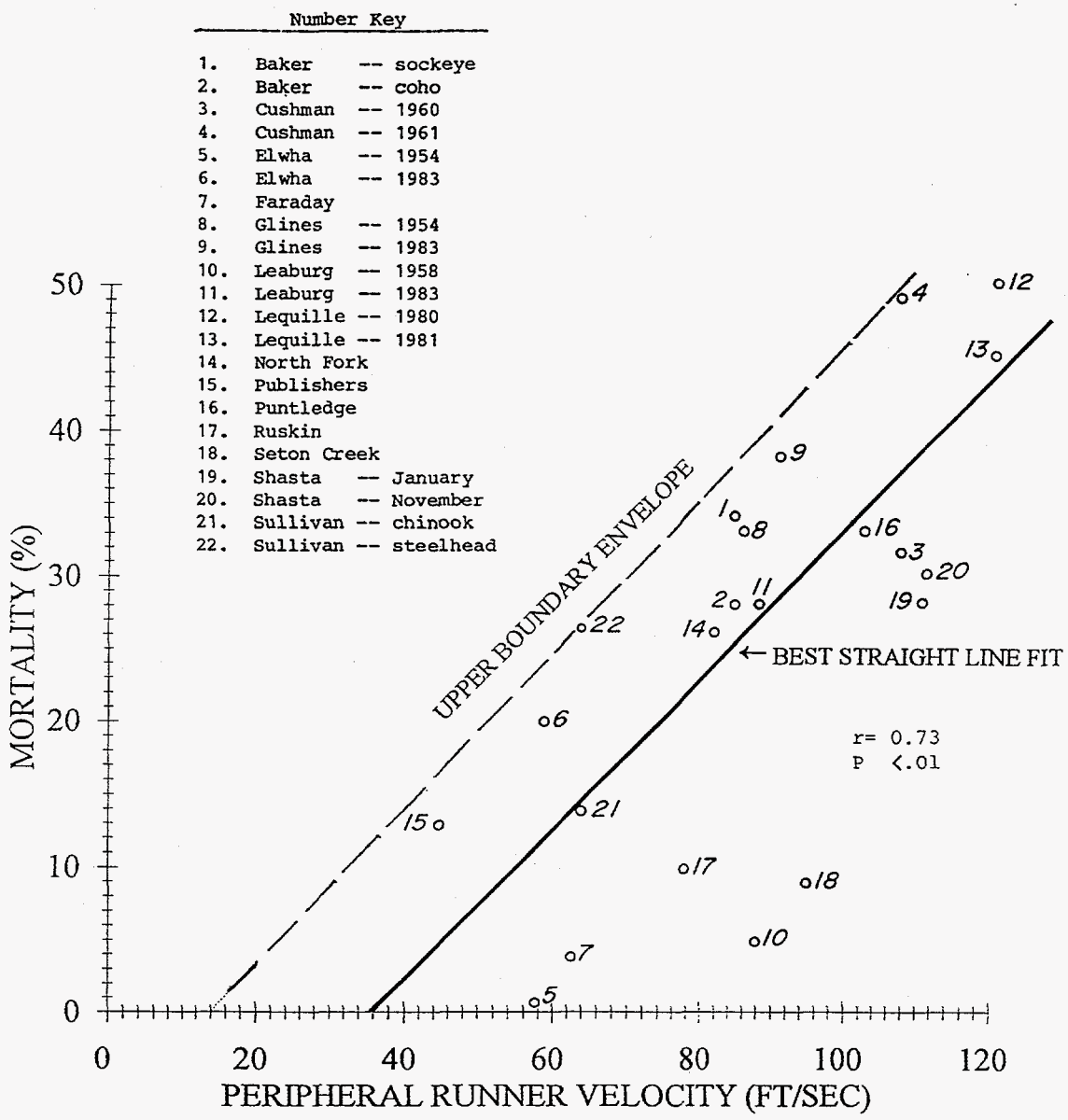

Figure 2-8
Relationship of Peripheral Runner Velocity to Mortality
for Francis Turbines, Source: Adapted from COE 1991

were about 45% in 1980 and 55% in 1981 at the Lequille Hydroelectric Project, 30% in 1960 and 50% in 1961 at the Cushman Hydroelectric Project, and 30% during January and November tests at the Shasta Hydroelectric Project. The predicted strike probability using equation (4) for these projects are 27 to 40% for Lequille, 18 to 35% for Cushman, and 8 to 24% for Shasta, as discussed above (COE 1991). The predicted strike probability using equation (4) for these projects are generally 50 to 70% of the mortality reported on Figure 2-8. The difference between the predicted strike probability and the mortality shown on Figure 2-8 is consistent with the results of the 1995 Lower Granite Dam studies which showed that 50% of observed injuries were attributed to mechanical source. Therefore, equation (4) does seem to predict the proper range of strike mortality.

Abrasion

Abrasion injury to fish is the result of rubbing contact with objects in the flow passage (COE 1995a). Turbine characteristics that may be related to abrasion injury are speed, flow, number of blades, shape of flow passage, and spacing of the blades (COE 1995a). There are no available data specifically addressing abrasion injury to fish passing through a turbine. The type of injury resulting from abrasion cannot be separated from the type of injury resulting from strike and grinding.

Grinding

Grinding damage results from fish being drawn into narrow gaps (COE 1995a). Information on grinding injury is limited because gap induced mortality may have been included in strike induced mortality studies conducted to date (COE 1991). The Chelan County Power Research Program has identified mortalities caused by gaps in Kaplan turbines (COE 1995a). High velocity zones exist at gaps in the turbine components where the leakage entrains fish (COE 1995a). Leakage occurs at gaps between rotating and stationary components, which includes the gap between the turbine blade leading edge and hub, and the gap between the blades and the throat ring (COE 1995a). The trailing edge hub-to-blade gap may not contribute to fish mortality as much as the blade tip-to-throat ring gap (COE 1995a). Although the gap between the blade tip and throat ring is small compared to the gap at the hub, the greater water flow at the periphery makes gap induced mortality at the periphery important (COE 1995a). Leakage also occurs at gaps between the wicket gates and stay vanes, and at gaps between the wicket gates and distributor ring (COE 1995a).

At the Rocky Reach Project (COE 1995a), Chelan County PUD is testing a new blade configuration. The gaps between the blade and the hub will be limited to 2 mm maximum with the leading edge of the blade recessed into the hub.

2) Cavitation

Cavitation occurs when the local pressure is low enough to cause water vapor bubbles to form. Downstream implosion of these bubbles occurs when the pressure is sufficiently increased. The intensity of the resulting shock waves varies but could be as high as 1,451 psia (Rodrigue 1986 cited in Cada 1991). The magnitude of the pressure wave decreases rapidly with the distance from the center of the bubble collapse (Cada 1991). Cavitation can be considered the extreme result of subatmospheric pressure within the turbine, most often occuring at high power loads (Cada 1991). Although damage to turbine components occurs only when such implosions are adjacent to surfaces, damage to fish can occur when such implosions occur anywhere in the flow field.

Cavitation can reduce turbine efficiency, seems to increase fish damage (COE 1995a),and may be the principal pressure effect causing fish mortality (Davies 1988 cited in COE 1995a). Brief exposure to vapor pressure followed by instantaneous return to atmospheric pressure has been shown to cause 50% mortality in fingerling salmon (Muir 1959 cited in Cada 1990). This mortality was attributed to the rapid, high-pressure shock waves associated with a collapsing vapor pocket in the test chamber (Muir 1959 cited in Cada 1990).

A parameter called sigma is a non-dimensional term representing pressure conditions at a turbine runner. The equation for calculating sigma is:

$$\sigma = (Hatm - Hs - Hv) / H \qquad \text{(eq. 5)}$$

where: σ = sigma;
Hatm = atmospheric absolute pressure (ft absolute);
Hs = runner setting relative to tailwater level (ft);
Hv = vapor pressure (ft absolute);
H = gross head (difference between headwater and tailwater) across turbine (ft).

Critical sigma is the value at which cavitation is initiated. Generally, critical sigma is lower than plant sigma, which reflects site conditions including elevation, water temperature, turbine runner setting, and the lowest tailwater during turbine operation. Critical sigma is typically the lowest runner sigma, the value of sigma for a particular location in a particular turbine runner. Turbine settings with a plant sigma higher than the runner critical sigma reduces the potential for cavitation damage to fish (COE 1995a). At the Foster Project, the highest fish survival occurred when the Kaplan turbine operated at 25% blade angle and the runner sigma was one-half to one-third the plant sigma (Bell 1981).

Conditions which precipitate or affect cavitation in turbine runners are: 1) general or local low pressure zones; 2) high velocity zones; 3) abrupt changes in flow direction; 4) blade surface roughness; 5) submergence; 6) atmospheric pressure; and, 7) the air content of water (COE 1995b). All of these factors affect the magnitude of the minimum pressures and the potential for cavitation at the runner blades. Low pressure zones, high velocity zones, abrupt changes in flow direction, surface roughness, and submergence are all design parameters affected by runner geometry. The runner geometry can be changed to adjust these parameters and create desired pressure distributions to minimize cavitation. Atmospheric pressure is dependent on site altitude and is an input parameter for determining a turbine setting to prevent cavitation. Air content is a function of the water quality at a site and is not typically considered to determine a turbine setting.

The best efficiency points for turbines are in zones where significant runner cavitation does not occur (COE 1995a). Operating turbines at the best efficiency point minimizes cavitation potential. However, leading edge and leakage related cavitation occurs even at efficient operating points (COE 1995a). Cavitation on runner blade surfaces is affected by submergence; leakage cavitation is not affected by submergence (COE 1995a). A true spherical throat ring would minimize gaps and leakage flow which would minimize leakage cavitation (COE 1995a).

During the fall of 1995, the Corps of Engineers conducted tests at Lower Granite Dam to evaluate the effects of cavitation on fish (Normandeau 1995). As discussed above in the section on strike, the tests evaluated observed injuries to fish released into a Kaplan unit operating near best efficiency and into the same unit operating under cavitation conditions. Test results did not indicate any significant differences in fish injury and mortality between the unit operating at best efficiency and under cavitation conditions (Normandeau, 1995). The cavitation condition was created by allowing excess flow for the blade angle, approximately 19,000 cfs compared to the 18,000 cfs for the on-cam flow rate (Normandeau 1995). Since flow for the cavitation condition was similar to the flow for the best efficiency condition, significant cavitation may not have been present during the cavitation test and the Lower Granite Dam test results may not represent actual fish injury potential related to cavitation. At Lower Granite Dam, 19% of the observed injuries, out of the total 2 to 6% mortality for the six test conditions, were attributed to pressure-related sources. Cavitation injury could not be differentiated from pressure injury.

3) Shear

Shear injury to fish passing through a turbine occurs in the zones between streams of water having different velocities (COE 1995b). Fish are injured when passing from one velocity zone to another

zone, that is, when the fish experience a velocity gradient. One portion of the fish would experience a different velocity than another portion, thus causing differential drag forces on the fish. The extent of injury is affected by the size of the shear zone relative to the fish size, by the pressure changes across the zone, and by the angle at which the fish passes through the zone (COE 1995a).

Velocities through a hydraulic turbine vary from near zero at solid boundaries up to 120 ft/sec, depending on the head, although the magnitude of typical velocity changes across shear zones may be on the order of 30 ft/sec (COE 1995a). Kaplan turbines do not have such significant velocity gradients, however, shear zones created by vortices are present in Kaplan turbines (COE 1995a). These vortices result from leakage through gaps between the moving and stationary components of wicket gates and runner blades, and from operation away from the best efficiency point producing flow separation off the leading edge of the blades (COE 1995a). Operating a Kaplan unit at maximum blade tilt reduces the gaps which reduces vortices (COE 1995a). Leading edge vortices can be minimized by matching the leading blade edge angle to the incoming velocity vector, which occurs when a Kaplan unit is operating on-cam (COE 1995a).

Draft tube swirl is the vortex in flow passage downstream of turbine runners. Draft tube swirl may be a primary source of shear damage in Francis turbines (COE 1995a).

Various studies have been conducted in an attempt to evaluate the effects of shear on fish mortality. Studies with salmonids introduced into a water body adjacent to submerged water jets with a velocity of 30 ft/sec (Groves 1972), 60 ft/sec (Theus 1972 cited in COE 1995b), and even as high as 67 ft/sec (Johnson 1970 cited in COE 1995b) indicate that there was no mortality. Similar tests with a four-inch nozzle indicated no mortality to salmonids with velocities less than 57 ft/sec (Johnson 1972 cited in Bell 1981). At ARL, alewives and smelt injected into the wider side of a rectangular submerged jet, approximately 3 inches downstream of the orifice, where the injection pipe was 1 inch from the core of the jet as depicted on Figure 2-9, showed no signs of injury at jet velocities of 30 ft/sec and 40 ft/sec (SWEC 1975).

Mortality data for entry of fish into water, as previously discussed, may also be useful to identify shear effects on fish. Freefall spill flow tests into a pool of water, conducted by the Corps of Engineers, indicated 0 to 2% mortality of salmonids at velocities less than 50 ft/sec (COE 1972). Mortality rates were 2 to 7% for salmonids entering a pool of water in a hydraulic jump or stilling pool with and without baffles (COE 1972).

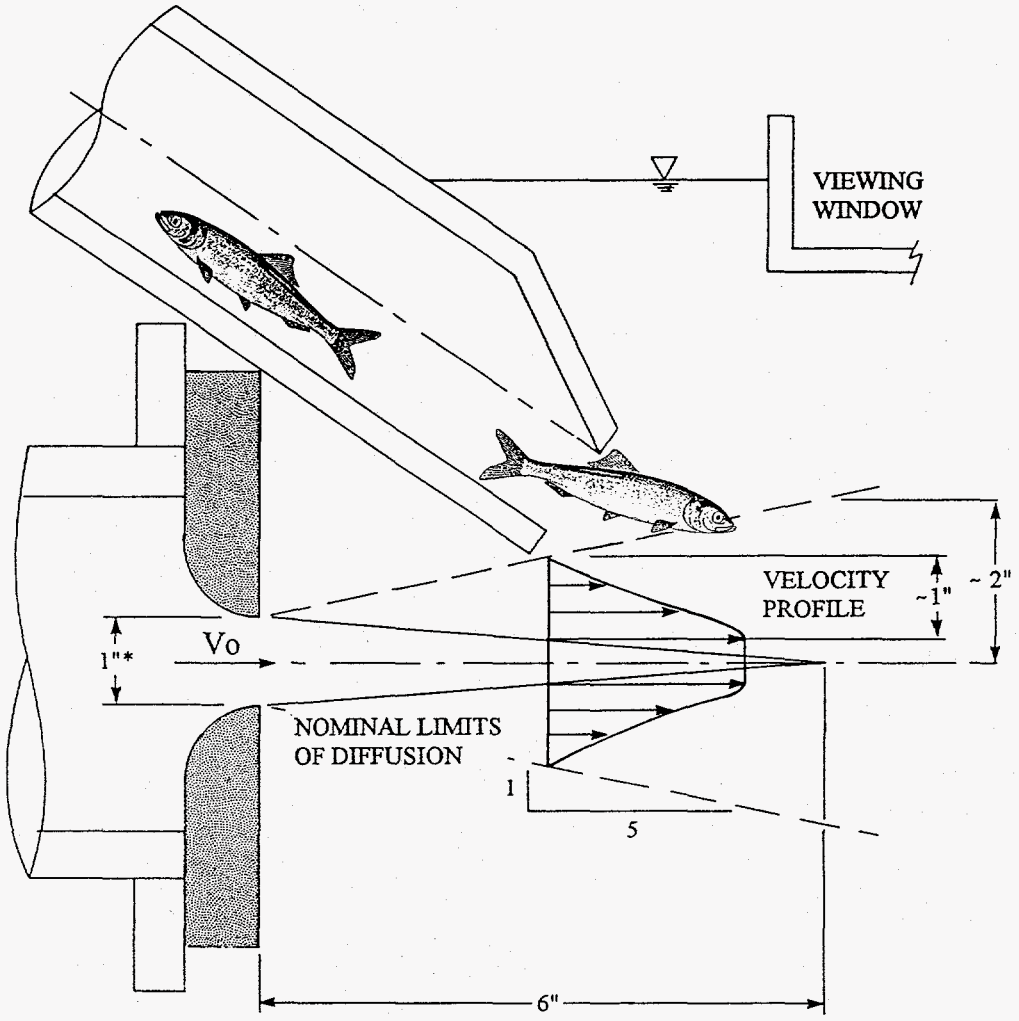

*INITIAL JET WIDTH = 3.5 INCHES

Figure 2-9
Jet Nozzle Model Tests
Source: Adapted from SWEC 1975

4) Pressure

Pressure damage is the result of rapid increases and/or decreases in pressure from which fish have acclimated. Pressure changes through a turbine are related to the head available at a hydroelectric site. Pressure changes through turbines typically range from 15 ft of water (7 psi or 0.5 atmospheres) at low-head sites to 170 ft of water (73 psi or 5 atmospheres) at high-head sites (COE 1995b). The pressure changes fish are subjected to depend on the water depth the fish are initially acclimated to before entering the turbine. The lower mortality rate associated with Kaplan units relative to the mortality rate associated with Francis units may be attributed, in part, to the lower differential pressures at many Kaplan unit installations (COE 1995b).

Fish may be more sensitive to pressure decreases than pressure increases, and injury to the swim bladder from decompression may be the main cause of pressure related mortality (Tsvetkov 1972 cited in Cada 1990). The absolute minimum pressure which can occur in any turbine is vapor pressure (COE 1995a), about 0.3 psia at 65°F water temperature, and minimum local pressures in turbines are generally near the cavitation limit (COE 1995a). Turbines with a runner elevation below tailwater have lower mortality than units with the runner elevation above tailwater (Cramer 1964) probably due to higher minimum pressures. However, a runner setting above tailwater could have the same or higher minimum pressures as a runner setting below tailwater depending on the runner design.

Sudden pressure reductions to 40% of acclimated pressures have been shown to burst swim bladders in 10 cm perch (Jones 1951 cited in Cada 1990). However, studies indicate that rapid pressure reductions to 14% of the acclimation pressure did not have any effect on striped bass larvae with swim bladders, and that striped bass larvae could survive rapid pressure reductions from depths of 157 ft or more (Beck et al. 1975 cited in Cada 1990). Whitefish fry and common carp exposed to a rapid increase in pressure from atmospheric to 725 psia, followed by a 10-minute depressurization back to atmospheric pressure experienced no mortality (Lampert 1976 cited in Cada 1990). Rainbow trout exposed to pressure increases of 35 to 185 psia in less than one minute followed by a nearly instantaneous release of pressure exhibited normal activity after depressurization with no mortality attributed to the test conditions (Rowley 1955 cited in Cada 1990). Fish slowly pressurized and then instantaneously depressurized to atmospheric and even to subatmospheric pressures did not experience any mortality (Harvey 1963 cited in COE 1995a). Brief exposure of fingerling salmon to vapor pressure in a gradual manner has been shown to cause no mortality (Muir 1959 cited in Cada 1990).

In 1974, ARL conducted tests with alewives in 43°F to 70°F water temperatures to simulate pressure conditions in a thermal power plant intake system (SWEC 1975). The fish were rapidly pressurized from 14.7 psia to 50.7 psia, held at 50.7 psia for about 15 minutes, and depressurized back to 14.7 psia over a 2 minute period. Visual observations indicated that the alewives had difficulty maintaining a horizontal attitude as a result of air bladder compression when first exposed to the high pressure, but were able to adjust to the 50.7 psia pressure within the 15 minute period. Over the range of water temperatures, the test fish mortality was similar to the control fish mortality.

The Corps of Engineers 1991 Revised Compendium on the Success of Passage of Small Fish Through Turbines concludes that "fish are killed by suddenly lowered pressure from their accustomed depth pressure. Such changes can and do cause embolism and swim bladder rupture" (COE 1991). The Revised Compendium presents theoretical information on mortality in salmonids relative to pressure change. This information, as shown on Figure 2-10, indicates that the minimum pressure for no mortality increases from about 4.5 psia to about 9 psia as the initial acclimation pressure increases from 14.7 psia to 29.4 psia. The upper portion of Figure 2-10 indicates no mortality can be expected if the minimum pressure is limited to about 30% of the initial acclimation pressure.

Relatively high head turbines are typically smaller units with a high rate of pressure change per time, and low head units are typically large units with a lower rate of pressure change per time (COE 1995a). Fish are depressurized from a pressure as great as 6 atmospheres absolute (88 psia) on the upstream side of the runner to a low pressure of minus one-half atmosphere absolute (7 psia) on the discharge side of the runner (COE 1995a). Energy density (the differential pressure per square inch of blade surface) affects the passage time through the runner, and the greatest rate of pressure change occurs in 0.1 to 0.2 seconds (COE 1995a). At McNary Dam, only 0.2 seconds are required for water to pass from the high pressure side to the low pressure side of the Kaplan blades (COE 1995a). For Kaplan units in general, the rate of pressure change across the blades is about 160 psi per second, assuming a 75 ft head (the mid-range of Kaplan turbines), and a 0.2 second time period from high to low pressure.

2.3 Biological Criteria

Available information relative to fish damage and mortality in hydroelectric turbines was assessed to compile design criteria for developing and evaluating a runner geometry to pass fish without damage. Although considerable information lends itself to only assigning qualitative guidelines relative to turbine characteristics that should minimize the potential for fish mortality, some turbine features

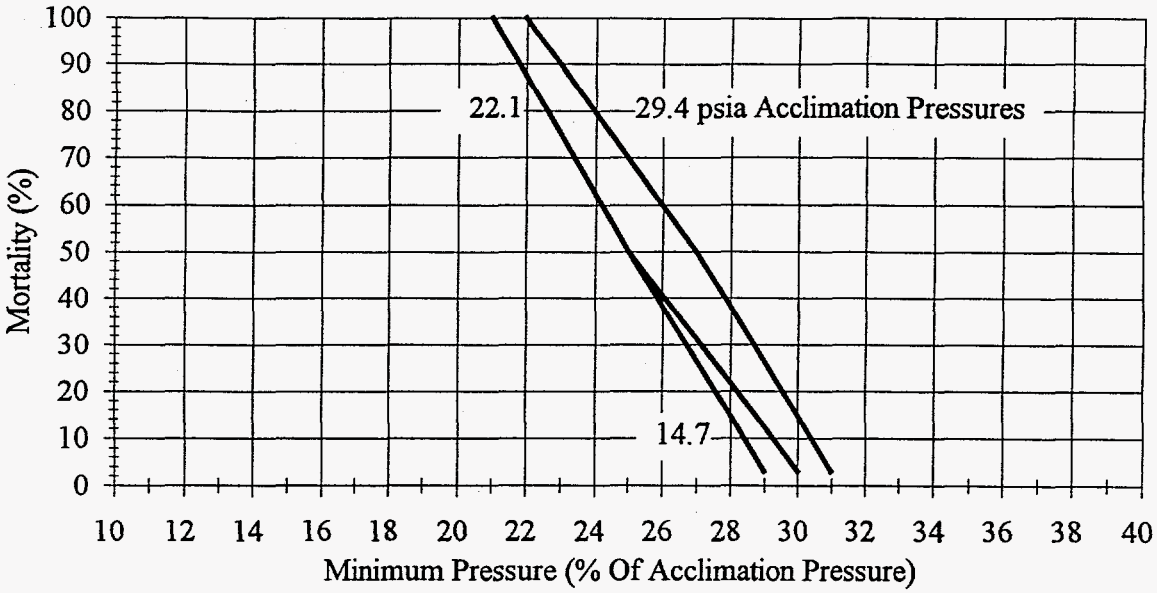

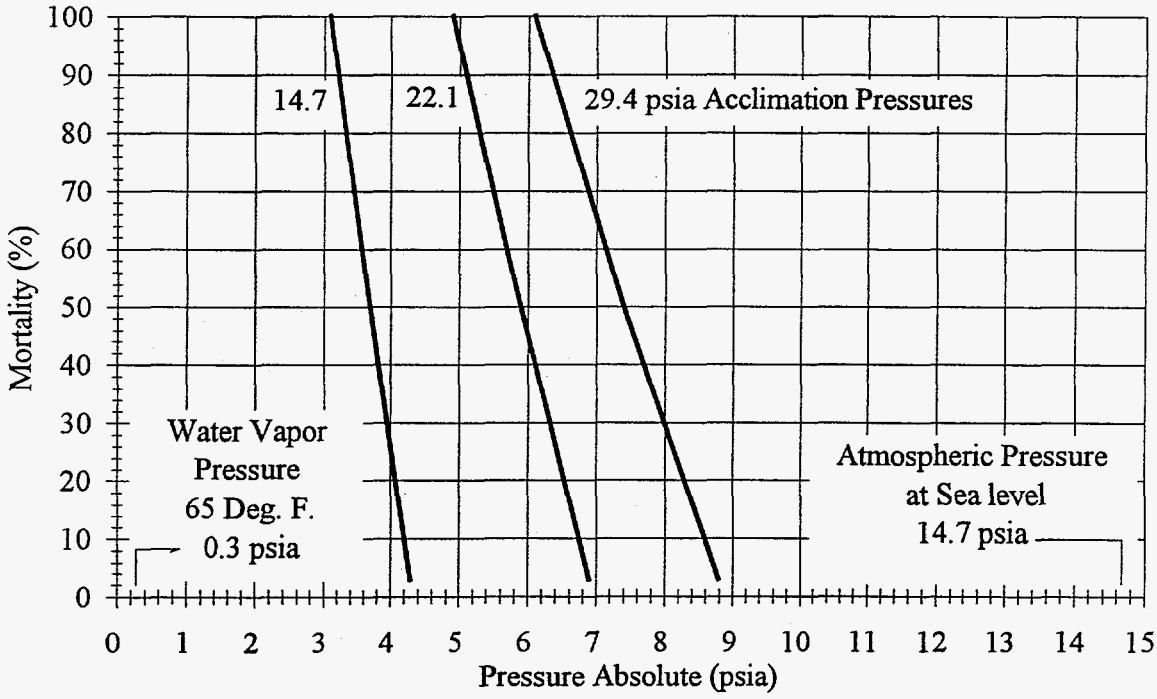

Figure 2-10
Pressure-Related Mortality of Salmonid Fish
Source: Adapted from COE

can be characterized by quantitative criteria to allow evaluation of runner geometries in a more specific manner.

The biological design criteria selected for design of the new runner are as follows.

1) Peripheral runner velocities should be less than 40 ft/sec

Low peripheral runner speeds should reduce the potential for fish damage resulting from the runner blades striking the fish, and from flow disturbances (shear zones and vortices) in areas between moving and stationary surfaces. Based on the Figure 2-8, peripheral runner velocities should be less than 40 ft/sec, preferably even 20 ft/sec or less, to minimize fish mortality.

2) Minimum pressure through the runner should be not significantly less than 10 psia

Figure 2-10 indicates that the minimum pressure for no mortality increases from about 4.5 psia to about 9 psia as the initial acclimation pressure increases from 14.7 psia to 29.4 psia, and that no mortality can be expected if the minimum pressure is limited to about 30% of the initial acclimation pressure. Assuming that downstream migrating fish are in the top 34 ft of water (about 30 psia maximum), the available data indicates that 10 psia is a reasonable minimum pressure limit.

3) The rate of pressure change through the runner should be less than 80 psi per second

The rate of pressure change through a Kaplan runner is about 160 psi per second, based on a 0.2 second travel time from the high to low pressure sides of the blade (COE 1995a) and based on an average head of 75 ft (the mid-range for Kaplan units). Low rates of pressure changes across the runner should minimize the potential for pressure-related injury. Since available data indicates that some pressure-related mortality may exist, even for Kaplan units, a conservative value for a rate of pressure change across a runner for acceptable fish passage would be 80 psi per second, or 50% of the rate of pressure change across a typical Kaplan runner.

4) The rate of velocity change across a shear zone should not be more than 15 ft/sec per inch

Low rates of velocity change across shear zones should minimize the potential for shear-related fish injury. Shear tests conducted at ARL indicate that alewives and smelt showed no signs of injury when subjected to a velocity change of 30 ft/sec per inch, see Figure 2-9 (SWEC 1975). Since alewives are a fragile species which are very susceptible to injury, limiting the rate of velocity change

across a shear zone to 15 ft/sec per inch, or 50% of the velocity change rate which does not cause injury to alewives, should minimize the potential for injury to any species.

5) The clearance between the rotating and stationary components should be less than 2 mm

Chelan County PUD is presently testing a new Kaplan blade configuration with a 2 mm clearance between the blade and the hub, both rotating elements (COE 1995a). The gap between the blades and the hub are suspected to be a major contributor to mortality in Kaplan turbines. Therefore, limiting clearances between rotating and stationary turbine components to 2 mm, similar to the clearance selected by the Corps of Engineers, should be adequate to prevent mechanical injury (abrasion and grinding) to fish.

6) The flow passage openings in the runner should be as large as possible

Large flow passage openings will increase the ratio of the volume of water within the runner at any instant to the surface area of the runner. A larger water volume to surface area ratio should reduce the potential for mechanical injury (abrasion) to fish.

7) The number and the length of runner blade leading edges should be minimized

Available information indicates that the number and the length of the runner blade leading edges may contribute to mortality of fish passing through turbines. The number of blades is a parameter included in the most recent mathematical models developed by Corps of Engineers to evaluate strike probability, equation (3) for Kaplan units, and equation (4) for Francis units. Minimizing the number of blades and the length of the blade leading edge should reduce the potential for mechanical injury (strike).

These criteria were used to evaluate the results of the CFD analyses of the new runner, and to identify modifications to the geometry that would provide effective fish passage. The intent of the criteria was to provide guidance for selecting changes to the runner geometry to improve fish passage, and to provide a basis for evaluating and comparing the potential for the various runner geometries to be biologically effective. Runner modifications were selected to improve performance relative to each criterion. A runner with greater compliance to these criteria was deemed to be more biologically acceptable than a runner with less compliance.

Two other criteria, which have not been addressed in the conceptual design of the runner, have been identified as possible sources of injury to fish passing through turbines. These criteria relate to the configuration of the project structures upstream of the turbine and flow control features for the turbine which are outside of the boundaries selected for flow analysis of the new runner and would be addressed during subsequent phases of the turbine development. These additional criteria are:

Travel time from the intake to the turbine runner should be minimized - Available information indicates that normal pressure increases from the hydroelectric plant intake to the turbine do not appear to cause fish injury and that the minimum pressure on the downstream side of the runner is the primary cause of pressure-related injury. Figure 2-10 indicates that fish acclimated to high initial pressures will have a higher mortality than fish acclimated to low initial pressures when rapidly depressurized to the same minimum pressure. Minimizing the travel time and the distance from the intake entrance to the turbine runner should prevent fish from becoming acclimated to the higher pressures at the runner inlet elevation and should limit potential injury from the pressure reduction across the runner.

The distance between the wicket gates and the runner should be maximized - Available data indicates that Kaplan units generally have lower fish mortality than Francis units. Wicket gates in Kaplan units are not typically located close to the runner, as shown on the figure provided in the glossary. Even bulb type Kaplan units have a large separation between the wicket gates and the runner. The wicket gates in Francis units are typically close to the runner as, shown on the figure provided in the glossary. Kaplan turbines have a larger gap between the wicket gates and the runner than Francis turbines, and the smaller gap between the turbine wicket gates and runner may contribute to the higher mortality of Francis units. Therefore, maximizing the distance between the wicket gates and the runner should reduce the potential for mechanical injury (abrasion and grinding) to fish passing through a turbine.

SECTION 3
SELECTION OF TURBINE DESIGN PARAMETERS

3.1 Operating Design Point

Available data in ARL's files on hydroelectric projects were reviewed to identify an operating design point for the fish tolerant turbine that would be representative of typical installations for existing turbines. The majority of hydroelectric turbines installed in the United States today have a flow capacity ranging between 500 cfs and 2,000 cfs, and an operating head (headwater to tailwater) ranging between 25 ft and 150 ft. Figure 3-1 shows the common application ranges for conventional hydraulic turbines.

The design point selected for the new turbine was 1,000 cfs and a head between 75 ft and 100 ft. A specific design head was not selected to allow comparison of runner geometries at the same power output. This design point is in the middle of the Francis and Kaplan turbine operating ranges and is at or above the upper limit of the bulb and tube turbine operating range relative to head. The selected design point is at the lower end of the flow range for Francis units, in the middle of the flow range for Kaplan and bulb units, and is greater than the maximum flow for tube units.

The efficiency characteristics of conventional turbines is shown on Figure 3-2. All of the turbine types have a peak efficiency in the 90% to 93% range. A minimum target efficency of 85% was selected for the new turbine to allow the new design to be competitive with conventional turbines.

3.2 Initial Runner Geometry

Pump characteristics for different models of the Hidrostal pump were obtained and reviewed to identify which model would be most appropriate to evaluate as a turbine runner geometry for the computational analyses. The range of operating characteristics for the solids handling pumps and for the fish handling pumps are shown on Figures 3-3 and 3-4, respectively. Schematic diagrams of the impeller shapes for each type of pump are presented on Figure 3-5. Six pumps were selected based on performance characteristics indicated on the selection charts and discussions with Hidrostal personnel. A summary of the data for the pumps initially selected as offering the greatest potential as the point of departure for the new turbine is presented on Table 3-1.

Model L12Q-SH was selected as the basis for the new runner. Even though this pump has a higher head than used in other fish pumps, and has an open back shroud designed to shear stringy material, the L12Q-SH model has the highest effiency when compared to other Hidrostal pumps operating at 1,000 rpm. The highest pump efficiency possible was deemed to be the most important parameter in selecting the initial geometry for the new runner so as to be competitive with the efficiency of existing turbines. Features incorporated into the pump to enhance fish survival, including a shroud around the runner and a rounded transition from the inlet to the volute similar to the L12F model, were considered to be components that could be added to the computational models after the initial geometry had been designed, if necessary.

To define the initial runner geometry, ARL procured an impeller casting from Hidrostal in Lima, Peru and prepared a computer file of the impeller geometry using "reverse engineering" techniques. Machining of the casting was superimposed on the computer sections based on drawings provided with the impeller. NREC then used the geometry to prepare the mesh for the analytical codes.

Table 3-1
Hidrostal Pump Characteristics

Model Number	Speed (rpm)	Best Efficiency Point			Impeller Opening * (inches)
		Efficiency (%)	Flow (gpm)	Head (ft)	
L12K-H	1,000	81	8,900	95	8.6
L12Q-SH **	1,000	82	6,100	125	6.0
L12F	1,000	75	4,675	88	7.9
L12F-H	1,000	77	3,600	82	5.8
I08F-M	1000	76	2,880	105	6.3
H12V-SS	1000	72	5,200	40	6.2

* Diameter of sphere which can pass through impeller

** Selected to start computational analyses

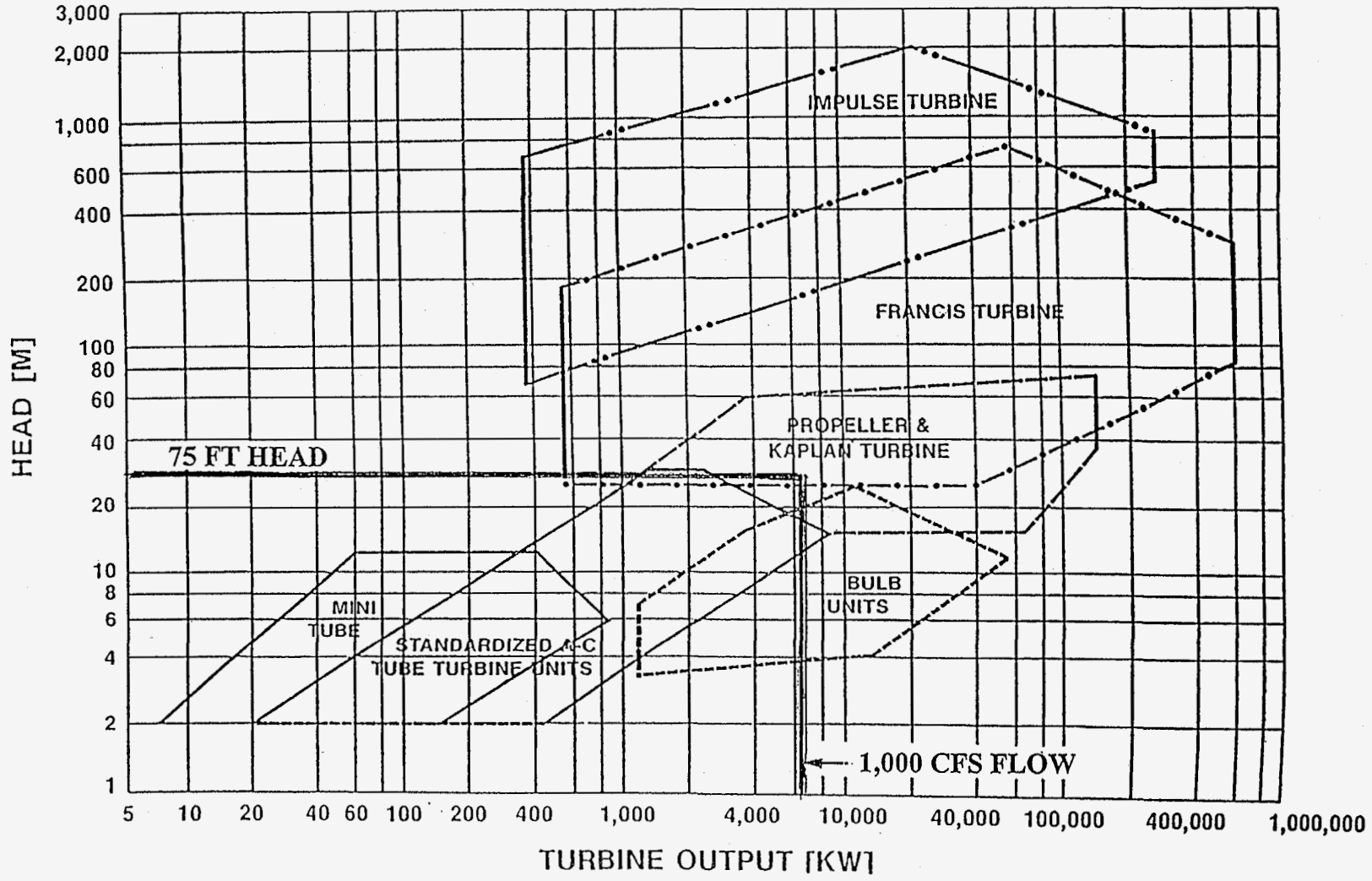

Figure 3-1

Common Application Ranges For Conventional Hydraulic Turbines

Source: Hydraulic Lecture Series

On Small Scale Hydropower, BSCE/ASCE 1980

CURVE A -- FIXED-BLADE PROPELLER TURBINE
CURVE B -- KAPLAN TURBINE, BLADE ANGLE ADJUSTED AUTOMATICALLY IN COORDINATION WITH GATE OPENING AND LOAD
CURVE C -- PELTON TURBINE
CURVE D -- FRANCIS TURBINE

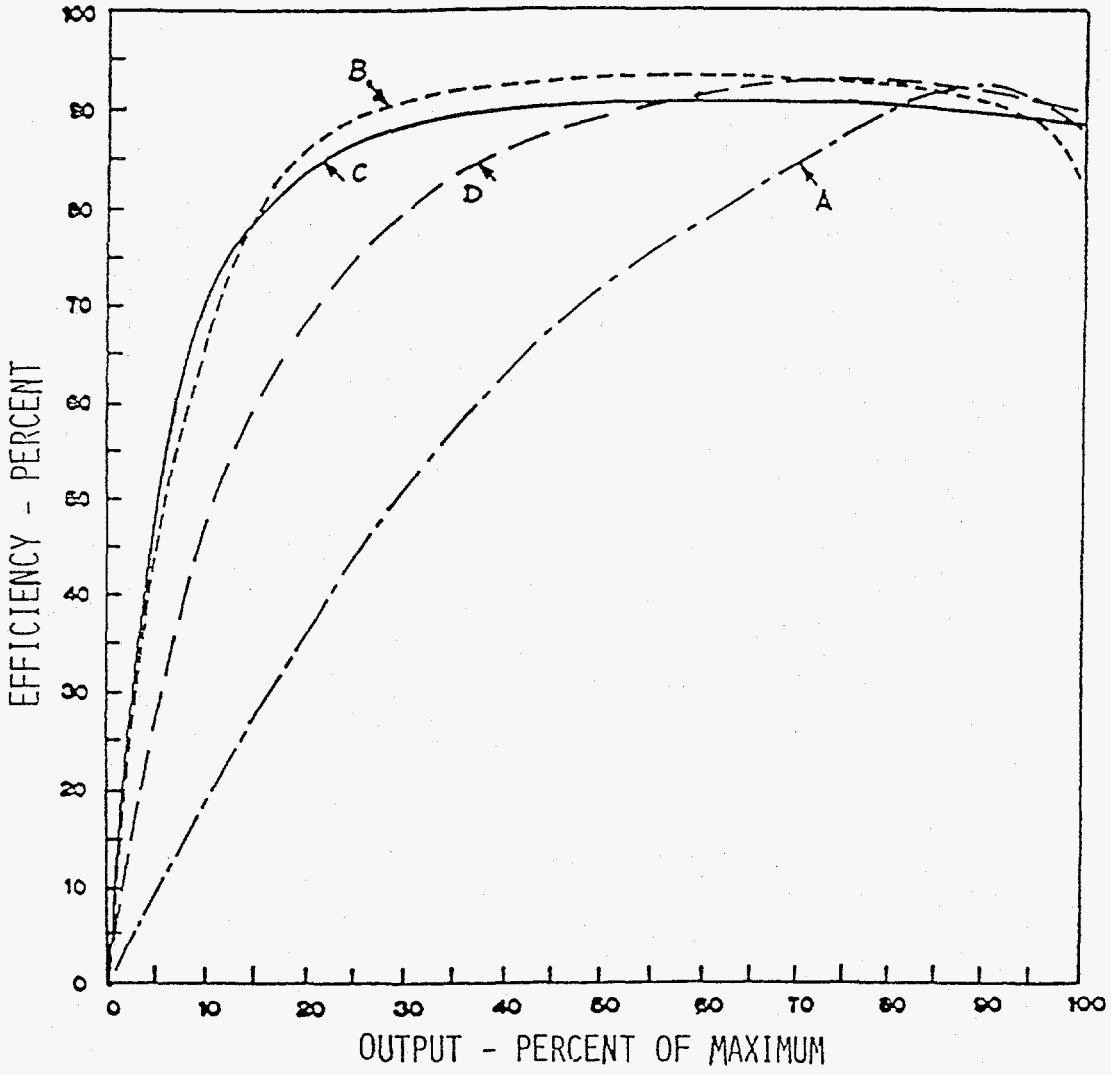

Figure 3-2
Efficiency Characteristics of Hydraulic Turbines
Source: Hydraulic Lecture Series
On Small Scale Hydropower, BSCE/ASCE 1980

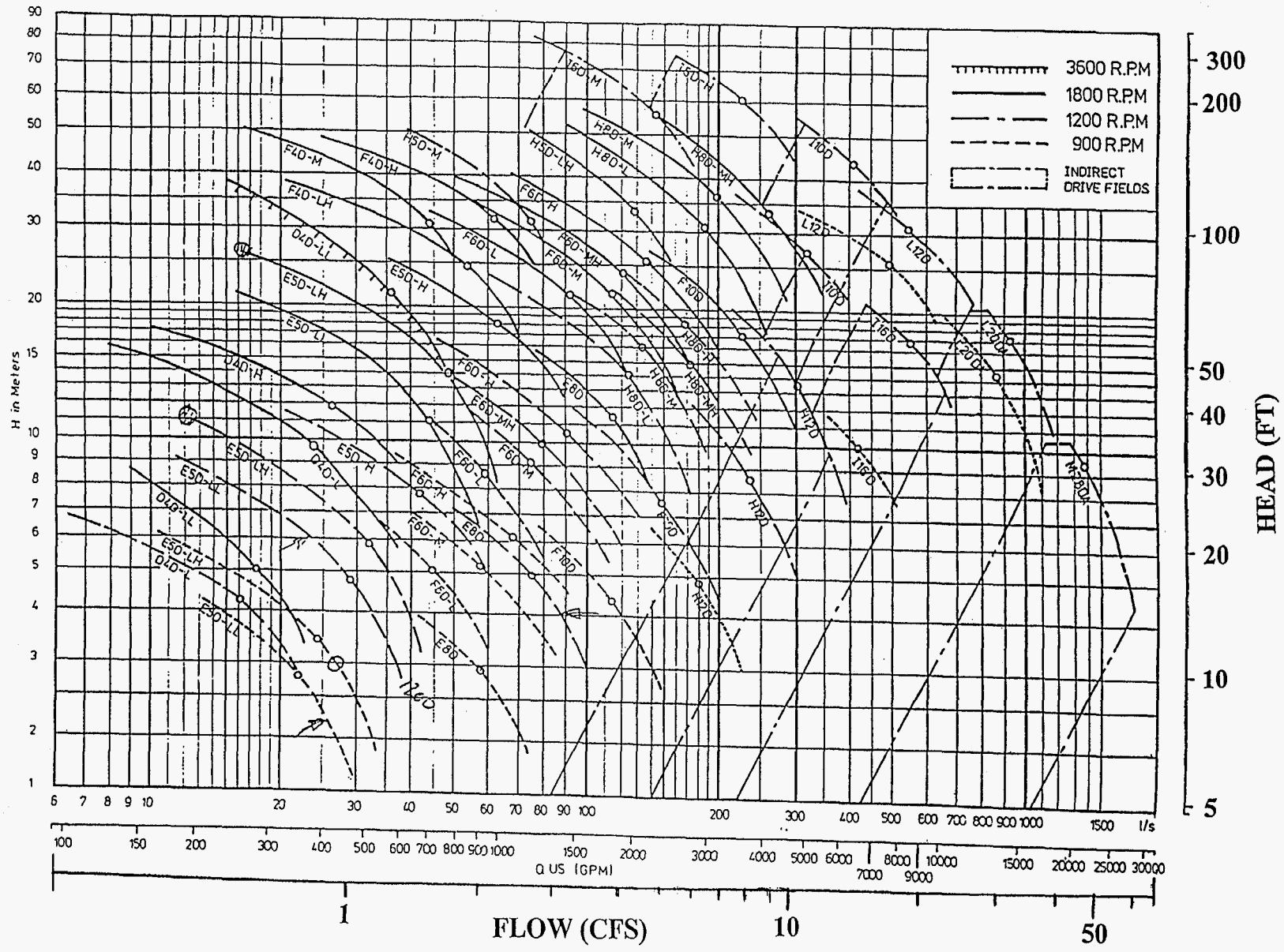

Figure 3-3
Hidrostal D-Type (Solids) Pump Selection Chart

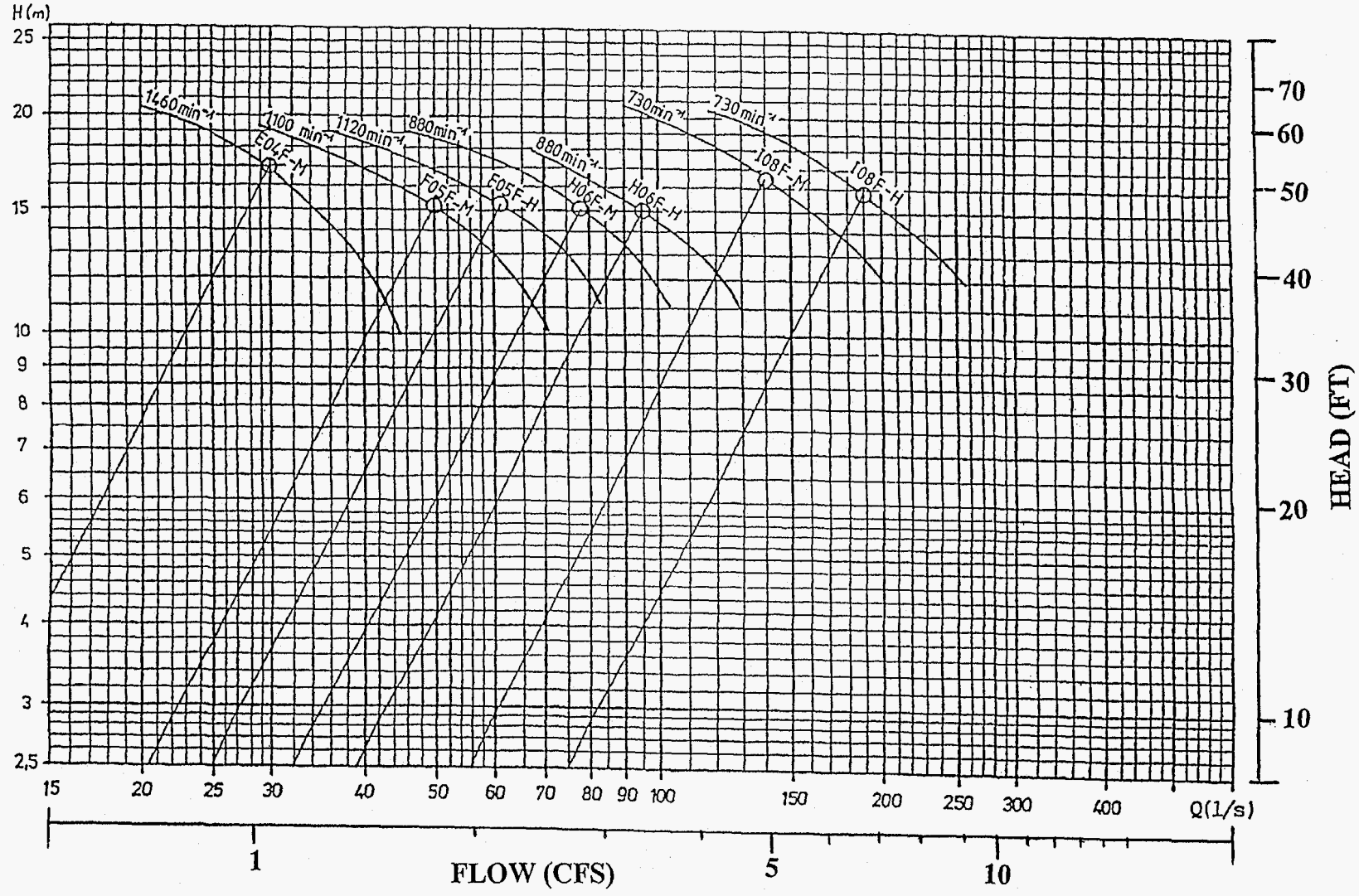

Figure 3-4
Hidrostal F-Type (Fish) Pump Selection Chart

Fig. 1 used for Fishpumping $n_q = 30$

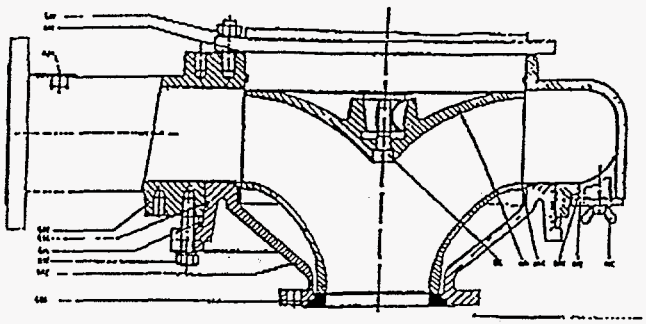

Fig. 2 High pressure type $n_q = 30$

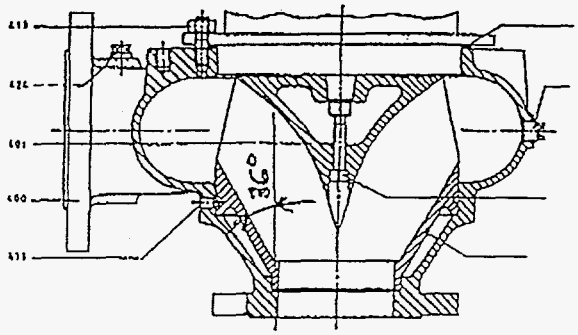

Fig. 3 Medium pressure type $n_q = 60$

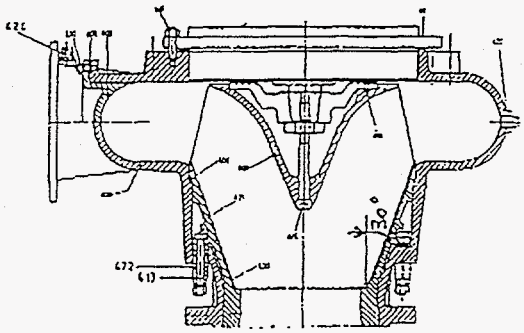

Fig. 4 low pressure type $n_q = 140$

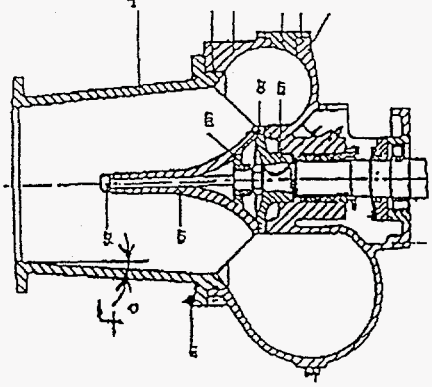

Figure 3-5
Schematic Diagram of Hidrostal Pumps

SECTION 4
THE HIDROSTAL IMPELLER CONCEPT AND PAST APPLICATIONS

4.1 Pump Design and Operation

WEMCO Pump Company is the U. S. representative of the Hidrostal pump, a solids handling pump adapted to move delicate food items with minimal damage. The pump is used in the food industry to transport fruits and vegetables and to off-load fish from commercial fishing boats. WEMCO has developed the Hidrostal pump for application as a fish pump in intake diversion and bypass systems.

The Hidrostal pump has a screw/centrifugal impeller with an open channel design. The impeller design has the clog-free features of a vortex pump, the gentle action of a screw pump, and the efficiency of a centrifugal pump. The Hidrostal pump impeller shape has design features which should reduce fish mortality in a turbine application. The single bladed impeller has only one leading edge, a long flow path minimizing sudden pressure changes, minimal or no clearances between the impeller and runner housing, and relatively large flow passages. The impeller used for pumping live fish has a shroud enclosing the entire impeller which is recessed into the pump casing. The fish pump impeller has a single gap between the impeller and the casing at the pump suction. A schematic diagram of the Hidrostal pump operating in the turbine mode is shown on Figure 4-1.

As shown on Figures 3-3 and 3-4, the general operating ranges for solids transport pumps are from 150 to 25,000 gpm, from 10 to 200 ft of head, and from 590 to 3,600 rpm, and for fish pumps from 320 to 3,960 gpm, from 30 to 65 ft of head, and from 875 to 1,750 rpm. Peak efficiency is about 80% for the solids handling pumps and is about 75% for the fish pumps.

The largest Hidrostal pump currently being manufactured is the 36 inch inlet diameter prototype being tested in the Red Bluff Diversion pilot study (discussed below). The recommended operating range for this particular pump is 90 to 110 cfs, 20 to 30 ft head, and 350 to 450 rpm shaft speeds. The specific speed of this pump is 6,270 at the design point (approximately 100 cfs, 23 ft head, and 350 rpm shaft speed). If the Red Bluff pilot study is successful, WEMCO will expand the pump size up to a 48 inch inlet diameter.

4.2 Experience as a Fish Pump

ARL has conducted biological evaluations of the pump to determine its potential for transporting fish in bypass systems back to their natural environment. As a result of these studies, Hidrostal pumps are currently in use in this capacity at a number of steam electric plants. A review of ARL's efforts and Hidrostal pump applications is presented in the following discussion.

In 1979, ARL evaluated the Hidrostal pump for transporting juvenile alewives, a fragile member of the herring family. The results of these tests, which were conducted with a 12 inch inlet diameter Hidrostal pump (Model No. L12F), are presented in an Empire State Electric Energy Research Corporation report (1981). The tests were conducted with the pump operating at 430 rpm. The mean mortality rate at 96 hours was 1.25%, the same mortality rate as for separately held control fish.

As a result of the studies conducted at ARL, the Hidrostal pump was selected for installation at three steam electric plants to return fish bypassed by screens to a safe location. At the Brayton Point Station in Massachusetts, four 12 inch inlet diameter Hidrostal pumps have been in operation since 1984 to return bypassed larval and juvenile fish to Mt. Hope Bay. Three 12 inch inlet diameter Hidrostal pumps have been in operation since 1985 at the Big Bend Station on Tampa Bay to return fish eggs and larvae collected on fine-mesh traveling screens to the bay. At the Danskammer Point Station on the Hudson River, a full-scale angled screen/Hidrostal pump system was evaluated from 1981 to 1983. Two 12 inch inlet diameter Hidrostal pumps were used to transport fish from the screen bypass to a collection and holding area. The evaluation of the fish diversion systems at all three plants focused on the screening systems and did not address mortality related to the pumps. The evaluation assumed that pump mortality was minimal.

A 16 inch inlet diameter Hidrostal pump was evaluated in 1987 at the Moses-Saunders Hydroelectric Facility on the St. Lawrence River to transport eels over the dam. The results of these tests are summarized in an Electric Power Research Institute (EPRI) report (1994). The tests indicated that eels passed through the pump, discharging 6.2 cfs at a 33 ft head and 1200 rpm, with no immediate mortality or latent mortality, and less than 3% injury (Patrick and McKinley 1987).

The U. S. Bureau of Reclamation is currently conducting a pilot study at the Red Bluff Diversion Dam on the Sacramento River to evaluate two 10 ft diameter Archimedes screw pumps and one 36 inch inlet diameter Hidrostal pump (Johnson et al. 1993). The pilot study is being conducted to determine if the pumps are biologically effective during the November through April period to supply water to the Tehama-Colusa Canal irrigation system. During this period, the diversion dam gates will

be opened to enhance upstream and downstream salmon migration. When the gates are open, pumps will be necessary to supply water to the irrigation canal headworks where a fish diversion and bypass system are located. The concept of using pumps with the diversion gate open has been identified as the most cost-effective alternative for minimizing the impacts of the project on salmon, provided that fish can be passed through the pumps with low mortality rates.

A summary of the pilot study at the Red Bluff Diversion Dam is presented in Johnson et al. (1993). A 36 inch inlet diameter Hidrostal pump was selected for the study because of the potential to pass fish with low mortality rates based on the 1979 ARL tests, discussed above, and because of the relatively low installation and operating cost compared to the overall pilot study costs. The pump has a 44.5 inch diameter impeller with a capacity of 100 cfs at 23 ft of head at a speed of 350 rpm. The pilot project has been partly operational since 1995. Preliminary biological results are encouraging (Cook 1996).

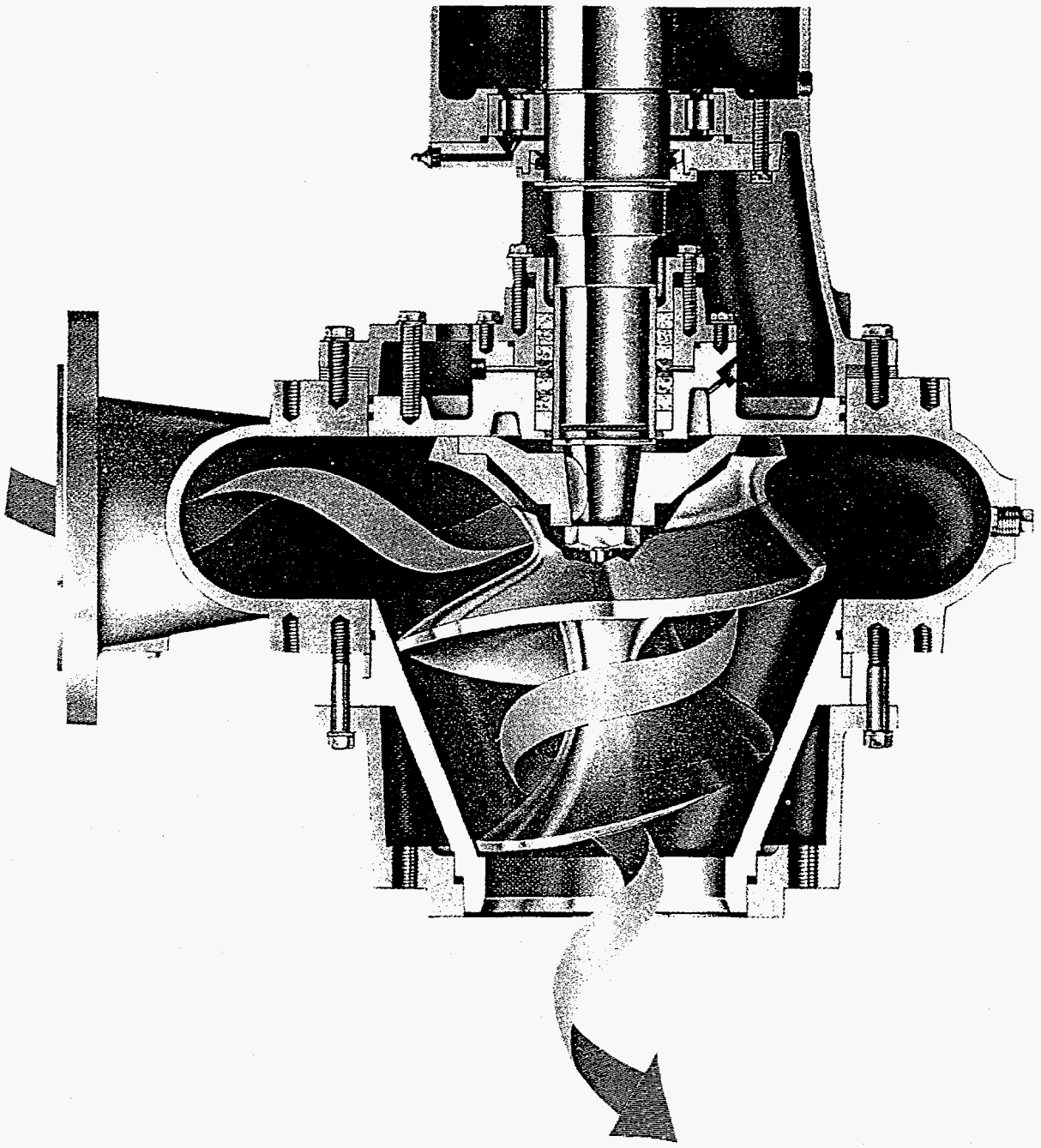

Figure 4-1
Hidrostal Impeller in Turbine Mode

SECTION 5
DESCRIPTION OF COMPUTATIONAL METHODS

5.1 General Approach

5.1.1 Design Process

The hydraulic turbine is a unique piece of turbomachinery equipment that has a long history, is rugged, and converts hydraulic energy very efficiently into mechanical energy. A typical high specific speed (high flow, moderate head) Francis (radial inflow) turbine is shown on Figure 5-1. The turbine is characterized by many relatively short blades that convert the hydraulic energy in a relatively short distance.

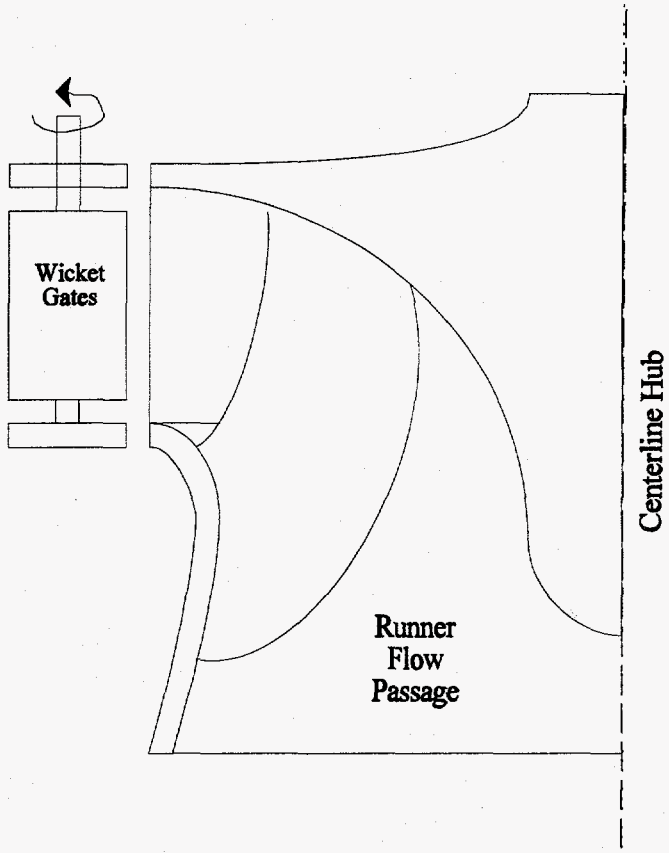

Figure 5-1
Schematic of Francis Turbine Runner

Design of the new fish tolerant turbine runner follows a design process commonly used for all modern turbomachinery components. The process includes three steps: preliminary design; detailed geometric design; and Computational Fluid Dynamic (CFD) analysis. A description of the design steps is provided in the following sections.

5.1.2 Preliminary Design

The preliminary design uses turbine specifications (such as flow and head) to arrive at a set of main dimensions that will satisfy the design requirements. The preliminary design is based on historic design information which is in the form of data bases embedded in computer programs. The results of the preliminary design are the main dimensions such as the inlet and discharge areas, wheel diameter, and blade heights, but do not include detailed geometric information. The basic method uses a one-dimensional analysis as described in Appendix A.

5.1.3 Detailed Geometric Design

Details of the flow path geometry are found in the next phase of the design process. Usually, hydraulic analysis is used that has proven to give reliable and repeatable results for high efficiency and cavitation-free operation. Similar to the preliminary design, historic experience is used during the detailed geometric design to judge whether one blade shape is better than another shape. The basic goal of the detailed geometric design step is to accurately predict the velocities and the pressures along the blade, hub, and shroud surfaces. Previous experience warns the designer when a certain velocity distribution will lead to a highly turbulent flow with vortices that cause high head losses. At the same time, pressure distributions that reach levels where water generates vapor (cavitation) should be avoided to prevent damage to the runner.

Detailed geometric design is usually doubly two-dimensional (also called quasi three-dimensional) in the sense that the analyses are performed in two steps. First, flow is calculated in streamtubes (usually between 9 and 30 streamtubes) from hub to shroud assuming an infinite number of blades as shown on Figure 5-2. Flow is then calculated in each of these streamtubes from one side of the blade to the other side as shown on Figure 5-3.

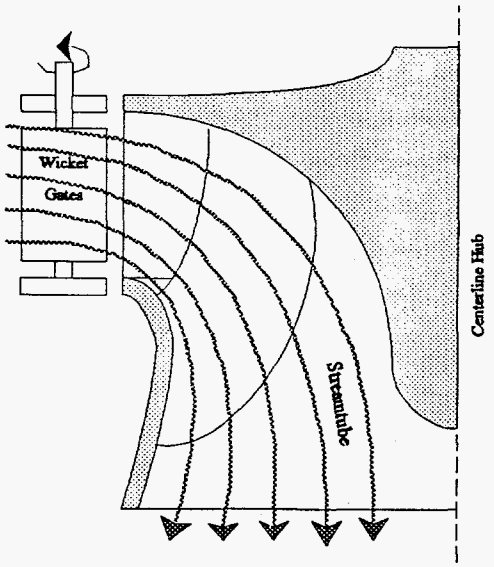

Figure 5-2
Quasi-Three-Dimensional Calculations
Part 1 Hub-to-Shroud Solutions

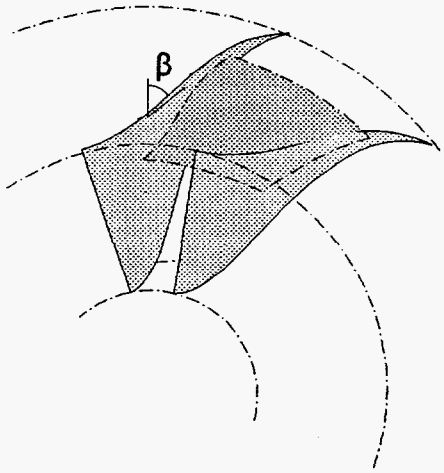

Figure 5-3
Quasi-Three-Dimensional Calculations
Part 2 Blade-To-Blade Solution.

Flow separation and resulting hydraulic losses are judged by inspecting the velocity decrements along the blade surfaces in one streamtube from inlet to exit. The suction surface of the blade in the streamtube located near the shroud is one area where flow separation is most likely to occur and is where the inspection of the velocities is focused in this phase of the design.

The detailed geometric design of the new runner has been conducted with NREC's well-established computer code COMIG®. Details of the code are provided in Appendix B.

5.1.4 Computational Fluid Dynamic (CFD) Analysis

CFD analysis is truly three-dimensional and allows precise assessment of the flow in the turbine passages. The flow around the leading edges, near the hub and shroud walls, and in the middle of the flow passages are influenced by secondary flows that are not accounted for by the quasi-three dimensional methods. CFD analysis is used as the final step in the design process when the overall dimensions are fairly well established and local refinements in the runner geometry are made to avoid severe turbulence and loss producing mechanisms.

The CFD analysis of the new runner has been accomplished with NREC's computer code called VISIUN™ . The code has been developed by NREC to conduct detailed analysis of flow through new turbine designs. A detailed description of VISIUN is provided in Appendix C. The starting point for analyzing the new runner was the geometry developed with the COMIG program and the flow conditions established during the preliminary design effort. The flow conditions established the boundary conditions including the inlet pressure, the outlet pressure (or head difference between inlet and discharge), and the wheel rotational speed.

The three-dimensional flow is governed by complicated Navier-Stokes equations that cannot be solved in closed form. The equations must be numerically integrated over very small distances. The first task in the three-dimensional analysis is to generate a grid of small volumes over which the differential equations can be applied in finite differences form. Grid generation requires special tools since the grid must be very fine in areas where large flow changes take place; such as near the boundaries and the leading and trailing edges. However, a coarse grid is preferable in the interior of the passage, since such a grid will speed up the calculations. The VISIUN program contains its own grid generator specially devised for turbomachinery components such as turbines and pumps.

The second task in the CFD analysis is the solution of the equations over the grid. The finite difference solution is iterative since it must use parameters that have not been calculated at the

beginning of the calculation scheme. There may be up to 3,000 iterations before a fully converged solution is obtained. The large number of iterations is one of the reasons why CFD calculations take such a long time to execute.

The third task in the CFD analysis is to display the results in a manner that allows the engineer to assess the results and render opinions regarding the design. NREC uses the Fieldview Flow Visualizer and the VISIUN post processor to produce views of the velocity and pressure fields in the flow passages and other parameters, which influence fish survivability. The results of the CFD analysis are presented in Section 6 using the available displays.

5.2 Flow Assessment

5.2.1 Introduction

Evaluating flow characteristics relative to velocities and pressures requires judgment regarding acceptability of the conditions to meet the intended goals for the turbine. There are two types of judgement factors for assessing the new turbine runner: a) those affecting the efficient operation of the turbine; and b) those affecting the survival of the fish while passing through the turbine. As can be expected, there are conflicts in the criteria for both types of judgement factors. Where one geometry may be desirable for high efficiency, the same geometry may be detrimental for fish survivability. Throughout the design process, judgments have been made to provide a balanced design rather than to exclusively favor either efficiency or fish survivability.

The following discussion describes both types of flow assessments in general terms relative to turbine efficiency and relative to fish survival criteria. In later sections where the actual results of the analyses are presented, flow assessments in specific terms are provided for each turbine design iteration, based on these general types of assessments.

5.2.2 Efficiency Criteria - Velocity Distribution

Experience has shown that losses are generated by flow separation caused by decreasing velocities. Therefore, velocity distribution is an important parameter to evaluate the runner design. The blade surfaces and the leading edge at the shroud are important areas to evaluate the velocity distribution

in the runner. Figures 5-4, 5-5, and 5-6 show typical velocity distributions along a blade surface. The best distribution in a turbine is shown on Figure 5-4, where the velocities continually increase and no flow separation is expected along the blade. Figure 5-5 shows a case where near the inlet the velocity becomes low and negative indicating a reverse flow, leading to losses. Figure 5-6 shows a case where the flow approaches the leading edge at a high incidence causing a rapid acceleration of the flow, followed by a deceleration and subsequent flow separation and losses.

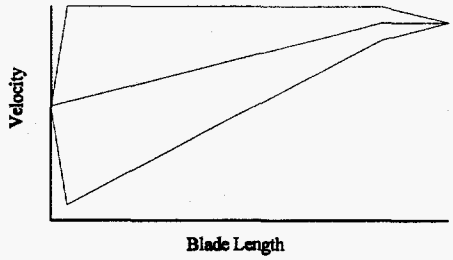

Figure 5-4
Optimal Velocity distribution

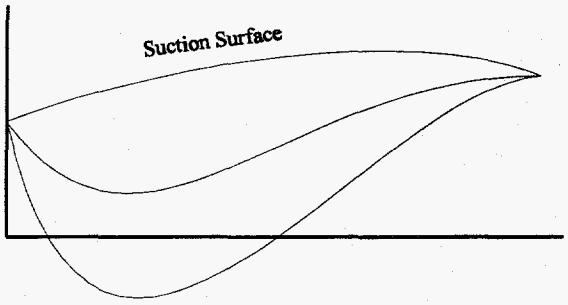

Figure 5-5
Velocity Distribution With
Low Inlet Velocity

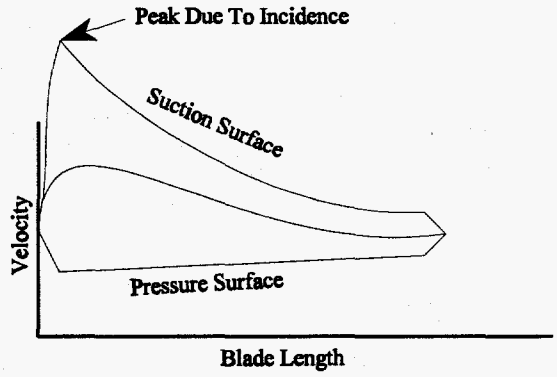

Figure 5-6
Velocity Distribution With High Approach
Flow Incidence Angle

5.2.3 Efficiency Criteria - Pressure Distribution

Two parameters relative to pressure distribution have been assessed, the rate of change of pressure and the actual pressure through the runner. Both are fish survival criteria and the actual pressure through the runner is also a parameter for finding cavitation within the turbine passages. When the pressure decreases below the saturation pressure at the prevailing temperature the water will vaporize. The ensuing train of bubbles will move downstream and collapse when the pressure becomes larger. The collapsing bubbles are the cause of cavitation damage and turbine designers

generally agree that the pressure should be kept above the saturation pressure to avoid cavitation problems. Figure 5-7 shows a normal pressure distribution along the blade surface, while Figure 5-8 shows a pressure distribution where the pressure drops below the vapor pressure.

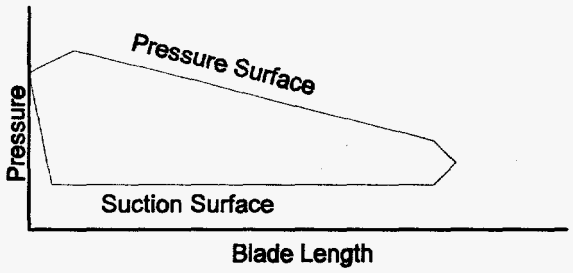

Figure 5-7
Normal Pressure Distribution
Along Blade Surface

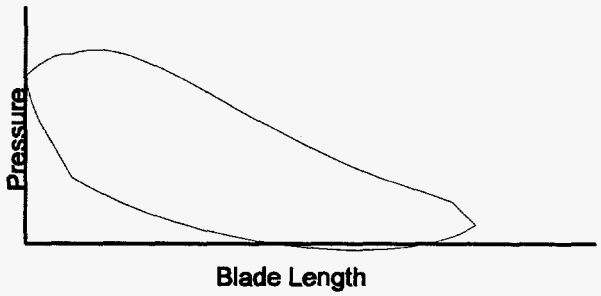

Figure 5-8
Pressure Distribution
Resulting in Cavitation

5.2.4 Fish Survival Criteria - Peripheral Speed

The head imposed on the turbine determines the peripheral speed of the runner. While minor changes in the blade shape may slightly affect the rotational speed, gross changes in the blade shape will adversely affect the unit efficiency. If the runner diameter is reduced, the rotational speed of the wheel must be increased to extract the work from the water, resulting in the same peripheral speed. Therefore, given a design head, the peripheral speed is a fairly fixed number. When the speed becomes higher than recommended for fish passage, limiting other parameters, such as the number and length of leading blade edges that fish encounter, is important for effective fish passage.

5.2.5 Fish Survival Criteria - Velocity Shear

The limit on the velocity gradient normal to the direction of flow is mainly encountered along the blade surfaces and at the leading edge when the inflow approaches the blade at a high incidence angle . As illustrated on Figure 5-9, the velocity is zero at the walls of the runner, but is at full value only a short distance into the flow (across the

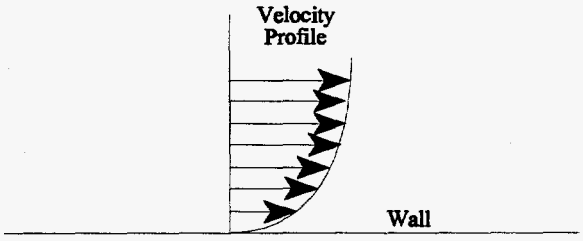

Figure 5-9
Boundary Layer Shear

boundary layer). This shear at the wall cannot be avoided, but can be limited by maintaining a very thin boundary layer which is accomplished by judicious choice of velocity gradient (i.e. minimize decelerating flows).

Other regions of shear occur when recirculating flows are generated within the flow field. Recirculating flows generally result from flow separation at a wall where a region of flow circulation is set up as shown on Figure 5-10. An approach flow incidence angle at the leading edge with the associtated adverse velocity gradients are the main cause of these shear zones. Flow separation is difficult to avoid when a turbine runs at "off-design" conditions, but can be avoided at the design condition through careful design.

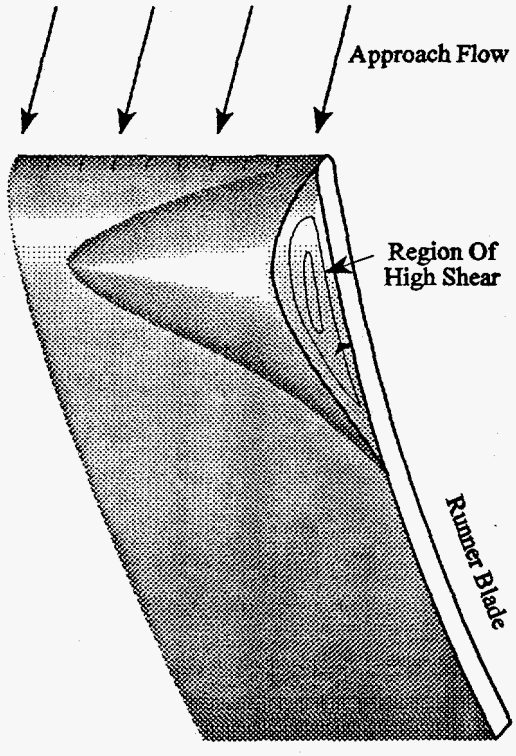

Figure 5-10
Flow Separation and Shear

5.2.6 Fish Survival Criteria - Pressure Changes

Rapid pressure change with time is a fish survival criterion that is not readily available from the analyses that are commonly done by hydraulic engineers. Pressure gradient with distance is a common variable used in turbine design. However, rate of pressure change with time is not a common variable for turbine design and is calculated as discussed in Section 6.7.3. This variable usually is largest near areas where the flow interacts with a stationary object, such as a blade leading edge. When the flow approaches a stationary object it reduces speed and comes to a halt at the stagnation point. The dynamic velocity head changes to pressure over a short distance and in a short period of time. Reducing the number of stationary objects, such as blade leading edges, will reduce areas of steep pressure gradients and will minimize areas of rapid pressure changes.

The absolute minimum pressure is also a fish survival criterion. In general, the pressure through the runner should be kept higher than 10 psia. This minimum pressure can be achieved by providing a high back pressure at the turbine exit upstream of the draft tube. Locating the turbine below tailwater

level is a possible solution which does not affect design of the runner flow passages. However, construction cost considerations may limit the turbine back pressure.

5.2.7 Fish Survival Criteria - General Rules

A hydraulic turbine that has a high power generation efficiency while at the same time has characteristics which allow fish passage with minimal injury must have satisfactory local flow and pressure distributions, and should have as few leading edges as possible. These general rules are reflected in the runner designs which have been evaluated in the conceptual design of the new turbine runner.

5.3 Basic Assumptions

5.3.1 Consequences of Biological Criteria

The fish survivability criteria which most significantly affect runner design are:

a) Flow openings should be as large as possible.

b) Number and the lengths of leading edges should be minimized.

c) Minimum pressure through the runner should not be significantly less than 10 psia.

d) Rate of velocity change across a shear zone should not be more than 15 ft/sec/in.

e) Rate of pressure change through the runner should be less than 80 psi/sec.

The first two and the last criteria indicate that the number of blades must be limited to two or three blades for a runner sized for the selected operating point (1,000 cfs and 75-100 ft head). With only a few blades, the blades must be longer, particularly in the radial flow portion of the blades, than the blade length for typical Francis turbine design. The longer length is necessary to extract the energy from the flow without excessive loading on the blades. For this reason, the new runner must have the blades wrapped further around the hub at the inlet with the inlet more tangential than conventional design. In addition, tangential flow requires more inlet area than usual for other turbines. The new runner diameter will be larger than conventional Francis turbines because the axial length of the inlet

is constrained by other geometric and hydraulic considerations. The diameter of the new runner will increase as the number of blades decrease.

A basic assumption in the new runner design is that fish injury can be minimized by eliminating rotating blades that sweep by stationary components. A shroud around the runner that rotates with the blades limits the areas in the flow passage where rotating and stationary components interface to the runner inlet and exit. Therefore, all of the designs discussed in this report include a rotating shroud on the runner.

Since total loading on the blades is fixed by design conditions, limiting the number of blades presents a challenge in distributing the loading from the inlet to exit of the rotor blade to satisfy the velocity and pressure change rates defined in the last three criteria listed above. The loading distribution is represented in terms of surface velocity distribution. The velocity difference across a blade passage (normal to the flow direction) represents the local loading. A high loading locally would create a fast local surface velocity on one surface and a slow local velocity on the other surface. A sufficiently high surface velocity will result in a surface pressure less than 10 psia, violating the minimum pressure criteria. In addition, a high surface velocity may also lead to a higher change in velocity across the flow passage, with possible violation of the maximum velocity change rate and the maximum pressure change rate criteria.

5.3.2 Velocity Diagrams

The velocity diagrams for the inlet and exit of the new hydraulic turbine are shown in Figure 5-11. The runner is turning in the clockwise direction in Figure 5-11 with the water entering the turbine runner with the velocity V_1. Because the leading edge of the blade is moving at the wheel speed U_1, the velocity V_{r1} is the velocity relative to the runner at the runner inlet. Similarly at the exit, water leaves the runner at the velocity V_2. The trailing edge of the blade is moving at the wheel speed U_2, resulting in the velocity V_{r2} relative to the runner at the exit.

In many hydraulic turbines, the inlet velocity diagrams are quite different from the one shown on Figure 5-11. In an impulse turbine, the tangential velocity component of V_1 is twice the runner speed U_1, and in a 50% reaction turbine, the tangential velocity component of V_1 is equal to the runner speed U_1. The new runner design is a high reaction design, in which the tangential component of V_1 is a little more than half the wheel speed. This high reaction design is what produces the large change in direction between V_1 and V_{r1}.

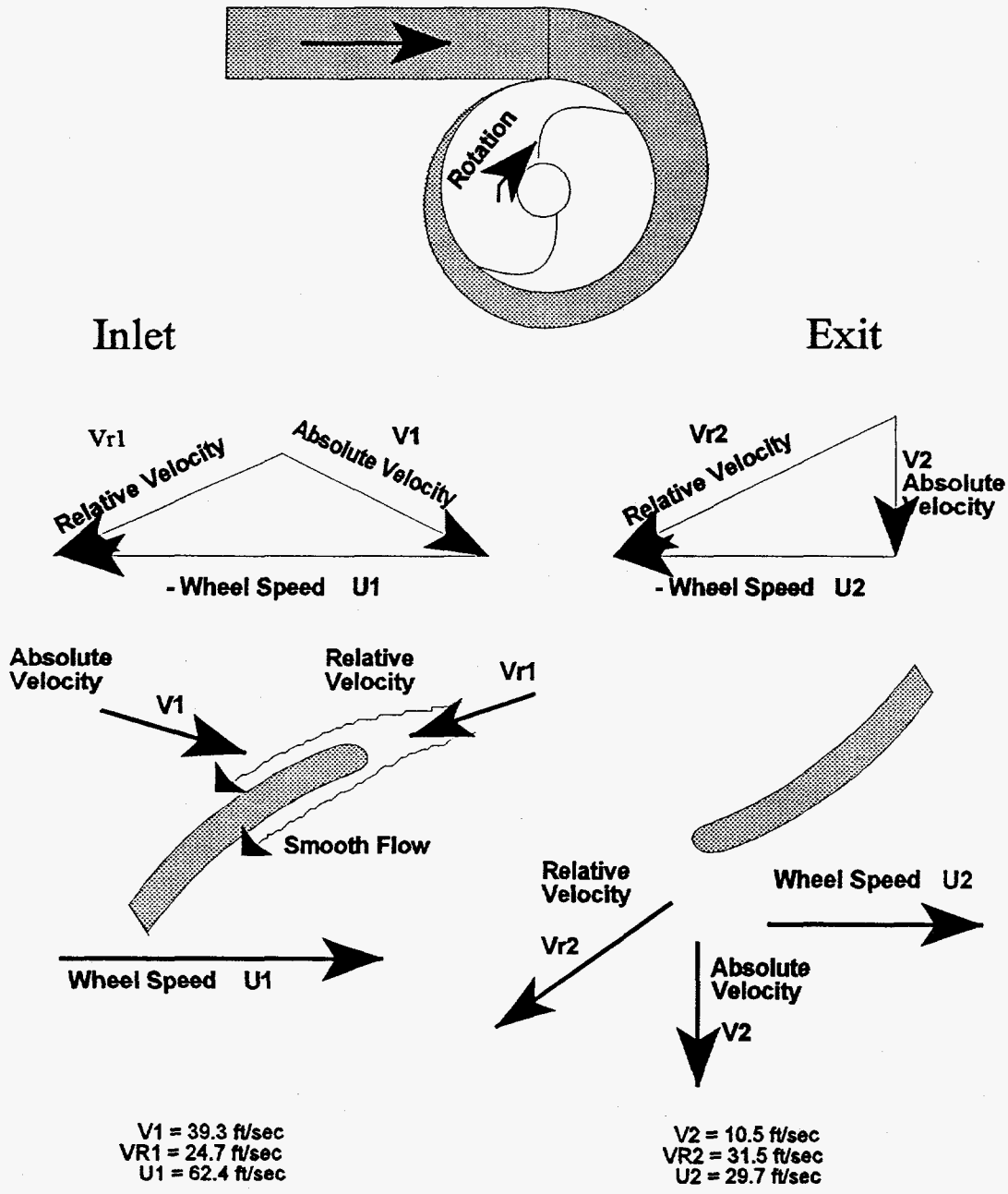

Figure 5-11
Velolcity Diagrams

5.3.3 Head Definition

Head across the runner (between the runner inlet and the runner exit) is one of the input parameters to the power performance model and is specified as the head available after the rotor friction, loading, and incidence losses. Scroll case and draft tube losses are not included as part of the head input to the performance model. Conceptual design of the new runner is based on the assumption that 75 ft of head is available for conversion to power after the rotor losses, which equates to a slightly higher head relative to tailwater. This assumption allows comparison of runner geometries for the same power output. The actual head to produce the same power will vary with the efficiency of each runner.

5.3.4 Efficiency Calculations

Power efficiencies presented in this report are based on the overall efficiency of the turbine with the 1,000 cfs design flow. The overall efficiency is based on the total head across the unit from the scroll case inlet to the tailwater, consistent with the American Society of Mechanical Engineers (ASME) definition of head. The ASME definition of head includes head losses associated with the scroll case, the wicket gates, the runner, and the draft tube. The International Electric Committee (IEC) does not include the draft tube losses. Therefore, the efficiencies for the new turbine presented in this report would be higher if the IEC code had been selected as the method for determining efficiency.

The one-dimensional power performance model used to determine efficiency with quasi-three-dimensional analysis included the scroll case but did not include the draft tube. The three-dimensional analysis only determines the efficiency of the runner. Therefore, the efficiency calculations for the new runner designs include estimates of the other components, the draft tube for the quasi-three-dimensional analysis, and the scroll case and draft tube for the true three-dimensional analysis. Head loss estimates are based on typical losses for hydraulic machinery in the hydroelectric industry. The overall efficiency is based on resulting decreases in the power output by about 2% for the scroll case and about 1% for the draft tube.

5.3.5 Wicket Gates

During the proposal preparation phase of the project, ARL/NREC decided to focus the conceptual design efforts on the turbine runner. ARL/NREC believe that flow control would be more appropriately incorporated into the turbine design after the runner has been developed to a stage at which the new runner has been proven to pass fish with minimal injury. Therefore, modelling of the

wicket gates or other flow control features was not included in the conceptual design of the new runner.

5.3.6 Scroll Case

The scroll case (spiral case) produces the kinetic energy in terms of velocity V_1, a portion of which the runner converts into useful work (Figure 5-11). Thus, a scroll case model was necessary to have to analyze the runner. A model of the scroll case is included in the NREC Program RITDAP™ described in Appendix A.

5.3.7 Draft Tube

In order to calculate the overall efficiency of the turbine, the draft tube was included in the model. In general, draft tubes typically have a 1:4 expansion area ratio which was assumed for the conceptual design of the new runner. An effectiveness of 0.7 was assumed for the diffuser corresponding to a loss coefficient of 0.28 in terms of the runner exit velocity head. For an exit velocity of 10.5 ft/sec at the rotor as shown on Figure 5-11, the dynamic head is 1.7 ft (0.74 psi). At the end of the draft tube, the velocity is 2.6 ft/sec and the corresponding head is 0.1 ft (0.05 psi). With a diffuser loss coefficient of 0.28, the draft tube head loss is 0.5 ft (0.21 psi). The total exit loss with the draft tube is 0.6 ft (0.26 psi) compared to 1.7 ft (0.74 psi) without the draft tube. This analyses indicates that the exit head loss with the draft tube is only one-third of the head loss without the draft tube.

5.3.8 Runner Exit Pressure

The runner exit was set 0.6 ft above the tailwater level for analysis of the first iteration design with the three-dimensional CFD model. This setting was selected to place the runner exit slightly above tailwater, as is customary for design of vertical axis turbines. To allow a direct comparison of the pressure distributions through the runner flow passages using the CFD model, all three design iterations assume the same runner exit pressure. At the design flow, the runner exit elevation is the same elevation as the energy grade line at the runner exit. Static pressure at runner exit is 13.7 psia for all three runner designs since the velocity head is the same, about 2.3 ft (1 psi).

SECTION 6
RESULTS OF COMPUTATIONAL ANALYSES

6.1 Validation of Pump Impeller Geometry

An inspection of the Hidrostal L12Q-SH pump impeller was performed to obtain the geometry for the initial analysis. The raw geometric inspection data was then transferred to electronic files using commercially available Computer Aided Design (CAD) software, and subsequently smoothed so that a representative blade shape for the pump impeller could be created for the computational analyses.

After the blade shape was created, the geometry was analyzed with PERFIG™, NREC's quasi-two dimensional pump analysis code. This code estimates the performance of the pump at both design and off-design operating points. The estimated performance from PERFIG was then compared to available performance test data from Hidrostal. This comparison, shown on Figure 6-1, indicates that the test data and the estimated performance from PERFIG match very well. Therefore, the blade shape derived from the inspection data was judged to be a close representation of the actual blade shape.

6.2 Scaled-up Impeller in Turbine Mode

The power performance model, described in Section 5.1.2 and Appendix A, was used to analyze the performance of a scaled-up version of the L12Q-SH pump impeller in the turbine mode for 1,000 cfs at 96 feet of head. The results are shown on Figure 6-2 which shows the overall turbine efficiency as well as efficiency decrements due to various loss effects. Figure 6-2 shows that the peak efficiency approaches 79% for a rotor tip diameter of about 22.2 ft. On both sides of this peak efficiency diameter, the efficiency drops precipitously.

The predicted efficiency with the impeller geometry was well below that of existing hydraulic turbines, which generally have efficiencies of over 90%. Also, the diameter of the runner at best efficiency was unusually large, and decreasing the diameter would result in major reduction in efficiency. Therefore, the pump impeller geometry was not considered a viable approach for the new turbine runner, and a new design had to be developed for the runner.

6.3 Development of Basic Runner Geometry

The initial effort in the development of the new basic runner geometry involved the optimization of the overall dimensions using the power performance model previously discussed in Section 5.1.2 and described in Appendix A. The results of the optimized runner geometry with two and three blades are compared with the results of the scaled-up pump impeller geometry operating in the turbine mode in Table 6-1.

The design optimization leading to Case 3 is shown on Figure 6-3. Figure 6-3 shows that the efficiency was fairly flat for a wide size range. As noted on Table 6-1, the Case 3 size could be reduced by 30% with about a 1% efficiency penalty. Such a reduction would reduce the tip diameter from 17.5 to 12.3 feet. Case 3 was preferred over Case 2 to minimize the number of blades.

Table 6-1
Optimization of Initial Runner Geometry

Case	Description	Number of Blades	Runner Diameter* ft	Runner Length ft	Rotational Speed rpm	Head ** ft	Overall Efficiency %
1	Scaled-up Pump Impeller as Turbine	1	22.2	10.8	61.2	96	79
2	New Turbine Design	3	16.2	12.3	73	84	90
3	New Turbine Design	2	17.5	13.3	68	85	89***

* Runner diameter at best efficiency.

** Head between scroll case inlet and tailwater.

*** For Case 3, the overall efficiency would be reduced by about 1% with a 30% reduction in runner diameter (12.3 ft diameter and 9.4 ft length).

However, if the large size of the new turbine becomes an important constraint in its application at hydroelectric sites, a three bladed design could be considered to reduce the diameter of the runner.

Next, an attempt was made to design blading for the preliminary design of Case 3 using NREC's COMIG program. As the detailed design progressed, the analysis indicated that the radial inlet created a large reduction in radius of the runner flow passages over a short distance resulting in large velocity and pressure loading at the upstream end of the runner. In order to reduce these large loadings and the corresponding susceptibility for flow separation at the runner inlet, the approach was turned from a radial inlet to a mixed flow inlet with meridional flow angles of 30 degrees from radial at the hub surface and 45 degrees from radial at the shroud. In addition, four degrees of incidence between the inlet flow angle and the inlet blade angle was introduced in order to further lower the large loadings, shown by COMIG, in the runner inlet area.

A detailed blade design was developed for the basic runner geometry to include a rotating shroud, an inlet blade angle of -70 degrees, an average inlet relative flow angle of -74 degrees, exit blade angles of -45.5 degrees at the hub surface, and -75.5 degrees at shroud surface. The quasi-three-dimensional flow analysis with COMIG was still predicting some areas of flow separation in the inlet of the basic runner geometry. However, CFD analysis was considered necessary at this point to ascertain if COMIG was properly analyzing the flow field for the two-bladed runner.

VISIUN was used to perform the three-dimensional analysis of flow through the basic runner geometry for the new turbine. Parameters related to the basic runner geometry (Design 1) and the overall efficiency based on the three-dimensional analysis are presented on Table 6-2. The VISIUN

Table 6-2
Results of Three-Dimensional Analysis

Design	Number of Blades	Runner Diameter* ft	Runner Length ft	Rotational Speed rpm	Head** ft	Overall Efficiency %
1	2	17.5	13.3	68	86	88
2	2	19.2	10	67.3	91	83
3	2	17.5	13.3	70.1	84	90

* Runner diameter at best efficiency.

** Head between scroll case inlet and tailwater.

results showed a turbine efficiency of 88% for Design 1, 1% lower than the efficiency predicted with the power performance model, confirming that the model produced reasonable results. The three-dimensional results also confirmed flow separation at the leading edge. The flow separation predicted by the COMIG and the VISIUN analyses indicates that the two-dimensional COMIG analysis is reasonably valid for this two-bladed runner.

However, the design had a noticeable problem: there was a separation of flow from the pressure surface of the blade. The separation started just downstream of the leading edge and continued to the middle of the blade where the flow finally reattached. The separation was largest at the hub and smallest at the mid-span. Additional discussion on the flow separation is presented in Section 6.6.2.2 with the flow separation shown on Figures 6-22 (mid-span of the blade), 6-27 (near the hub surface), and 6-30 (near the shroud surface).

The analysis also showed that the four degrees of incidence had not sufficiently reduced the loading at the leading edge of the blade to prevent the separation of flow, as intended with the basic design. The incidence was reduced to zero for the second design because the incidence was ineffective in preventing flow separation and that any incidence could be detrimental to approaching fish.

6.4 Refinements to Basic Runner Geometry

Because of the large separation zone on the pressure surface, several changes were made to the basic runner geometry to reduce the loading in the runner inlet and to eliminate the negative velocities calculated by COMIG. To reduce the loading on the blades, the blades must be longer for a given meridional distance. Longer blades spreads the loading across a greater area, resulting in a lower pressure differential between the surfaces. The easiest way to make the blade longer is to make it more tangential at the inlet. Another method to reduce the loading is to increase the meridional length of the blade by radially extending the inlet of the blade. Both of these techniques were used to develop the second iteration runner geometry.

The inlet radius for the second iteration runner geometry was increased to 115 inches from 105.2 inches. The inlet blade angle and average relative flow angle were changed to be equal at -78 degrees (zero incidence angle), both angles increased from the -70 degree blade angle and the -74 degree average relative flow angle used in the initial runner design. These inlet radius and incidence angle changes resulted in a more tangential leading edge for the blades and longer blades than the initial runner geometry.

The second iteration geometry also included inlet meridional angles of 50 degrees at the shroud and 40 degrees at the hub, greater than the mixed flow angles for the initial basic runner geometry. These greater inlet meridional angles helped to lower the radius reduction for a discrete meridional distance which also decreases the inlet loading on the runner blades. The size parameters for the second iteration runner design (Design 2) are presented above in Table 6-2.

Another change incorporated into the second iteration design was shorter axial length of the runner to reduce the blade length at the runner exit. The VISIUN and COMIG analyses of the basic runner geometry indicated that the loading in the exit of the turbine was very low. If the loading is low in a section of the blade, that section of the blade is not contributing to power output as much as the blade sections with higher loadings. Therefore, a shorter blade would reduce friction loss over low loading sections of the blade and would have power outputs comparable to the longer blade with low loading sections. The axial length of the runner was reduced from 160 inches for the initial runner geometry to 120 inches for the second iteration runner. The net effect of all the changes was a 30% increase in the blade lengths from the initial geometry to the second iteration design.

The final refinement to the first iteration design was reducing the thickness of the blades to the minimum amount necessary to maintain structural integrity. The scaled-up thickness of the pump impeller had been used for the first design iteration. For the second and third design iterations, the blade normal thicknesses were reduced from an average thickness of 9 inches to an average thickness of 4 inches. This blade thickness change was done to lower the meridional velocity within the runner flow passages, thereby reducing blade friction losses, and to reduce the overall weight of the runner.

6.5 Refinements to Second Iteration Design

The VISIUN results for the second iteration design iteration indicated an overall turbine efficiency of about 83%, about 5% lower than the initial design. The VISIUN results also showed that the flow separation and recirculation area found in the initial design had been completely eliminated in the second design, similar to the COMIG results. After evaluating the output from both the first and second iteration design VISIUN analyses, the lower efficiency for the second iteration runner was attributed to the higher relative flow velocities resulting from the more tangential angles in the second design. Since both designs have the same flow and both designs have approximately the same passage width (i.e. the meridional velocities are approximately equal), the design with the more tangential blade angles (the second design) should have higher relative velocities. These higher velocities result in greater skin friction on the blades and more head losses.

The results of the analyses of the first and second iteration designs indicated that the runner geometry should have a meridional flow path similar to the first design (which achieved a high efficiency) and that the flow angles should be slightly more tangential than the first design, but not as tangential as the second iteration design. The third iteration design geometry was defined to provide a compromise between the first and second designs, a geometry with no flow separation and with a reasonable efficiency. The size parameters for the third iteration runner design (Design 3) are presented above in Table 6-2.

For the third iteration design, the inlet blade and average relative flow angles were set at -76.5 degrees, and the exit blade angles were changed to -76 degrees at the shroud and to -46.5 degrees at the hub. The results of the COMIG analyses for this third iteration indicated no negative velocities (no separation) and lower relative velocities than the second iteration design (a higher efficiency).

To more accurately model the trailing edge as it would actually be manufactured, Design 3 had a rounded trailing edge instead of the square cut trailing edges used in Designs 1 and 2.

The VISIUN results for the third design iteration showed a turbine efficiency of about 90%, about 2% higher than the initial runner geometry and about 7% higher than second iteration design. The VISIUN results also showed that the third iteration design had a smaller flow separation and recirculation area than the first design, but did not eliminate flow separation as indicated by the COMIG results for the third iteration design.

6.6 Predicted Operating Characteristics

6.6.1 Three-Dimensional Flow Modeling

As is discussed in Appendix C, the VISIUN turbomachinery flow modeling system was developed to analyze compressible flow in turbomachinery components and stages. To expand its capabilities into incompressible flow analysis, several changes had to be implemented. The most important change was to diminish the approximate factorization error that grows as the Mach numbers become smaller. The approximate factorization error can be partially eliminated with the use of subiteration, but convergence can still be a problem. To insure the convergence of the algorithm, the minimum Mach number in the bulk of the flow should not fall below 0.05 which is possible if the characteristic speed of sound is kept at a very low level. A low level characteristic sound speed was accomplished by decreasing inlet total temperature by a factor of 80. At the same time, the inlet total pressure was increased by a factor of 10. Those two changes resulted in a significant increase of Mach numbers

and also brought the characteristic density to the level of water which gave the correct mass flow rate. Because the inlet total pressure was changed (by the factor of ten), the exit static pressure also had to be adjusted to have a correct total head drop. The original ratio of the static pressure at the exit to total pressure at the inlet was around 0.32. In the calculations, this ratio was changed to around 0.77 depending on the flow conditions and the losses such that the resulting mass flow rate was close to the specified 1,000 cfs.

To evaluate the efficiency of a particular design, an expression for the polytropic efficiency

$$\eta = \ln\left(\frac{T_{t,ma,in}}{T_{t,ma}}\right) \Big/ \left(\frac{\gamma-1}{\gamma} \ln\left(\frac{P_{t,ma,in}}{P_{t,ma}}\right)\right)$$

was used. In this expression $T_{t,ma,in}$ and $P_{t,ma,in}$ are the mass averaged total temperature and pressure at the inlet to the computational domain, $T_{t,ma}$ and $P_{t,ma}$ are the total mass averaged temperature and pressure at a particular station along the flow path. The value of gamma (γ) was set to 1.4.

6.6.2 Three-Dimensional Results

Flow analysis was performed using the VISIUN Computational Fluid Dynamics Program. The grid and flow property figures presented in the following sections were created using the Fieldview™ Flow Visualization Program and the pressure loading diagrams were plotted with the VISIUN Post-Processor. These visualizer and post-processing programs translate the enormous quantities of computed flow field property values into easily-interpreted visual displays of scalar and vector distribution fields. These displays have been used to evaluate the three design iterations of the new turbine runner in terms of computed flow field properties.

6.6.2.1 Computational Grid

Computational Fluid Dynamics (CFD) solves the equations of motion on small volume elements. The collection of corner points of these elements comprise the computational grid. Before a CFD solution can be attempted, a procedure must be applied to divide the turbine passage volume into small elements. This procedure is known as grid generation. Because the flow both upstream and downstream of the turbine blades is affected by the turbine, the grid must include regions that extend upstream of the leading edge and downstream of the trailing edge. Grid generation is a science in itself and frequently is the most difficult step in CFD analysis. However, the VISIUN-2FR

computational system includes an automatic algebraic grid generator used to generate the three-dimensional grids used in the CFD analysis of the new turbine runner.

Figure 6-4 shows a side view of the mesh of small elements along the hub surface of the turbine used in the analyses of the third iteration design (Design 3), the last geometry analyzed for conceptual design of the runner. The flow enters the turbine at the top of the runner shown on Figure 6-4 in the inward radial direction (towards the machine axis) and exits at the bottom in the axial direction. The blades are shown on Figure 6-4 for reference. Grids for all three designs are similar within the blade passage. However, the grids for the initial and second iteration runner geometries (Designs 1 and 2) did not include a draft tube, while the grid for Design 3 includes a draft tube with an expansion area ratio of 1:4. The grids for Designs 1 and 2 have 114 points in the streamline direction, 62 points from blade to blade, and 24 points from hub to shroud (114 x 62 x 24 grid) with a total 169,672 points in the entire grid. The grid for Design 3 is a 140 x 62 x 24 grid with a total of 208,320 points with the additional points associated with the draft tube grid.

Additional grid details are illustrated on Figure 6-5, where a side view of the mesh (grid) is shown on the mid-span surface halfway between the hub and the shroud (crown). The grid extends both upstream and downstream of the turbine blades. Both blade flow passages are shown on Figure 6-5 with the blade surfaces beyond mid-span omitted because they would obscure the grid. The diagonal stripes shown on the figure represent the intersection of the blades with this surface. The darker areas denote regions of grid clustering (dense grid point concentration) near the blade surfaces and near the leading edges (LE) and trailing edges (TE) of the blades. Concentrations of grid points are necessary to accurately calculate the rapidly varying flow that occurs at these locations. Figure 6-6 is similar to Figure 6-5, but shows only one blade flow passage to illustrate the spiraling of the passage around the axis from leading edge to trailing edge.

A view of the turbine from below (end view) is shown on Figure 6-7 which also has the blade surfaces removed for clarity so that only the intersections of the blades with the hub surface are shown. The dense grid at the leading edge, extending around the passage from blade to blade, was necessary to resolve the rapidly varying flow at the entrance to the turbine wheel. Grid concentration is also evident at the blade surfaces, where boundary layers occur. The grid extends through the draft tube where the radius of the hub is reduced to a small value, as shown by the small white opening at the axis. A similar view of the mid-span grid is shown on Figure 6-8. The larger white opening at the center illustrates that the mid-span surface diameter remains large throughout the draft tube.

A hub-to-shroud grid surface midway between the blades is shown on Figure 6-9 to illustrate the clustering of the grid at the trailing edge and the dense packing of grid lines near the hub and shroud surfaces. Twenty-two (22) surfaces are located between the hub and shroud. The sixth, twelfth, and nineteenth surfaces shown on Figure 6-9, counting outward from the hub, represent the near hub, mid-span, and near shroud surfaces, respectively, referenced in the discussions and figures presented in the following section. At the left side of Figure 6-9, the grid curves follow the blade shape. The grid at the right, downstream from the trailing edge, on Figure 6-9 is part of the draft tube. Figure 6-10 shows the same surface shown on Figure 6-9 extended to the end of the draft tube where the cross-sectional area is four times the area at the runner exit (1:4 expansion area ratio).

6.6.2.2 Computed Flow Field

The flow field has been computed on a grid that moves with the turbine wheel, and all flow properties shown on the following figures are relative to this reference frame. A complete set of figures is presented for Design 3 with additional figures shown for Designs 1 and 2 to show contrasts for some flow properties. The figures for Design 3 do not show flow in the draft tube since flow details would not be visible at a scale that shows the runner with the draft tube.

Velocity Magnitude

Figures 6-11 through 6-13 show the hub surface, blades (clipped at the hub or mid-span), and contours of relative velocity magnitude for Design 3 grid surfaces near the hub, at mid-span, and near the shroud, respectively. The contours shown on the figures are curves of constant relative velocity magnitude colored according to the spectrum shown in the legends. Near the hub refers to surface 6, mid-span refers to surface 12, and near the shroud refers to surface 19 as shown in Figures 6-9 and 6-10. The relative velocities cannot be shown on the hub or shroud surfaces because the viscous wall boundary condition sets the velocity to zero. The blades are truncated at each display surface so that the flow will not be obscured.

The distribution of velocity in the Design 3 runner, as shown on Figures 6-11, 6-12, and 6-13, indicates regions of flow reversal and flow separation leading to increased losses and reduced turbine efficiency. The highest relative velocities (colored red) occur at the inflow boundary, where the swirling incident flow has not yet felt the influence of the blades. The lowest velocities (blue) occur along the blades and in regions adjacent to the pressure (convex) surface, where the extended region of low velocity indicates the possibility of flow separation, especially near the hub and shroud. The velocity contours also indicate that the separated flow reattaches to the blade surface. The small

yellow regions behind the leading edges indicate flow acceleration around the leading edge. The three-dimensional nature of the flow is revealed by the differences in the flow near the hub, at mid-span and near the shroud. For example, the upstream influence of the blades is stronger at mid-span than the influence near the hub or shroud. Velocities along the suction surface appear higher near the hub than at mid-span or near the shroud, and the indication of flow separation is stronger near the hub than at mid-span or near the shroud. The strong three-dimensionality of the flow pattern for Design 3 is physically consistent with a flow that enters almost radially and turns 90 degrees to exit axially.

The velocity magnitude distribution can also be displayed as regions of continuously changing color shading instead of as contours. Figures 6-14 through 6-16 show the same information as the previous three figures, but show the velocity distribution as shaded regions. These figures show a large region of low velocity on each of the three surfaces, and the largest region, which extends furthest downstream, is located near the hub. Near the shroud, the region of low velocity terminates closest to the blade leading edge. These regions of rapidly decreasing flow velocity magnitude lead to flow separation. Additional refinement of the runner geometry would be necessary during the next phase of the runner development to minimize the magnitude of decreases in velocity.

Velocity Vectors

Another method of visualizing the velocity field is to display velocity vectors, which show both velocity magnitude and direction. Figures 6-17 through 6-19 show velocity vectors colored with velocity magnitude (speed) on the same Design 3 grid surfaces presented on the previous six figures. The velocity magnitude is shown both by the vector color and length. In these figures, the turbine is rotating counterclockwise resulting in relative velocity vectors that show the flow moving into the runner in the clockwise direction. These three figures show that the relative velocity is zero at the blade surfaces and that the velocity vectors align with the blades near the blade surfaces. At the turbine exit, the relative velocities have a large swirl (tangential) component that corresponds to almost axial absolute velocities (in the non-rotating reference frame) with very small tangential components. The velocity within the passage is higher at mid-span and near the shroud than the velocity near the hub, which is also apparent on the previous three figures.

Closer views of the velocity vector field reveal additional information. Figure 6-20 shows that the mid-span flow proceeds in the through-flow direction along both sides (low and high pressure) of the portion of the blade shown on the figure. Figure 6-20 indicates that the flow velocity magnitude behind the leading edge on the pressure side is low in the region close to the blade surface, and that

the flow has not separated from the blade. An even closer view of the leading edge region, shown on Figure 6-21, confirms that the velocity is low close to the blade and that the flow does not separate from the blade. This figure also shows that the local incidence angle is small and negative, and that the stagnation point, shown by the dark blue arrows at the leading edge, occurs towards the pressure side of the blade. This assessment is confirmed by the increased velocity (yellow and orange arrows) on the suction surface just behind the leading edge, which indicates acceleration due to leading edge curvature.

Similar leading edge region velocity vector distributions are shown for Designs 1 and 2 on Figures 6-22 and 6-23. Design 1 has a thicker blade than Design 3, but has a similar flow pattern to Design 3 behind the leading edge. Design 1 has an incidence angle near zero and Design 3 has a small negative incidence angle, even though the approach flow as determined by COMIG for Design 1, had an incidence angle of four degrees, and the approach flow for Design 3 had an incidence angle near zero. Thus both Designs 1 and 3 turn the approach flow towards negative incidence as the flow approaches the leading edge. Design 2 has a thin blade, a near zero local incidence angle, and higher velocities in the leading edge region than either Designs 1 or 3. Figure 6-24, a closer view of Figure 6-20, shows a region of the Design 3 mid-span velocity field further downstream on the blade than the velocity field shown on Figure 6-21. The low velocity in the thick boundary layer on the pressure surface and the higher velocity near the blade on the suction surface (thinner boundary layer) are evident at this location for Design 3. Figure 6-25 shows a similar mid-blade view of the velocity vectors near the hub for Design 3. The recirculation adjacent to the suction surface is clearly shown by the blue velocity vectors that point in the upstream and cross-stream directions. Figure 6-26 superimposes the calculation grid on the previous figure and increases the velocity magnitude scale to better show the recirculation in Design 3. Addition of the grid to the figure illustrates that the velocity vector tails are located at grid points and that the locations of the vectors on all velocity figures are determined by the locations of grid points.

To complete the description of the leading edge flow, Figures 6-27, 6-28, and 6-29 show the velocity vectors near the hub for Designs 1, 2, and 3, respectively, and Figures 6-30, 6-31, and 6-32 show the corresponding velocity vectors near the shroud. All three designs show a slight outward flow (away from the runner axis) upstream of the leading edge near the hub. Only Design 1 shows this outward flow behavior upstream of the leading edge near the shroud (Figure 6-30). This outward flow component is caused by the rotating wall that centrifuges a small region of the flow radially outward in the wall boundary layer. In all six figures, the suction side boundary layer remains attached. Design 1 shows a large high pressure region with flow separation, starting just behind the leading edge near the hub (Figure 6-27) and near the shroud (Figure 6-30), where recirculation and the

resulting vortices are clearly visible. Design 2 shows no pressure surface separation near the hub (Figure 6-28) and near the shroud (Figure 6-31). Design 3 shows flow separation regions on the pressure surface (Figures 6-29 and 6-32), but these regions are smaller and start farther downstream along the blade compared to Design 1.

The radially outward flow for Design 3, present at the hub but not at the shroud, is shown on Figure 6-33. Figure 6-33 presents the velocity on four surfaces oriented approximately normal to the through-flow direction, and illustrates the three-dimensional pattern of the flow at the runner entrance and exit. At both locations, the magnitude and direction of the velocities are different at the hub, the mid-span, and the shroud.

Pressure Distributions

Pressure distributions are another important measure of turbine performance. An investigation of contours of constant pressure (isobars) has been conducted to identify the location and values of maximum and minimum pressure through the runner, and to determine the extent of the lowest pressure regions. This pressure information has been used to determine if local pressures reach values low enough to initiate cavitation in the water leading to fish and blade damage. Figures 6-34 through Figures 6-48 display the static pressure distribution, which is the same in the relative and stationary (absolute) reference frames, through each of the three runner designs .

Figures 6-34 through 6-36 show the Design 3 pressure distribution on surfaces near the hub, at mid-span, and near the shroud. All of the figures show that the pressure decreases at a reasonably uniform rate as the flow proceeds through the turbine runner from the highest values at the inlet to lowest values at the runner exit. The highest value of pressure occurs in the stagnation region around the blade leading edge, which is difficult to see on the figures because of the scale of the grid in this region. The lowest value occurs at the blade trailing edge. Pressure levels near the hub are lower than pressure levels at mid-span and pressure levels at mid-span are lower than pressure levels near the shroud. In addition, the pressure variations across the flow passage in the blade-to-blade direction are stronger near the hub than at mid-span or near the shroud. The pressure contours have been used to compare the runner hydraulic characteristics with the biological design criteria selected for evaluating the runner's potential of the runner designs to pass fish with minimal injury.

Closer views of the mid-span trailing edge region are shown on Figures 6-37, 6-38, and 6-39 for Designs 1, 2, and 3, respectively. In each case, the lowest pressure is confined to a very small region right at the low pressure side of the trailing edge. Designs 1 and 2 were modeled with sharp trailing

edges cut off at a constant axial location. To better model the actual blade, which may be fabricated or cast, Design 3 included a rounded trailing edge. The extent of the lowest pressure region is seen to be smallest in design 3. The lowest pressure at the trailing edge for Design 1 was about 5.4 psia, for Design 2, about 4.0 psia, and for Design 3 about 8.6 psia.

Figures 6-40 through 6-48 present pressure loading diagrams at the hub, at mid-span, and at the shroud for Designs 1, 2 and 3. Pressure distributions on the pressure (high pressure) surfaces (convex) of the blades are shown as circles and distributions on the suction (low pressure) surfaces (concave) are depicted by x's.

The point of highest pressure on each figure represents the stagnation point. The abscissa on all of the pressure loading diagrams is meridional distance, not camberline distance. The zero meridional distance point corresponds to the point of highest radius (point M on Figure 6-49), not to the point where the camberline intersects the leading edge (point C) and not to the stagnation point (point S). For designs with near tangential inlets, when the stagnation point occurs near point C, the part of the pressure surface between point M and the stagnation point is plotted as part of the suction surface and the two curves will cross within the first five percent of meridional distance. The loading at any value of meridional distance is defined as the difference between the pressure and suction surface pressures. All three designs exhibit negative loading near the leading edge at the hub, and less negative loading at the shroud than at the hub. Design 3 has the lowest negative loading because the stagnation point is closer to the point of highest radius than for the other two designs. At the shroud, Design 3 has no negative loading. Design 3 at mid-span has a greater loading over the first 30 percent of the blade and less loading over the remainder of the blade when compared to Design 2. Design 3 has greater loading over the entire blade when compared to Design 1.

The lowest pressure occurs on the suction (low pressure) side at the trailing edge and is confined to a very small region for all three designs. This region corresponds to the dark blue closed contours at the trailing edge shown on Figures 6-37 through 6-39. All three designs show suction surface pressures ranging between 13 psia and 16 psia over the last 40 percent of meridional distance.

Path Lines

Another interesting way of looking at the flow behavior in the turbine runner and the potential effects on the fish is to display flow path lines. These curves represent the paths that particles embedded in the flow would follow in time as the particles pass through the turbine runner. Because the flow is steady in the relative reference frame moving with the turbine, path lines representing relative flow

provide the most meaningful display. Each path line starts from a seed point where a particle is introduced into the flow. Fish that do not swim against or across the flow would follow the path line from the seed point where the fish enters the turbine inlet through the runner to the turbine exit.

Figures 6-50, 6-51, and 6-52 show eight colored path lines seeded at mid-span points on a curved line of constant radius near the blade leading edge for Designs 1, 2, and 3. There are two path lines of each color, one for each flow passage, shown on each figure, with the same colors used for similar seed points for all three designs. The yellow and green path lines for Design 1 (Figure 6-50) start right in front of the blade leading edge where they collide with the blade surface. The dark blue path line for Design 1 (Figure 6-50) moves along the pressure surface until it encounters the flow separation region. At this point the path line turns towards the shroud, loops through the recirculation zone, and is centrifuged out in the shroud boundary layer. Five of the path lines from the center of the flow passage for Design 1 move downstream through the turbine (Figure 6--50).

The path lines for Design 2, shown on Figure 6-51, indicate a somewhat different pattern. The yellow, green, and purple path lines end on the blade or hub surfaces and the dark blue path line moves to the hub and is centrifuged out in the hub boundary layer (Figure 6-51). Only four path lines from the center of the flow passage move downstream through the Design 2 turbine runner.

The path lines for Design 3 (Figure 6-52) are similar to those for Design 1 (Figure 6-50), but exhibit some improved characteristics. All eight path lines move downstream through the turbine runner. The green and dark blue path lines move together along the pressure surface migrating towards the shroud where they encounter the flow separation region and loop through the recirculation zone. However, both of these path lines pass inside the next blade and continue through the passage. The yellow path line moves along the suction surface of the blade and continues to the exit. None of the eight mid-span path lines shown for Design 3 (Figure 6-52) are entrained by the hub or shroud boundary layers, and none are therefore centrifuged outward.

Figure 6-53 shows path lines seeded near the shroud leading edge for Design 3. The black grids show the periodic boundary surfaces upstream and downstream of the turbine blades. These periodic surfaces are boundaries of the computational domain used by the VISIUN™ flow analysis program. Because of a limitation of the flow visualization program, path lines terminate when they intersect periodic boundaries. All of the path lines shown in Figures 6-50 through 6-53 that proceed through the turbine terminate at periodic boundaries downstream of the turbine. Review of the termination positions at the downstream periodic surfaces shown in Figure 6-53 indicate that the flow entering the turbine near the shroud twists as it moves through the runner flow passages and exits the runner

mixed with the flow that entered the runner at other locations between the hub and shroud. In addition, the path lines that are centrifuged upstream of the runner leading edges terminate at the periodic boundary upstream of the leading edge.

6.7 Comparison of Flow Characteristics to Biological Criteria

6.7.1 Introduction

The results of the CFD analyses described in Section 6.6 were presented in terms of computed flow field characteristics that can be compared to the biological design criteria selected for evaluating the runner designs. The figures presented in Section 6.6 and in this section are intended to show flow properties that represent the biological criteria, and to show the regions where the values of these properties approach or exceed the critical values defined by the criteria. The biological criteria that can be compared to flow characteristics are as follows:

- Minimum pressure 10 psia or greater;
- Maximum pressure change rate not to exceed 80 psia/sec; and,
- Maximum velocity change not to exceed 15 ft/sec/in.

The hydraulic characteristics of the three runner designs defined by CFD analyses are compared to these biological criteria in the following sections.

6.7.2 Minimum Pressure

Static pressure distributions for Designs 1, 2, and 3 are shown on Figures 6-34 through 6-48. The displays of the distribution of mid-span pressure near the trailing edge (Figures 6-37, 6-38, and 6-39) reveal that the pressure falls below 10 psia only in a small region just behind the runner trailing edge. The pressure loading diagrams, presented on Figures 6-40 through 6-48, also clearly show that the minimum pressure along the blade surface is restricted to a very small region at the trailing edge and confined to the suction (low pressure) surface at the hub, at mid-span and at the shroud for all three designs. Rounding the trailing edge in Design 3 reduces the extent of this low pressure region. The minimum pressure in this small region is 5.4 psia for Design 1, 4.0 psia for Design 2, and 8.6 psia for Design 3, all less than the minimum pressure criterion of 10 psia.

Since minimizing the low pressure regions along the blades is important for fish survival, the pressure distribution displays and pressure loading diagrams have been reviewed to approximate the size of

the lowest pressure regions. As shown on Figures 6-37, 6-38, and 6-39, the lowest pressure region for all three designs is at the trailing edge and is limited to less than the width of the blade. As shown on Figures 6-40 through Figure 6-48, lowest pressures generally occur over the last (downstream end of runner) 40% of the suction (low pressure) surface for all three designs. Except at the trailing edge, the pressure in this region ranges from about 13 psia up to about 17 psia. The minimum pressure criterion (10 psia) is violated only in the very small region at the trailing edge, which for Design 3 amounts to less than 1/10,000 of one percent (<0.0001%) of the runner flow passages total volume.

6.7.3 Maximum Pressure Change Rate

For steady flow, the rate of pressure change has been calculated as the scalar product of the pressure gradient (∇p) and the velocity vector (V):

$$\frac{dp}{dt} = V \cdot \nabla p$$

The units for this parameter are pounds per square inch per second (psi/sec). The pressure change rate is a measurement of the time rate of change of pressure experienced by a fish moving along a path line.

The pressure change rates for the mid-span surface are shown on Figures 6-54, 6-55, and 6-56 for Designs 1, 2, and 3, respectively. The maximum value of pressure change rate occurs near the leading and trailing edges of the blades for all three designs. At the leading edge, flow first decelerates as it approaches the blade and then accelerates around the leading edge. These accelerations create a high positive (red) rate of pressure change approaching the leading edge and then change to a high negative (dark blue) rate around the blade. At the trailing edge, the high pressure change rates are associated with accelerations in the vicinity of small low pressure zones.

The pressure rate of change magnitude exceeds 80 psi/sec, the maximum pressure change rate criterion, only in the small uncolored regions within the last blue or red contours as shown on Figures 6-54, 6-55, and 6-56. The minimal size of these zones indicates that only a small fraction of the flow passage volume is subjected to unacceptably high levels of pressure change rate. The high pressure change rate zones are located very close to the runner blade surfaces. Fish that enter these high pressure change rate regions have a high likelihood of impacting the blade because these regions are so close to the blade leading and trailing edges. The contours on Figures 6-54, 6-55, and 6-56

indicate that Design 3 (Figure 6-56) should have less fish injury from pressure change rates than Design 1 and Design 2 (Figures 6-54 and 6-55) for three reasons: (1) the Design 3 leading edge region does not have the high negative pressure rate change zone on the pressure side of the blade that occurs for Designs 1 and Design 2; (2) Design 3 has a smaller positive maximum pressure change zone than Designs 1 and 2; and, (3) the high pressure change rate zones at the Design 3 trailing edge appear smaller than the same zones predicted for Designs 1 and 2. A rough size approximation of these high pressure change rate zones indicates that volume of these zones for Design 3 is about one percent of the total volume of the runner flow passages.

6.7.4 Maximum Shear

Shear zones in the turbine flow passages for Design 3 can be quantified by the vorticity, ω, of the flow. Vorticity is a measure of the rate of change of velocity with distance and has been computed by:

$$\omega = \nabla x V$$

where ∇ x is the curl operator and V is the velocity vector.

As shown in Figure 6-57, the regions of maximum vorticity for Design 3 are entirely within the boundary layers near the blade surfaces. The regions of maximum vorticity identified for Design 1 and Design 2 were the same regions shown for Design 3. The high shear zones close to the runner walls should not increase injury to fish beyond that resulting from collision with the blade surfaces.

This page intentionally left blank.

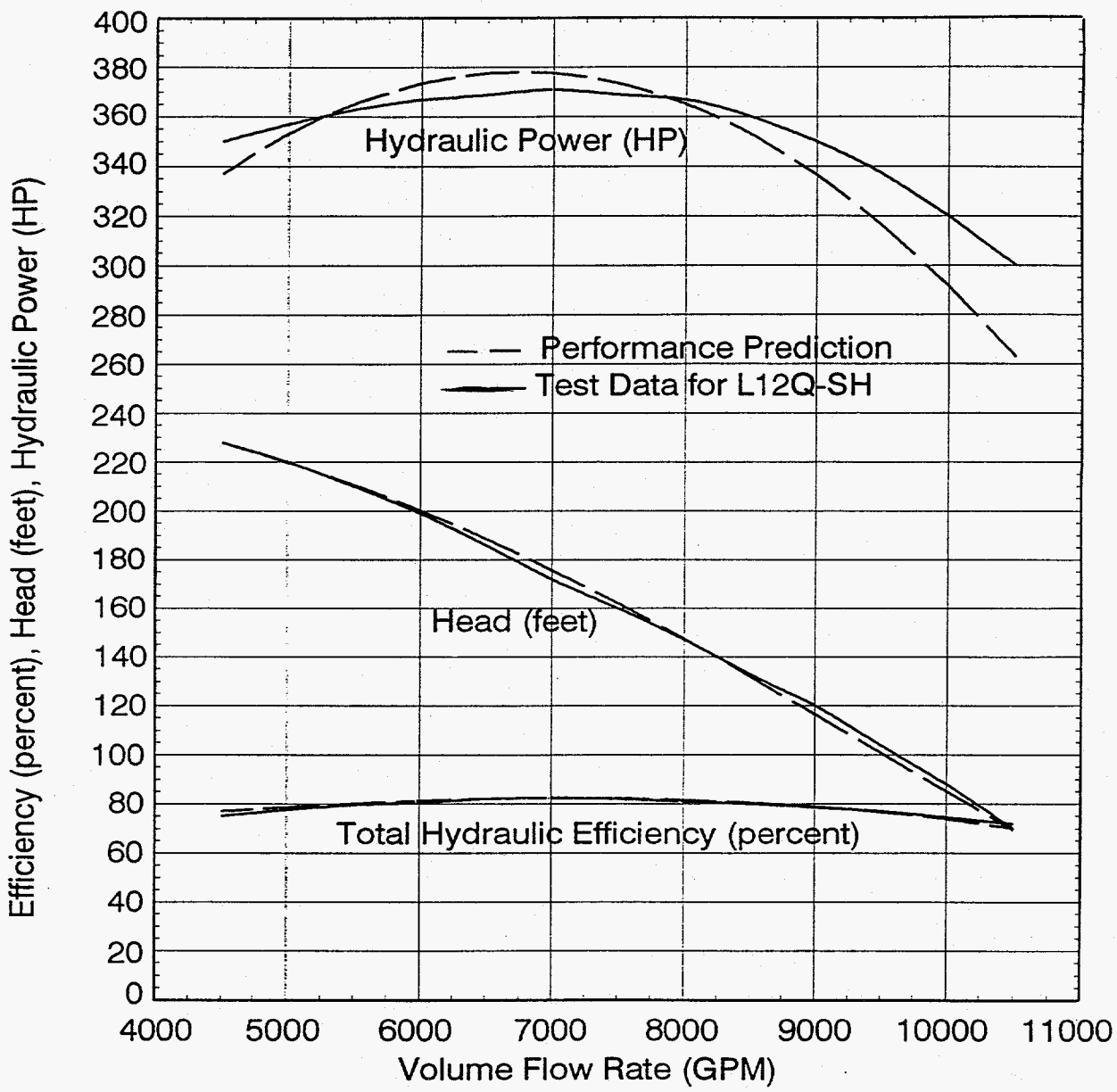

Figure 6-1
Validation of Two-Dimensional Model

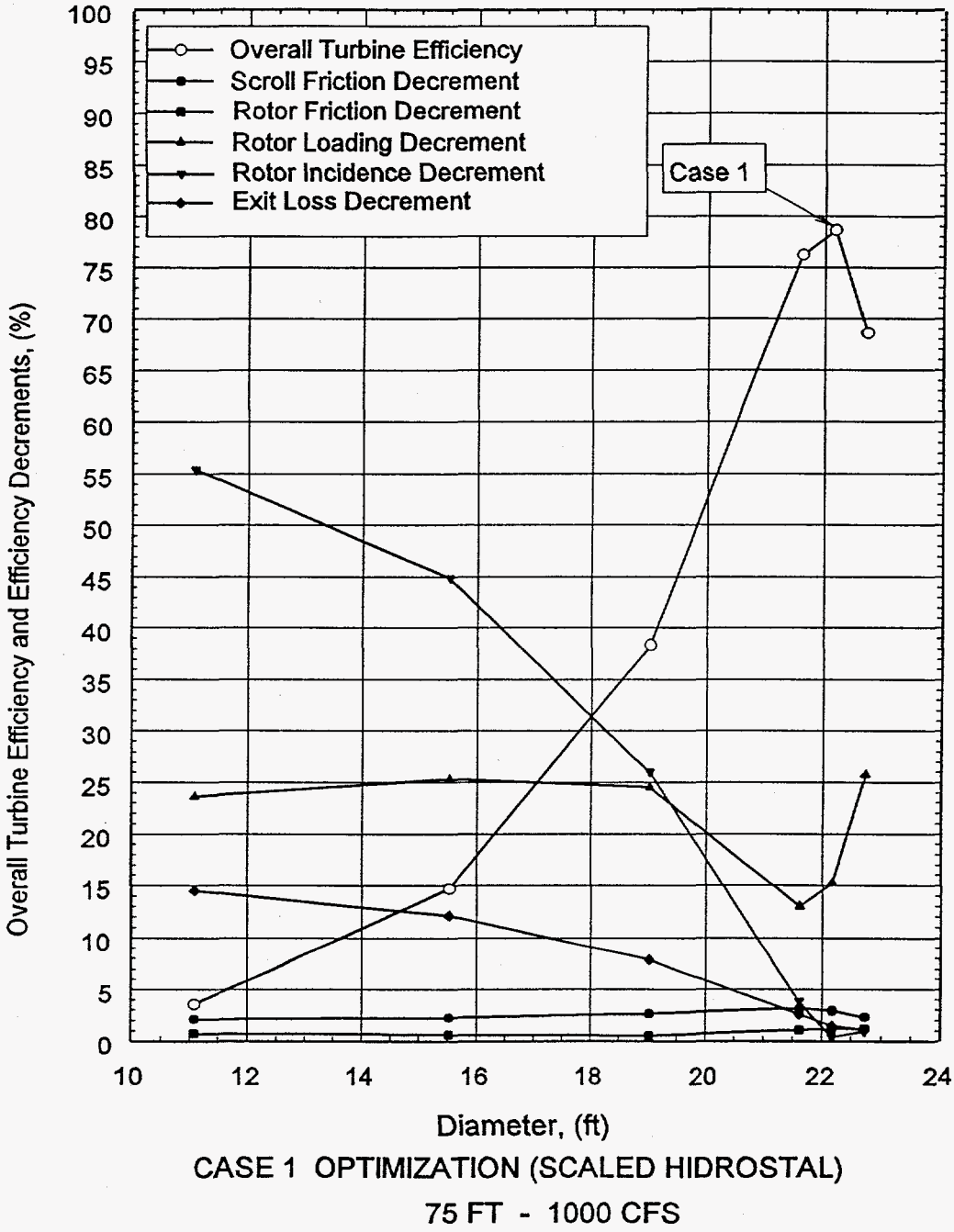

Figure 6-2
Case 1 Optimization (Scaled Pump Impeller)

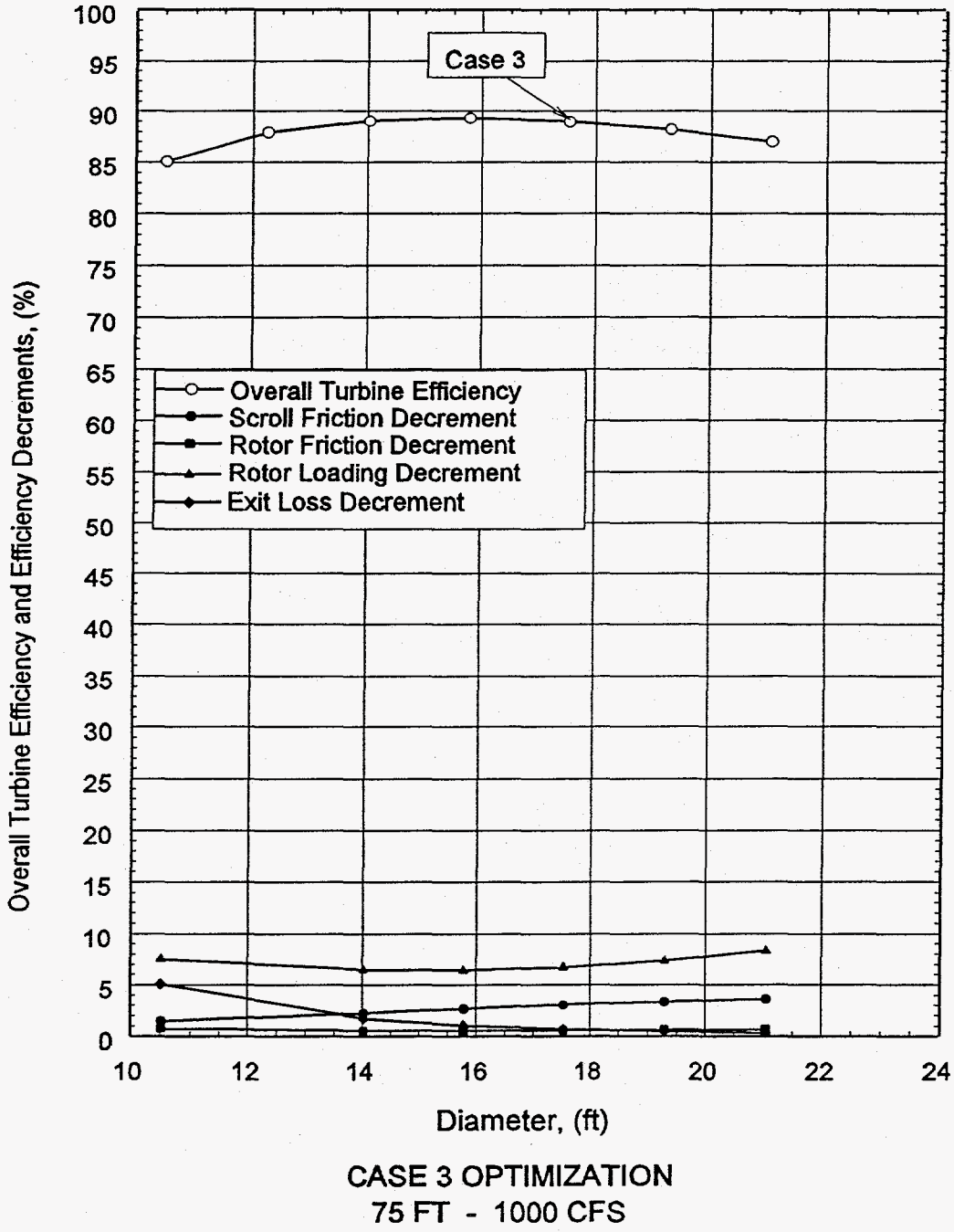

CASE 3 OPTIMIZATION
75 FT - 1000 CFS

Figure 6-3
Case 3 Optimization (Initial Runner Geometry)

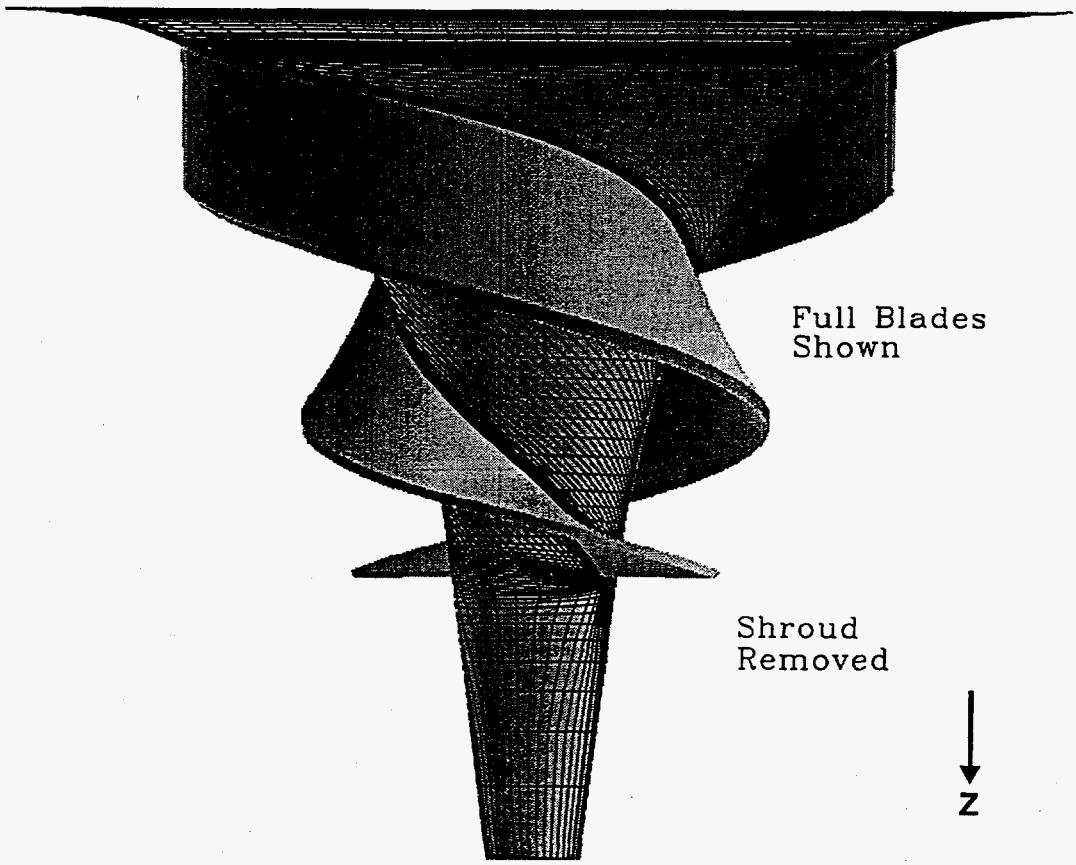

Figure 6-4
Design 3 - Side View Grid on Hub Surface

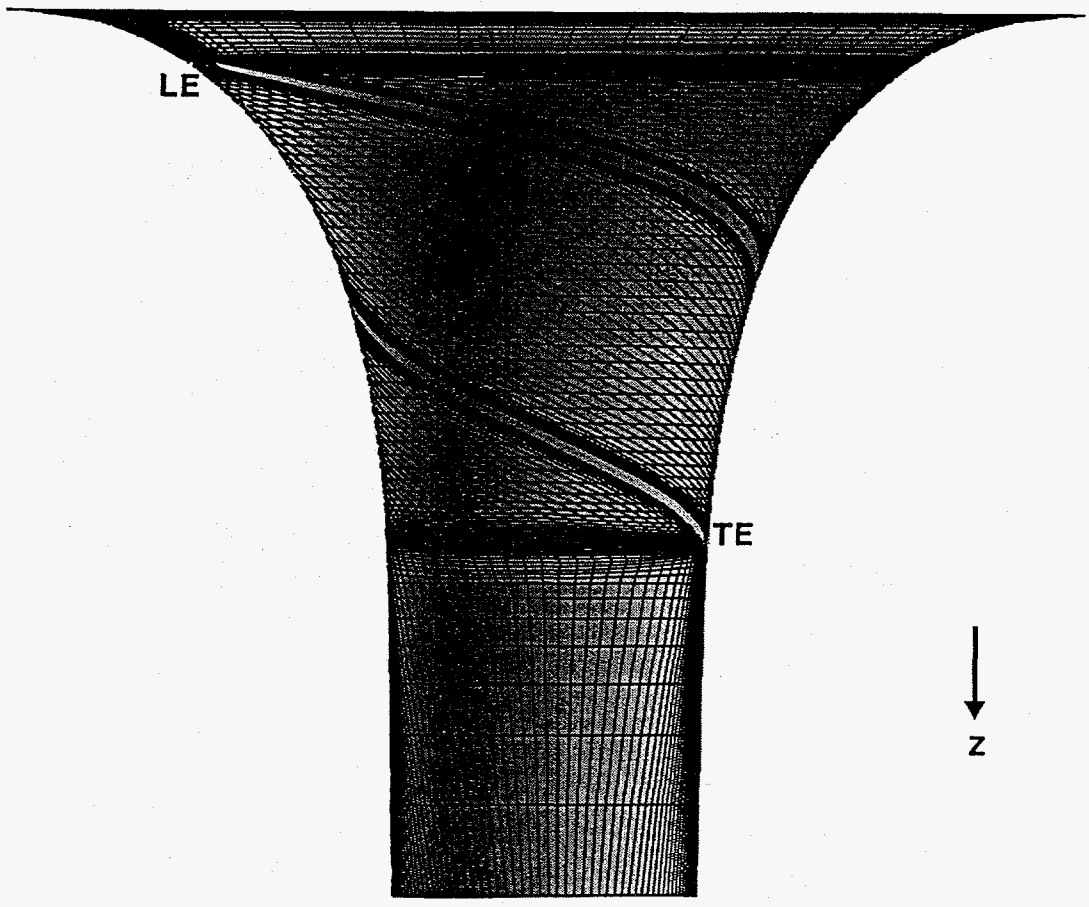

Figure 6-5
Design 3 - Side View Grid on Mid-Span Surface

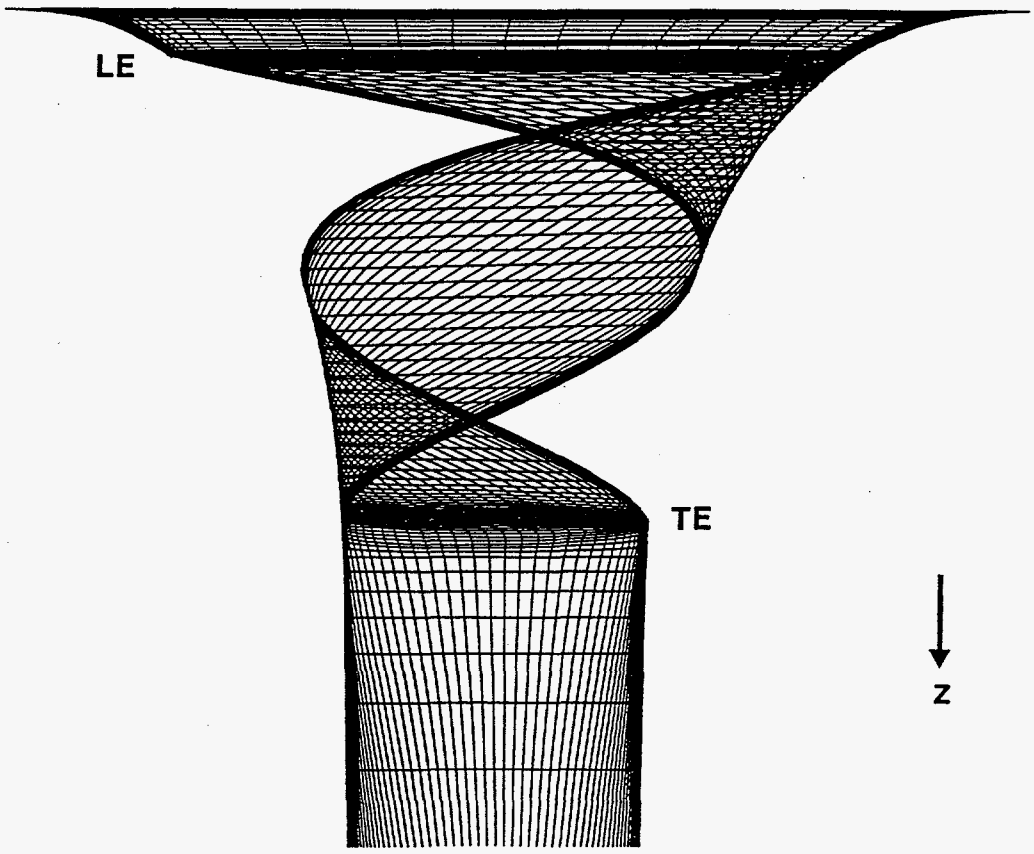

Figure 6-6
Design 3 - Side View Grid on Mid-Span Surface Single Passage

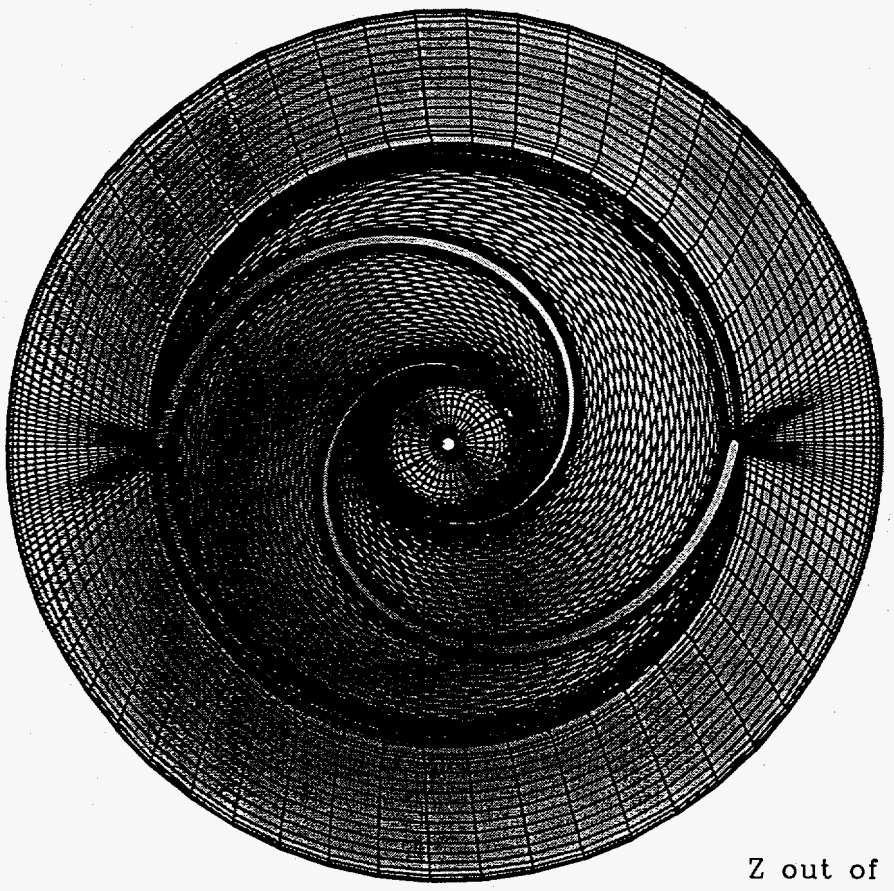

Figure 6-7
Design 3 - End View Grid on Hub Surface

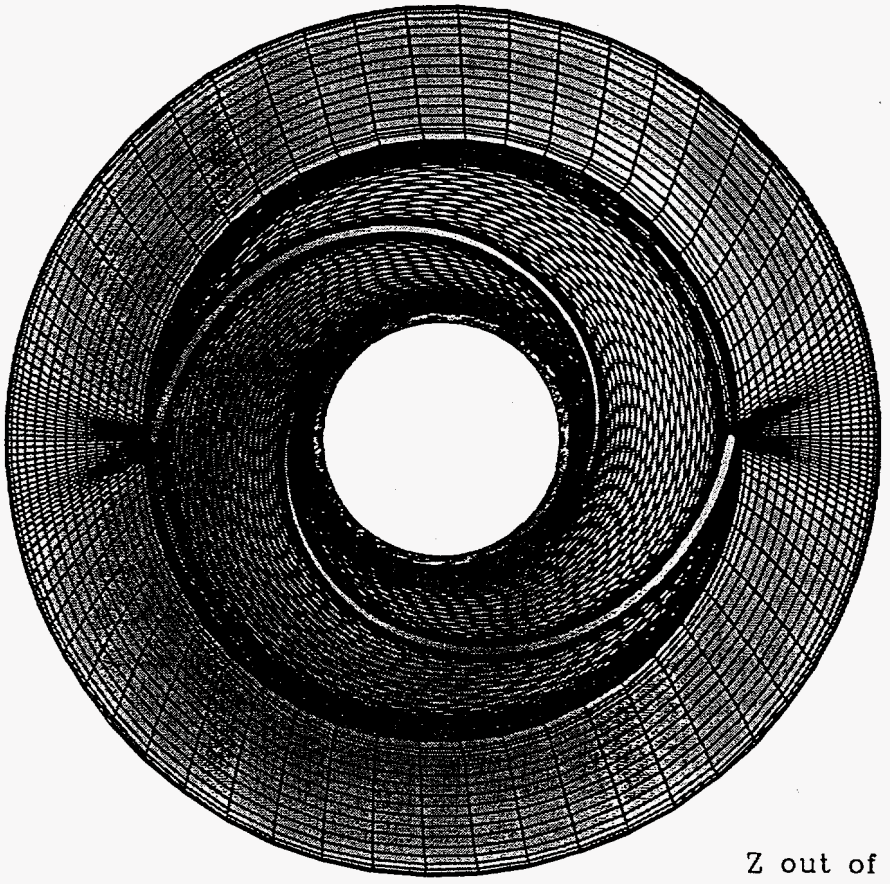

Figure 6-8
Design 3 - End View Grid on Mid-Span Surface

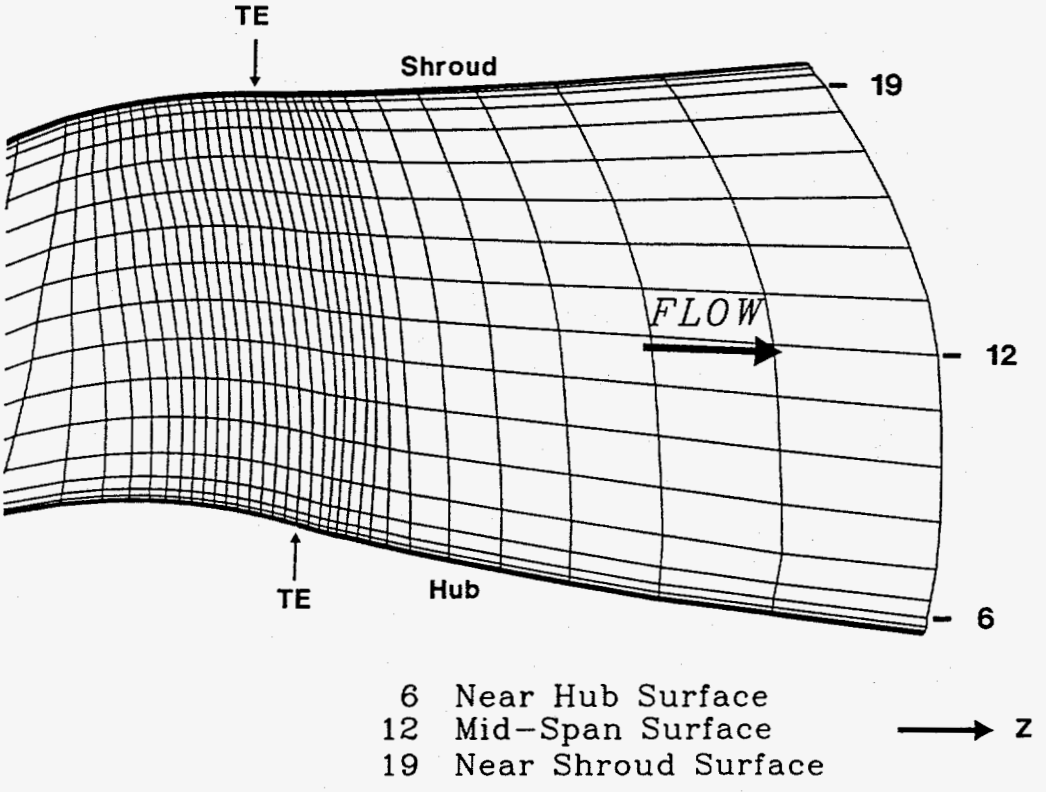

Figure 6-9
Design 3 - Hub-to-Shroud Grid Surface Midway Between Blades At Trailing Edge

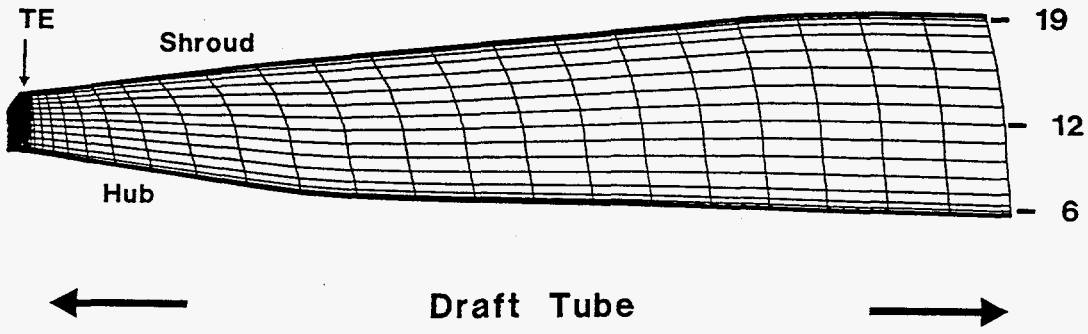

6 Near Hub Surface
12 Mid-Span Surface
19 Near Shroud Surface

Z

Figure 6-10
Design 3 - Hub-to-Shroud Grid Surface Midway Between Blades Extended Though Draft Tube

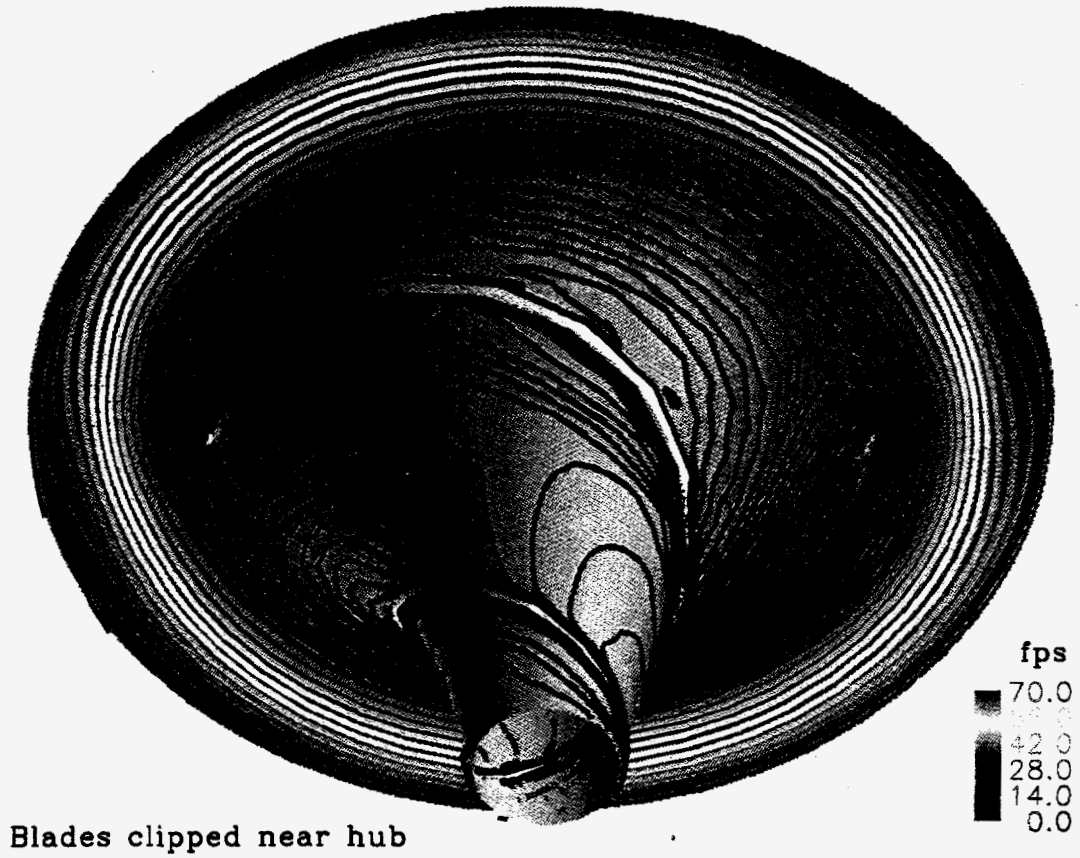

Figure 6-11
Design 3 - Velocity Magnitude Near Hub (Defined by Contours)

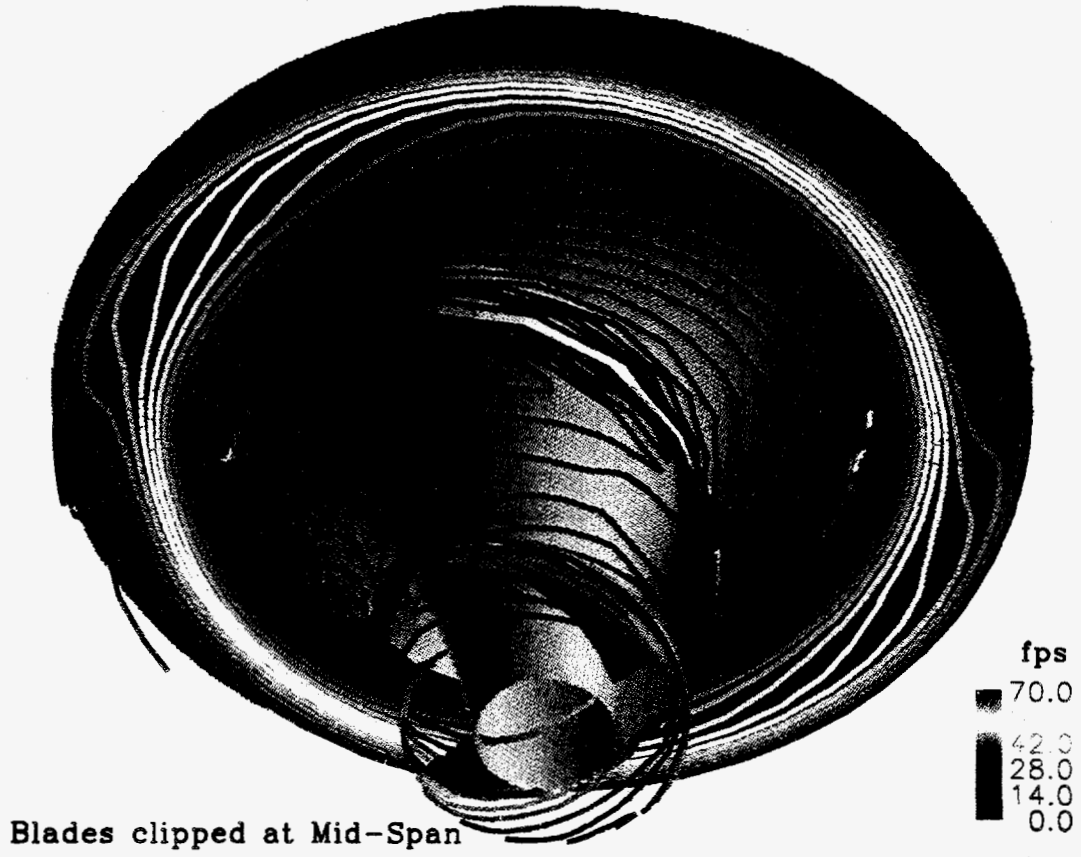

Figure 6-12
Design 3 - Velocity Magnitude at Mid-Span (Defined by Contours)

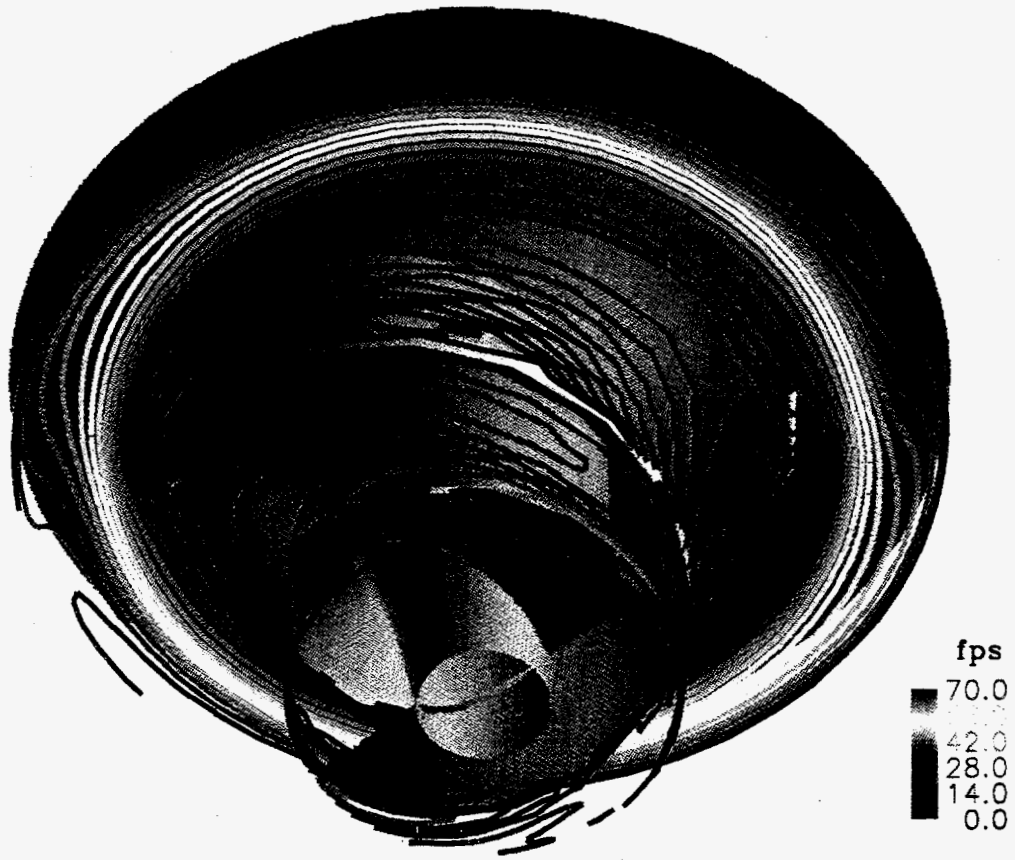

Figure 6-13
Design 3 - Velocity Magnitude Near Shroud (Defined by Contours)

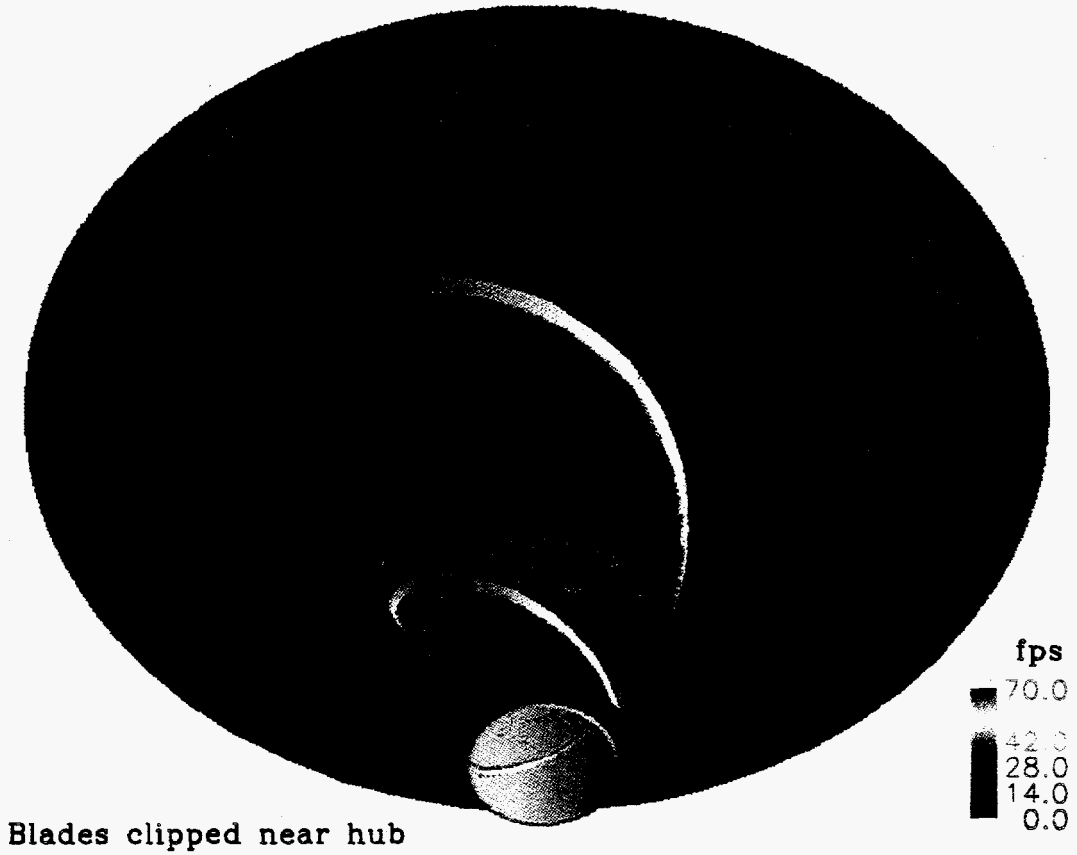

Figure 6-14
Design 3 - Velocity Magnitude Near Hub (Defined by Shading)

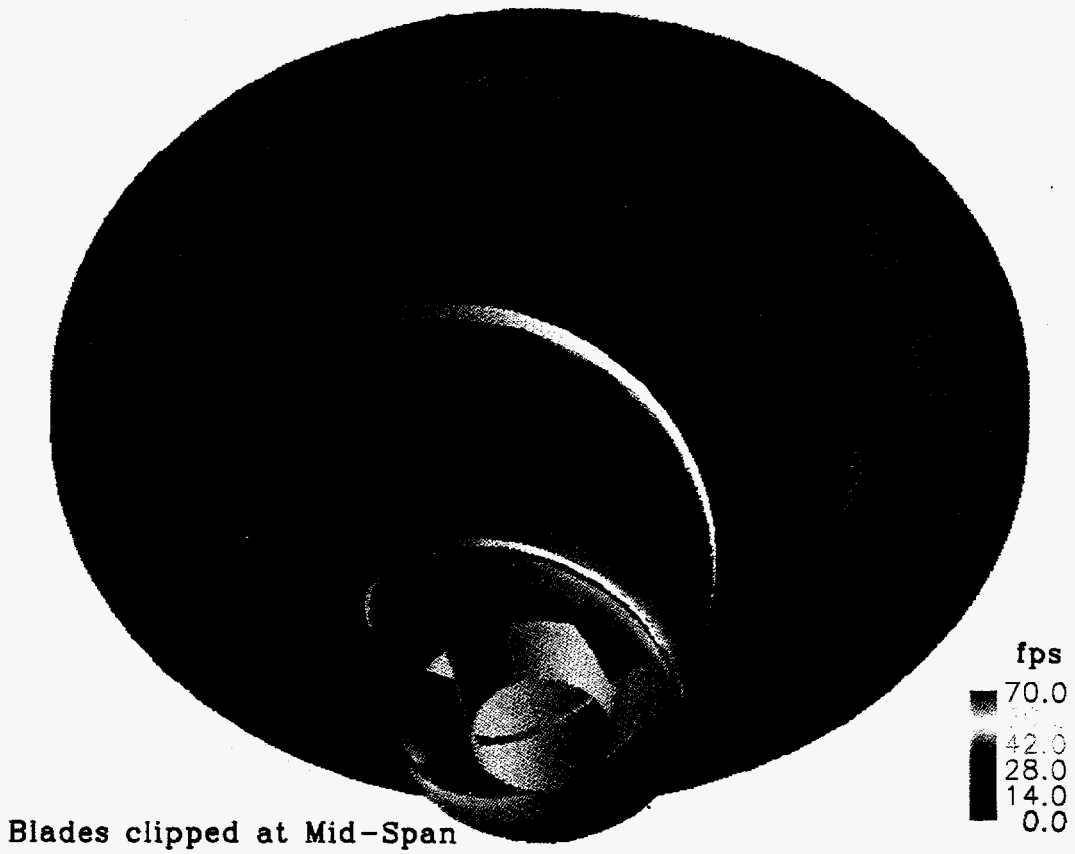

Figure 6-15
Design 3 - Velocity Magnitude at Mid-Span (Defined by Shading)

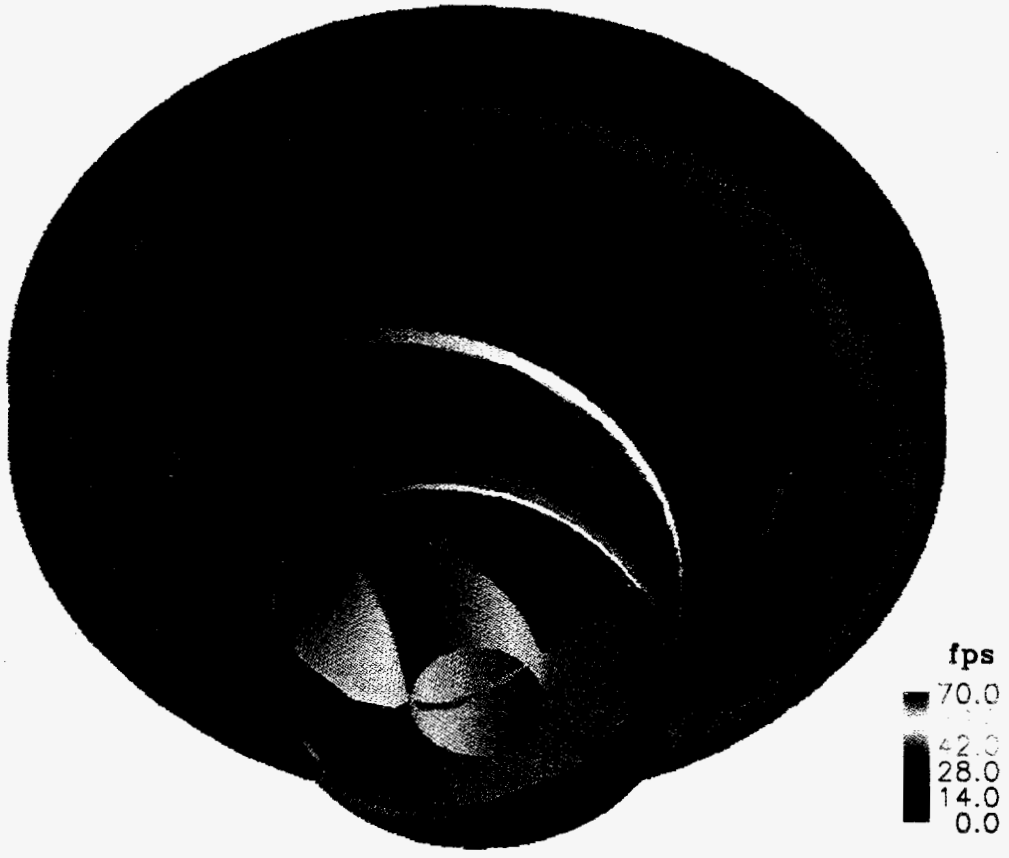

Figure 6-16
Design 3 - Velocity Magnitude Near Shroud (Defined by Shading)

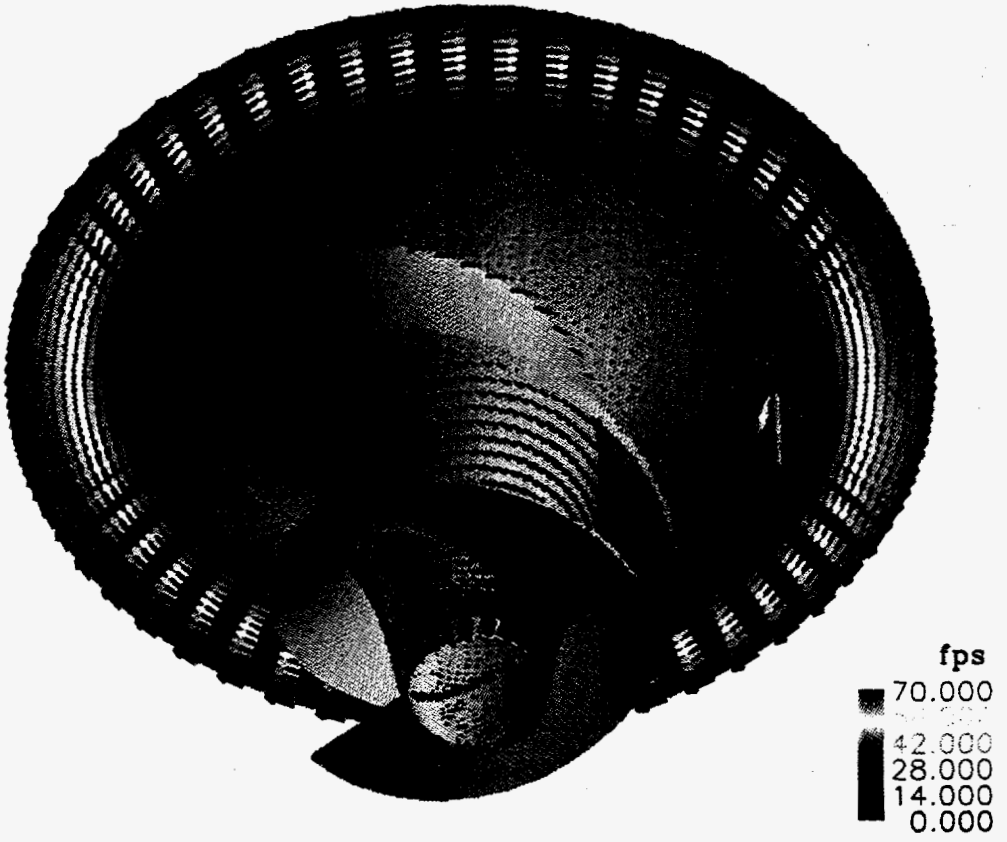

Figure 6-17
Design 3 - Velocity Colored With Speed Near Hub

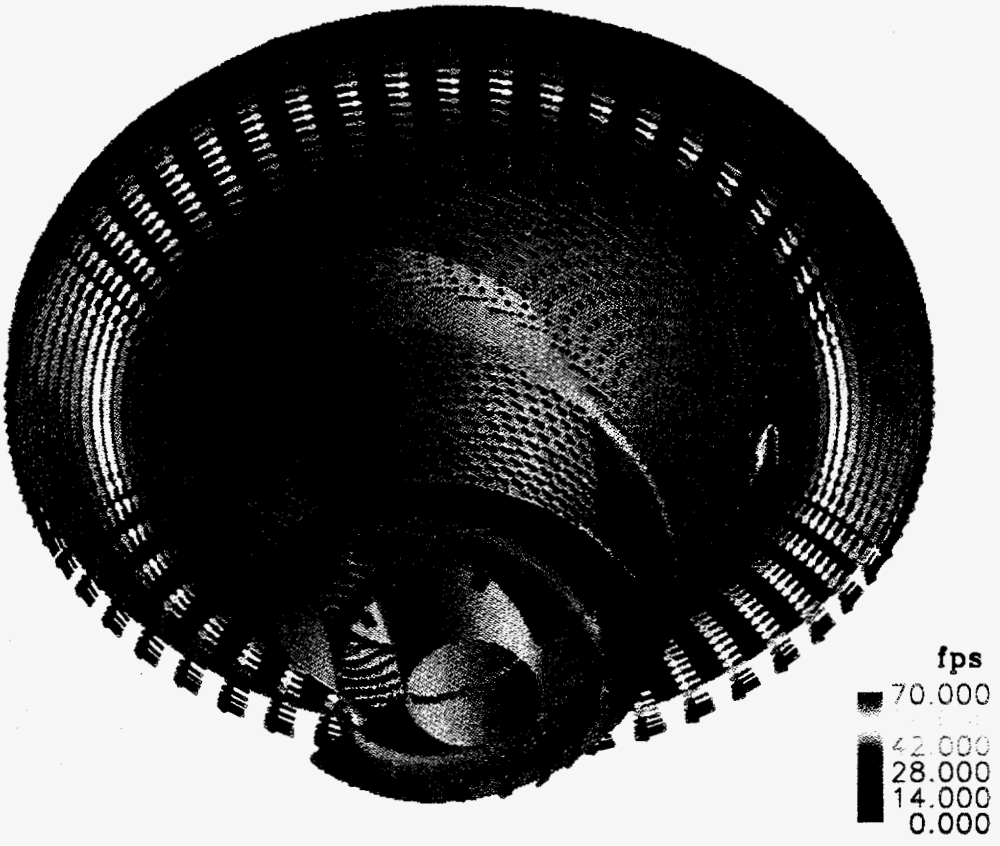

Figure 6-18
Design 3 - Velocity Colored With Speed At Mid-Span

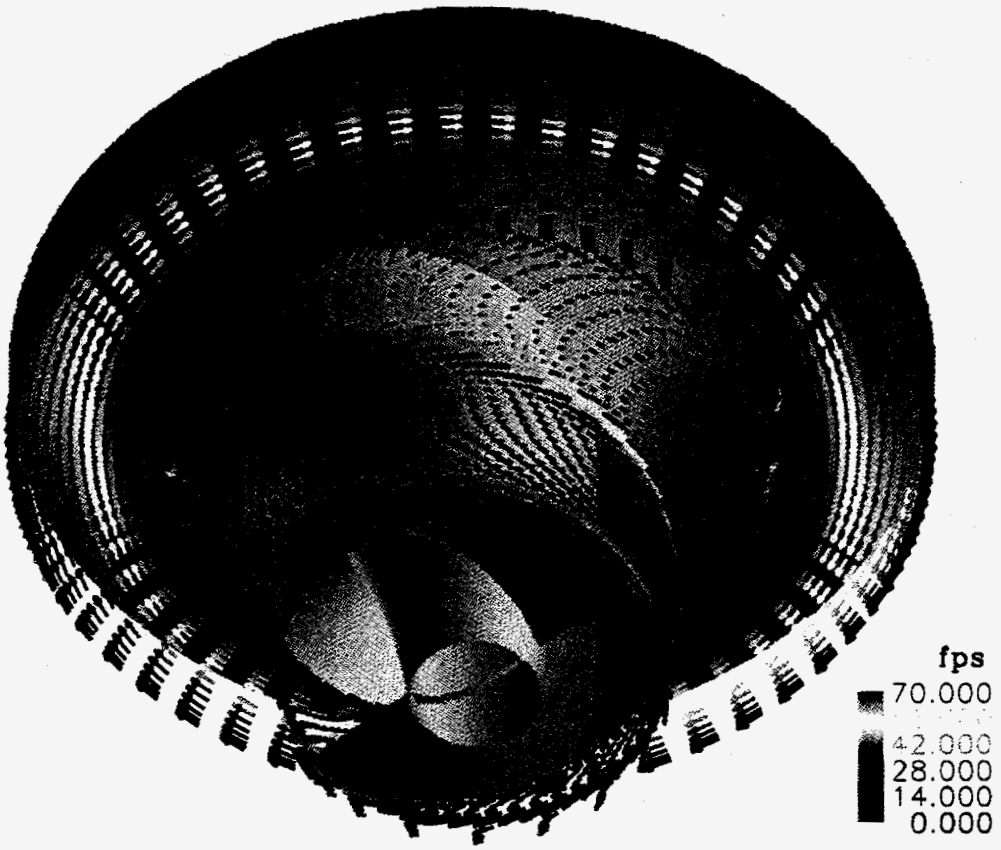

Figure 6-19
Design 3 - Velocity Colored With Speed Near Shroud

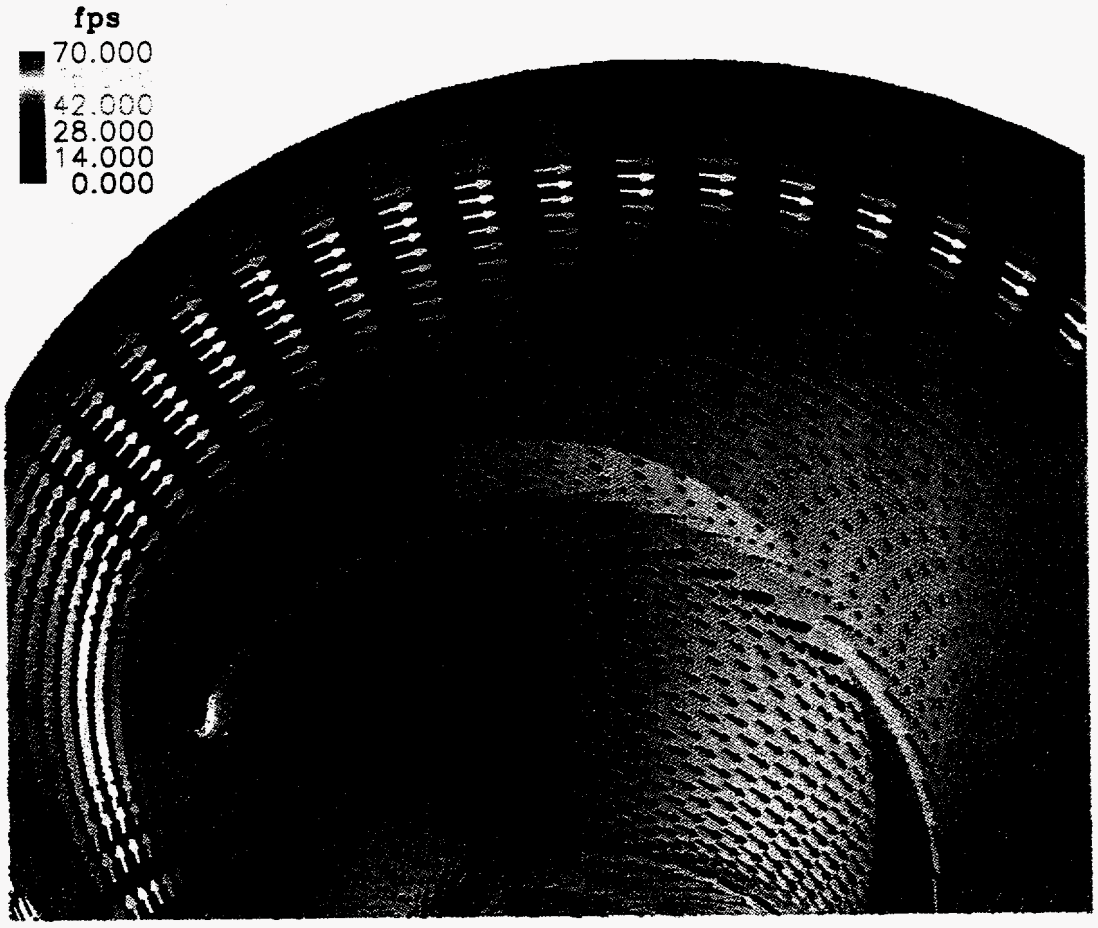

Figure 6-20
Design 3 - Velocity Colored With Speed At Mid-Span

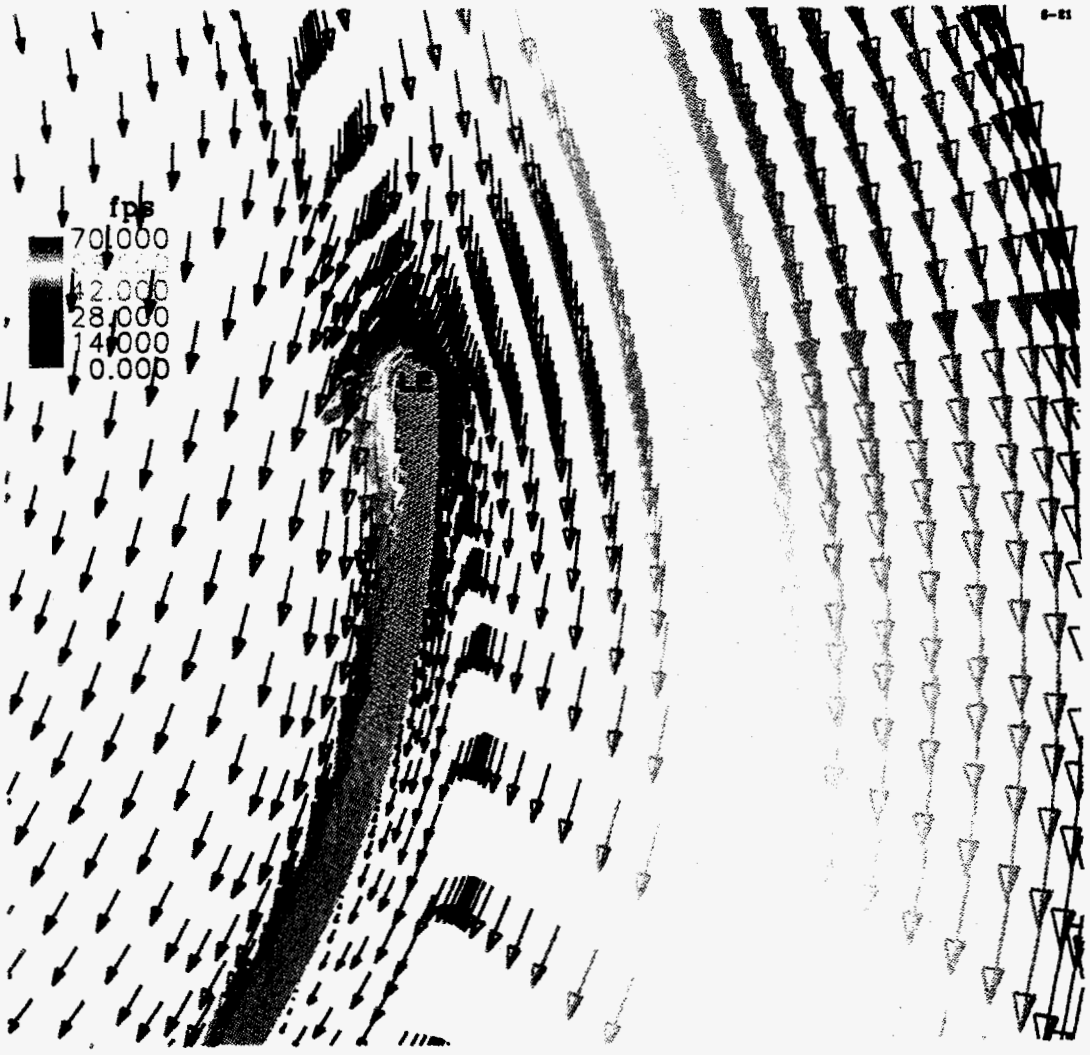

Figure 6-21
Design 3 - Leading Edge Velocity Colored With Speed At Mid-Span

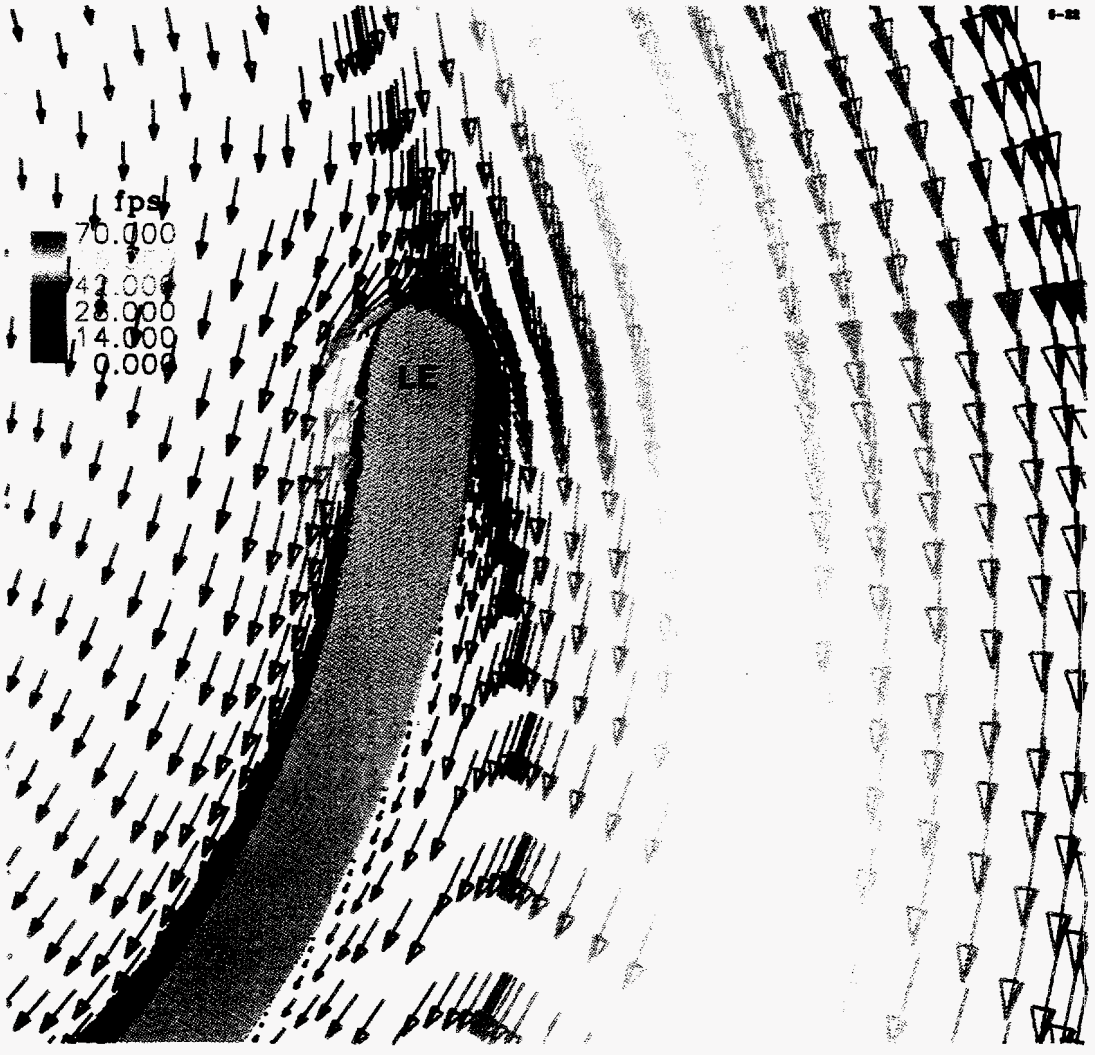

Figure 6-22
Design 1 - Leading Edge Velocity Colored With Speed At Mid-Span

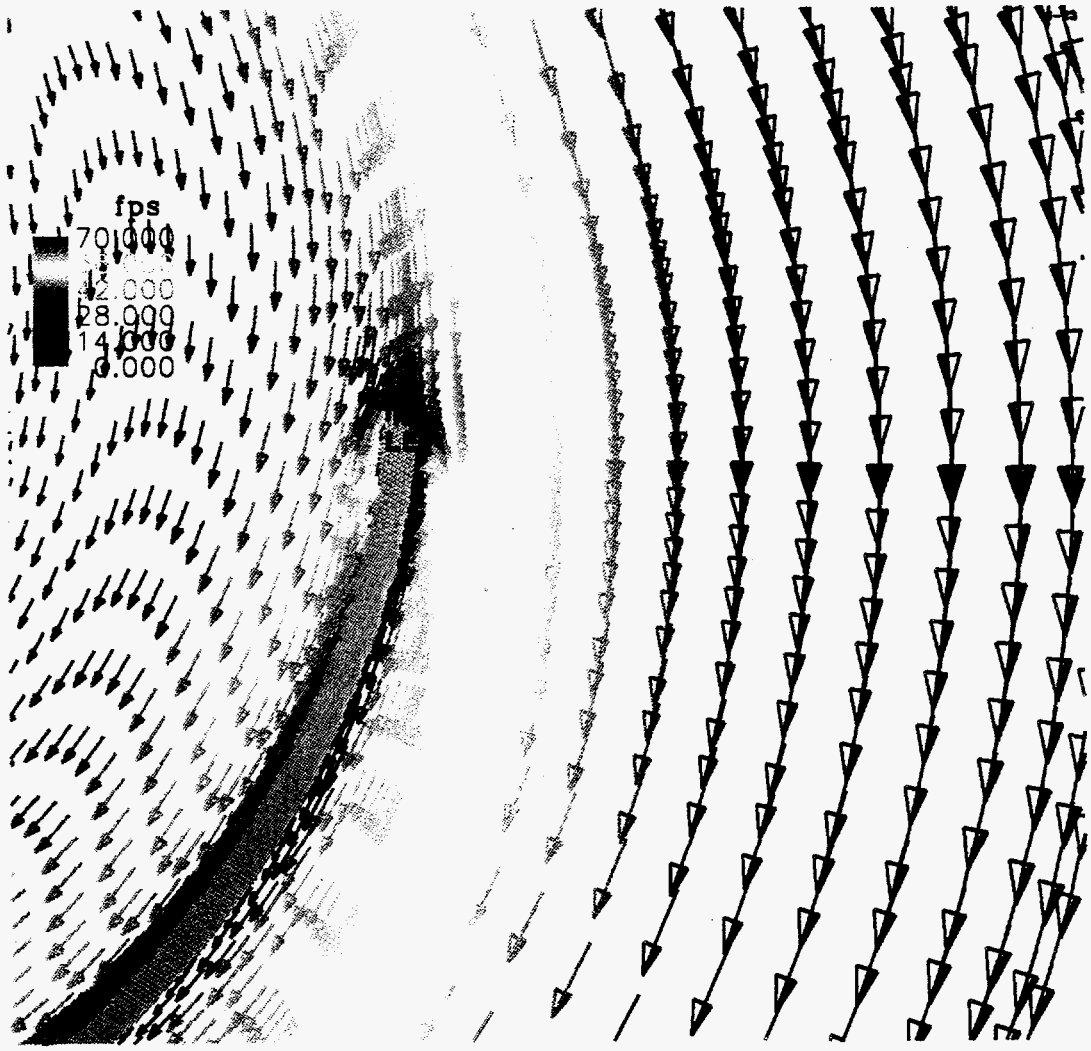

Figure 6-23
Design 2 - Leading Edge Velocity Colored With Speed At Mid-Span

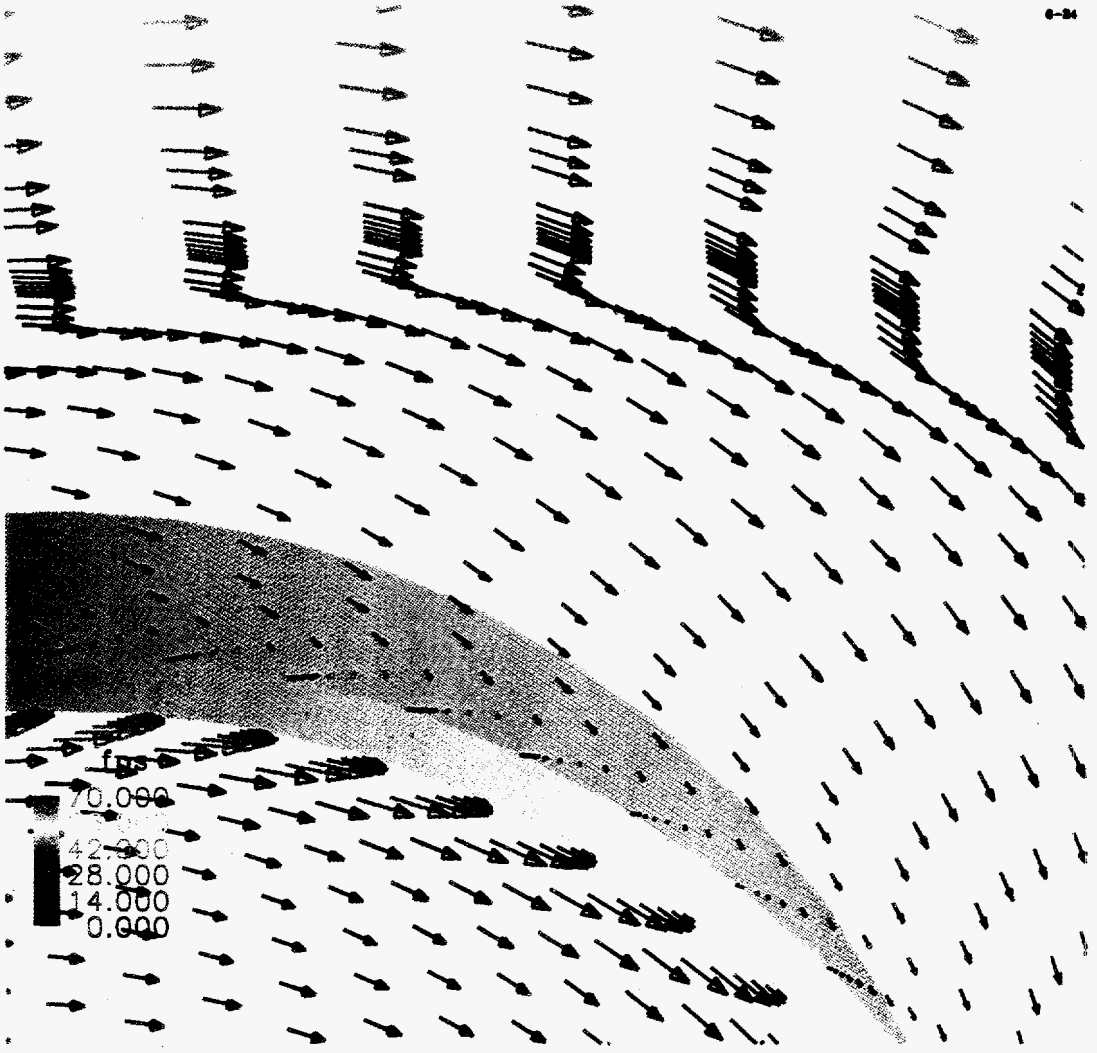

Figure 6-24
Design 3 - Mid-BladeVelocity Colored With Speed At Mid-Span

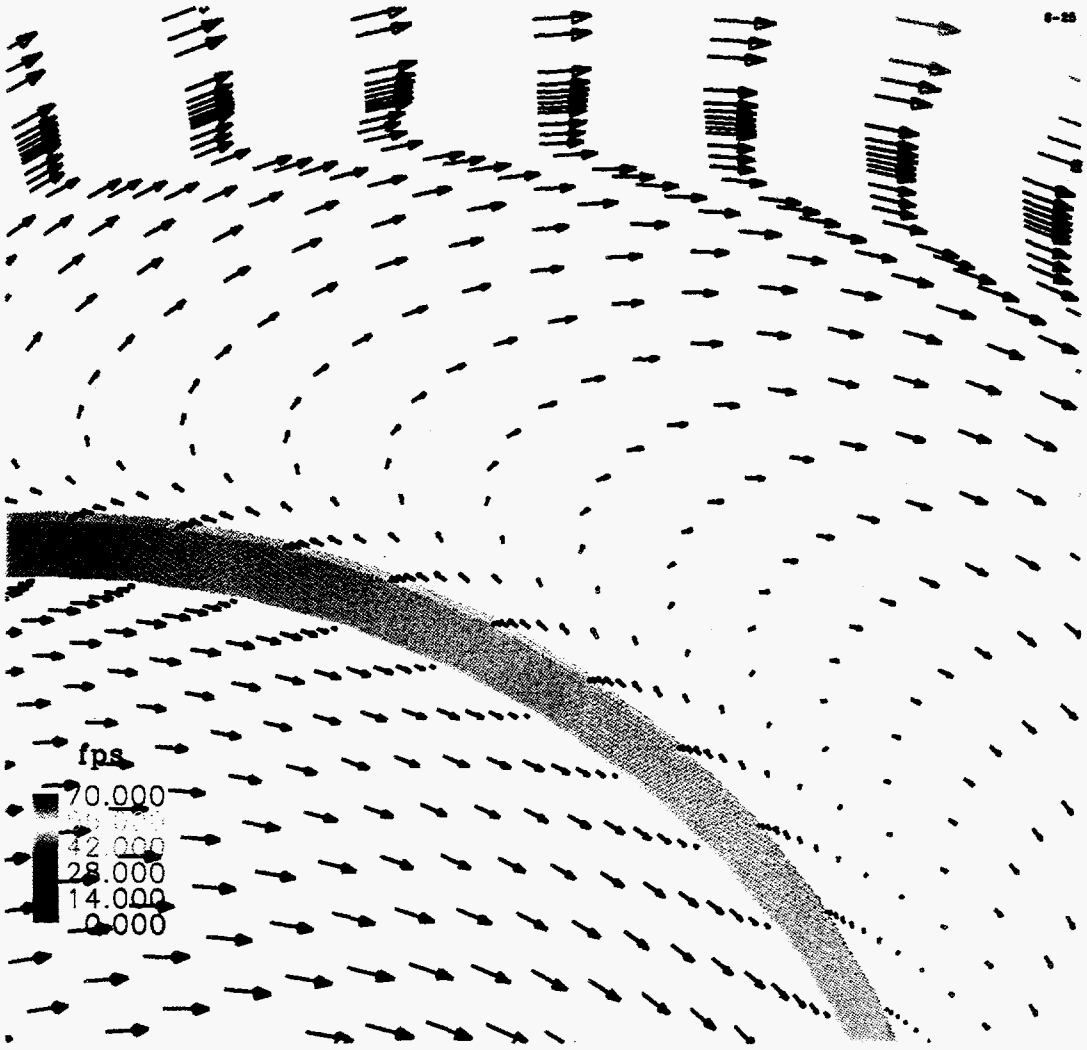

Figure 6-25
Design 3 - Mid-BladeVelocity Colored With Speed Near Hub

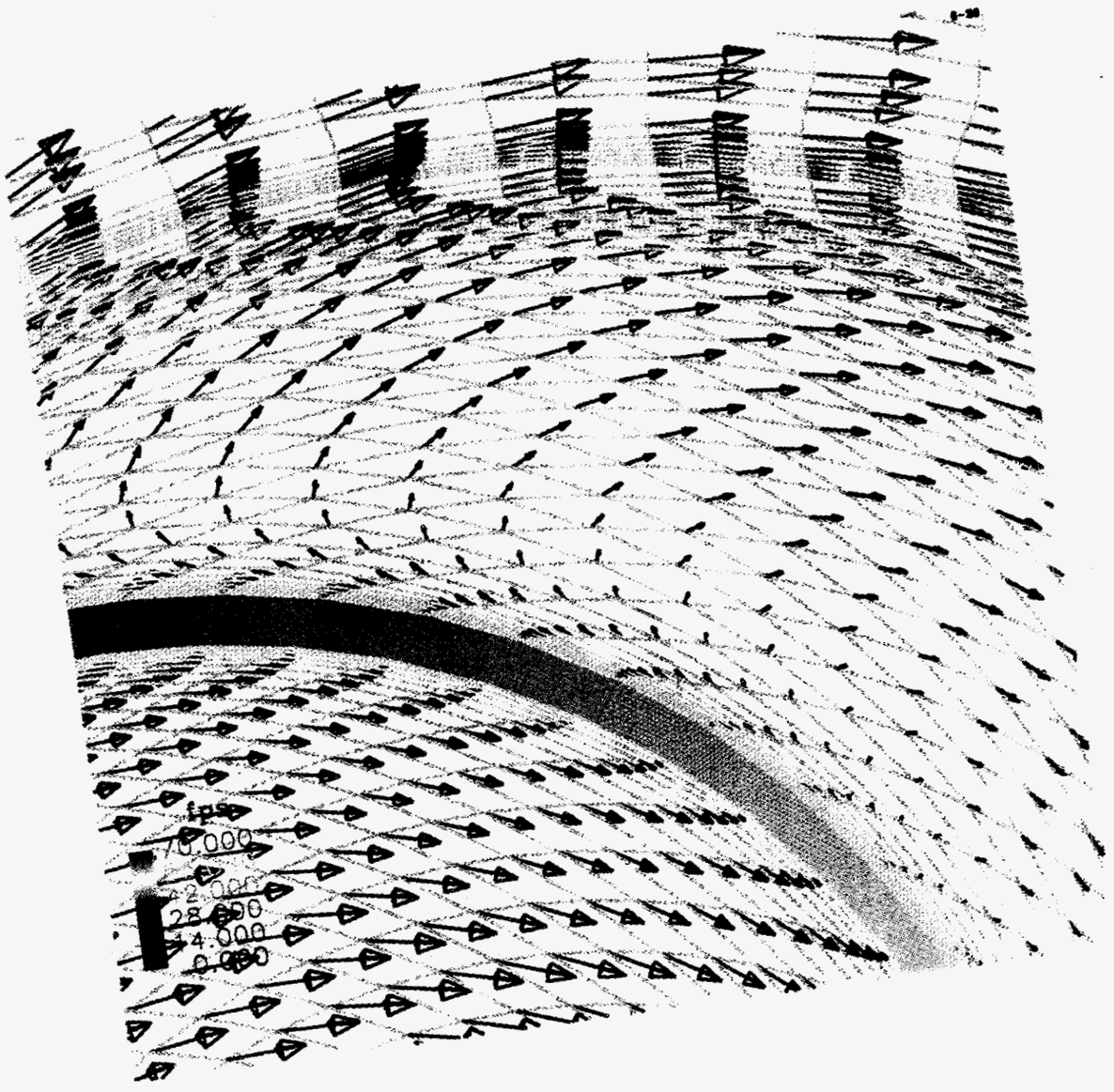

Figure 6-26
Design 3 - Mid-BladeVelocity Colored With Speed Near Hub Scale Magnified

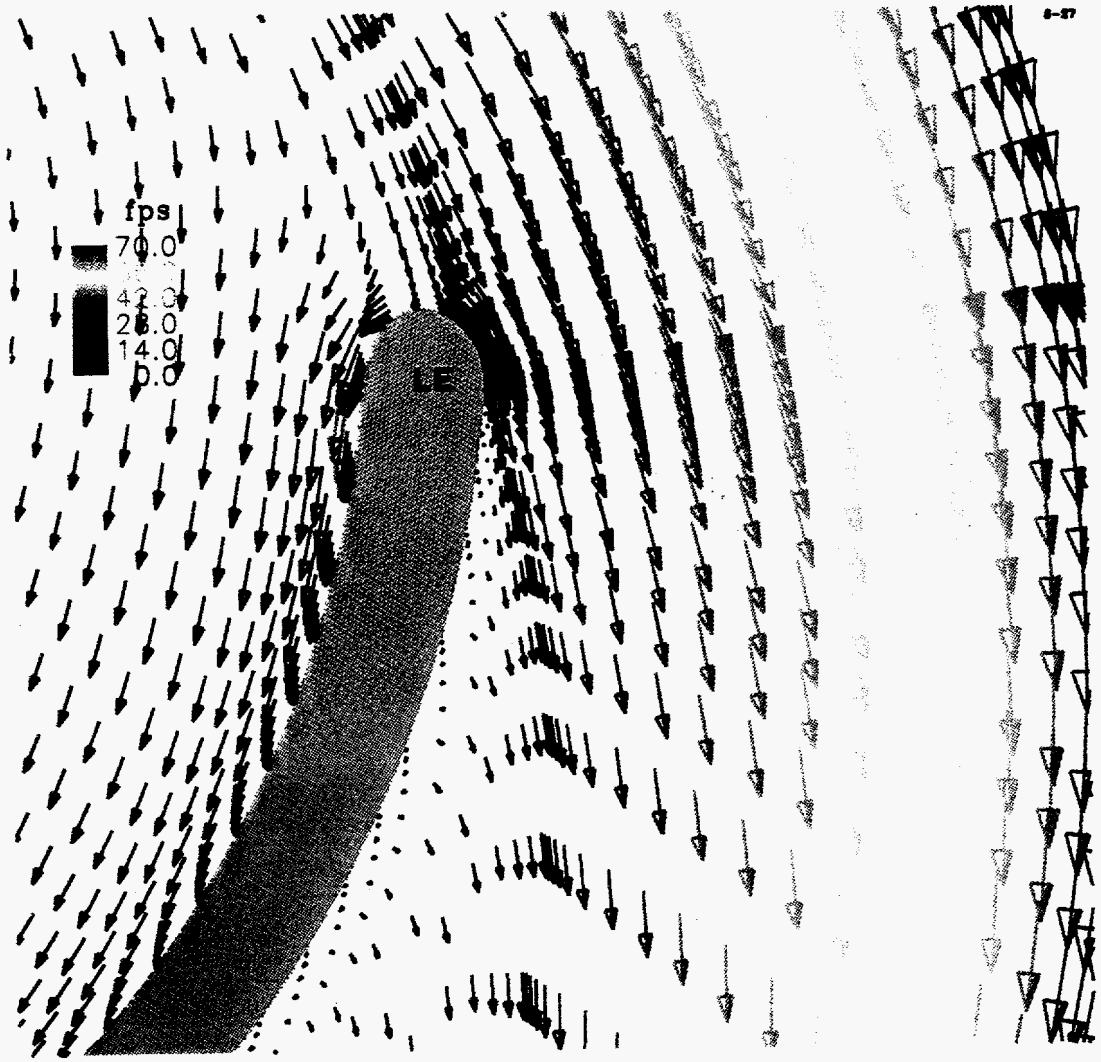

Figure 6-27
Design 1 - Leading Edge Velocity Colored With Speed Near Hub

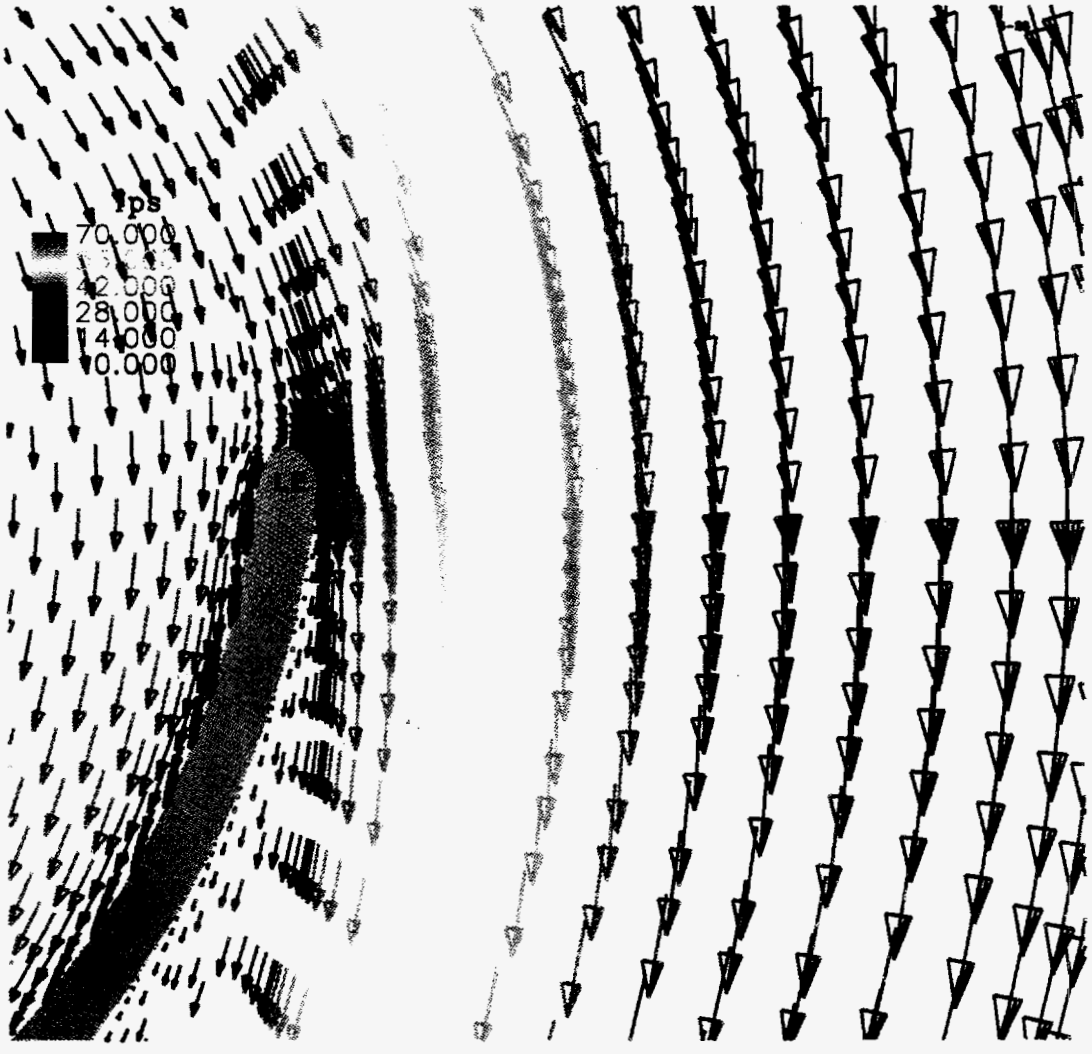

Figure 6-28
Design 2 - Leading Edge Velocity Colored With Speed Near Hub

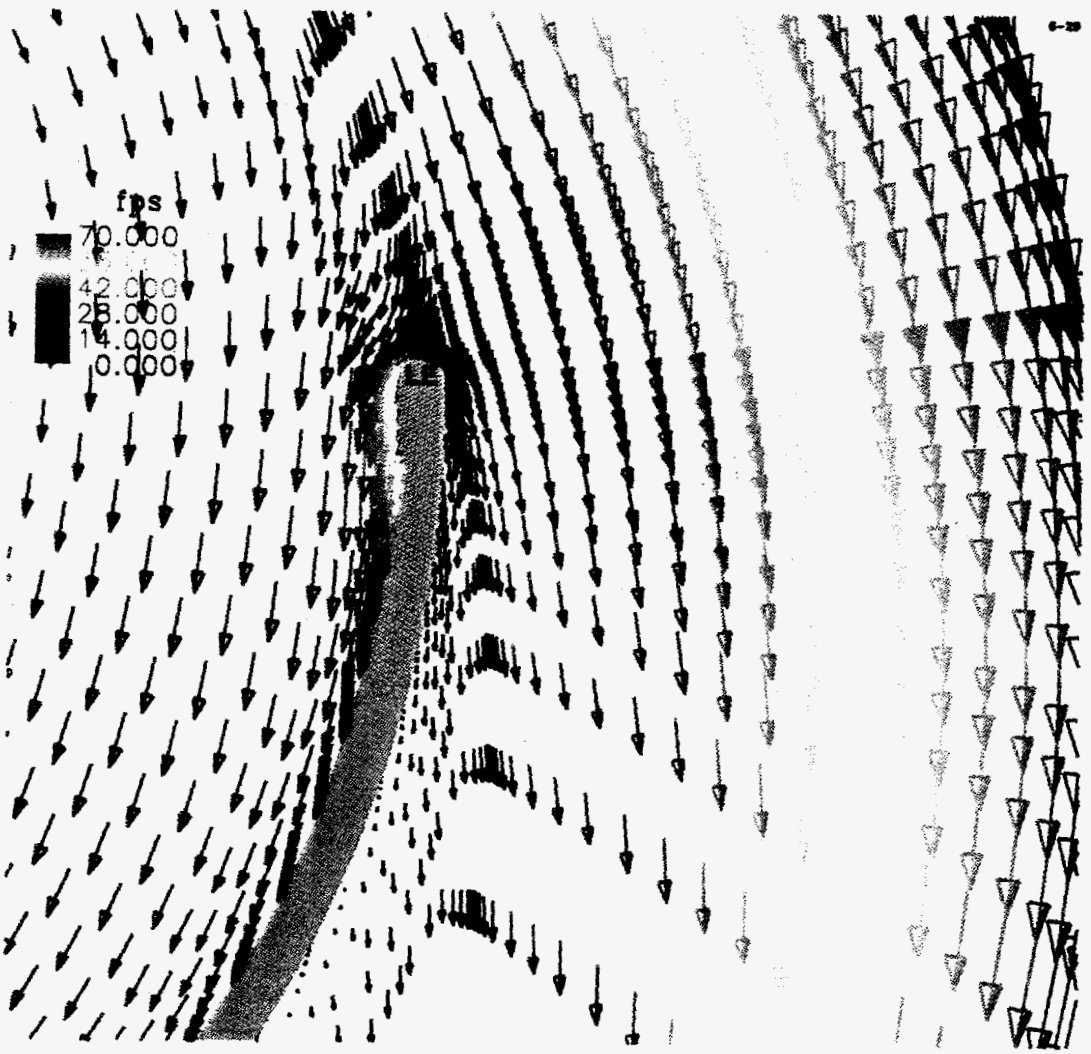

Figure 6-29
Design 3 - Leading Edge Velocity Colored With Speed Near Hub

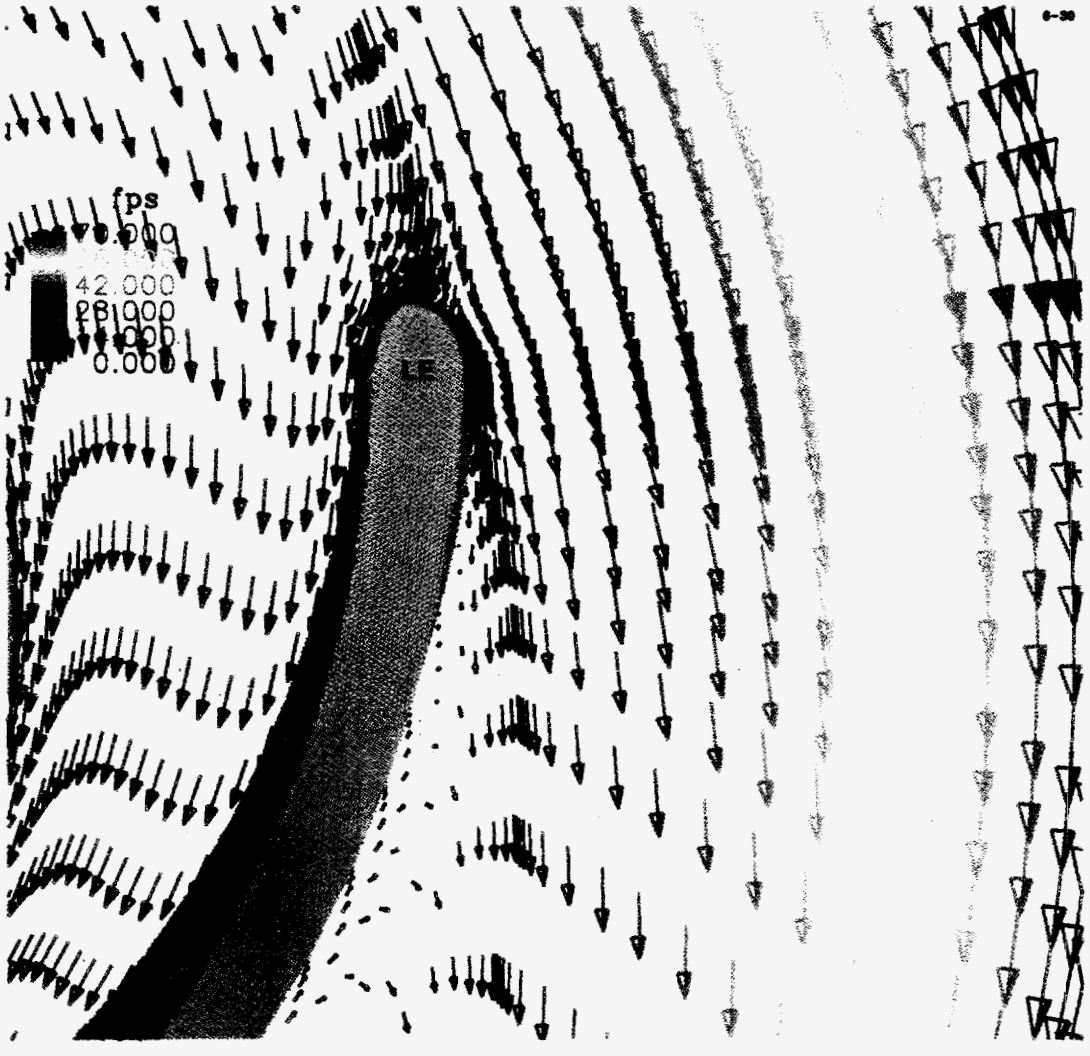

Figure 6-30
Design 1 - Leading Edge Velocity Colored With Speed Near Shroud

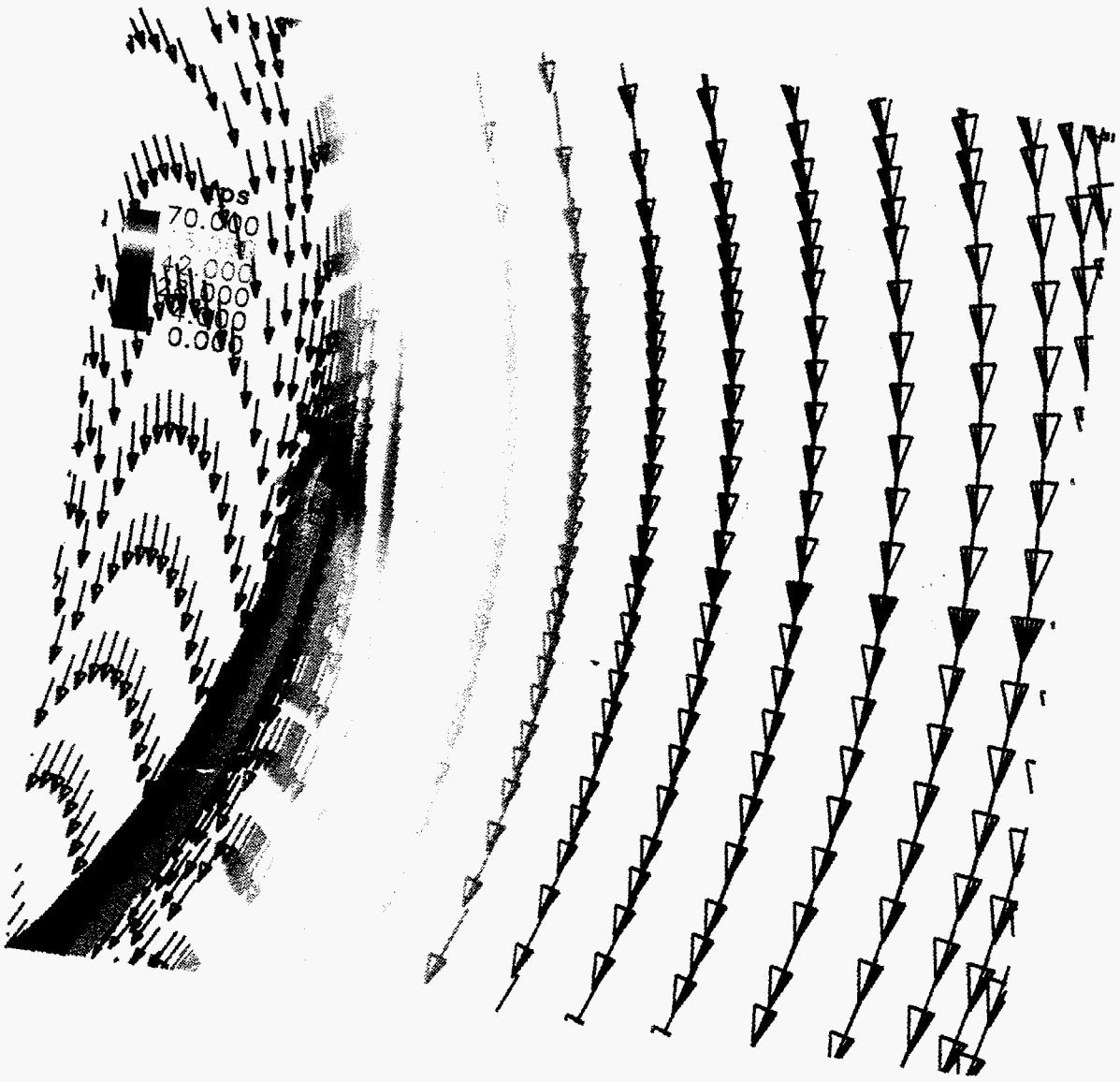

Figure 6-31
Design 2 - Leading Edge Velocity Colored With Speed Near Shroud

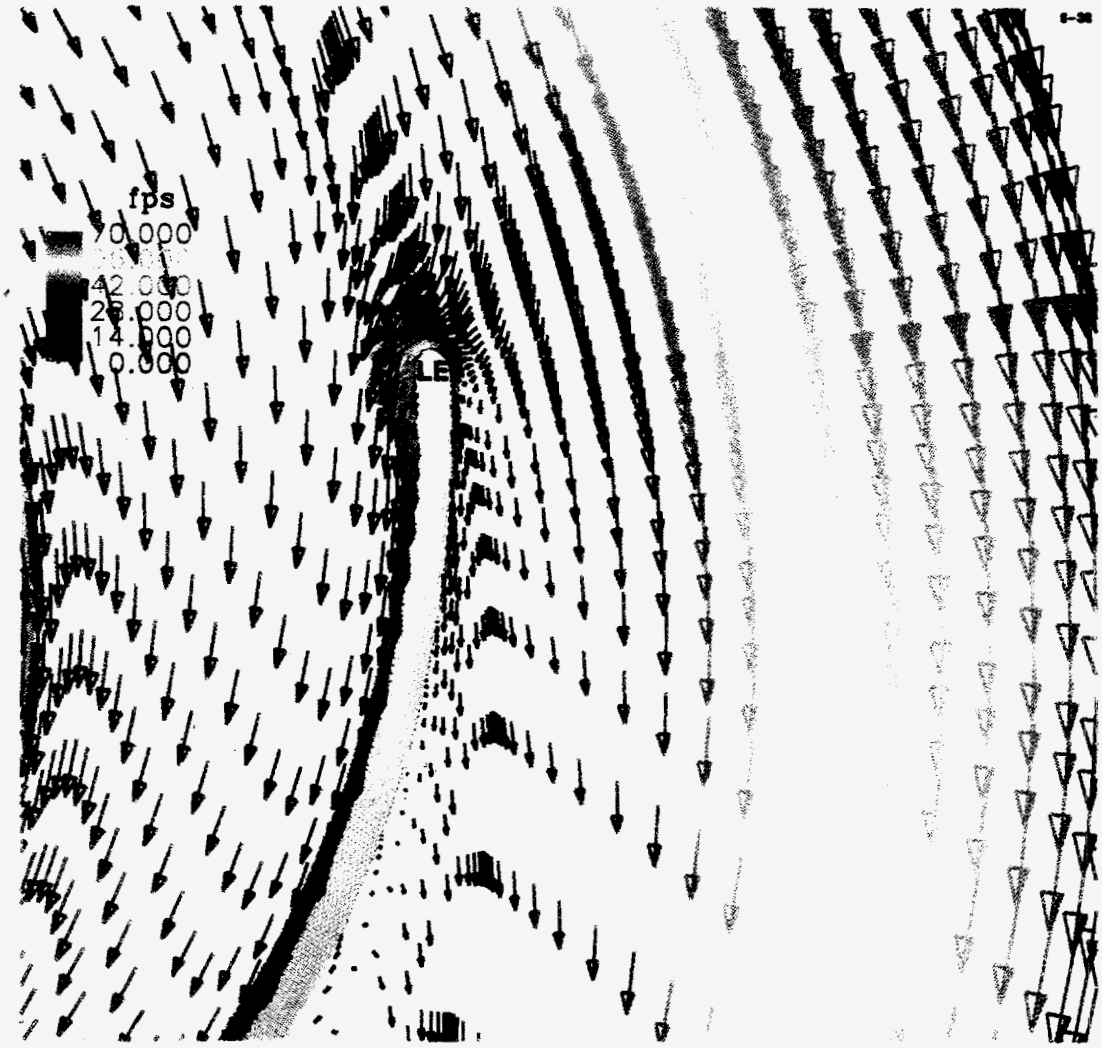

Figure 6-32
Design 3 - Leading Edge Velocity Colored With Speed Near Shroud

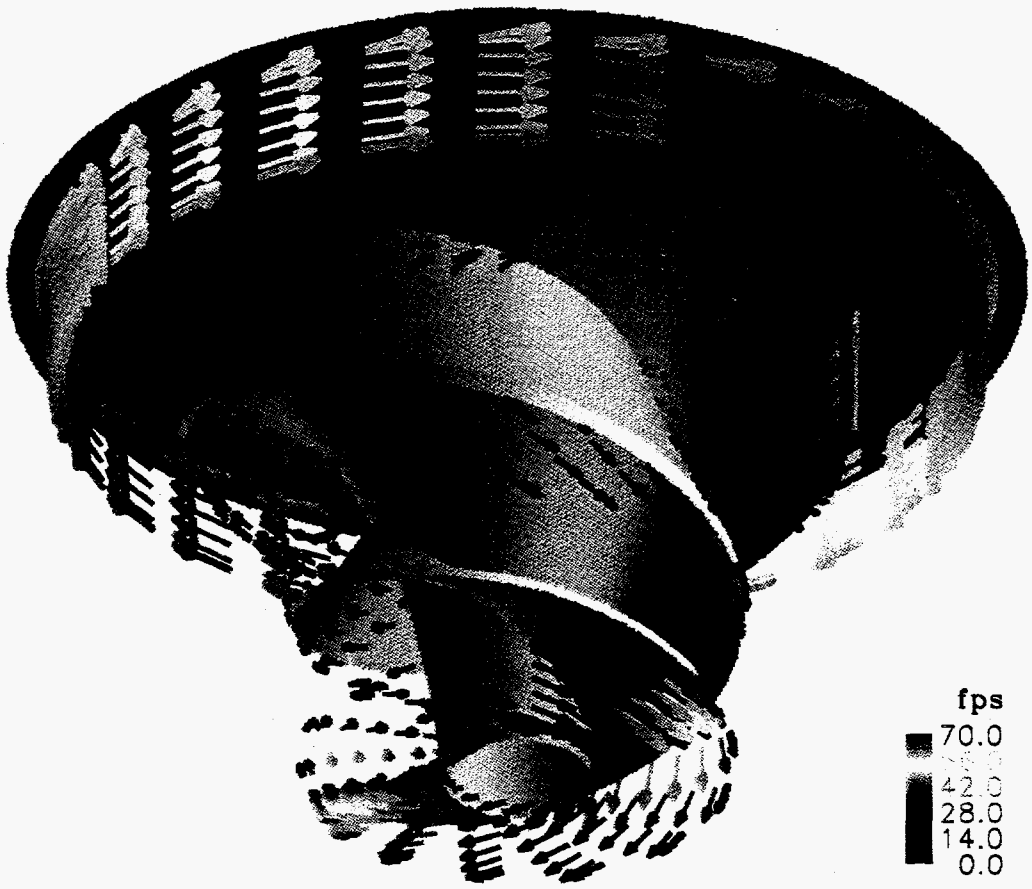

Figure 6-33
Design 3 - Velocity Vectors Colored With Speed

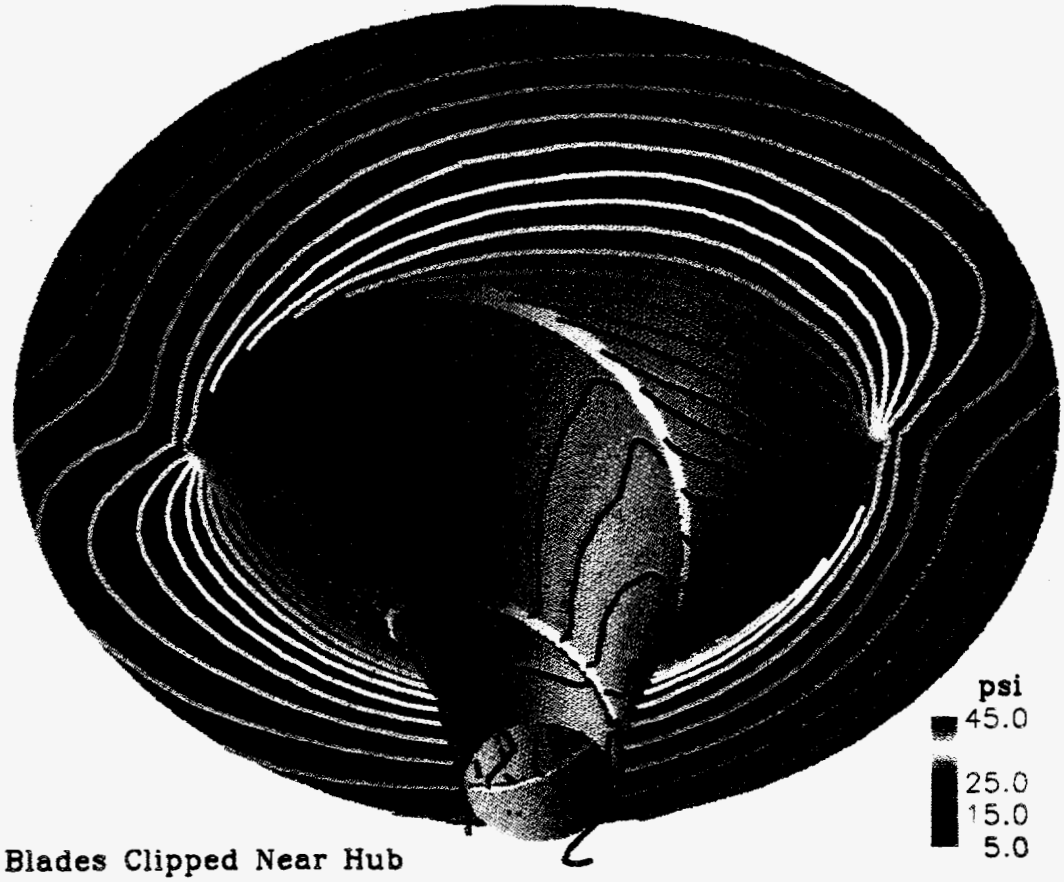

Figure 6-34
Design 3 - Pressure Near Hub

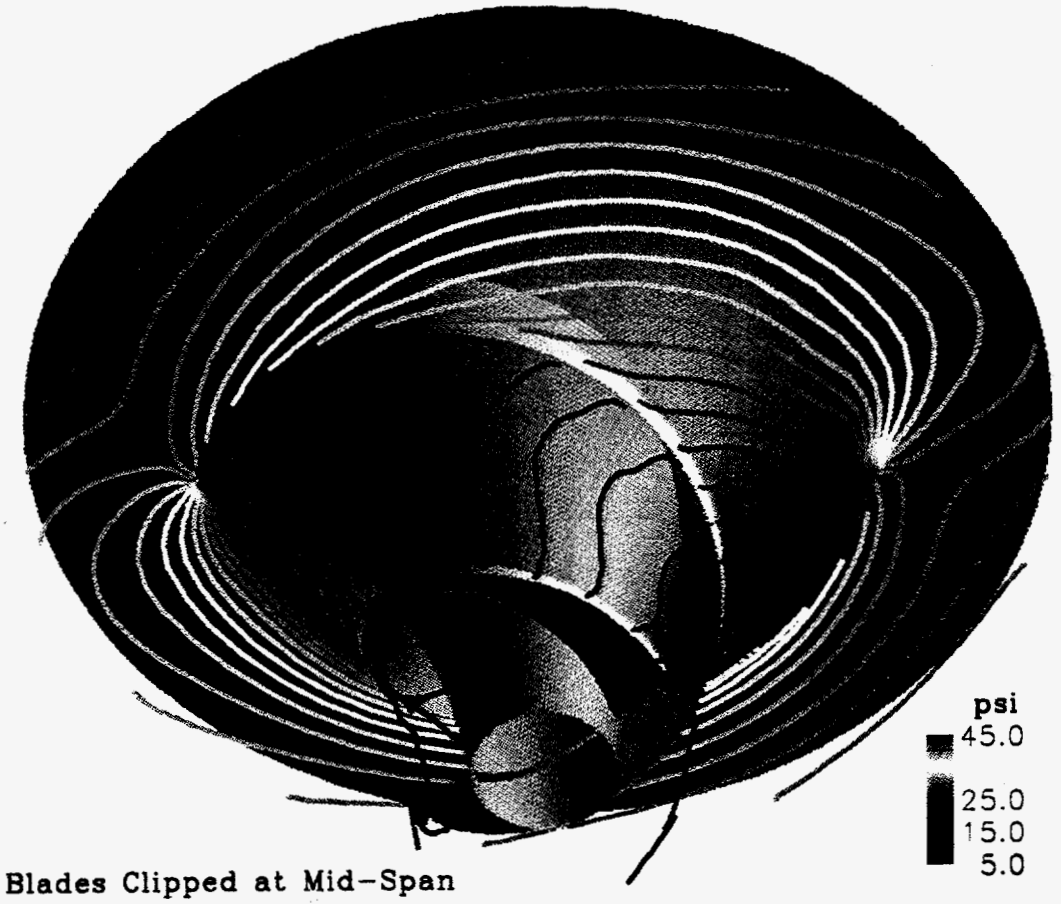

Figure 6-35
Design 3 - Pressure At Mid-Span

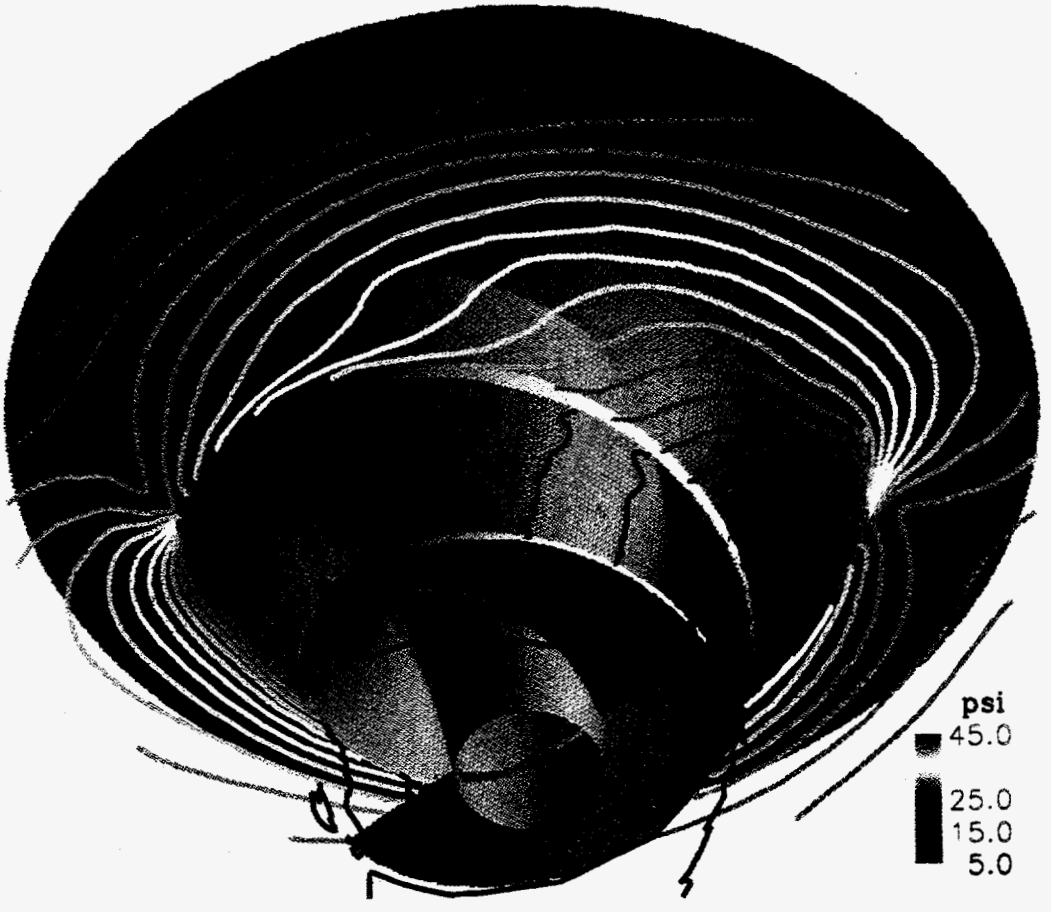

Figure 6-36
Design 3 - Pressure Near Shroud

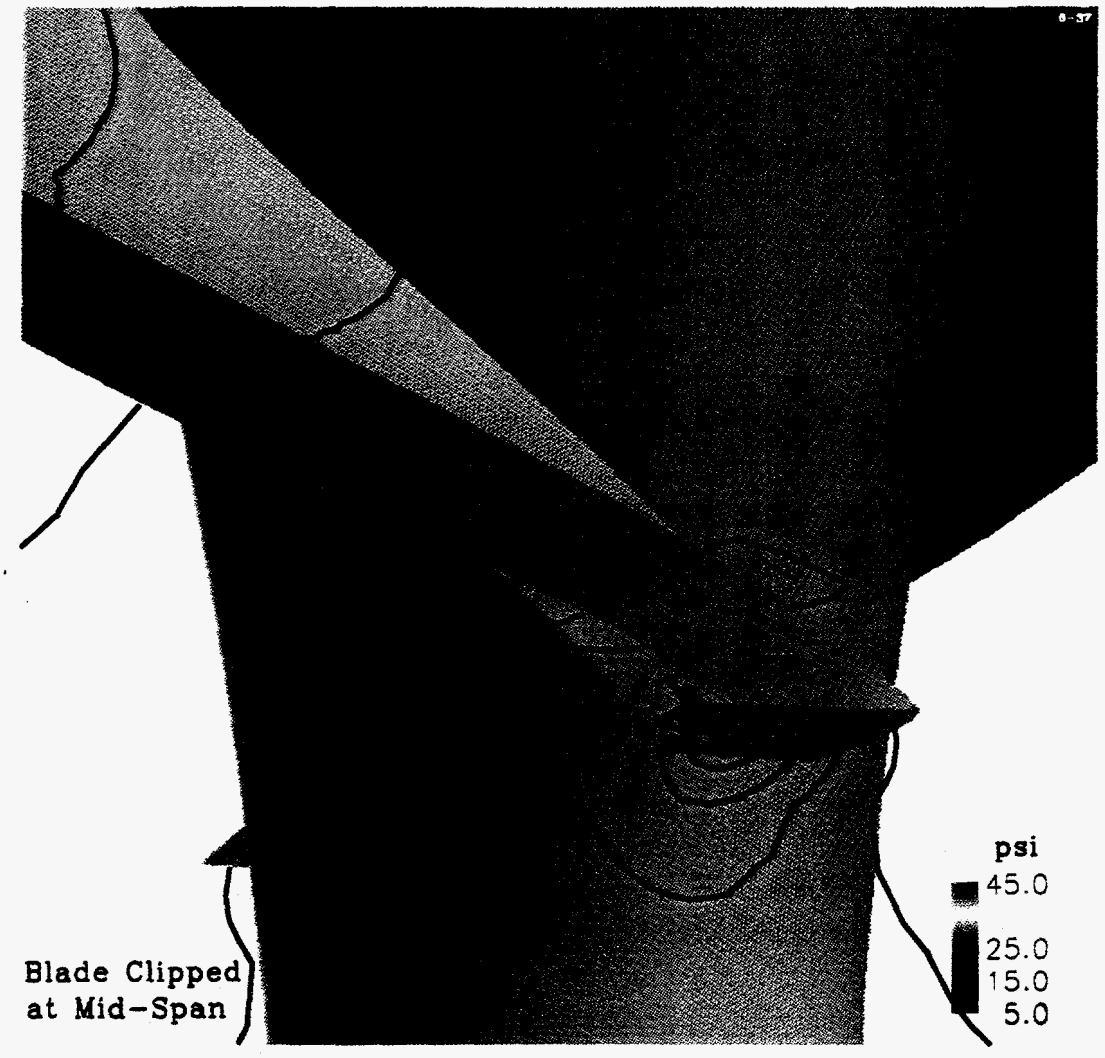

Figure 6-37
Design 1 - Trailing Edge Pressure At Mid-Span

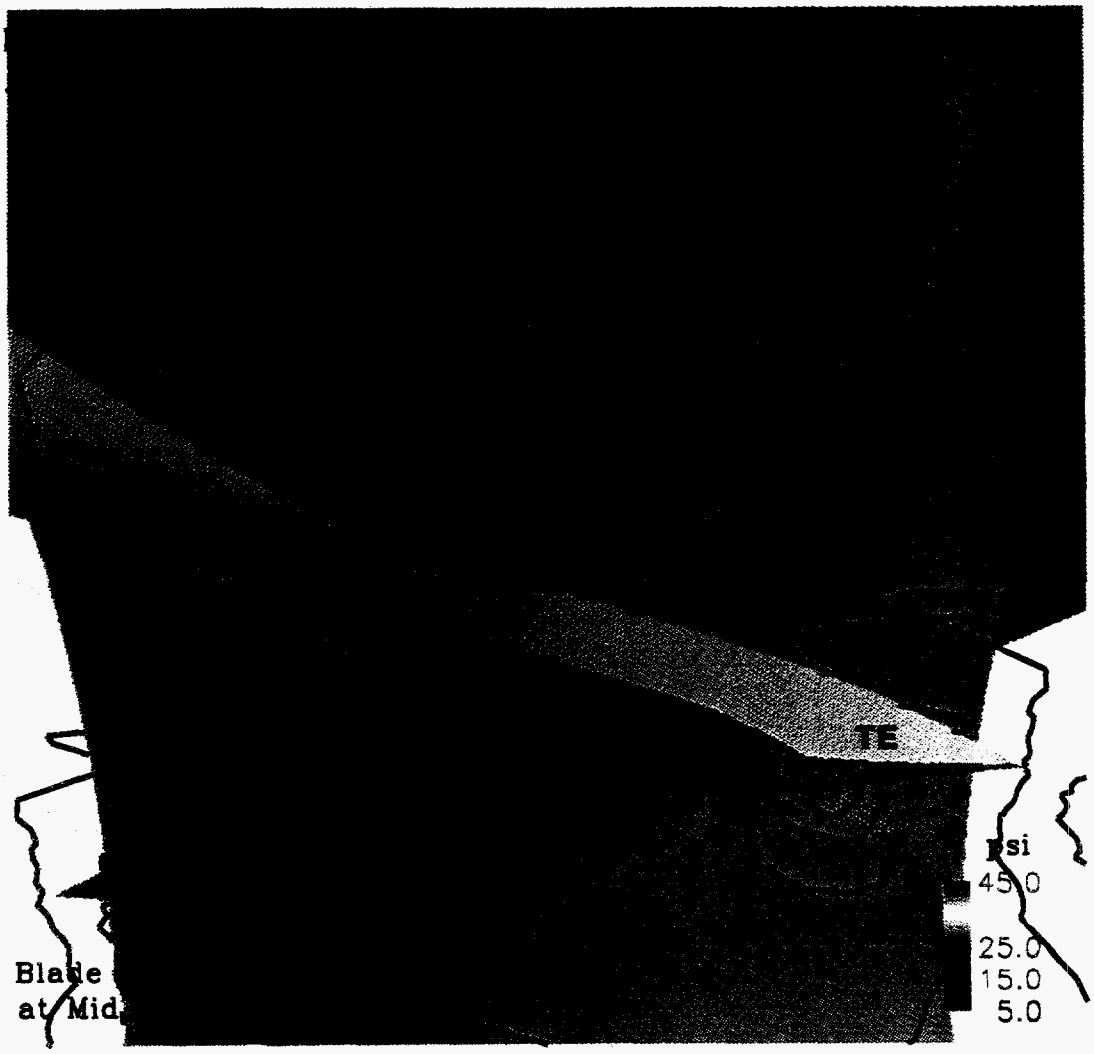

Figure 6-38
Design 2 - Trailing Edge Pressure At Mid-Span

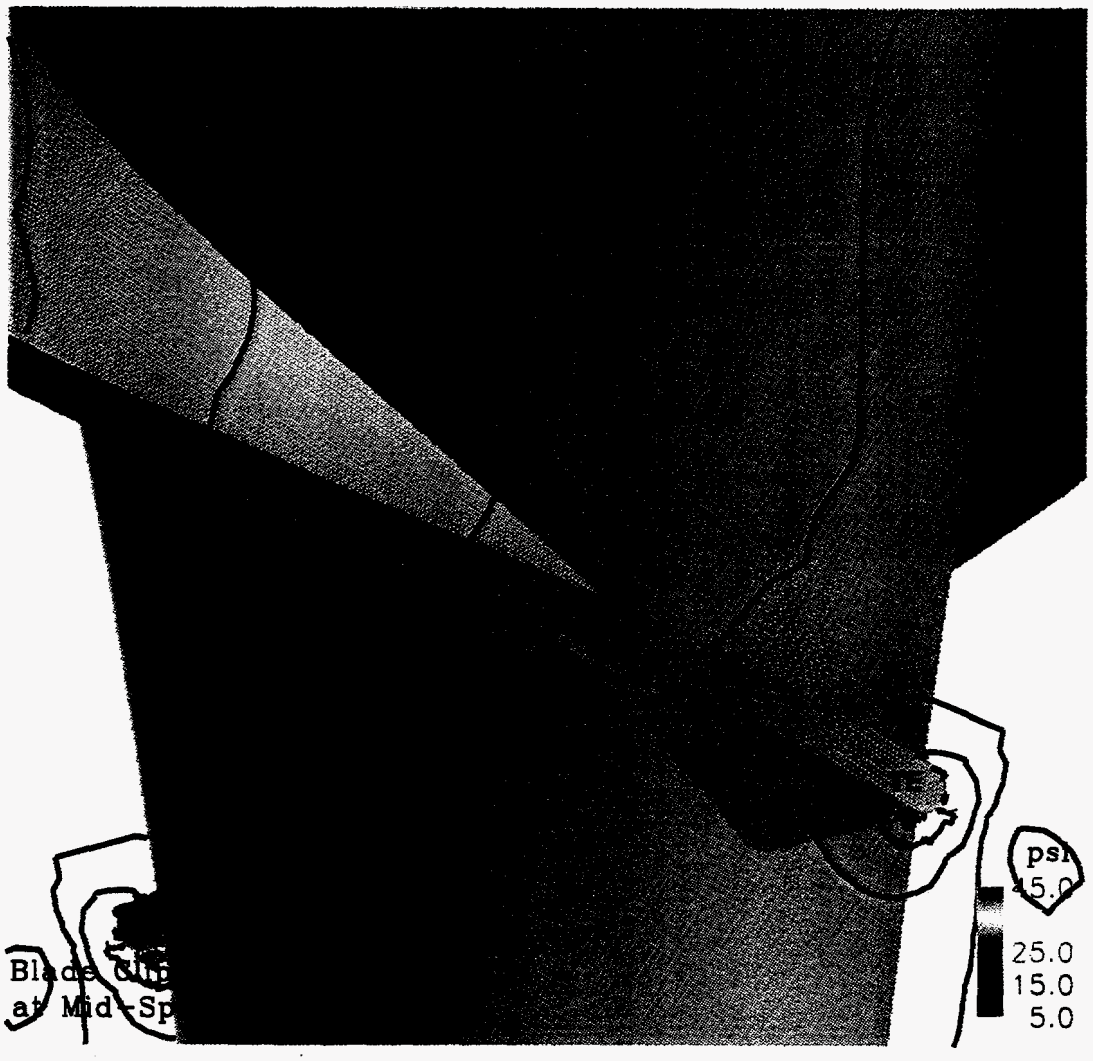

Figure 6-39
Design 3 - Trailing Edge Pressure At Mid-Span

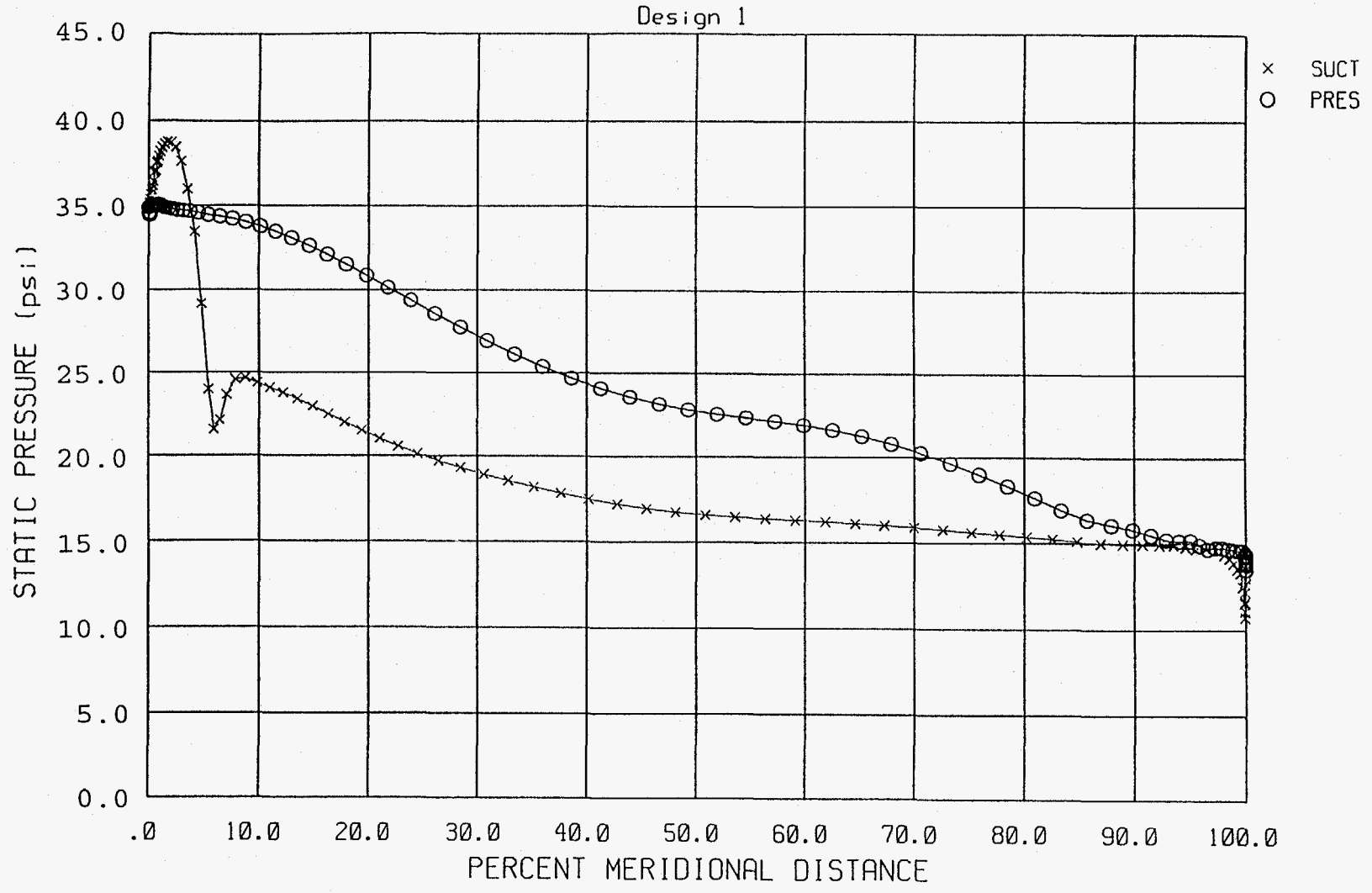

Figure 6-40
Design 1 - Pressure Loading Diagram At Hub

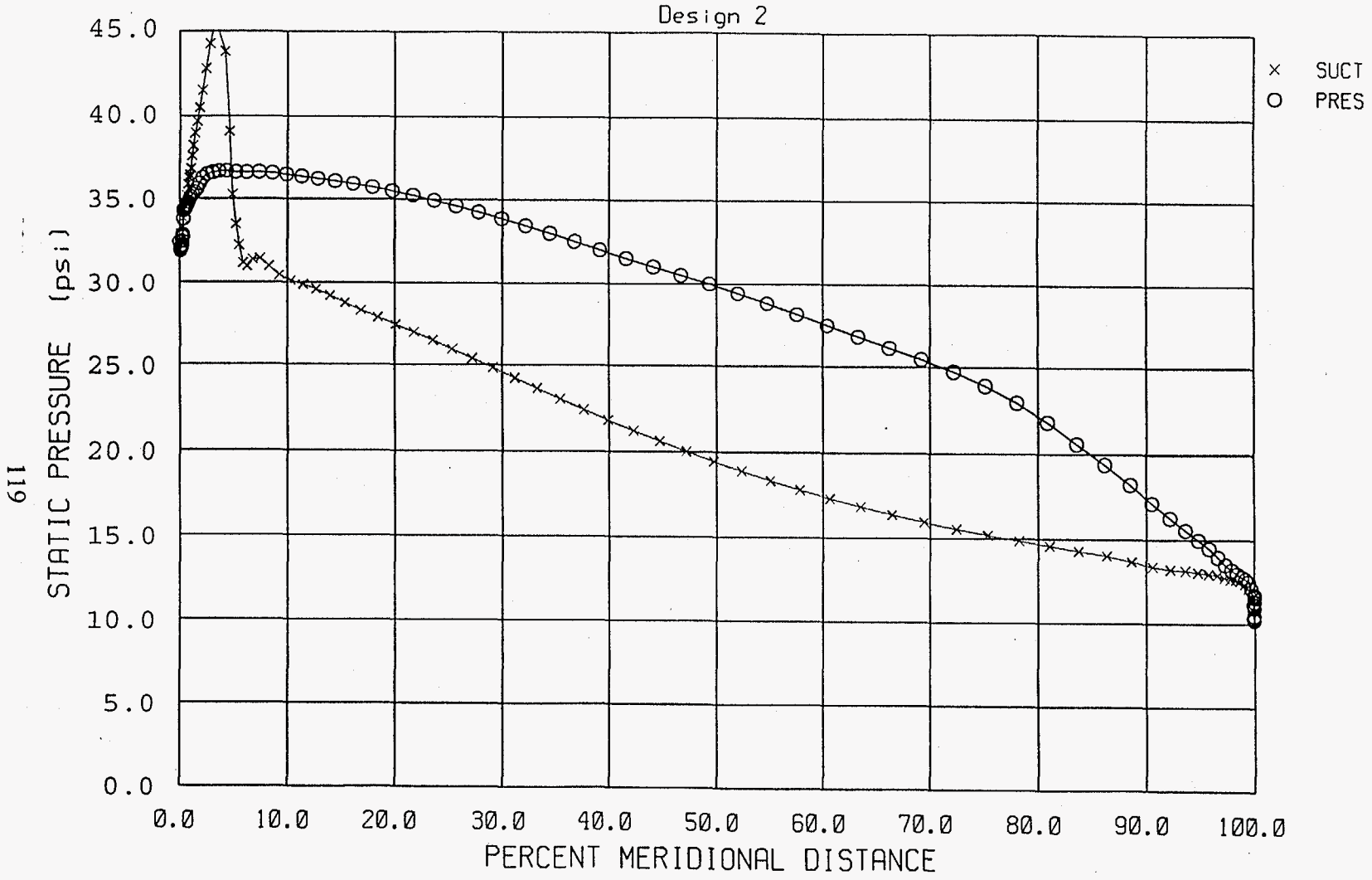

Figure 6-41
Design 2 - Pressure Loading Diagram At Hub

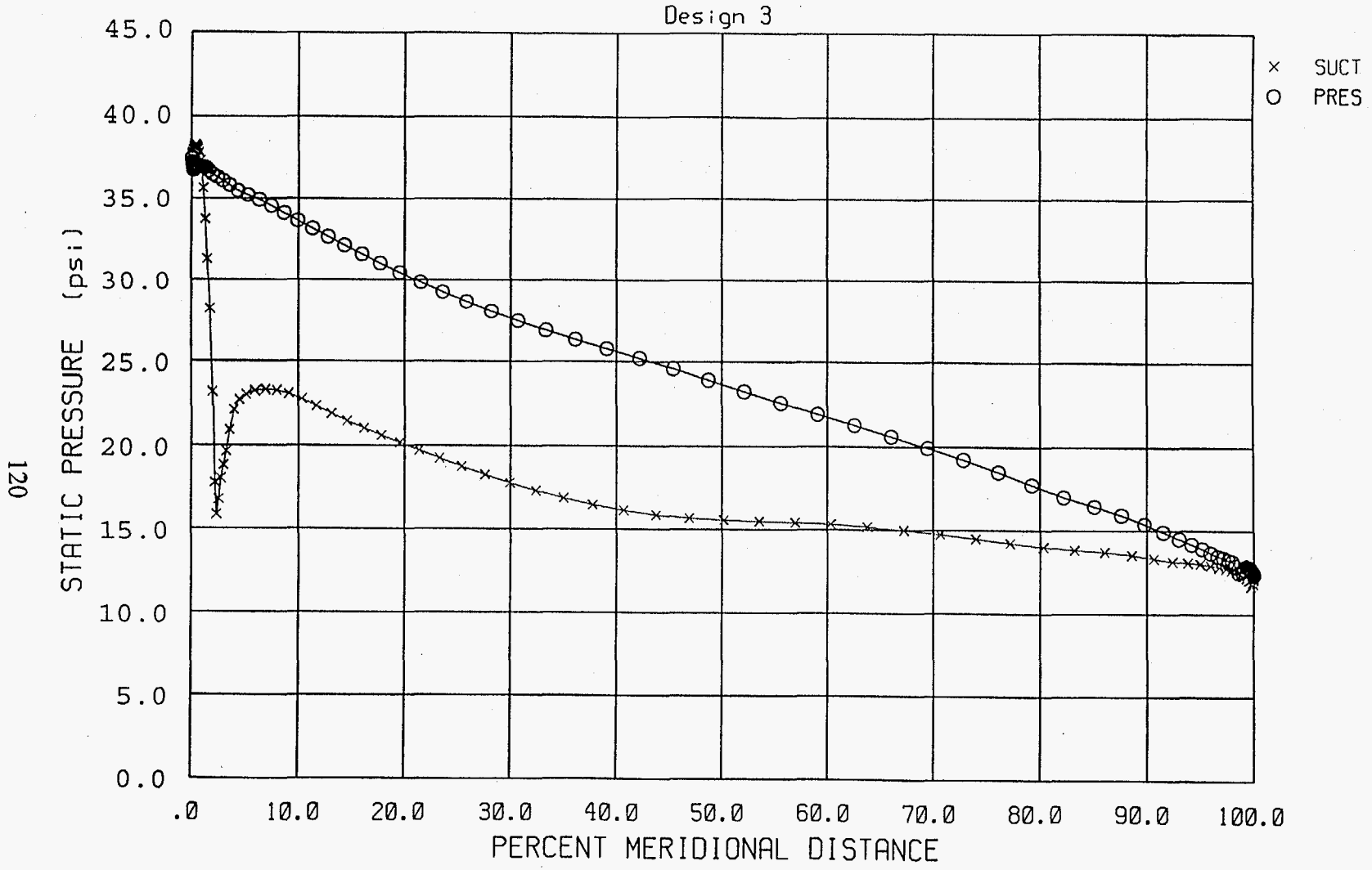

120

Figure 6-42
Design 3 - Pressure Loading Diagram At Hub

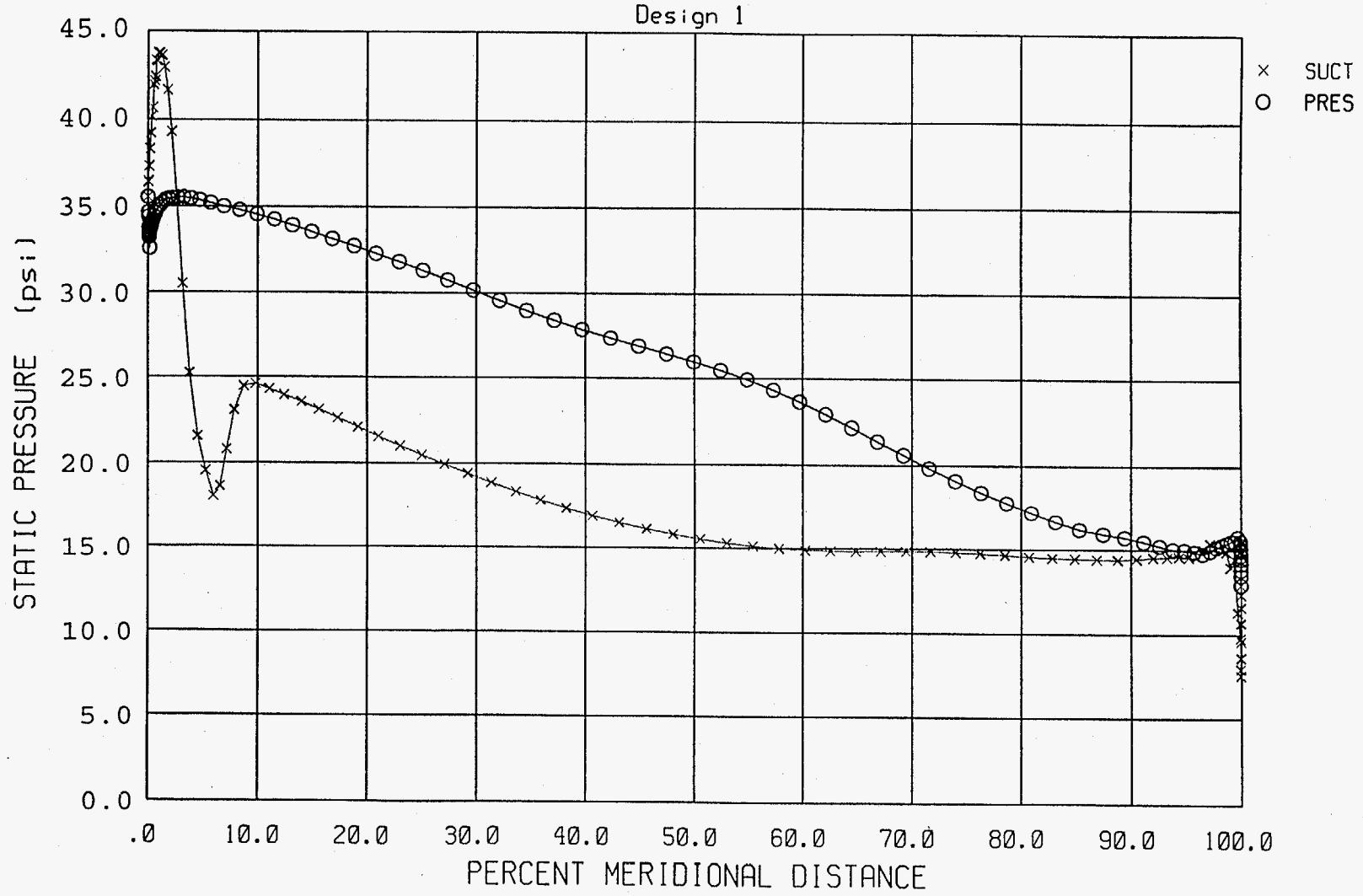

Figure 6-43
Design 1 - Pressure Loading Diagram At Mid-Span

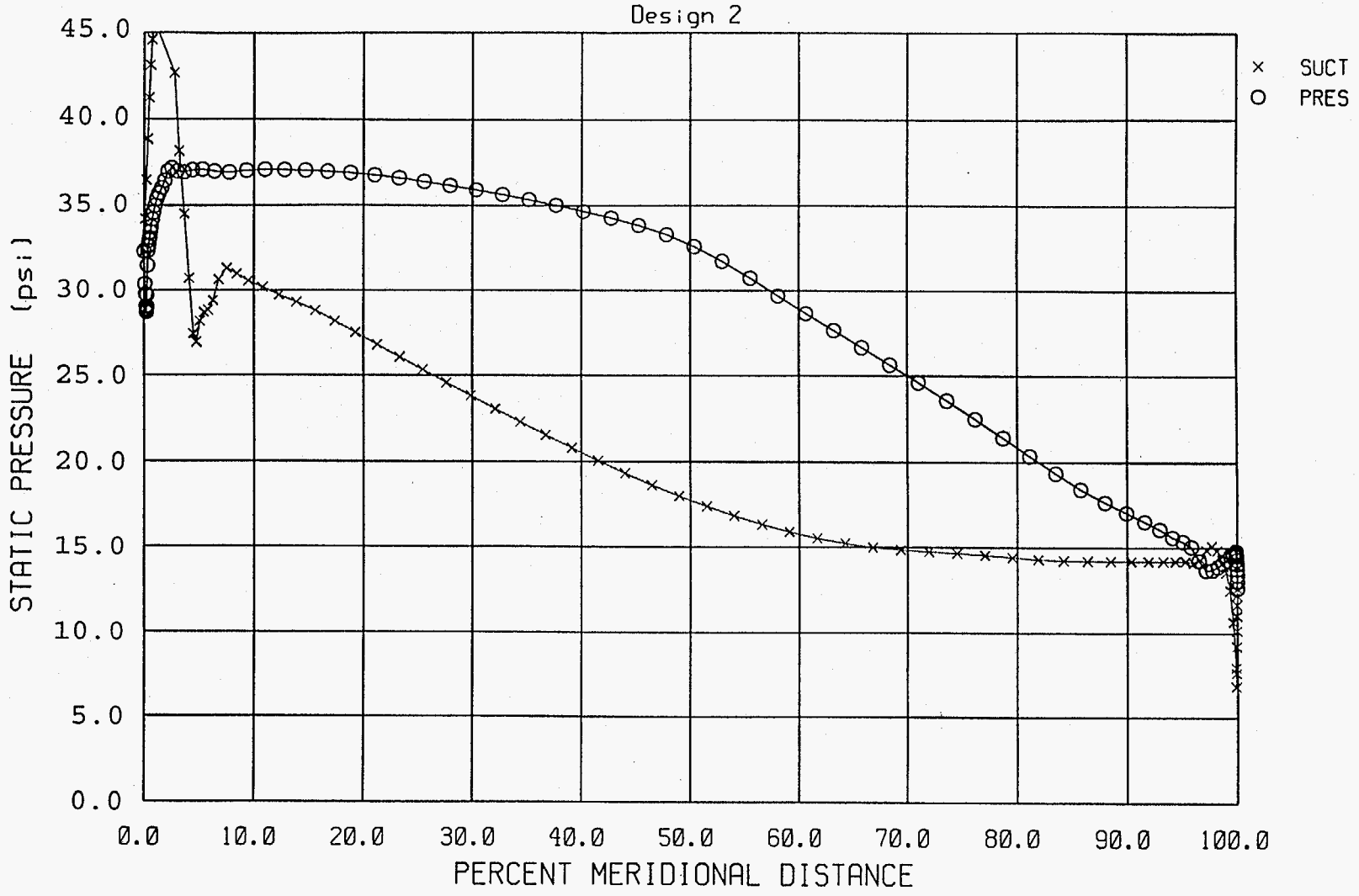

Figure 6-44
Design 2 - Pressure Loading Diagram At Mid-Span

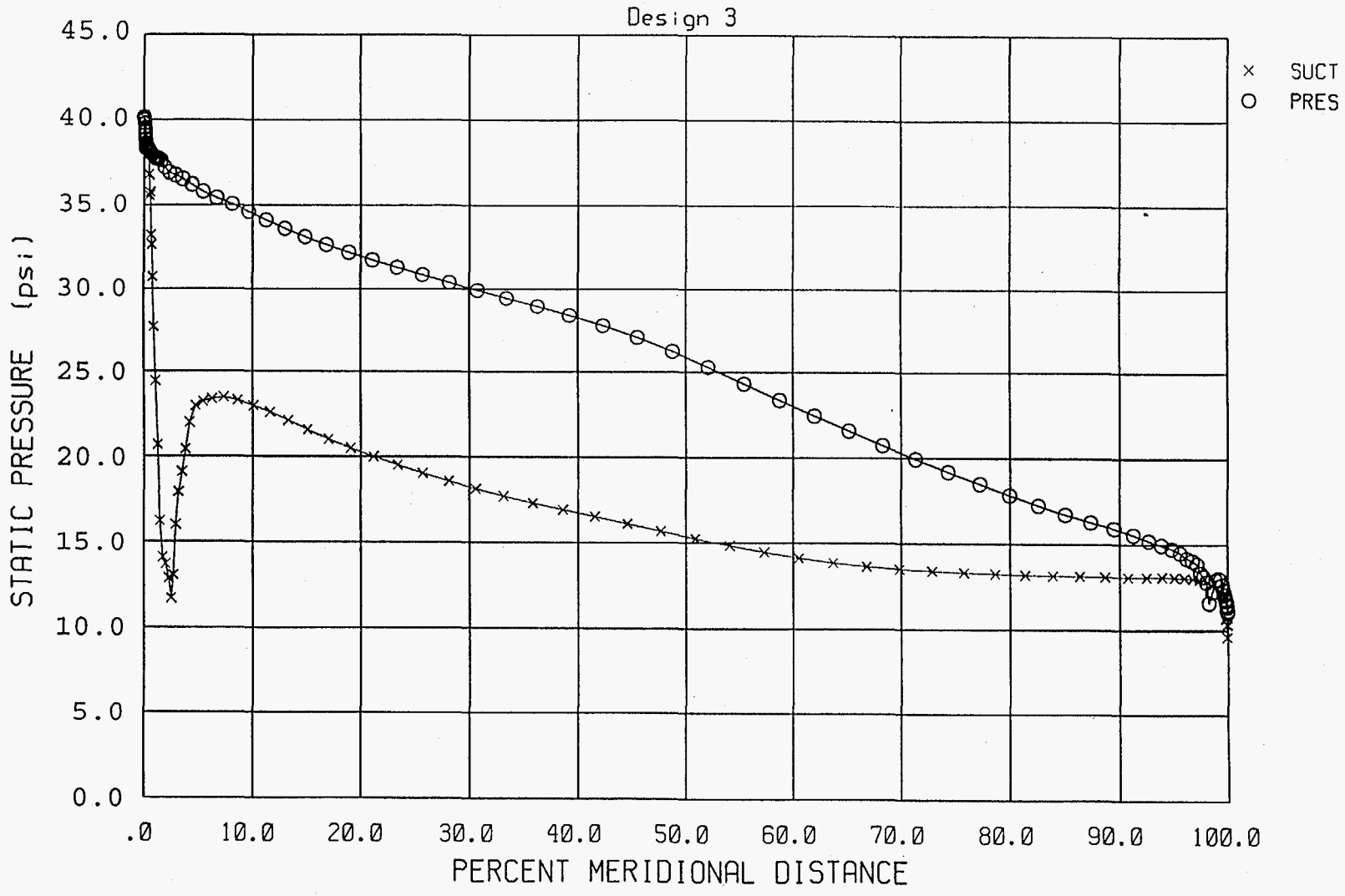

Figure 6-45
Design 3 - Pressure Loading Diagram At Mid-Span

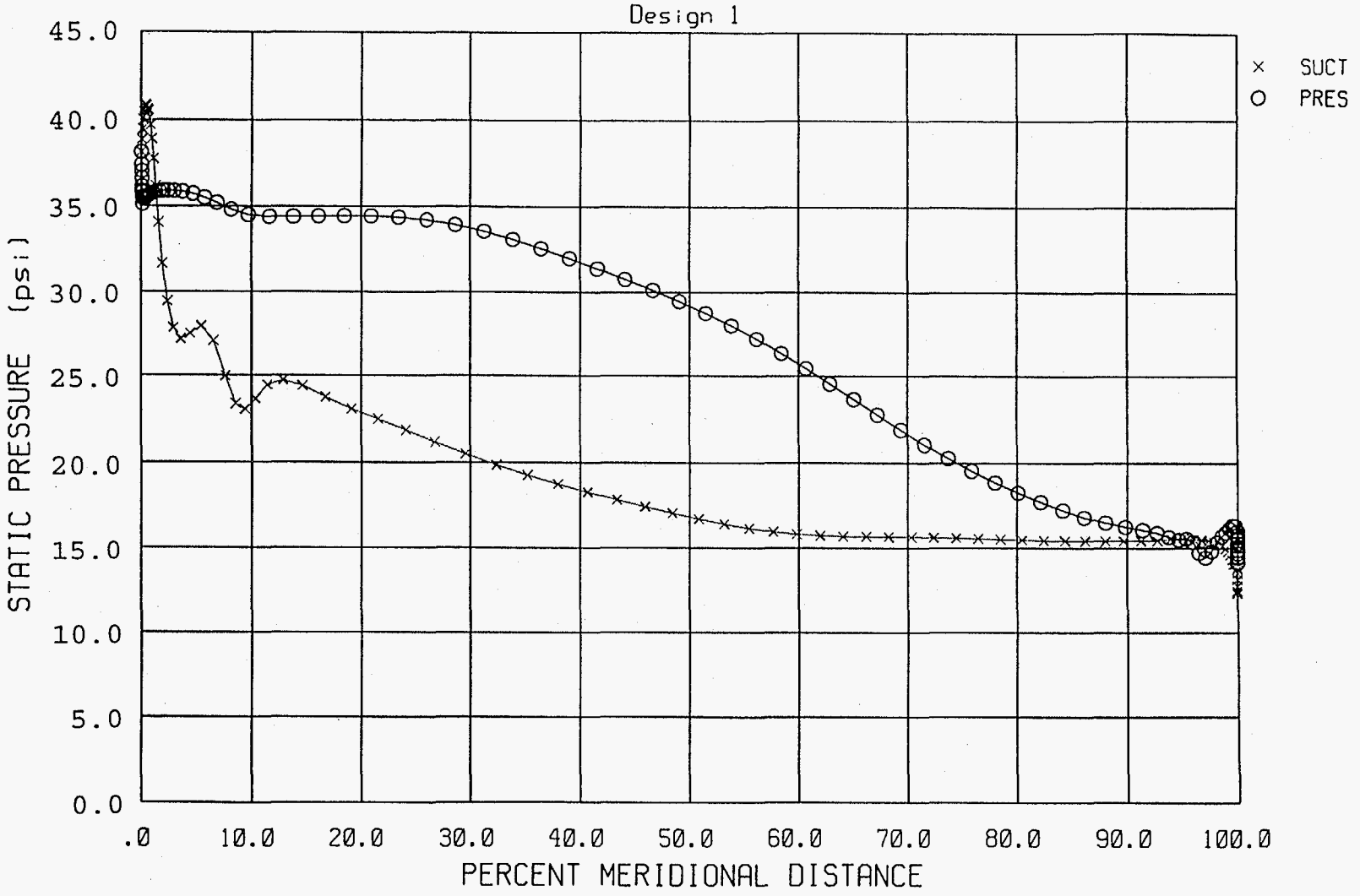

Figure 6-46

Design 1 - Pressure Loading Diagram At Shroud

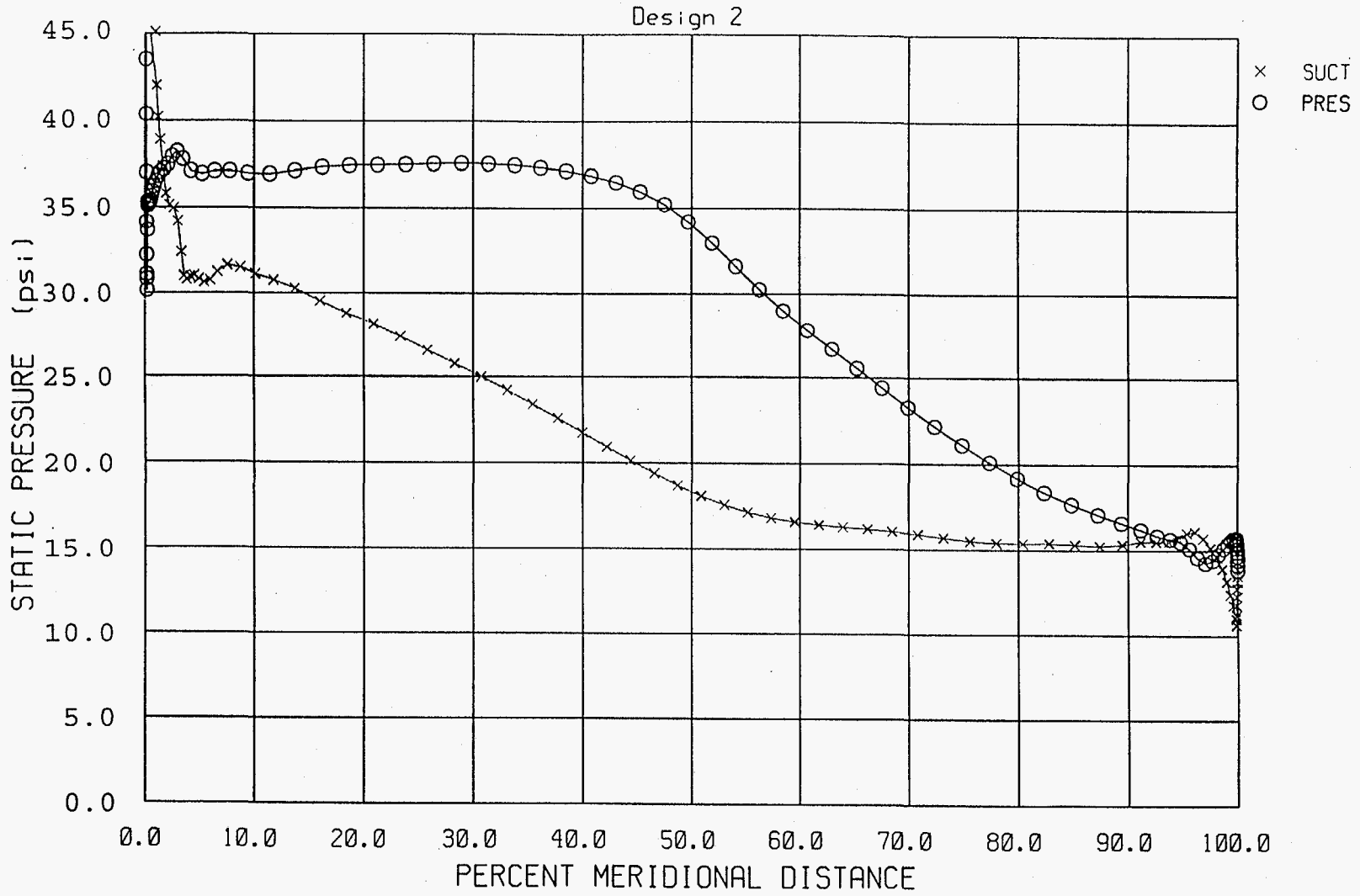

Figure 6-47
Design 2 - Pressure Loading Diagram At Shroud

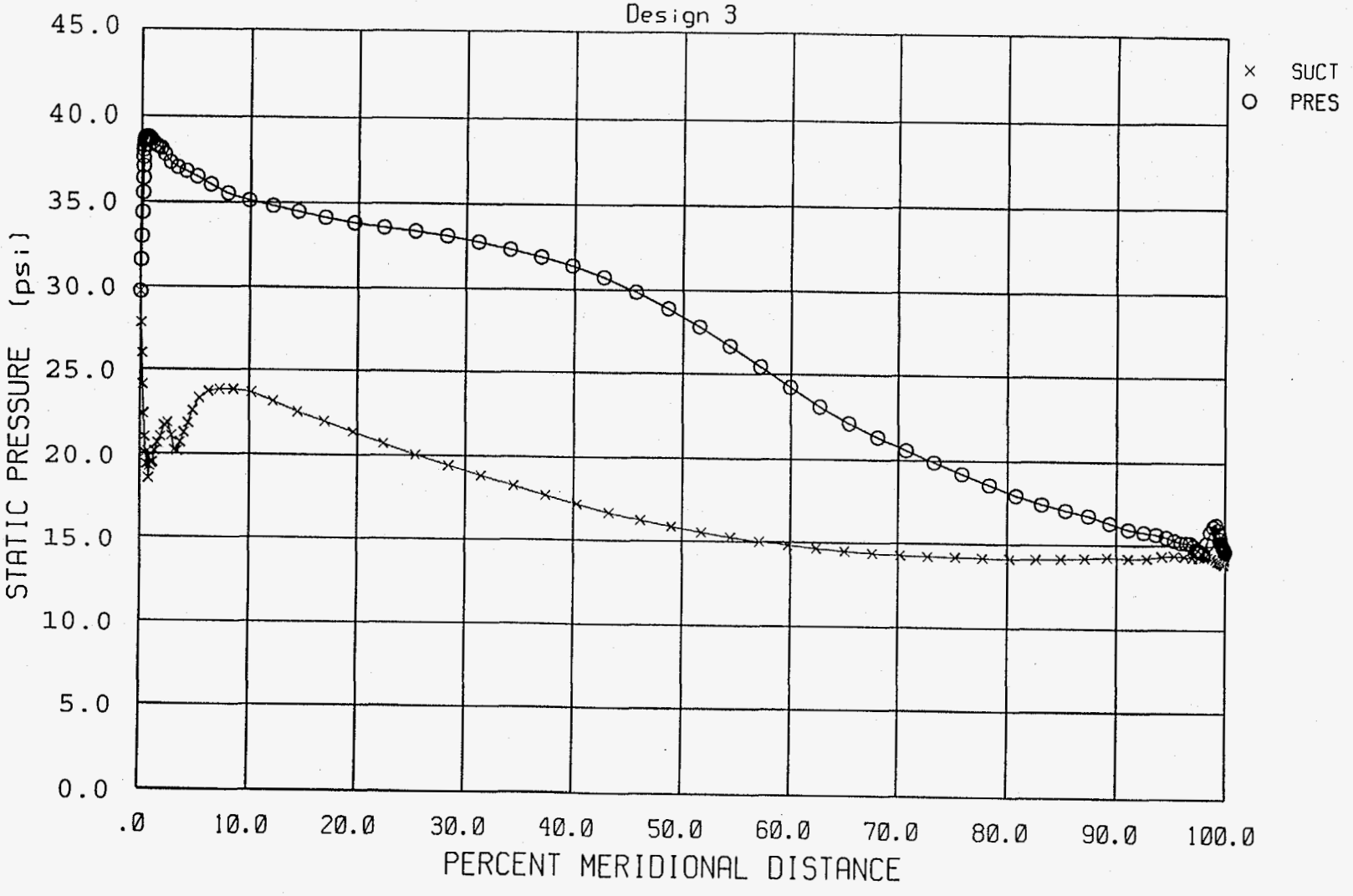

Figure 6-48

Design 3 - Pressure Loading Diagram At Shroud

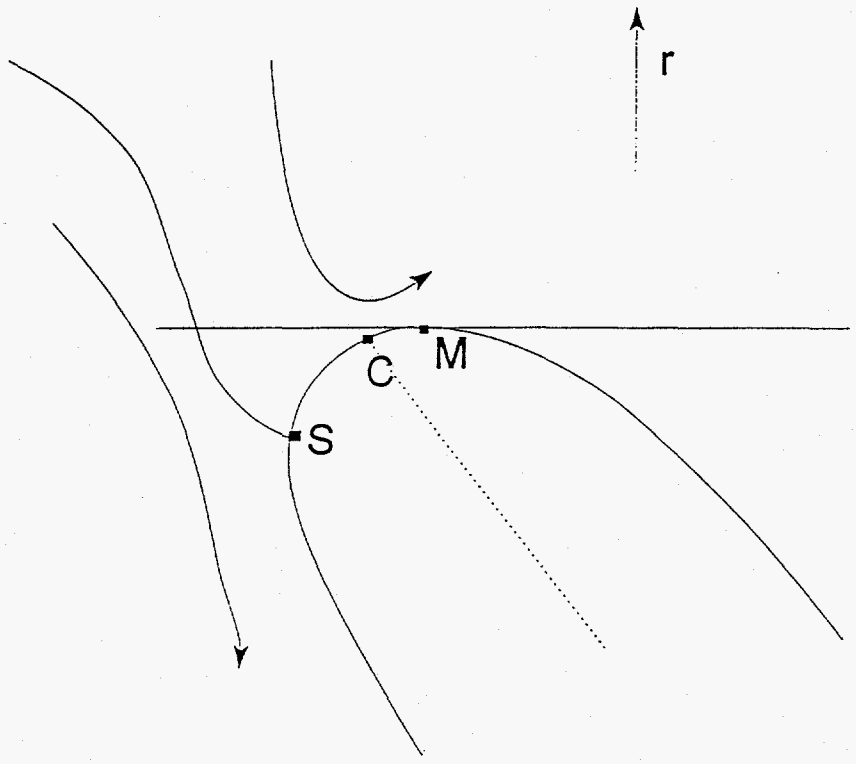

Figure 6-49
Leading Edge Detail

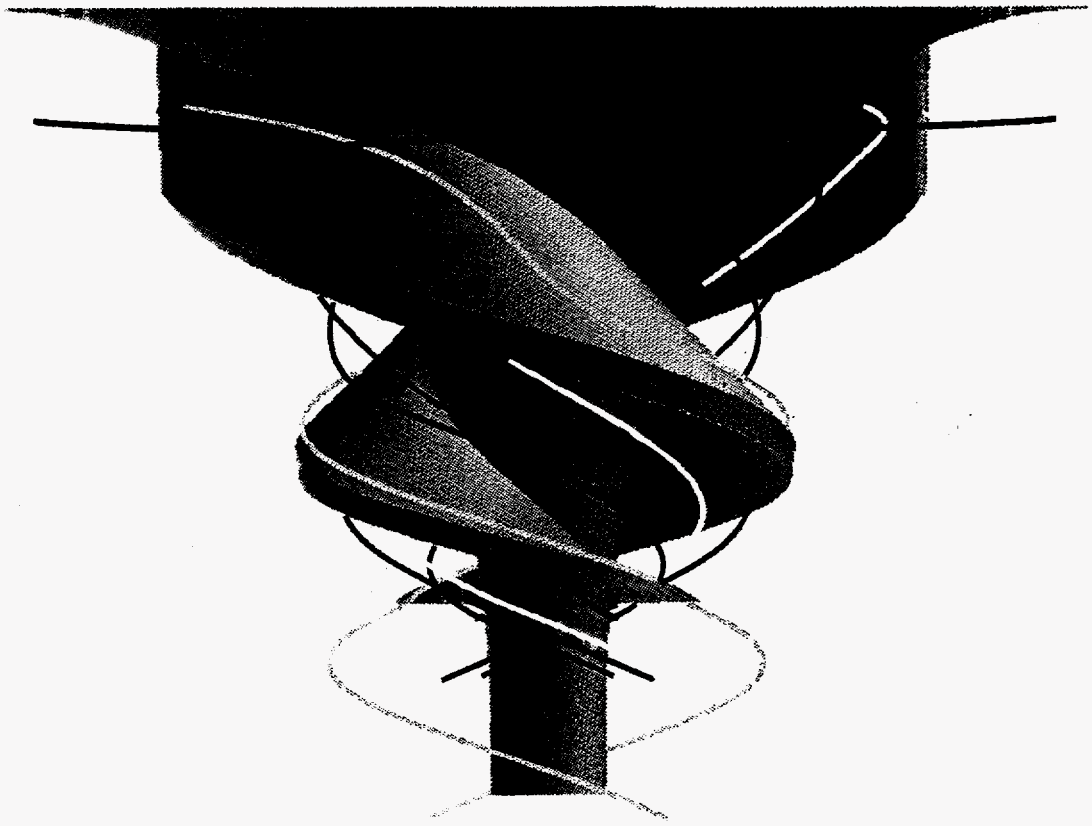

Figure 6-50
Design 1 - Path Lines Seeded Near Leading Edge At Mid-Span

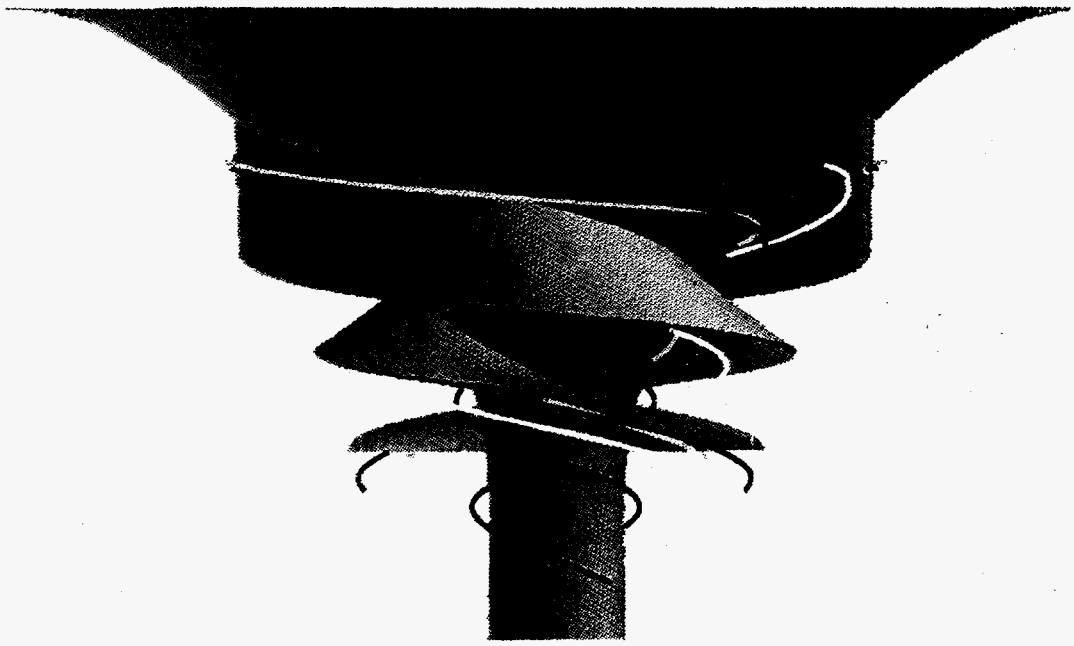

Figure 6-51
Design 2 - Path Lines Seeded Near Leading Edge At Mid-Span

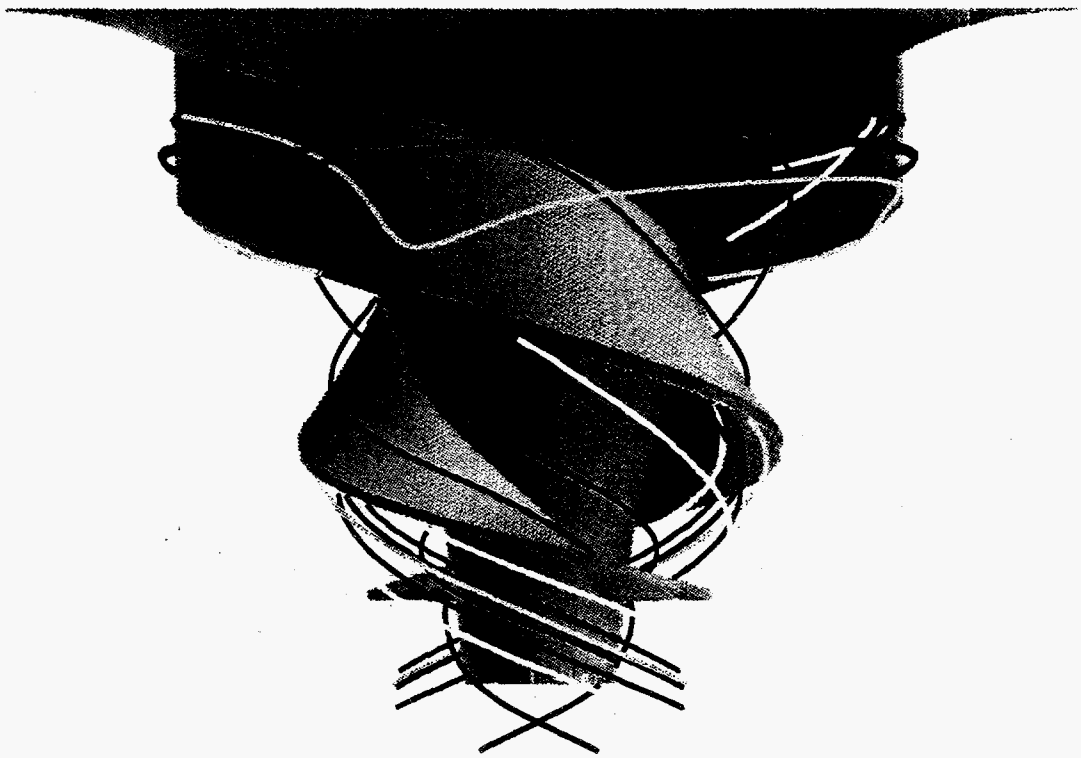

Figure 6-52
Design 3 - Path Lines Seeded Near Leading Edge At Mid-Span

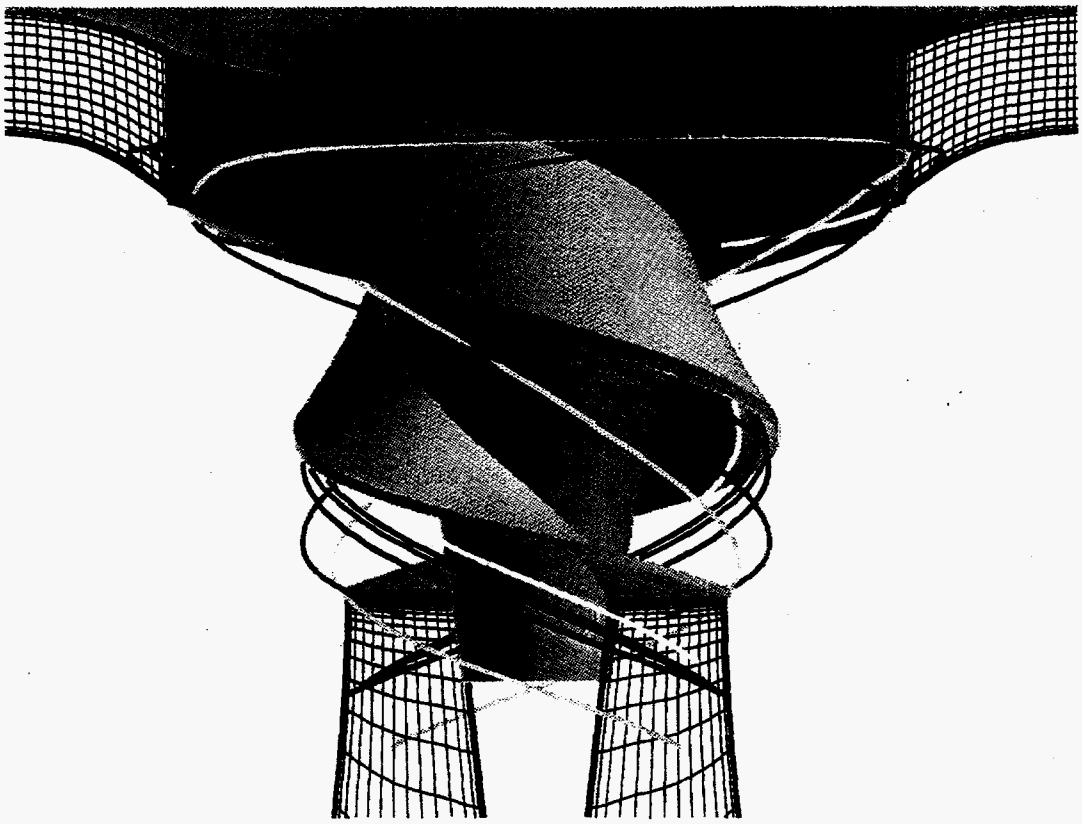

Figure 6-53
Design 3 - Path Lines Seeded Near Leading Edge Near Shroud

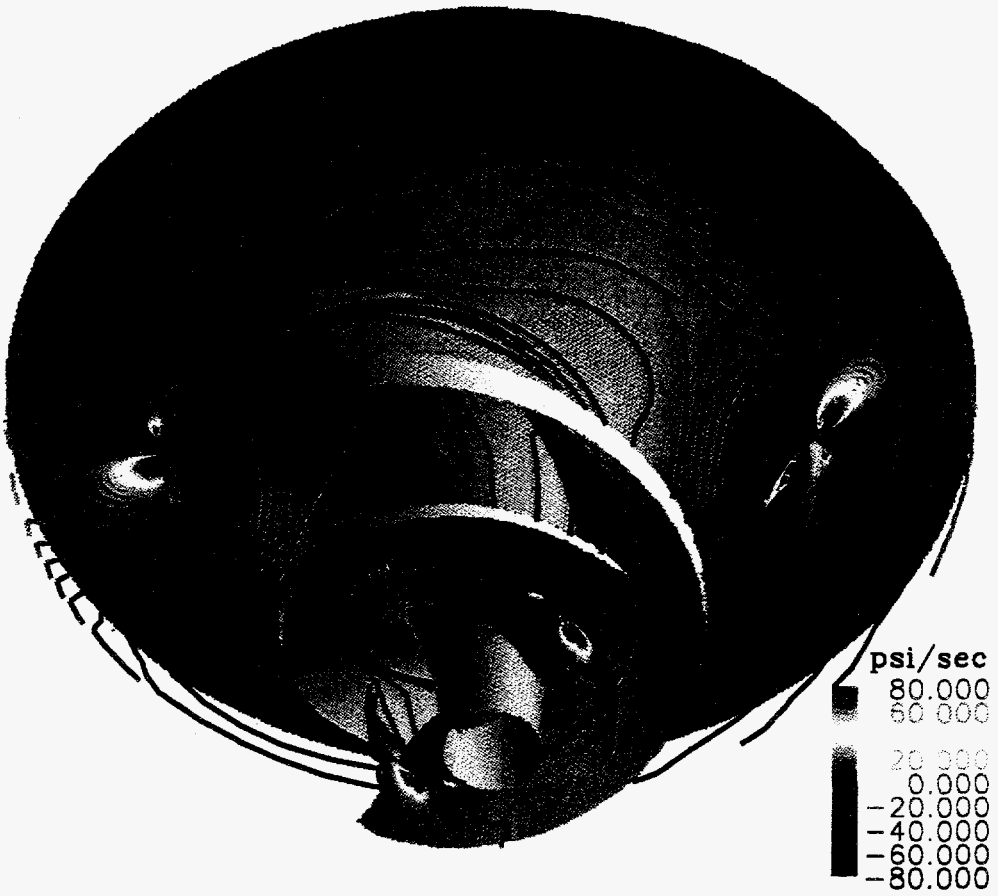

Figure 6-54
Design 1 - Pressure Change Rate At Mid-Span

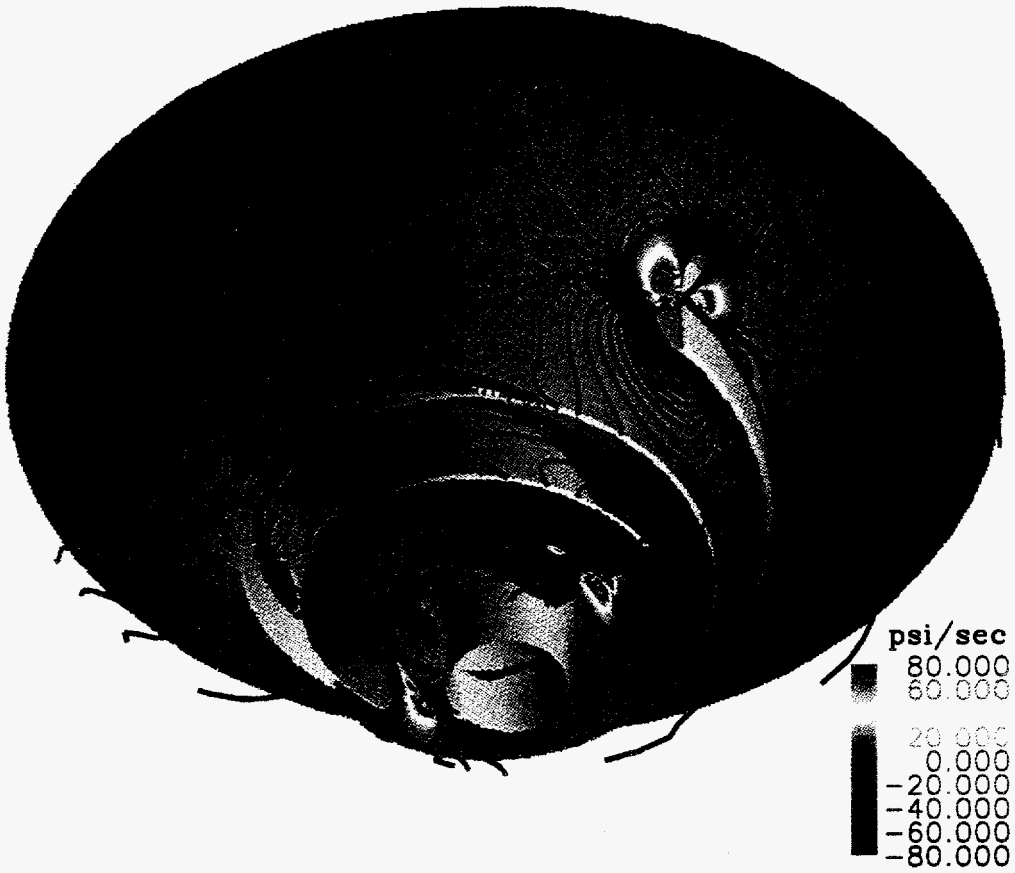

Figure 6-55
Design 2 - Pressure Change Rate At Mid-Span

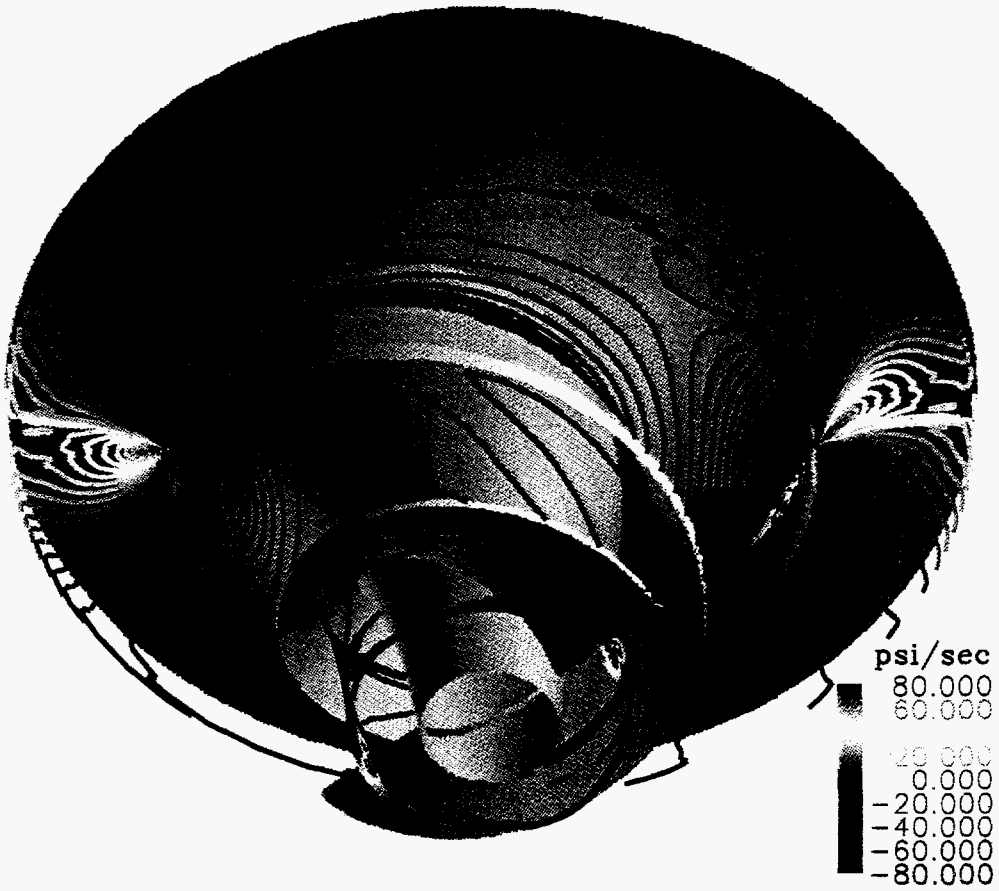

Figure 6-56
Design 3 - Pressure Change Rate At Mid-Span

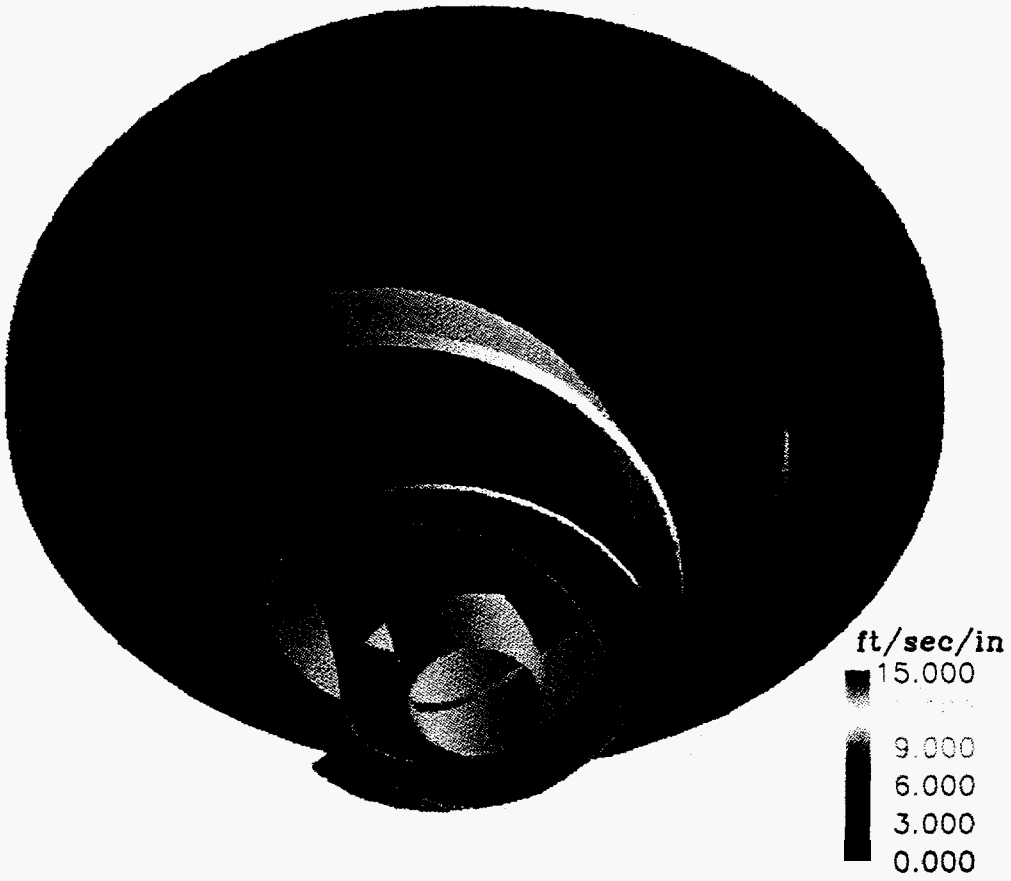

Figure 6-57
Design 3 - Shear (Vorticity Magnitude) At Mid-Span

SECTION 7
EVALUATION OF FINAL RUNNER DESIGN

7.1 Fish Biology Considerations

The new runner flow characteristics have been compared to the biological criteria identified as important parameters relative to passage of fish through turbines without injury. The criteria selected are:

- 40 ft/sec maximum peripheral runner speed;
- 10 psia minimum pressure;
- 80 psi/sec maximum pressure change;
- 15 ft/sec/inch maximum shear;
- Minimum number and total length of leading blade edges;
- Maximum distance between runner and wicket gates, and minimum clearance between other components; and,
- Maximum size flow passages.

Conceptual design of the new turbine runner has focused on computational analyses of the flow characteristics between the runner inlet just upstream from the runner blade leading edges and the runner discharge just downstream from the trailing edge of the blades. The CFD models do not include the inlet scroll case and the entire discharge draft tube. Therefore, the criterion relative to the maximum distance between the runner and the wicket gates has not been addressed in the biological evaluation of the final runner characteristics developed during the Phase I conceptual design.

A comparison of the preliminary two-dimensional analyses results for the L12Q-SH pump impeller, the same but scaled-up impeller geometry in the turbine mode, and the first iteration two-bladed runner to the biological criteria is presented on Table 7-1. The data provided on Table 7-1 shows how the basic runner geometry evolved during the preliminary design process. The pump impeller and the scaled-up impeller were single-bladed mixed flow units. The first iteration runner was modeled as a two-bladed unit with mixed inflow.

The Hidrostal pump L12Q-SH impeller two-dimensional analysis indicated that the pump has a peripheral speed of 116 ft/sec and a maximum pressure change rate of greater than 400 psi/sec,

significantly greater than the 40 ft/sec speed and the 80 psi/sec pressure change evaluation criteria. The maximum calculated shear for the impeller was less than 12 psi/sec, less than the 15 psi/sec criteria. The minimum pressure in the impeller flow passage occurred at the pump inlet (0 psia) and was a function of the assumed atmospheric inlet pressure. As shown on Table 7-1, the pump impeller has only one blade with the blade leading edge only 5.5 inches long. The 5 inch minimum size flow passage is large relative to the 12 inch discharge diameter of the pump. Evaluation of the L12Q-SH pump to identify characteristics which are favorable for fish passage may not be valid, especially speed and pressure change characteristics, since this particular pump impeller is not used to transfer fish.

As shown on Table 7-1, the two-dimensional analyses indicated that all of the turbine runner characteristics, based on a scaled-up impeller geometry, meet the biological evaluation criteria, except for peripheral speed and minimum pressure. The maximum pressure change rate was less than 20 psi/sec and the maximum shear rate was less than 2 ft/sec/inch for the scaled-up impeller geometry. Two-dimensional analyses of the scaled-up impeller used in the turbine mode resulted in a peripheral runner speed of 71 ft/sec, exceeding the 40 ft/sec criterion. Peripheral speed is a relatively fixed characteristic since head and diameter determine the rotational speed necessary to extract power from the water. Minimum pressure for the scaled-up impeller geometry for the turbine runner was 8 psia, slightly less than the 10 psia minimum pressure set as the criterion. Since the minimum pressure on the blade is a function of the blade shape and the assumed pressure at the runner discharge, the minimum pressure in the runner can be adjusted by changing the discharge pressure in the mathematical model, or by changing the elevation of the runner relative to tailwater level at a prototype site. For this reason, the minimum pressure criterion is not considered as important as the pressure change rate and the shear criteria.

The first iteration with a two-bladed runner and with radial inflow was selected to increase the efficiency. Increasing the number of blades decreased the runner diameter at best efficiency from 28.8 ft to 22.2 ft with mixed flow, and modifying the inlet conditions reduced the two-bladed diameter at best efficiency from 22.2 ft for mixed flow to 17.5 ft for radial inflow. These changes resulted in an increase in efficiency from about 81% to 88%. The reduced runner diameter had a 62 ft/sec peripheral speed, less than the scaled-up impeller but still greater than the 40 ft/sec criterion, as shown on Table 7-1. A three-bladed runner was investigated in an attempt to reduce the runner diameter and the peripheral speed, and to further increase the efficiency. The results of this preliminary two-dimensional analysis indicate that an additional blade would only reduce the diameter by about one foot and would only increase the efficiency by about one percent. The three-bladed runner was eliminated from further consideration because: a three blade geometry was too much of a departure

Table 7-1
Biological Evaluation Of Results From Two-Dimensional Analyses

Evaluation Criteria	L12Q-SH Pump Impeller	Scaled L12Q-SH Impeller As Turbine	First Iteration Runner
40 ft/sec Maximum Peripheral Runner Speed	116 ft/sec	71 ft/sec	62 ft/sec
10 psia Minimum Pressure	0 psia	8.0 psia on Blades Assuming 14.7 psia at Runner Exit (No Draft Tube)	10.0 psia on Blades Assuming 13.7 psia at Runner Exit (Draft Tube Area Expansion Ratio 1:4)
80 psi/sec Maximum Pressure Change Rate	> 400 psi/sec	< 20 psi/sec	< 20 psi/sec
15 ft/sec/inch Maximum Shear	< 12 ft/sec/inch	< 2 ft/sec/inch	< 2 ft/sec/inch
Minimum Number And Total Length of Leading Edges	1 Blade 5.5 inches	1 Blade 55 inches	2 Blades 64 inches
Maximum Distance Between Runner and Wicket Gates; Minimum Clearance Between Other Components	NM	NM	NM
Maximum Size Of Flow Passages (Minimum Width)	5 inches	50 inches	32 inches
Minimum Travel Time From Intake To Runner	NM	NM	NM

NM = Not Modeled

from the original one-blade concept; three blades significantly increase the total length of blade leading edges; and, three blades significantly decrease the maximum size flow passages. Increasing the number of blades to reduce the peripheral runner speed was considered to have more of a detrimental effect on fish than the high peripheral speed relative to the evaluation criteria.

A comparison of the three-dimensional CFD analyses results for the three runner geometry iterations to the two-dimensional analyses results for the first iteration, and to the biological evaluation criteria is provided in Table 7-2. The important criteria in this comparison are maximum pressure change rate and the maximum shear. As discussed above, the minimum pressure is a function of the discharge pressure assumption, and are reflected in the minimum pressures in Table 7-2.

The three-dimensional analyses of all three iterations of the runner geometry indicate a maximum pressure change rate greater than 80 psi/sec in small regions at the leading and trailing edges of the blades. These small regions amount to about one percent of the total the runner flow passage volume for Designs 1 and 3 and about two percent of the total passage volume for Design 2. These pressure change rates are significantly larger than the maximum pressure change rate of less than 20 psi/sec predicted with the two-dimensional model. The high pressure change rates in the three-dimensional model occurred where there was flow separation near the blade leading edges. This area is not accurately modeled in two-dimensional analyses, which is one reason why three-dimensional modeling is necessary. Graphic illustration presented in Section 6 show that Design 3 has the smallest maximum pressure change rate regions, and should minimize injury to fish.

The regions of maximum shear, in all three iterations of the runner geometry, occur in the boundary layers at the blade surfaces. Since the boundary layer is about 2-3 inches thick, shear zones adjacent to the runner blades should not increase fish injury beyond any injury that may result from fish contacting the blades.

The new turbine runner has apparent internal flow characteristics conducive for fish passage with minimal injury. The CFD analyses of the final geometry indicate that the velocity changes and pressure gradients through the new runner are low, that the minimum absolute pressures and flow patterns should be acceptable for fish passage, and that the flow characteristics of the runner meet the selected turbine evaluation criteria to the maximum extent possible during the conceptual design phase for the new runner development. However, some parameters relating to the biological evaluation criteria and the importance of each criterion relative to fish injury have not been addressed by the computational analyses performed in the conceptual runner design phase. Parameters such as

Table 7-2
Biological Evaluation Of Results From Three-Dimensional Analyses

Evaluation Criteria	First Iteration Runner	Second Iteration Runner	Third Iteration Runner
40 ft/sec Maximum Peripheral Runner Speed	62 ft/sec	68 ft/sec	64 ft/sec
10 psia Minimum Pressure	5.4 psia at Trailing Edge of Blade Assuming 13.7 psia Average Pressure at Runner Exit	4.0 psia on Trailing Edge of Blade Assuming 13.7 psia Average Pressure at Runner Exit	8.6 psia on Trailing Edge of Blade Assuming 13.7 psia Average Pressure at Runner Exit
80 psi/sec Maximum Pressure Change Rate	< 80 psi/sec Except Near Leading Edge	< 80 psi/sec Except Near Leading Edge	< 80 psi/sec Except Near Leading Edge
15 ft/sec/inch Maximum Shear	< 2 ft/sec/inch (Outside Boundary Layer)	< 2 ft/sec/inch (Outside Boundary Layer)	< 2 ft/sec/inch (Outside Boundary Layer)
Minimum Number And Total Length of Leading Edges	2 Blades 71 inches	2 Blades 66 inches	2 Blades 71 inches
Maximum Distance Between Runner and Wicket Gates; Minimum Clearance Between Other Components	NM	NM	NM
Maximum Size Of Flow Passages (Minimum Width)	33 inches	32 inches	36 inches
Minimum Travel Time From Intake To Runner	NM	NM	NM

NM = Not Modeled

the distance between the runner and the wicket gates, the size of the flow passages, and the travel time from the intake to the runner can only be addressed by testing with fish in a protype installation.

7.2 Engineering Considerations

7.2.1 Runner Setting

The conceptual design of the new turbine reflects a mixed flow condition (flow entering at an angle to the radius of the wheel) at the runner inlet. This flow condition is similar to many conventional Francis and Kaplan turbine designs, generally vertical shaft units with a scroll case. However, some turbines with radial or mixed flow inlet designs are installed in a flume or pit type intake where the approach flow conditions are controlled by turning vanes and gates. These open flume type of turbine installations are applicable to low head sites, generally less than 25 ft. At higher heads, a scroll case design is generally more economical than a flume type design due to lower costs for the intake structure and the shorter shaft between the turbine and the generator.

The new runner would probably have a vertical axis shaft, similar to other large conventional turbines. A vertical shaft simplifies runner and generator support, and eliminates support shaft struts in the flow passage at the runner exit, which would be required with a horizontal shaft axis. The shaft bearings system is more complicated for a horizontal shaft than a vertical shaft because the thrust is in two directions (vertical and axially) with a horizontal shaft rather than just one direction (axially) with a vertical shaft unit.

The conceptual design of the new runner was based on a vertical shaft runner with the minimum absolute pressure on the blades slightly lower than the minimum pressure specified in the biological criteria (10 psia). Design 3 represents the highest runner setting which satisfies the minimum pressure evaluation criteria. Raising or lowering the runner relative to the tailwater would affect the minimum pressure at the runner exit and on the blades. A low runner setting relative to tailwater would be preferred for effective fish passage because of the higher minimum pressures, and would be preferred to avoid potential damage to the runner from cavitation. Unfortunately, low turbine settings relative to tailwater usually cost more for excavation and civil works than higher settings.

The results of the CFD analysis indicates that cavitation should not be a problem with the new runner. The third iteration runner evaluated with CFD analyses showed that the minimum absolute pressure was 8.6 psia with the assumed average pressure of 13.7 psia at the runner discharge. This minimum

pressure is well above the pressures where cavitation would occur. Actual tests with a model turbine would define any cavitition limits for the new runner.

Minimum pressures in modern conventional turbines at the runner exit are typically about 5 psi below atmospheric pressure, corresponding to an absolute pressure of about 10 psia. Minimum average pressures at the runner exit in modern turbines are generally based on cavitation limits. Low runner outlet pressures allow the highest possible runner setting relative to tailwater, and minimize construction costs for the civil works. In addition, an absolute pressure of about 10 psia is necessary for a self-aspirating turbine venting system to address water quality issues in the tailwater.

The new turbine could be set at a higher level relative to tailwater than assumed in the conceptual design of the runner. If the new turbine was set at an elevation such that average pressure at the new runner exit was 10 psia rather than 13.7 psia (a setting about 8.5 ft higher than assumed in the CFD analyses), the minimum pressure at the trailing edge of the blades would be 8.6 psia minus 3.7 psia or 4.9 psia. All of the pressures through the new runner would be 3.7 psi lower than reported in Section 6. However, a higher elevation setting could be more damaging to fish because of the lower absolute minimum pressure. The pilot test study and subsequent phases of the turbine development will address the new runner setting to minimize fish injury and to avoid cavitation damage to the runner.

7.2.2 Flow Control

The conceptual design of the new turbine did not include wicket gates between the scroll case and the runner. Flow control may not be necessary in some types of installations for the new turbine, such as minimum flow or fish diversion bypasses where the flow rate would be nearly constant. However, use of the new runner for a typical hydroelectric installation would require some form of flow control for the turbine. Valves, gates, and possibly other new types of flow control devices could be used upstream of the scroll case, or the usual wicket gates could be used for flow control to the new turbine runner.

Upstream flow control would severely reduce the efficiency of the runner when operating off the design point. This reduction in turbine efficiency at off-design operation results from improper approach flow at the runner inlet. The new runner is designed for a zero incidence angle at the runner blade inlet (the average relative velocity angle and the blade angle are equal) at the design point (1,000 cfs at 75-100 ft head). Although not included in the conceptual design of the new runner, the scroll case is also designed to provide the desired approach flow conditions at the runner inlet. Any

changes in the flow upstream of the scroll case will change the runner inlet approach flow conditions, resulting in reduced turbine efficiency.

Wicket gates can be incorporated into the design of the scroll case for the new runner. Wicket gates for conventional turbines are typically close to the runner to minimize the size of the scroll case. When full open, the downtream end of the gates are usually immediately upstream of the runner blades with very little clearance between the gates (stationary) and the blades (rotating). As such, the upstream end of the gates are generally near the inside boundary of the scroll case. To improve fish passage, the scroll case design for the new runner could provide more distance between the wicket gates and the runner inlet, one of the biological criteria. The approach to designing the wicket gates would be similar to the design of the runner. The number of gates would be decreased, which would increase both the distance between the gates and the length of the gates. The gates could be designed to improve approach flow conditions over a range of operating conditions, which would minimize the reduction in efficiency when the turbine operates at off-design settings. All of these changes would increase the inside diameter of the scroll case beyond typical scroll case diameters. Other aspects of the scroll case design would be similar to conventional hydraulic turbine design.

Design of the flow control system and the scroll case for the new runner will be evaluated during the next phase of the runner design, the pilot test study, and subsequent phases of the turbine development.

7.2.3 Runner Diameter

The new runner, as conceptually designed, has a larger than conventional diameter at best efficiency to meet the biological criteria for effective fish passage. As discussed in Section 6, the analysis indicates that a 30% smaller diameter runner would have only a 1% reduction in best efficiency from the larger diameter runner used to investigate the runner flow characteristics with CFD analyses. A smaller diameter runner would have a lower cost and better potential for application at existing hydroelectric plants than the larger runner. A smaller diameter runner may be as effective for fish passage as the larger diameter runner, but a comparison of biological effectiveness of the two different size runners is not possible without actual testing with fish.

Additional CFD analysis with a smaller diameter runner is planned at the beginning of the pilot test studies to compare the flow characteristics of the smaller runner to the CFD results for the larger runner presented in this report. This analysis will allow selection of the runner design for the pilot tests.

7.2.4 Draft Tube

The overall efficiency of the new turbine has been calculated based on the difference in head (pressure) at the inlet to the scroll case and the tailwater level, and include a draft tube friction and exit loss of about 0.6 ft. As discussed in Section 6, draft tubes are used with hydraulic turbines to recover velocity head at the runner exit. As conceptually designed, the new runner will have a typical draft tube similar to draft tubes used for conventional turbines. Design of the draft tube would be consistent with industry practice.

7.2.5 Off-Design Operation

Conceptual design of the new runner has been completed with the goal of developing a runner geometry to pass fish with minimal injury. The conceptual design efforts have focused on evaluation of the hydraulic characteristics of the runner operating at design point. Evaluation of the runner operating at off-design conditions would be completed in a subsequent phase of the turbine development after the new runner design had been proven to effectively pass fish without injury. The next phase for the runner development is the pilot test study with a small (prototype) turbine tested with fish at the design point to assess if the runner is biologically effective. During the pilot test study, some additional CFD analyses will be conducted to evaluate flow characterictics during off-design point operation. However, the pilot test study will focus on biological evaluation of the runner operating at design point and hydraulic measurements to verify the design point flow characteristics predicted with the CFD analyses. Further assessment of operation at off-design points will be conducted during a subsequent phase of the turbine development.

7.3 Manufacturing Considerations

The new fish tolerant turbine can be manufactured in the same manner as conventional Francis or propeller units. However, for the pilot test project, where only one turbine is required in a short time, a combination of manufacturing processes may be considered for the different components. The majority of the turbine system for the new runner consists of components that are similar to those currently used in the industry with the major novel item being the turbine runner itself.

A common manufacturing method for pump and turbine wheels involves five-axis machining methods. The procedure requires procurement of a "pancake" forging, and machining a shroud profile with a vertical lathe. The blades would then be produced from the forging by milling out the material in the flow passage on a five-axis milling machine. The shroud would be welded on the blading with a

special process that ensures that the shroud and blades are fully fused together. This method would be fast since time-consuming patterns and castings are eliminated from the process. In addition, the advantages of machining versus casting are the high dimensional and material quality of the final product.

For the pilot test project and subsequent commercial production, machining may not be an efficient or economical method to manufacture the new runner. The fact that the flow passage is large and long means that considerable material removal would be necessary, which would be very expensive. Other manufacturing processes may be less costly. These processes include:

a) Near Net Casting - In this process the impeller is cast in very rough form with an inexpensive pattern. Final finish is obtained with a machining process.

b) Fabrication - In this process the hub, blades and shroud will be individually cast and welded together. Also the blades could be machined from near net castings.

c) Blade Fabrication - In this process the blades will be welded together from rolled plate to form the completed blade. The entire unit will then be welded together similar to the fabrication method.

Various methods for manufacturing the turbine components will be more thoroughly assessed in the next new runner development phase. In addition, the next phase of the new runner development will include an assessment of the maximum practical size for manufacturing the runner with available technology.

7.4 Installation Considerations

7.4.1 Retrofit Options

The new runner, as conceptually designed, is larger (diameter and length) at its best efficiency than conventional turbine runners having the same flow and head design point. Even with a 30% size reduction, resulting a small reduction in efficiency as discussed in Section 7.2.3, the new runner would still be larger than other turbines. Some additional reduction in size is possible with the three bladed design. However, replacement of conventional turbine runners at existing hydroelectric projects with the new runner may result in some reduced power output. The new runner could be adapted to an existing turbine scroll case and draft tube, but this runner may not have the flow

capacity of the original turbine. This reduction in power output would make existing runner replacement most favorable for those projects where fish injury is of primary concern.

New turbine installation in an existing turbine bay may require major modifications to the powerhouse structure, if the new turbine is designed for the same power output as the original unit. To pass fish without injury, the runner and the scroll case at best efficiency are larger than conventional turbines. Retrofit of the new turbine may require rebuilding the existing scroll case. These changes may be expensive and would be mainly justified for those projects where fish injury is of primary concern.

A good option for the new turbine at an existing hydroelectric plant would be installation in an existing turbine bay which has been previously constructed for future expansion of the plant. Installation of the new turbine in an available bay would require minimal modifications to existing structures and would have the least impact on plant operations during construction.

7.4.2 New Applications

The new turbine offers an innovative option for generating power with minimum flow releases and with bypass flow discharged from fish diversion systems. Many hydroelectric projects must release sufficient water to maintain the fisheries habitat or to add dissolved oxygen to the water in the river reach downstream from dams. Some projects have fish diversion structures to prevent fish from passing through the turbines, and these diversion structures require flow to attract and transport the fish. These flows are not generally utilized for power generation because fish protection and passage then again become issues.

The new turbine could be installed downstream of most minimum flow release structures. Typically, these structures are gated or valved outlets in the existing dam which could be modified to become an intake for the new turbine. Fish screening systems would not be required if the new runner could be proven to pass fish without injury. If necessary, the new turbine intake could include gates or overflow weirs to provide a discharge capacity comparable to the existing spillway and outlet works.

The new turbine could also be installed in the return piping for fish diversion systems. A properly designed fish diversion system requires flow to be guided into a bypass to convey fish in a return system to the tailrace downstream of the powerhouse. This diversion flow can be as high as 5% of the river flow. Larger diversion systems typically incorporate secondary screening to recover most of the diverted flow. Secondary diversion systems are generally designed to minimize spilled water

(maximize power generation). Using the new turbine in the bypasses of primary diversion systems could eliminate the need for (and costs) secondary screening systems.

Diversion systems are usually installed in locations which have the best construction access and the shortest distance to the tailwater or natural river channel. To minimize costs, the new turbine could be installed at the end of the fish return system without any additional intake or pipe. A consideration with locating the new turbine at the end of a return pipe from a fish diversion system is access for civil works construction and turbine and generator component installation.

SECTION 8
CONCLUSIONS

A new turbine runner has been conceptually designed, using Computational Fluid Dynamics (CFD) analysis, to pass fish with minimal injury. The new runner reflects biological criteria which were derived as part of this design effort from a re-evaluation of available studies previously conducted by the hydroelectric industry to evaluate sources of injury to fish passing through hydraulic turbines. Specific flow criteria used to design the new runner include: a maximum pressure change rate of 80 psi/sec; a maximum velocity shear of 15 ft/sec/inch; and, a minimum absolute pressure of 10 psia. Other criteria reflected in the design include: mimimizing the number and total length of the leading edges; minimizing the peripheral runner speed; minimizing the clearances between the runner and the turbine housing; and, maximizing the size of the flow passages. Two other criteria that will be addressed in future runner design phases are: maximizing the distance between the wicket gates and the blade leading edges, and minimizing the travel time from the intake to the runner.

The operating design point selected for the new turbine runner (1,000 cfs at 75-100 ft head) is representative of the operating range for the majority of hydraulic turbines in the United States. The initial runner geometry for starting the analysis was based on an existing solids handling pump adapted to transfer live fish at flow diversion facilities. Two-dimensional analyses determined that the pump impeller was not suitable as a turbine runner, and additional analysis was used to develop a new geometry for turbine operation at the design point.

The new runner is two-bladed and has a screw/centrifigal shape with large flow passages; each blade wraps around the hub about 360 degrees. At maximum efficiency, the runner has a diameter of 17.5 ft and a length of 13.3 ft for the operating design point. The runner diameter can be reduced significantly with a small drop in efficiency. Flow passages are enclosed by a rotating shroud attached to the blade edges to eliminate gaps that may damage fish. Overall best efficiency of the turbine at the design point is about 90%, including losses from the scroll case inlet to the tailwater, and reflects a 1:4 draft tube expansion but does not include losses associated with wicket gates.

Three-dimensional CFD analysis indicates that flow characteristics through the runner are generally consistent with the criteria established to pass fish without injury. There are small regions at the leading and trailing edges of the blades where the maximum pressure change rate exceeds the evaluation criterion of 80 psi/sec. The flow volumes associated with these maximum pressure change rates is about one percent of the total volume of the runner flow passages. The maximum shear

criterion is only exceeded in the boundary layer next to surfaces. Minimum pressure is at the turbine runner exit and is controlled by the runner setting relative to tailwater. CFD analysis of the final runner iteration indicates that the minimum absolute pressure is 8.6 psia at the trailing edge of the blades, slightly less than the 10 psia criterion, with the assumed 13.7 psia average pressure at the runner exit. The flow volume associated with this lowest pressure is less than 1/10,000 of one percent (<0.0001%) of the runner flow passage total volume. No cavitation is expected anywhere in the runner. CFD analysis results indicate that the new runner has flow characteristics that should not injure fish.

Fish diversions or minimum flow installations are ideal applications for the new runner, allowing use of greater bypass flows with no loss in power generation. Retrofit of the new turbine at existing hydro plants depends on the size of the existing turbine components. Two-dimensional analysis of the basic runner geometry indicates that a 30% reduction in the runner diameter would only reduce the overall efficiency by about 1%. Some additional reduction in runner size can be obtained using a three bladed runner, although this increases the number and total length of leading edges. Further three-dimensional CFD analysis of the smaller runner is necessary to improve flow characteristics through the runner for diameters and lengths compatible with current turbine installations.

Conceptual design study results indicate that the new turbine runner should pass fish without injury. Actual tests with several species of fish are needed to verify this prediction. Therefore, the next phase in the development of the new runner is to conduct a pilot study to evaluate fish injury with the runner in a test facility. Additional CFD analysis will be needed to further refine the runner geometry and model the flow characteristic of the actual turbine to be used in the pilot study. A pilot scale turbine with a 3 to 4 ft diameter would be fabricated and tested at the full design head. Hydraulic measurements would be included to verify the predicted power efficiency.

SECTION 9
FUTURE EFFORTS TO VERIFY SAFE FISH PASSAGE

Phase I conceptual design efforts have resulted in development of a new runner to the point where the internal flow characteristics (flow patterns, velocities, and pressures) and hydraulic efficiency at the design point are reasonably well known, at least to the level of uncertainty inherent in modern CFD codes. The basic unknown with the new turbine design is whether fish will pass through the runner without injury. Therefore, the next logical step in advancing the new fish friendly runner is a pilot scale test with fish. After effective fish passage through the runner has been demonstrated, additional CFD analysis of the runner can be completed to refine the geometry. If necessary, hydraulic model testing of the turbine can also be conducted to verify the predicted efficiency at the design point and determine the turbine performance characteristics at off-design conditions.

The recommended pilot scale test is a minor deviation from the Phase II - Hydraulic Model Tests originally planned by the DOE for the Advanced Hydropower Turbine Program. Expending funds to construct and test a hydraulic model of the new turbine to verify the CFD analyses of flow conditions and efficiency would not be appropriate until the survivability of fish passing through the runner was directly demonstrated. Even basic separate effects experiments on fish, which are a possible part of the DOE's Phase II efforts, would not address simultaneous and cumulative effects of potentially damaging phenomena on fish passing through the new turbine, or even conventional turbines. The recommended pilot study for the fish tolerant turbine would reflect the combined effects on fish of all hydraulic conditions in the new runner. Should the fish testing results be positive, as envisioned, then ample justification would exist to check the results of the CFD analyses with a model study and to further refine the runner design.

Pilot scale tests would concentrate on evaluation of injury to fish passing through the runner, but would also include measurements of basic flow characteristics and efficiency. A runner diameter of 3 or 4 ft would be tested to insure adequate (minimum) passage area between blades, one of the Phase I evaluation criteria. Minimum size openings would be 5.5 inches for a 3 ft diameter runner and 7.5 inches for a 4 ft diameter runner. The pilot scale turbine would be free standing with an approach penstock and a draft tube (tailrace piping). The head across the runner (83 ft for Design 3) would be a critical parameter in the site selection, since fish should be subjected to actual velocities and pressure changes. For this range of runner diameter, the flow would range from 50 cfs to 100 cfs, and power output for the two runner sizes would be about 400 HP and 900 HP at the design head.

The pilot scale tests could be conducted in a laboratory or at a hydroelectric site. At a hydro site, the new turbine could be installed in an unused bay or in a test stand constructed adjacent to the existing powerhouse. Water would be conveyed to the new turbine through a test pipe that would withdraw water from an existing penstock or from an existing intake at the headpond. The test pipe would include a flow control valve and instrumentation to monitor the turbine flow. A fish injection system would be installed in the test pipe sufficiently far upstream of the turbine inlet to allow fish to orient into the flow before reaching the runner. Tailrace netting techniques would be employed at the exit of the new turbine draft tube to recover all test fish. Figure 9-1 presents a schematic layout of the pilot scale test facility at a typical site.

In the laboratory, the new turbine would be installed in a closed flow loop using a test stand adjacent to one end of a flume. A pump would be located at the other end of the flume to convey flow to the turbine inlet through a return pipe. The return pump line would include a flow control valve and instrumentation to monitor the flow. A fish injection system would be installed a sufficient distance upstream of the turbine inlet to allow the fish to orient into the flow prior to reaching the turbine inlet. An angled screen fish collection system would be installed in the flume to recover the test fish. The fish collection system would include secondary screening to facilitate and minimize handling of the fish. A schematic layout of the pilot scale test facility in the laboratory is shown on Figure 9-2.

Conducting the pilot test at a hydro site or in the laboratory each have advantages and disadvantages. At an appropriate hydro site, flow and head would be available in a physically representative manner, and many of the components necessary to test the turbine, including an intake, penstocks, or turbine bays, could be available. The large flow and high head would be a major design factor for the laboratory test facility. A large pump would be required to convey flow to the turbine and a large flume would be necessary for collecting the fish in the laboratory. Power requirements would be an important cost factor associated with a pump system.

In the laboratory, strict control would be available over operational and environmental factors. A more effective fish collection and holding facility could be installed in the laboratory than at a hydro site, where space available for the fish handling facilities may be limited or located far from the test turbine, and access to the field test facility may be difficult for test personnel. Weather, debris, and water availability may be factors affecting the pilot tests at a hydro site which would not affect tests in the laboratory. The site selection process and sending personnel to the field would be cost factors associated with conducting the pilot tests at a hydro site. In general, conducting the pilot scale tests in the laboratory would be less time consuming and less costly than conducting the tests at a hydro site, and would result in more controlled test conditions.

For these reasons, testing of the new turbine with fish in the laboratory is recommended as the next step in the turbine development. The tests would include CFD analyses of the runner to define the pilot test runner flow characteristics. The results of CFD analyses would provide data to identify areas where fish injury may occur for comparison to any observed injury. Measurement of flow, head, and power would be included to verify the efficiency of the turbine predicted by the conceptual design computations.

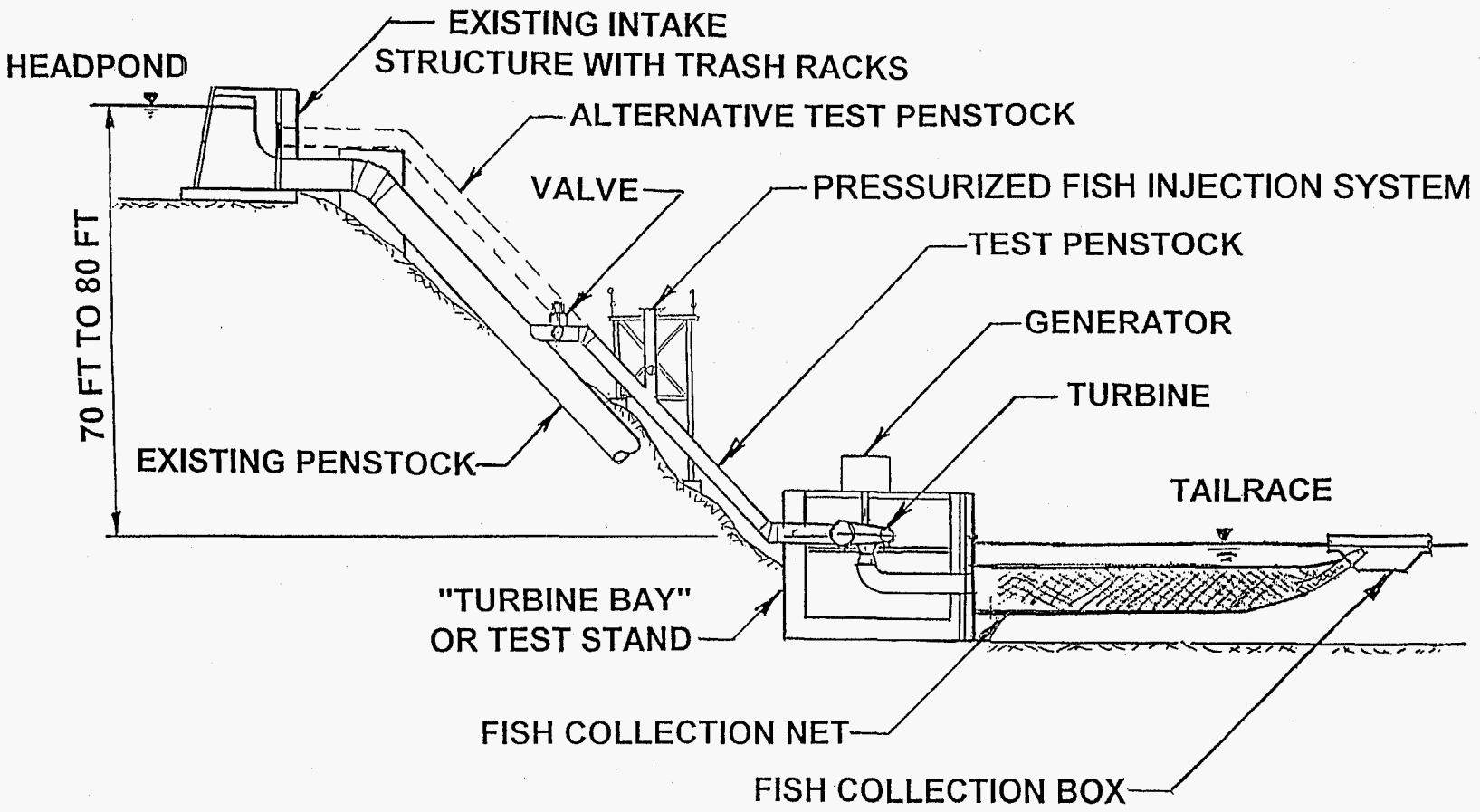

Figure 9-1
Pilot Scale Test Facility At Hydro Site

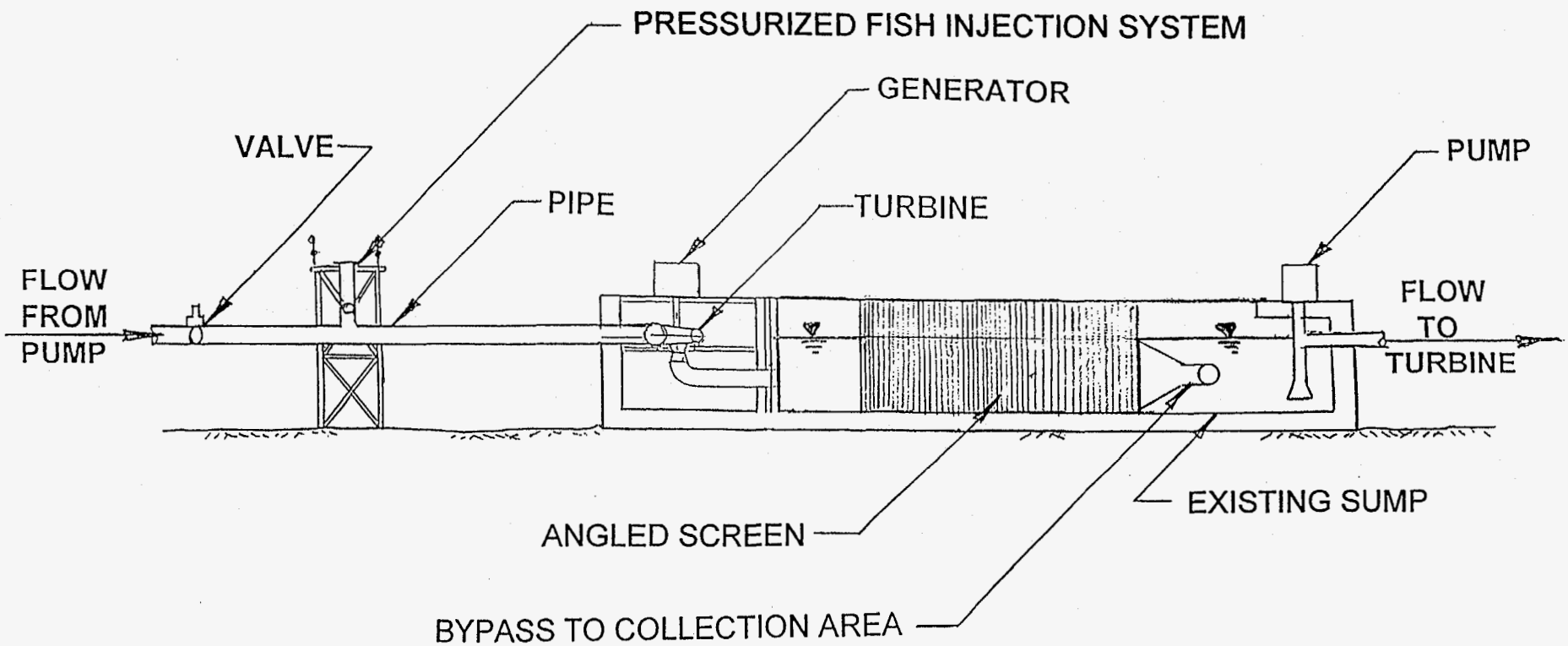

Figure 9-2
Pilot Scale Test Facility In Laboratory

SECTION 10
LITERATURE CITED

Bell, M.C. 1981. Updated compendium on the success of passage of small fish through turbines. Prepared for U.S. Army Corp. of Engineers, North Pacific Division, Portland, Or.

Cada, G.F. 1990. A review of studies relating to the effects of propeller-type turbine passage on fish early life stages. North American Journal of Fisheries Management 10:418-426.

Cada, G.F. 1991. Effects of hydroelectric turbine passage in fish early life stages. Pages 318-326. Reprints from Proceedings of the international conference on hydropower, WaterPower'91: a new view of hydro resources, DOE/ID-10439. U. S. Depart. Energy, Idaho Operations Center, ID.

Collins, N.H. 1984. Potential fish mortality associated with large hydroelectric turbines. In: Canadian Technical Report of Fisheries and Aqautic Sciences, No. 1256: 551-563.

Cook, T.C., Maass E. 1996. personal communication.

Cramer, F.K. and R.C. Oligher. 1964. Passing fish through hydraulic turbines. Transactions of American Fisheries, No. 93(3), pp 243-259.

Doland, J.J. 1954. Hydro power engineering, a textbook for civil engineers. The Ronald Press Company, New York, NY.

Electric Power Research Institute (EPRI). 1986. Assessment of downstream migrant fish protection technologies for hydroelectric application. EPRI AP-4711, project 2694-1 final report, Palo Alto, CA.

Electric Power Research Institute (EPRI). 1987. Turbine-related fish mortality: review and evaluation of studies. EPRI AP-5480, project 2694-4 final report, Palo Alto, CA.

Electric Power Research Institute (EPRI). 1992. Fish entrainment and turbine mortality review and guidelines. EPRI TR-101231, project 2694-01 final report, Palo Alto, CA.

Electric Power Research Institute (EPRI). 1994. Update on fish protection technologies for water intakes. EPRI TR-104122, project 2694-01 final report, Palo Alto, CA.

Empire State Electric Energy Research Corporation. 1981. Laboratory evaluation of fish protection devices at intakes. New York, NY.

Groves, A.G. 1972. Effects of Hydraulic Shearing Actions on Juvenile Salmon. Summary Report. National Oceanic and Atmospheric Administration Northwest Fisheries Center, National Marine Fisheries Service, Seattle, WA.

Johnson, P. L., A. Watkins, C. N. Liston, and R. C. Kristof. 1993. Use of pumping as an alternative to gravity diversion at Red Bluff Diversion Dam, California. Pages 141-146. Proceedings of fish passage policy and technology symposium. Bioengineering Section, Am. Fish. Soc., Portland, OR.

Patrick, P.H. and R.S. McKinley. 1987. Field evaluation of a Hidrostal pump for live transfer of American eels at a hydroelectric facility. North American Journal of Fisheries Management. 7:303-305.

Personal communication. 1996. T. C. Cook (ARL) and E. Maass (WEMCO Pump Company).

RMC Environmental Services, Inc. (RMC). 1994. Survival of fishes in turbine passage through the Townsend Dam, Pennsylvania (FERC project no. 3451). Prepared for Beaver Falls Municipal Authority, Beaver Falls, PA.

Stone & Webster Engineering Corporation (SWEC). 1975. Studies to alleviate potential fish entrapment problems - summary report, 1973-1974 efforts, Nine Mile Point Nuclear Power Station - Unit 2. Prepared for Niagara Mohawk Power Corporation, Syracuse, NY.

U.S. Army Corps of Engineers (COE). 1972. A Compendium on the Survival of Fish Passing Through Spillways and Conduits. Fisheries Engineering Research Program. Portland District, Portland, OR.

U.S. Army Corps of Engineers (COE). 1991. Revised Compendium on the Success of Passage of Small Fish Through Turbines. North Pacific Division, Portland, OR.

U.S. Army Corps of Engineers (COE). 1995a. Proceedings: 1995 Turbine Passage Survival Workshop. Portland District, Portland, OR.

U.S. Army Corps of Engineers (COE). 1995b. Draft agenda: turbine passage survival workshop, May 31-June 1, 1995. Portland District, Portland, OR.

SECTION 11
OTHER LITERATURE REVIEWED

Blaxter, J. H. S., and D. E. Hoss. 1979. The effect of rapid changes of hydrostatic pressure on the Atlantic herring *Clupea harengus*. The Response of the Auditory Bulla System in Larvae and Juveniles. J. Exp. Biol. Ecol. 41:87-100.

Ferguson, J. 1991. Relative survival of juvenile chinook salmon through Bonneville Dam on the Columbia River. Pages 308-317 *in* editors initial & last name, ed. WaterPower'91 Proceedings of the international conference on hydropower. Reprint DOE/ID-10439, U. S. Depart. Energy, Idaho Operations Center, ID.

Ginn, T. C., G. V. Poje, and J. M. O'Connor. 1977. Survival of planktonic organisms following passage through a simulated power plant condenser tube. Pages 91-101 *in* L. P. Jensen, ed. Fourth national workshop on entrainment and impingement. Ecological Analysts Communications, Melville, NY.

Heisey, P. G., D. Mathur, and E. T. Euston. 1995. Fish injury and mortality in spilllage and turbine passage. 2:1416-1423 *in* J. J. Cassidy, ed. Waterpower'95 Proceedings of the international conference on hydropower. ASCE, New York, NY.

Iwamoto, R. N. and J. G. Williams. 1993. Juvenile salmonid passage and survival through turbines. Report of Research. Coastal Zone and Esturine Studies Division, Northwest Fisheries Science Center, National Marine Fisheries Service, Seattle, WA.

Kao, P. T. 1985. New hydraulic design for improved water quality and reduced fish mortality. Pages 403-408 *in* F.W. Olson, R.G. White, and R.H. Hamre, editors. Proceedings of the symposium on small hydropower and fisheries. Western Division and Bioengineering Section, Am. Fish. Soc., Aurora, CO.

Ruggles, C. P. and T. H. Palmeter. 1989. Fish Passage Mortality in a Tube Turbine. Canadian Technical Report of Fisheries and Aqautic Sciences, No. 1664: 551-563.

Schoeneman, D. E., R. T. Pressey, and C. O. Junge, Jr. 1961. Mortalities of downstream migrant Salmon at McNary Dam. Transaction American Fisheries Society, 1961, No. 90, pp.58-71.

Turbak, S. C., D. R. Reichle, and C. R. Shriner. 1981. Analysis of environmental issues related to small-scale hydroelectric development: fish mortality resulting from turbine passage. *ORNL/TM-7521*. Oak Ridge National Laboratory, Oak Ridge, TN.

U.S. Army Corps of Engineers (COE). 1996. Turbine passage survival baseline turbine report. Contract DACW57-94-D-0002. Portland District, Portland, OR.

Williams U. P., D. A. Scruton, R. F. Goosney, C. E. Bourgeois, S. C. Orr, and C. P. Ruggles. 1993. Proceedings of the workshop on fish passage at hydroelectric Develpments. Canadian Technical Report of Fisheries and Aquatic Sciences, No. 1905.

APPENDIX A
POWER PERFORMANCE MODEL (ONE-DIMENSIONAL)

The power performance model for the hydraulic turbine is a customized version of the NREC Program RITDAP™. The standard version of RITDAP is used to predict the performance of radial inflow turbines for compressible fluids. The method is described in NREC Report 1372, An Interactive Design and Performance Prediction of Radial Inflow Turbines (see Appendix C, Section C.10 References, Jansen and Qvale 1967). Customizing the program to analyse the new runner mainly consisted of modifications to introduce incompressible relationships. The customized program calculates the turbine performance with a scroll case upstream of the rotor and a downstream diffuser.

The scroll case loss consists only of friction, whereas friction is only one of the various loss mechanisms in the turbine rotor. Friction losses are calculated from the Darcy-Weisbach pipe-flow presure-loss equation. The loss calculation is obtained from a general relationship representing the Moody diagram, which contains the friction coefficient as a function of Reynolds number and relative roughness. The Reynolds number is internally calculated from flow conditions. The relative roughness is calculated from the specified geometry and surface roughness. The other rotor losses are associated with loading, incidence angle, and clearance. These losses are calculated from the appropriate relationships given in RITDAP.

The diffuser losses are input to the program as the diffuser effectiveness (efficiency) to recover the velocity head at the runner exit. The diffuser effectivenes was calculated using typical loss coefficients for draft tubes.

APPENDIX B
BLADE GEOMETRY MODEL (TWO-DIMENSIONAL)

NREC uses the program COMIG® to generate and analyze the blade geometry. This code has been developed by NREC to analyze compressor and turbine blade geometries using both incompressible and compressible fluids. The method used is described in the American Society of Mechanical Engineers Journal of Engineering for Power entitled "Flow Analysis in Francis Turbines" (see Appendix C, Section C.10 References, Jansen 1967).

APPENDIX C
THREE-DIMENSIONAL FLOW ANALYSES

C.1 Introduction

The flow modeling system VISIUN™, developed at NREC, can be used to analyze the three-dimensional flow through turbomachinery (including centrifugal and axial components and stages). It is capable of simulating both viscous and inviscid, steady and unsteady flow situations. VISIUN™ has been described in detail in NREC Report No. 1628 (Oreper et al. 1990; Oreper et al. 1991; Oreper et al. 1993). The following short description concentrates on the VISIUN™ features pertinent to the numerical modeling of the flow through a hydraulic turbine.

The VISIUN™ system consits of a grid generator, a flow analysis module, and a post-processor that allows designers to quickly evaluate properties of the simulated flow field. Also included are a pre-processor with a graphical user interface, and two modules used to generate boundary and initial conditions. The numerical method used by the flow analysis module is based on the fully implicit, approximately factored algorithm developed by Beam and Warming (1976), implemented by Pulliam and Steger (1980), and later diagonalized by Pulliam and Chausee (1981). To diminish the approximate factorization and linearization error associated with this method, subiterations are included as an option (Rai and Chakravarthy 1986). The convective terms in the governing equations are approximated with forth order accuracy while the diffusion terms are approximated with second order accuracy. The algorithm is first or second order time accurate, depending on whether subiterations are used. The stability of the central difference scheme is maintained with the use of the A. Jameson (Jameson et al. 1981) dissipation model enhanced by directional eigenvalue scaling. Velocity scaling (instead of speed of sound scaling) is used to decrease artificial dissipation in boundary layers (Siclari, 1989). The turbulence is modeled algebraically based on the approach developed by Baldwin and Lomax (1978).

The earlier version of VISIUN™ flow analysis module was similar to the 1984 version of the ARC3D program written for the external flow analysis by Dr. Thomas H. Pulliam of the NASA Ames Research Center (Pulliam 1984).

C.2 Equations and Algorithm

The Navier-Stokes equations, solved numerically by the flow analysis module, are written in strong

conservation law form in transformed body-fitted coordinate system ξ, η, ς coordinates and time τ as:

$$\partial_\tau Q + \partial_\xi(E - E_v) + \partial_\eta(F - F_v) + \partial_\xi(G - G_v) = 0$$

where the inviscid (E, F, G) and viscous (E_v, G_v, F_v) fluxes are defined in Pulliam (1980). All the equations in the analysis module are normalized with respect to characteristic physical parameters so that all the terms are dimensionless. Since total rather than static inlet conditions are usually known when dealing with internal flow problems, the characteristic physical parameters of VISIUN™ have been specified as follows: total speed of sound, a_t, and total density, ρ_t, of the incoming stream as the characteristic velocity and density; 1 m as the characteristic length L; L/a_t as the characteristic time scale. The characteristic viscosity is also evaluated from the total conditions of the incoming stream.

C.3 Steady-State Formulation

The simulation was performed in a frame of reference rotating with the turbine which allows the problem to be treated using a steady state analysis . There are many advantages in performing a steady-state (instead of an unsteady) flow analysis including several techniques for accelerating convergence. To make use of the steady state approach, the governing equations must be rewritten in a rotating non-inertial frame of reference. This is done with use of the transformation described below.

For a constant angular velocity Ω, the absolute velocity in terms of relative velocity u' is:

$$u = u' + \Omega \times r$$

where r is the position vector in the rotating frame,

$$\Omega = \begin{pmatrix} 0 \\ 0 \\ \omega \end{pmatrix},$$

and ω is the angular velocity of rotation around Z-axis. Using this transformation, the governing equations are re-written as:

$$\partial_\tau Q + \partial_\xi (E - E_v) + \partial_\eta (F - F_v) + \partial_\zeta (G - G_v) = H$$

where vector H on the right-hand side is given by:

$$H = J^{-1} \begin{bmatrix} 0 \\ \rho v \omega \\ -\rho u \omega \\ 0 \\ 0 \end{bmatrix},$$

In the above, J is the Jacobian of the transformation defined by Pulliam (1980), u and v are the x and y Cartesian velocity components, and ρ is the density of the fluid.

The components of vector H represent the rotational forces. Using this set of governing equations, the flow in a turbine can be treated as steady-state. Moreover, there is no need to recalculate the metric coefficients and grid point location at each time step because the computational grid is stationary. All the metric coefficients, including unsteady ones, still have to be calculated, but only once at the beginning of the calculation process. The unsteady metrics are used to calculate relative velocities.

C.4 Time Step Modifications

For a steady-state flow analysis, a convergence accelerating procedure can be used. The acceleration procedure implemented in VISIUN™ is based on a local time step modification. The local time step is usually restricted by the stability limit, even for an implicit algorithm, because of the non-linear nature of the governing equations; however, the restriction is not as severe as for the explicit algorithm. Usually, a smaller time step is required in the regions where grid lines are clustered, whereas for the rest of the computational domain, a much larger time step can be used. Thus, the solution can be advanced in time with a time step that is optimal for each grid point. In the VISIUN™ code, a constant Courant number (a quantity related to the stability of the solution scheme) is used everywhere in the field. For example, in the j-direction we have:

$$\Delta t_j = \frac{CFL}{\left(U + a\sqrt{\xi_x^2 + \xi_y^2 + \xi_z^2} + \frac{2u}{Re\,\rho}\left(\xi_x^2 + \xi_y^2 + \xi_z^2\right) \right)}$$

where CFL is the Courant number, Re is the Reynolds number, U is the contravariant velocity component in j-direction (defined later), a is the local speed of sound, μ is the molecular viscosity and the third term in the denominator represents viscous correction. The metric coefficients ξ_x, ξ_y, ξ_z, are defined in Pulliam (1981). The minimum value of Δt among all three coordinate directions gives the maximum allowable time step. Sometimes this approach fails over a few iterations at the beginning of the run when large fluctuations in the physical variables take place due to large changes in the local flow variables. The stability can be maintained if the time step is limited by the relative change of the pressure or density. In the VISIUN™ analysis module, the maximum Δt is set to:

$$\Delta t = \min\left[t_{max}, \frac{PC}{\max \frac{\Delta \rho}{\rho}} \right]$$

where PC is the maximum specified percentage of change. The same procedure is implemented with respect to the static pressure change and the minimum Δt is used as the time step.

C.5 Boundary Conditions

The VISIUN flow analysis module works with five types of boundaries: inlet, exit, inviscid and viscous solid walls, and periodic surfaces. Specification of five flow variables are required at each boundary.

At the inlet, where the flow is considered to be inviscid, non-reflective inlet boundary conditions based on the total flow properties at the inlet plane are specified. The known quantities at the inlet boundary are usually the total pressure, the total temperature or density, along with two flow angles and/or velocity components. At this boundary four pieces of information can be imposed. The nature of the hyperbolic governing equations dictates that one of the boundary quantities must be extrapolated from inside the computational domain to the inlet boundary. The flow variables with which VISIUN™ operates are static density, three momentum components, and total energy. Thus, the boundary procedure in VISIUN™ extrapolates the static pressure, and calculates the static density, the three momentum components, and the total energy.

At the exit boundary, the static pressure is specified and the other four variables are linearly extrapolated. In the case of flow re-entering the domain due to recirculation at the exit boundary, the total pressure is set to the static pressure outside of the recirculation zone. The nondimensional total temperature is set to 1, and the two flow angles are extrapolated from inside the computational domain. It is also possible to use the specified total exit pressure and density in case of backflow at the exit boundary. Since those values are usually not known, it is preferable to extend the computational domain to avoid backflow due to flow recirculation.

In the case of an axial exit a simple radial equilibrium is imposed and the static pressure is found from:

$$\frac{\partial p}{\partial r} = \rho \frac{u_\theta^2}{r^2}$$

where u_θ is the velocity component in the circumferential direction.

Periodic boundary conditions are specified in the vaneless space under the assumption that H-type grids are used. The imposed periodic boundary conditions are second-order accurate in space. It is assumed that the values of all dependant variables as well as the gradients of the variables normal to the periodic boundary are equal on both sides of the periodic boundary.

In terms of a 3-D curvilinear coordinate system (ξ, η, ζ), the boundary conditions for a normal gradient and values of the flow variables are:

$$\nabla Q \cdot \nabla \eta|_1 = \nabla Q \cdot \nabla \eta|_2, \; Q_1 = Q_2$$

where subscripts 1 and 2 refer to the periodic boundaries 1 and 2, respectively. The ∇Q is the gradient of any variable and $\nabla \eta$ is a unit vector normal to the periodic boundary surface (k = 1 or k = kmax) which in this case is calculated as:

$$\nabla \eta = \frac{\eta_x \cdot i}{\sqrt{\eta_x^2 + \eta_y^2 + \eta_z^2}} + \frac{\eta_y \cdot j}{\sqrt{\eta_x^2 + \eta_y^2 + \eta_z^2}} + \frac{\eta_z \cdot k}{\sqrt{\eta_x^2 + \eta_y^2 + \eta_z^2}}$$

The derivatives of the gradient ∇Q in the above expressions along the periodic surfaces are evaluated using second order differences. For the derivatives normal to the periodic boundary surfaces, one-sided second order differences are used.

This procedure is repeated for all points along the periodic boundary. After applying the approximate factorization, a set of algebraic equations with a tridiagonal matrix is formed. The boundary conditions for these equations are the values of the flow variables at the leading or the trailing edge, the inlet , the hub and the shroud, and the tip of the blade. The values of flow variables at those points are calculated by solid wall, and inlet or exit boundary procedures. The points that are on the intersection of periodic boundaries and the inlet or exit surfaces are also calculated by the periodic boundary procedure, but with the use of simple averaging. In this manner the values of the flow variables at the periodic boundary are obtained by averaging the values of flow variables taken from the grid lines next to the periodic boundary.

The solid wall boundary conditions support both inviscid and viscous flow analysis. In the case of an inviscid wall, the contravariant velocity component (defined later) normal to the solid wall is set equal to zero and the contravariant components parallel to the wall are extrapolated. The extrapolation can be zero or first order accurate. The Cartesian components of velocity are obtained from the following equation:

$$\begin{pmatrix} u \\ v \\ w \end{pmatrix} = \begin{pmatrix} \xi_x & \xi_y & \xi_z \\ \eta_x & \eta_y & \eta_z \\ \zeta_x & \zeta_y & \zeta_z \end{pmatrix}^{-1} \begin{pmatrix} U - \xi_t \\ V - \eta_t \\ W - \zeta_t \end{pmatrix}$$

where:

$$U = \xi_t + \xi_x u + \xi_y v + \xi_z w, V = \eta_t + \eta_x u + \eta_y v + \eta_z w, W = \varsigma_t + \varsigma_x u + \varsigma_y v + \varsigma_z w$$

Here U, V, W are the contravariant velocity components and $\xi_t = \eta_t = \varsigma_t = 0$ if there is no rotation. For a viscous wall, $U = V = W = 0$.

The pressure on the body surface is obtained from the normal momentum equation, which is solved at all walls of the passage. For example, the equation for a wall at l = constant (hub or shroud) is:

$$(\nabla\xi \cdot \nabla\zeta)p_\xi + (\nabla\eta \cdot \nabla\zeta)_\eta + (\nabla\zeta \cdot \nabla\zeta)p_\zeta$$

$$= \rho(\partial_\tau\zeta_t + \mathbf{u} \cdot (\nabla\zeta)_\tau) - \rho U(\nabla\zeta \cdot \mathbf{u}_\zeta) - \rho V(\nabla\zeta \cdot \mathbf{u}_\eta)$$

Similarly for a k-wall (pressure and suction side of the blade) the normal momentum equation is written as:

$$(\nabla\xi \cdot \nabla\eta)p_\xi + (\nabla\eta \cdot \nabla\eta)p_\eta + (\nabla\xi \cdot \nabla\eta)p_\xi =$$

$$\rho(\partial_\tau\eta_\tau + \mathbf{u} \cdot (\nabla\eta)_\tau) - \rho U(\nabla\eta \cdot \mathbf{u}_\xi) - \rho W(\nabla\eta \cdot \mathbf{u}_\xi)$$

and for a j-wall (leading or trailing edges):

$$(\nabla\xi \cdot \nabla\xi)p_\xi + (\nabla\eta \cdot \nabla\xi)p_\eta + (\nabla\xi \cdot \nabla\xi)p_\xi =$$

$$\rho(\partial_\tau\xi_\tau + \mathbf{u} \cdot (\nabla\xi)_\tau) - \rho V(\nabla\xi \cdot \mathbf{u}_\eta) - \rho W(\nabla\xi \cdot \mathbf{u}_\xi)$$

Here **u** is the velocity vector in the Cartesian coordinate system.

The normal momentum equations are valid for high Reynolds number flows. For stationary coordinate systems, time derivatives of the metrics coefficients are set to zero. The resulting equations are rewritten in an approximately factored form and discretized with second-order differences. Central differences are used for the derivatives along the walls, and one-sided differences are used in the direction towards the wall. An ADI procedure is then applied to solve the resulting set of finite difference equations.

After the static pressure at the solid wall is found, the density at the slip wall is found by using the static pressure and the extrapolated entropy $S = p/\rho^\gamma$ (Barton and Pulliam, 1984; Chima, 1985). For viscous walls, the density instead of the entropy is extrapolated. The solid wall boundary procedure is valid for the adiabatic walls.

As was shown, in a steady-state formulation for the flow analysis in a rotational frame of references, extra terms are added to the right hand side of the normal momentum equations to represent the rotational forces. The addition of the rotational forces in the governing equations will also add rotational forces to the normal momentum equation for the pressure boundary condition. The corresponding rotational forces are:

$$\rho v\Omega\xi_x - \rho u\Omega\xi_y, \quad \rho v\Omega\eta_x - \rho u\Omega\eta_y \quad \text{and} \quad \rho v\Omega\zeta_x - \rho u\Omega\zeta_y$$

for j, k, and l walls.

C.6 Turbulence Modeling

The turbulence model used in the present turbine calculations is that of Baldwin and Lomax (1978) modified to provide values of turbulent viscosity for the case of multiple walls. In this model, the length scale calculation in the three dimensional flow field is based on the reduced vorticity value. This value is the vorticity component parallel to the current wall and normal to the local velocity vector. This procedure estimates values of Fmax (See Baldwin and Lomax, 1978 for details) even when the search for Fmax is along a grid line located in the boundary layer of another wall. The turbulent viscosity is calculated across boundary layers and wakes separately for each wall. The contribution from each wall into the final turbulent viscosity is calculated according to the formula:

$$\mu_{turb} = \frac{1}{\sqrt{\sum_{i=1}^{n} \frac{1}{d_i^2}}} \sum_{i=1}^{n} \frac{\mu_{turb,i}}{d_i}$$

where n is the maximum number of solid walls that can contribute to the turbulent viscosity value and d is the distance to a particular wall. If there is no solid wall at a boundary, such as an inlet, exit or periodic boundary, then the contribution from the wall is eliminated by setting d very large.

It should be mentioned that in a three-dimensional flow field several maxima of Fmax are possible. After the first maximum is found, the search for the Fmax continues, and if a second maximum is found, the largest of the two value is used. This is particularly important for regions of separated flow where two maxima in the F function distribution exist.

In VISIUN, the search for the Fmax and its corresponding Smax is restricted to the region between the wall and some specified distance from the wall. This eliminates false values of Fmax that might be in the inviscid region of the flow or in the boundary layer of the opposite wall. If that is not done, turbulent viscosity might have erroneously large values. The region for the Fmax search is evaluated as a distance from the wall to the location that corresponds to $Y^+ = 1500$. Thus, the current procedure finds the location of the first and the second maximum, but within the distance restricted by $Y^+ = 1500$.

Constants used in the Baldwin-Lomax turbulence model were not changed, except for the wake constant. This constant was set to 2 instead of 0.25 according to the recommendation of Chan (1993).

C.7 Grid Topology

VISIUN™ uses compound H-type body-fitted grids to conduct flow analysis within complex geometries. The transformation to body-fitted coordinates maps the entire geometrical domain into a cube which is subsequently split into regions. The boundaries of a typical region consist of solid walls, periodic boundaries, inlet and exit planes, and depend on the direction of the integration. For example there are three regions for the integration in the blade to blade direction: in front of the leading edges, between the blades and after the trailing edges. The compound H-type grid is a combination of simple H-type grids that are continuous at a region's boundaries. If an enclosure has to be modeled, such as a blade or a splitter, grid lines will go through the enclosure. This allows for a better clustering of grid lines in critical areas, such as leading edges, so that a sufficient spatial resolution can be maintained there. The calculations are only performed outside of the enclosure, and a solid wall boundary condition is imposed at the boundary of the enclosure.

The grid generator availible in VISIUN™ is tuned to generate body-fitted coordinates for turbomachinery components and stages. The x, y, and z coordinates of the blade surface are read from a file containing blade cross-section coordinates at the hub and at the shroud. The coordinates of the hub and the shroud for the entire passage, including inlet and exit regions are read from a separate file. The blade coordinates for locations other than the hub and shroud are calculated by interpolation with the restriction that hub and shroud coordinates are connected with a straight line. This results in ruled blade surfaces. For a sculptured blade, multiple blade cross-sections are allowed. If the leading edge coordinates are not known, an elliptical leading edge can be specified. The trailing edge can also be specified as an elliptical or, alternatively, blunt. The periodic lines are extended upstream and downstream. This extension can be radial, parallel to the blade Camberline, or at a specified angle. The grid is generated on surfaces of revolution with boundaries at the inlet, exit, periodic regions and the blade surfaces. The grid generation is repeated at each spanwise location of the desired grid surface. Those surface grids will fill out the space between the hub and the shroud specified in the geometry file with hub and shroud contours. To generate a grid for an unshrouded turbomachinery component the tip of the blade is cut back at a specified tip clearance, which can vary from leading to trailing edge. The clustering of the grid points can be acheived in any direction by specifying clustering functions accessible from the user interface, and can be manipulated by dragging points on the distribution curve with the mouse. After the distributions of the clustering functions

are defined, the grid is generated by a modified transfinite interpolation procedure. Finally, an elliptical grid generator is used to smooth grid points distribution in the areas of excessive clustering and skewness.

With the boundary conditions specified at each boundary, the algorithm solves the finite-differenced governing equations for a grid line. The calculations proceed direction by direction starting at one boundary and ending at the corresponding one.

C.8 Solution Algorithm

The solution proceedure used in the calculations is an iterative, block structured algorithm. In this method the equations are solved by using an approximate factorization and linearization algorithm developed by Pulliam (1981). The algorithm is first order accurate in time and has an approximate factorization and linearization error. This algorithm in delta form is:

$$T_\xi\left[1 + h\delta_\xi\Lambda_\xi\right] N \left[1+ h\delta_\eta\Lambda_\eta\right] P \left[1+ h\delta_\xi\Lambda_\xi\right] T_\xi^{-1} \Delta Q^n = R^n$$

where:

$$\Delta Q^n = Q^{n+1} - Q^n,\ h = \Delta t,$$
$$R^n = -h(\delta_\xi(E^n + E_v^n) + \delta_n (F^n + F_v^n) + \delta_\xi (G^n + G_v^n))$$

In the above, δ is the central difference operator and the matrices T, N, and P, along with the inviscid (E, F, G) and viscous (E_v, F_v, G_v) flux vectors are defined in Pulliam (1980: 1981).

To improve the time accuracy and to minimize the approximate factorization error, M.M. Rai (1986) suggested an iterative algorithm which is also based on approximate factorization and linearization. This algorithm uses a Newton type iteration proceedure to drive the approximate factorization error to zero at each time step. A somewhat different formulation was implemented in VISIUN™. The new second order time accurate iterative algorithm in delta form is as follows:

$$\left[T_\xi\left[I + h\delta_\xi\Lambda_\xi\right] N \left[I + h\delta_\eta\Lambda_\eta\right] P \left[I + h\delta_\zeta\Lambda_\zeta\right] T_\zeta^{-1}\right]^p \Delta Q^p = R^p$$

where:

$$\Delta Q^p = Q^{p-1} - Q^p,$$

Here Q^p is an approximation to Q^{n+1}. When $p = 0$, $Q^p = Q^n$. If the above equation is iterated to convergence for a given time-step, $Q^p = Q^{n+1}$. Since the left-hand of this equation can be driven to zero at each time step, the linearization and approximate factorization error can be eliminated. For a steady-state solution, the iteration is not required to converge at each time step. If the number of iterations is one, the scheme becomes a conventional non-iterative scheme, such as the diagonal version of the Beam and Warming algorithm (Beam and Warming 1976). This scheme was used to arrive at the steady-state solution for the Fish Friendly Turbine. In that case the stability and convergence of the compressible flow algorithm can be maintained even for very low Mach number flows with the use of subiterations that diminish the approximate factorization and linearization error.

C.9 Output

The main output of the VISIUN™ analysis consists of four files: a grid file, a flow field values file, a run summary file, and a file with mass averaged values and values of the flow variables along a specified grid line. The run summary file contains residuals, time steps, and maximum residuals for each variable in the flow field. A summary of mass averaged values at the inlet and exit of the computational domain are printed out at the specified number of iterations. The values of the x, y, and z coordinates, density, velocity, total energy, static and total pressure, and enthalpy can also be printed at specified grid locations. Cylindrical coordinates r, z, and θ, along with density, Mach number, static pressure, and total pressure can also be printed out.

C.10 References

Baldwin, B., and H. Lomax. 1978. Thin-Layer Approximation and Algebraic Model for Separated Turbulent Flows, AIAA Paper 78-257.

Barton, J.T. and T.H. Pulliam. 1984. Airfoil Computations at High Angles of Attack, Inviscid and Viscous Phenomena, AIAA Paper 84-0524.

Beam, R. and R. F. Warming. 1976. An Implicit Finite-Difference Algorithm for Hyperbolic Systems in Conservation Law Form, Journal of Computational Physics, Vol. 22, pp. 87-110.

Chan, W.M., NASA Ames. 1993. Private Communication.

Chima, R.V. 1985. Inviscid and Viscous Flows in Cascades with a Explicit Multiple Grid Algorithm, AIAA Journal, Vol. 23, pp. 1556-63.

Jameson, A., W. Schmidt and E. Turkel. 1981. Numerical Solutions of the Euler Equations by Finite Volume Methods Using Runge-Kutta Time-Stepping Schemes, AIAA Paper 81-1259, AIAA 14th Fluid and Plasma Dynamics Conference, Palo Alto.

Jansen, W., and E. B. Qvale. 1967. A Rapid Method for Predicting the Off-Design Performance of Radial-Inflow Turbines, ASME Paper 67-WA/GT-3.

Jansen., W. 1967. Flow Analysis in Francis Water Turbines, ASME Journal of Engineering for Power, p. 445.

Oreper G.M. (Principal investigator) et al. 1990. Analysis of Three-Dimensional Unsteady Flow in Centrifugal Compressors. NREC Report No. 1628-1, Phase One: Diffuser Performance.

Oreper G.M. (Principal investigator) et al. 1991. Analysis of Three-Dimensional Unsteady Flow in Centrifugal Compressors. NREC Report No. 1628-2, Phase Two: Impeller Performance.

Oreper G.M. (Principal investigator) et al. 1993. Analysis of Three-Dimensional Unsteady Flow in Centrifugal Compressors. NREC Report No. 1628-3, Phase Three: Stage Performance.

Pulliam, T. H. and J. L. Steger. 1980. On Implicit Finite Difference Simulation of Three-Dimensional Compressible Flow, AIAA Journal, Vol. 18, p. 159.

Pulliam, T. H. and D. S. Chaussee. 1981. A Diagonal Form of an Implicit Approximate Factorization Algorithm, Journal of Computational Physics, Vol. 39, p. 347.

Pulliam, T. H. 1984. EULER AND THIN LAYER NAVIER-STOKES CODES: ARC2D, ARC3D, Notes for COMPUTATIONAL FLUID DYNAMICS USER'S WORKSHOP. The University of Tennessee Space Institute, Tullahoma, Tennessee, March 12-16.

Rai M. M. and S. R.Chakravarthy. 1986. "An Implicit Form for the Osher Upwind Scheme," AIAA Journal, Vol. 24, No. 5, p. 735.

Siclari, M.J., P. Del Guidice and A. Jameson. A Multigrid Finite Volume Method for Solving the Navier-Stokes Equations for High Speed Flows, AIAA paper 89-0283, AIAA 27th Aerospace Sciences Meeting, Reno, Nevada.